INSTITUTO DE TECNOLOGÍA QUÍMICA (UPV–CSIC)

UNIVERSITAT POLITÈCNICA DE VALÈNCIA

IN COTUTELLE WITH

LEBANESE UNIVERSITY

Catalysts and catalytic processes for the transformation of tars and other non-conventional feedstocks into fuels and chemicals

PhD in Sustainable Chemistry

Doctoral candidate: Zaher Raad

Directors: Dr. Marcelo E. Domine and Prof. Tayssir Hamieh

Valencia, September 2021

Acknowledgements

"*The sweetness of success erases the bitterness of patience*."

Imam Ali Ibn Abi Talib

"*Patience is bitter, but its fruit is sweet*."

Jean-Jacques Rousseau

I would like to express my deepest gratitude to all who have helped me during the development of this thesis:

To "Islamic Center Association for Guidance and Higher Education", Universitat Politècnica de València (UPV) and the Spanish government for their financial support during this period.

To both Instituto de Tecnología Química ITQ (UPV - Spain) and Laboratory of Materials, Catalysis, Environment and Analytical Methods MCEMA (Lebanese University - Lebanon) for my PhD development.

To my supervisor Dr. Marcelo E. Domine for your invaluable advice, guidance, continuous support, and patience during my PhD study. It is such a pleasure to work with you and thank you sincerely for everything.

To my supervisor Prof. Tayssir Hamieh for your helpful advice and support during this period. To Prof. Joumana Toufaily for this great collaboration between Lebanese University and Universitat Politècnica de València. I really appreciate your effort.

To Prof. Sébastien Paul for his kind reception during my fruitful stay at REALCAT platform at Ecole Centrale de Lille (France), for including me as

one member in his group, and to Dr. Svetlana Heyte for her kind help and support.

To all ITQ people responsible for characterization techniques (Maribel, Amparo, Maria Jesus, Fani…), workshop (mechanical and informatics), administration staff, along with the Microscopy service at UPV for their collaboration and help.

To José Gaona for your help, practical and insightful suggestions (me has ayudado mucho).

To my friends and colleagues of the laboratory: Marvin, Alberto, Susana, Cristina, Chelo, Miriam (special thanks for your help with microscopy), Jaime, Claudia, Lina, Borja, Paola, Maria, Madalina, Mari, Zoel, Byron, Pau, Marta, Fran, Javi, Verónica, Carlos, Carles and Karen. To Dr. Miguel Angel, as well. Thanks for your support and the great company inside and outside ITQ. Special thanks to Claudia and Paola for your kindness and encouragement.

To all my colleagues at ITQ for your appreciated support and encouragement.

To my friend Jaime for your great company during these years, sharing the tough and the good moments, and for all the great discussions we have had during coffee time. Thanks, my little friend.

To my friend Yannick for always being here for any doubt. Grand Merci pour ton aimable aide et tes conseils ingénieux mon ami.

To my friend Marvin, thanks for your kind and appreciated help and support since the very first moment at ITQ.

To Jaime, Yannick, Marvin, Ferran (gràcies amigo!!), Dani, Agustin, Silvia, Pascual, Luismi, and Dr. Marta Feliz. Thanks for your company and the great moments we have shared.

To Rosa for your kind support all through my stay at ITQ. Thank you for showing me such kindness.

To my friend Abdessamad for your support and the great company, becoming part of my second family in Valencia.

To Mouin, Moussa and Salman for your support, becoming part of my second family in Valencia, as well.

To Zeinab for your kindness, support, encouragement, and for being by my side despite the distance. You gave me strength when I really needed it.

It would not have been possible to complete this work without the support, encouragement, unconditional love, and nurturing of my family: my parents Mohamad and Sanaa, my brother Maher, and my sister Sarah. To my cousin Jad, the rest of my family and my close Lebanese friends, thanks for your appreciated support.

I really appreciate it!

Zaher Raad

Abstract

Because of the depletion of petroleum sources, the increased demand for energy and transportation fuels, and the need for both reduction of greenhouse gases (GHG) emissions and the dependence on fossil resources, the utilization of sustainable alternative sources to produce fuels and chemicals becomes essential. In this context, the valorization of light tars (formed during petroleum refining and biomass gasification processes) and other non-conventional sources (i.e., fatty acids), and their conversion into high-added value chemicals will be an interesting and challenging option.

In this work, solid catalysts, and catalytic processes for the transformation of light tars via mild hydrotreatment process are developed. This process is studied by employing different polycyclic aromatic hydrocarbons (PAHs) as model molecules representative of light tars feedstocks. The tars-type compounds of this model mixture are transformed into C9-C15 partially hydrogenated hydrocarbons that could be applied as jet fuel additives (improvers) or as chemicals and solvents for industry.

First, the tars mild hydrotreatment is studied over Pd supported on TiO_2 possessing different crystalline phases. The hydrotreatment activity and selectivity towards the desired hydrogenated products (i.e., tetralin and others) increase by increasing both acidity and surface area of the catalyst, along with the presence of small and well distributed Pd nanoparticles. The Pd/TiO_2 Nano catalyst reveals remarkable hydrotreatment activity and stability after several reuses with practically no changes in TiO_2 structure, quite low carbon deposition, any Pd leaching detected and maintaining both small Pd particle size and their adequate distribution, even after regeneration of the catalyst. Additionally, Pd/TiO_2 Nano catalyst demonstrates to be more effective to the production of C9-C15 hydrocarbons than other commercial and previously reported hydrotreatment catalysts.

In addition, Pd supported on TiO_2-Al_2O_3 mixed oxide, prepared via optimized co-precipitation method, is evaluated in the tars mild hydrotreatment, displaying good activity and stability after several reuses. Its hydrotreatment activity is compared with that of Pd/TiO_2 Nano and Pd/γ-Al_2O_3 catalysts; while its application

scope is extended to other demanding hydrogenation reactions, such as the reductive amination of bio-derived acetol with ethylenediamine to produce 2-methylpiperazine. Furthermore, a novel Pd supported on TiO_2/γ-Al_2O_3 (Ti precursor impregnated onto alumina as support) developed catalyst demonstrates good activity in the mild hydrotreatment of tars-type compounds.

Finally, Ni-based catalysts are prepared and tested in the tars mild hydrotreatment, Ni/TiO_2/Al_2O_3 catalyst being the most active among them. Additionally, Ni catalysts show excellent catalytic performance when applied as catalysts in the selective hydrogenation of fatty acids to produce hydrocarbons, Ni/TiO_2/Al_2O_3 and Ni/TiO_2/ZrO_2 catalysts offering the highest selectivity to n-heptadecane (C17). Interestingly, Pt doping is encountered to increase the activity of the latter Ni catalysts.

Summarizing, different metal supported catalysts developed in this study are capable to transform light tars and fatty acids under mild reaction conditions, thus offering a viable and more sustainable option to produce useful hydrocarbons from other non-conventional sources.

Debido al agotamiento de las fuentes de petróleo, la mayor demanda de energía y combustibles para el transporte, y la necesidad de reducir las emisiones de gases de efecto invernadero y la dependencia de los recursos fósiles, la utilización de fuentes alternativas sostenibles para producir combustibles y productos químicos se vuelve esencial. En este contexto, la valorización de alquitranes ligeros (formados durante los procesos de refinación de petróleo y gasificación de biomasa) y otras fuentes no convencionales (es decir, ácidos grasos) y su conversión en productos químicos de alto valor agregado será una opción interesante y desafiante.

En este trabajo se desarrollan catalizadores sólidos y procesos catalíticos para la transformación de alquitranes ligeros mediante el proceso de hidrotratamiento suave. Este proceso está estudiado empleando diferentes hidrocarburos aromáticos policíclicos (HAP) como moléculas modelo, representativas de materias primas de alquitrán ligero. Los compuestos de tipo alquitrán de esta mezcla modelo se transforman en hidrocarburos C9-C15 parcialmente hidrogenados, que podrían aplicarse como aditivos (mejoradores) del combustible de aviación, o como productos químicos y disolventes para la industria.

Primero, se estudia el hidrotratamiento suave de alquitranes empleando Pd soportado sobre TiO_2, que posee diferentes fases cristalinas. La actividad de hidrotratamiento y la selectividad hacia los productos hidrogenados deseados (es decir, tetralina y otros) aumentaron al aumentar tanto la acidez como el área superficial del catalizador, junto con la presencia de nanopartículas de Pd pequeñas y bien distribuidas. El catalizador Pd/TiO_2 Nano revela una notable actividad de hidrotratamiento y estabilidad después de varios reusos sin prácticamente cambios en la estructura del TiO_2. Además, no se observa prácticamente deposición de carbono, ni lixiviación de Pd, manteniéndose tanto el tamaño de partícula como la adecuada distribución del Pd, incluso después de la regeneración del catalizador. Además, el catalizador Pd/TiO_2 Nano demuestra ser más eficaz para la producción de hidrocarburos C9-C15 que otros catalizadores de hidrotratamiento comerciales y reportados anteriormente.

Además, el Pd soportado en el óxido mixto TiO_2-Al_2O_3 preparado mediante el método de co-precipitación optimizado, se evalúa en el hidrotratamiento suave de alquitranes, mostrando buena actividad y estabilidad después de varios reusos. Su actividad de hidrotratamiento se compara con la de los catalizadores Pd/TiO_2 Nano y Pd/Al_2O_3; mientras que su ámbito de aplicación se extiende a otras reacciones de hidrogenación más exigentes, como la aminación reductora de acetol bioderivado. Además, un nuevo catalizador desarrollado con Pd soportado sobre TiO_2/Al_2O_3 (precursor de Ti impregnado sobre alúmina como soporte) demuestra una buena actividad en el hidrotratamiento suave de compuestos de tipo alquitrán.

Finalmente, los catalizadores a base de Ni se preparan y prueban en el hidrotratamiento suave de alquitranes, siendo el catalizador Ni/TiO_2/Al_2O_3 el más activo entre ellos. Además, los catalizadores de Ni muestran un excelente rendimiento catalítico cuando se aplican como catalizadores en la hidrogenación selectiva de ácidos grasos para producir hidrocarburos, catalizadores de Ni/TiO_2/Al_2O_3 y Ni/TiO_2/ZrO_2, ofreciendo la más alta selectividad hacia n-heptadecano (C17). Curiosamente, se encuentra que el dopaje con Pt aumenta la actividad de los últimos catalizadores de Ni.

En resumen, diferentes catalizadores soportados por metales desarrollados en este estudio son capaces de transformar alquitranes ligeros y ácidos grasos en condiciones de reacción suaves, ofreciendo así una opción viable y más sostenible para la producción de hidrocarburos útiles de otras fuentes no convencionales.

Degut a l'esgotament dels depòsits petrolífers, hi hagut un increment de la demanda d'energia i de combustibles; al mateix temps que la necessitat de reduir les emissions de gasos GHG i la dependència als recursos fòssils; esdevé essencial la utilització de fonts d'energia alternativa per a produir combustibles líquids i productes químics. En aquest context, la valorització de quitrans lleugers (formats durant els processos de refinament del petroli i de gasificació de la biomassa) i d'altres fonts d'energia no convencionals com per exemple àcids grassos; i la seva conversió en productes químics d'alt valor afegit són una opció interessant i prometedora.

En aquest treball, es desenvoluparan catalitzadors sòlids i processos catalítics per a la transformació de quitrans lleugers a través del procés d'hidrotractament en condicions suaus. Aquest procés s'estudia utilitzant diferents hidrocarburs policíclics aromàtics (PAHs) com a molècules model representatives de la matèria prima que constitueixen els quitrans lleugers. Els quitrans d'aquesta mescla representativa es transformen a hidrocarburs C9-C15 parcialment hidrogenats que poden ser utilitzats com a querosè o com a productes químics i dissolvents per a la indústria.

Primer, l'hidrotractament en condicions suaus dels quitrans va ser estudiat utilitzant materials de Pd suportat sobre TiO_2 de diferents fases cristal·lines. L'activitat de l'hidrotractament i la selectivitat del procés als productes hidrogenats desitjats (i.e tetralina i altres) augmenta en augmentar l'acidesa i l'àrea superficial del catalitzador, junt amb la presència de petites nanopartícules de Pd adequadament distribuïdes. El catalitzador Pd/TiO_2 Nano presenta una destacada activitat en la reacció d'hidrotractament i resulta estable després de reutilitzar-lo en diverses ocasions sense pràcticament canvis en l'estructura TiO_2, malgrat que té lloc certa sedimentació de carboni, no es detecta lixiviació i es manté tan la distribució com les dimensions de les partícules després de la regeneració del catalitzador. A més a més, el catalitzador Pd/TiO_2 Nano resulta ésser més efectiu per a la producció d'hidrocarburs C9-C15 que altres catalitzadors comercials i d'altres descrits prèviament en la bibliografia.

A més a més, s'ha estudiat el Pd suportat en l'òxid mixt TiO_2-Al_2O_3 preparat a través de l'optimització del mètode de la coprecipitació en la reacció

d'hidrotractament de quitrans en condicions suaus. Aquest catalitzador mostra una bona activitat i estabilitat després de reutilitzar-lo en vàries ocasions. La seva activitat en dita reacció es compara a la que presenten els catalitzadors de Pd/TiO_2 Nano i Pd/Al_2O_3; i també s'ha comprovat el seu abast en altres reaccions d'hidrogenació d'interès, com per exemple l'aminació reductiva d'acetol provinent de la biomassa. A més a més, s'ha desenvolupat un nou catalitzador de Pd suportat sobre TiO_2/Al_2O_3 (on el precursor de Ti s'impregna sobre l'alúmina que actua com a suport) que mostra una bona activitat en la reacció d'hidrotractament de compostos tipus quitrans en condicions suaus.

Finalment, els catalitzadors basats en Ni han estat preparats i testats en reaccions d'hidrotractament de quitrans en condicions suaus, sent el catalitzador $Ni/TiO_2/Al_2O_3$ el més actiu de tots. Addicionalment, els catalitzadors de níquel mostren excel·lents activitats catalítiques quan s'utilitzen com a catalitzadors per a la hidrogenació selectiva d'àcids grassos per a la producció d'hidrocarburs. Els catalitzadors de $Ni/TiO_2/Al_2O_3$ i $Ni/TiO_2/ZrO_2$ presenten la major selectivitat a *n*-heptadecà (C17). Cal mencionar, que el dopatge amb Pt tendeix a augmentar l'activitat de l'últim catalitzador de Ni.

Resumint, s'ha demostrat que diferents catalitzadors basats en metall suportat que han estat desenvolupats durant aquest estudi són capaços de transformar els quitrans lleugers i els àcids grassos en condicions suaus de reacció, oferint d'aquesta forma una opció viable i més sostenible per a produir hidrocarburs d'interès industrial a partir de fonts no convencionals.

Chapter 1. Introduction

Chapter 2. Objectives

Chapter 3. Experimental procedure

Chapter 4. Titanium oxide-supported Pd as an efficient and stable catalyst for the mild hydrotreatment of tars-type compounds

Chapter 5. Titania-alumina-supported Pd catalysts for the mild hydrotreatment of tars-type compounds

Chapter 6. Ni-based catalysts for hydrogenation reactions

Chapter 7. General conclusions

Chapter 8. List of figures and tables

Chapter 9. Annex

CHAPTER 1.

INTRODUCTION

1.1. Use of conventional petroleum sources and heavy oils and residues

Total oil need in the world is expected to increase up to 123 million barrels per day (mmbpd) by 2025, according to the United States Energy Information Administration. In addition, referring to the organization of petroleum exporting countries (OPEC), its production is estimated to 61 mmbpd by 2025 (62 mmbpd by 2025 according to non-OPEC countries), which is less than half of the oil demand [1].

World-wide fuels and petrochemicals are obtained mainly from fossil sources and petroleum refining. These fossil fuels, which include coal, oil, and natural gas, supply about 80% of the world's energy, providing electricity, heat, and transportation [2]. Fossil fuels are considered to be non-renewable sources of energy, taking into account the rate of their formation (millions of years) and consumption. In addition, burning fossil fuels is a mayor reason of net carbon dioxide releasing to the atmosphere, contributing to severe environmental problems like global warming and climate change [3].

In the last decades, the continuous depletion of petroleum (fossil) sources, the increasing demand for energy and high quality transportation fuels [4,5,6], the shrinking supply of conventional crude oils [7], and the increasing in petroleum prices [8], have forced the petroleum refinery industries to explore heavy oils and residues to upgrade them. Therefore, heavy oils or extra heavy oil refineries coud partially replace petroleum refineries in the near future [9,10]. In this

sense, heavy oils, light cycle oil (LCO), oils or tar sands, vaccum residue (VR), bitumen, tars, among others have been explored and processed. In addition, they are considered as an alternate carbon suitable source for energy, value-added chemicals and fuels to fulfill the requirements of modern civilization [6,11].

Tars are defined as all hydrocarbons with molecular weight higher than benzene, according to the meeting about tars measurement protocol held in Brussels in the Spring of 1998, between the International Energy Agency (IEA), the Directorate General for Energy of the European Commission (DG XVII) and the Energy Department of the United States [12]. In this context, tars, which are liquid (semi-solid) dense mixtures, are generally produced during petroleum refining process or petroleum distillation. For example, LCO (Light Cycle Oil) and PFO (Pyrolysis Fuel Oil) are considered as residues generated from fluid catalytic cracking (FCC) and naphtha cracking, respectively. These petroleum derived fractions contain important amounts of poly-aromatic hydrocarbons (PAHs). These PAHs are mainly composed by two- and three- aromatic ring hydrocarbons such as naphthalene, methylnaphthalene, anthracene and phenanthrene, among others. For instance, the aromatic content of LCO can be as high as 80-90wt% with the two-ring aromatic content being over 70%, along with higher amount of sulphur and nitrogen. However, lower amounts of sulphur and nitrogen are found in PFO. In general, PAHs in LCO (and other feedstocks) having low cetane number (CN), unwanted cold flow properties and high densities, exhibit poor ignition properties in diesel

engines. Thus, the PAH blending in the diesel pool is limited. Consequently, LCO is usually employed as a blending stock in heavy fuel oils to adjust viscosity [13-24].

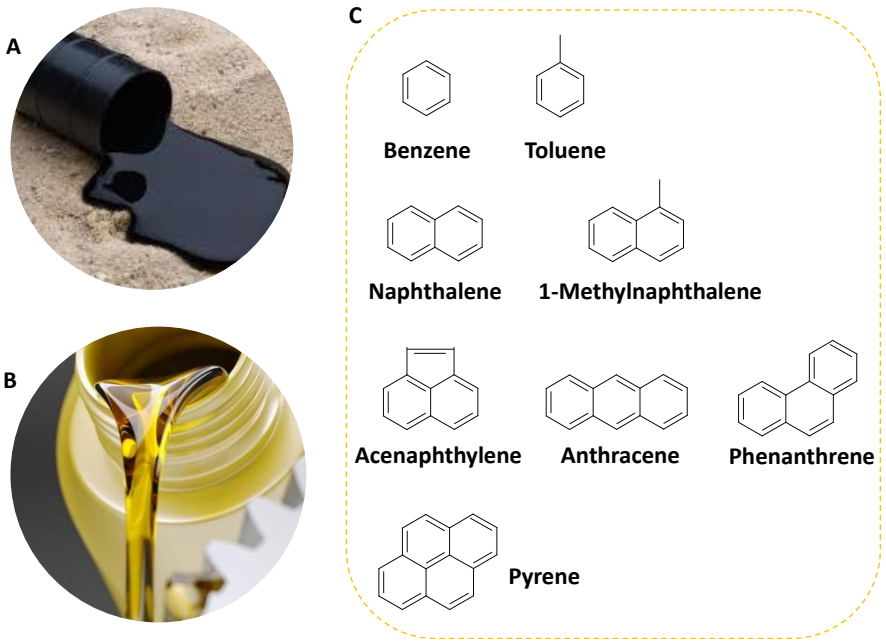

Figure 1.1. A) Heavy petroleum tars [25], B) Light cycle oil (LCO) feedstock [26] and C) typical composition of tars.

Because of their undesired characteristics already mentioned, petroleum derived feedstocks (i.e., LCO and PFO) required further transformation to be employed as high-added value liquid fuels and chemicals. In this sense, catalytic hydrotreating and hydrocracking are extensively explored for petroleum derived tars (such as LCO and PFO) upgrading or hydrotreatment [13-24]. In this sense, low-quality fossil tars (such as LCO and PFO) are hydroprocessed by means of catalytic

hydrocracking (or selective ring opening in this case) to obtain high-quality transportation fuels (high-octane gasoline and high-cetane diesel) [13,17]. In general, hydrotreating process is needed before hydrocracking, to obtain ultralow sulphur and nitrogen products. Moreover, these feedstocks could be transformed by catalytic hydrocracking into petrochemicals (benzene, toluene and xylene BTX enriched fractions) [13,16,19-24]. Both hydrotreatment and hydrocracking catalytic processes will be discussed in detail in section 1.7.2. In addition, tars can be transformed into gases (mainly hydrogen and carbon monoxide) by means of catalytic reforming [27,28]. However, most reported studies on tars (or molecules representative of tars) reforming are related to those produced from biomass gasification, which will be discussed deeply in section 1.7.1, as well.

1.2. Biomass as an alternative to fossil fuels

As it was mentioned in the previous section, heavy oils and tars could be used as non-conventional fossil sources for the production of transportation fuels and petrochemicals.

In addition, tars are formed during coal or biomass thermo-chemical processes such as pyrolysis and gasification [29]. As above-mentioned, due to fossil fuel depletion and their environmental issues, bioenergy, which is a clean and alternative sustainable energy derived from biomass, has attracted great importance in recent years [30,31]. Because biomass is inexpensive, renewable and abundant source of carbon, it is considered as promising alternative energy source [8], and

it contributes to 10-14% of the world's energy supply [3]. Compared with fossil fuels, biomass is considered to be CO_2 neutral, as the CO_2 released during combustion or other conversion processes will be re-consumed by the regrowth of the biomass through photosynthesis, and therefore, emissions generated during its thermal conversion can be considered neutral [3]. For all these above-mentioned reasons, biomass is considered as an excellent and adequate sustainable feedstock to produce transportation fuels and chemicals.

1.3. Biomass classification

Biomass refers to all organic material derived from living species like plants or animal residues that is now alive or was alive a short time ago. In addition, it is the plant material produced from the reaction between CO_2, water and sunlight through photosynthesis, to generate carbohydrates that form the building blocks of biomass. It is a stored source of solar energy in the form of chemical energy, which can be released when the chemical bonds between adjacent oxygen, carbon and hydrogen molecules are broken by different biological and thermo-chemical processes [3].

According to supply sector, biomass can be classified into: energy crops, agricultural and forestry residues, industrial (food processing wastes, wood), and urban wastes (sewage sludge and organic components of municipal solid wastes MSW) [3,32]. Biomass is generally composed of cellulose, hemicellulose and lignin as three main components, together with lipids, proteins, sugars, starches and

minerals (inorganic compounds like alkali metals mainly potassium, calcium, sodium, silicon, phosphorus, magnesium and chlorine) [3,33,34]. In comparison with fossil fuels, biomass has much higher volatile matter content (80% in biomass vs. 20% in fossil fuels), therefore, biomass has a high ignition stability and can be easily processed thermo-chemically into other higher-value fuels, such as methanol and hydrogen [35].

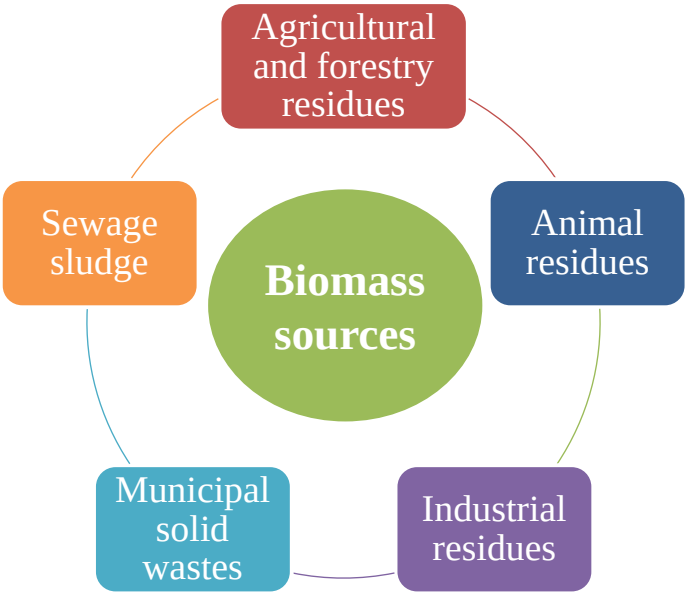

Figure 1.2. Different types of biomass resources.

1.4. Biomass conversion: bio-chemical and thermo-chemical processes

Biomass can be converted into bioenergy by means of two main types of processes: bio-chemical (fermentation, anaerobic digestion) and thermo-chemical processes (combustion, gasification, pyrolysis, liquefaction). Biomass gasification technology will be further discussed in detail, as the tars generated in this process are the main field of this work.

1.4.1. Bio-chemical processes: fermentation and anaerobic digestion

Fermentation is generally used to produce ethanol from sugar crop and starch crop. Part of the biomass is transformed into sugars using enzymes. Then, the sugar is converted into ethanol or other chemicals with the help of yeast [36,37].

Anaerobic digestion is carried out in the absence of oxygen, when organic material is directly converted to biogas, a mixture of mainly methane and carbon dioxide [38].

1.4.2. Thermo-chemical processes

Generally, thermo-chemical processes are more efficient than bio-chemical processes regarding the lower reaction time needed (a few seconds or minutes for thermo-chemical processes vs. several days, weeks or even longer for bio-chemical processes), and the superior ability to destroy most of the organic compounds. For example, lignin

materials are non-fermentable, and thus are not able to completely decompose using biological processes, whereas they are decomposable via thermo-chemical processes [39,40]. In general, the demand of energy required in thermo-chemical processes is compensated by the high yield of attained gases and liquid products.

1.4.2.1. Combustion

Combustion is the most widely used thermo-chemical process for biomass conversion. It contributes to over 97% of world's bioenergy production. It is an exothermic reaction between oxygen and hydrocarbons present in biomass. Here, the carbon is oxidized into carbon dioxide and the hydrogen into water (steam). Biomass still provides heat for cooking and warmth, especially in rural areas. Electricity, the foundation of all modern economic activities, may be also produced from biomass combustion. First, steam is generated by burning biomass in a boiler, and then electricity is produced through a steam turbine [41]. However, fouling and corrosion of the combustor are typical problems found with biomass combustion. Fouling is commonly associated with the presence of alkali metals and some other elements (such as silicon, sulphur, chlorine, calcium, and iron) in the biomass ash. Afterwards, these elements tend to condense and form deposits of chlorides, silicates, or sulphates inside the combustor, reduce heat transfer and lead to severe corrosion at high temperatures [40-43]. The ash deposition depends on the biomass type. Generally, herbaceous biomass, such as straws and grass which contain higher amounts of alkali, sulphur, chlorine, among others, has a higher

probability of ash deposition and corrosion in comparison with woody biomass [34,40,41]. Biomass co-firing with coal is an option to reduce fouling and corrosion, compared with using biomass alone, because alkali metals are diluted and consumed when they interact with sulphur or silica in the coal. This co-process could also reduce greenhouse emissions, compared with using coal alone [44]. In addition, biomass co-firing with natural gas could be processed [40]. Co-combustion is particularly applicable to biomass having high moisture content (>60%) that cannot be individually burned [40].

1.4.2.2. Liquefaction

Liquefaction is a low-temperature and high pressure thermo-chemical process transforming solid biomass into liquid fuels. During this process, biomass is decomposed into fragments of small molecules in water or another suitable solvent. Due to their instability and reactivity, these light fragments, can then be converted into oily compounds with various ranges of molecular weights [45,46].

1.4.2.3. Pyrolysis

Unlike combustion, pyrolysis is a thermo-chemical treatment process that takes place in the absence of oxygen. Biomass is converted into solid charcoal, liquid (bio-oil), and gases at elevated temperatures [34,47-49]. Depending on the reaction temperature and residence time, pyrolysis can be divided into fast (or flash) and slow pyrolysis. Typically, fast pyrolysis is a process with high heating rate (as high as hundreds of °C/min) and an extremely short residence time (≈1-3 s, <1

s for flash pyrolysis), and performed at temperature of approximately 500 °C. The formation of liquid products (60-75%, up to 75% for flash pyrolysis) is particularly favoured. The latters (bio-oils) are composed of an aqueous phase containing oxygenated organic compounds of low molecular weight, and a non-aqueous phase (tar) including high molecular weight insoluble aromatic organic compounds. Slow pyrolysis process, with a relatively long vapor residence time (5 to 30 min) and low heating rate, has been used to produce mainly charcoal for thousands of years [47,49].

Direct liquefaction and pyrolysis share some similarities in terms of the obtained liquid products. However, they differ in the operational conditions. Specifically, liquefaction is carried out at lower reaction temperatures but higher pressures than pyrolysis (5–20 MPa for liquefaction vs. 0.1–0.5 MPa for pyrolysis). In addition, it is not necessary to dry the feedstock for direct liquefaction, but it is important for pyrolysis. Moreover, using catalysts is always essential for liquefaction, whereas it is not the case for pyrolysis [46].

1.4.2.4. Gasification

Gasification is a thermo-chemical process where biomass is converted into combustible gases (also called producer gas or syngas), composed by H_2, CO, CO_2 and CH_4. This process is carried out at higher temperatures using gasifying agent such as air (or oxygen), steam, carbon dioxide or mixture of them [50]. Producer gas can be used in internal combustion engines or turbines to generate power and heat

[51], gas turbines [52], fuel cells [53], and as raw material for the synthesis of chemicals and liquid transportation fuels via Fischer Tropsch [54,55] and hydrogen production [55].

When the gasifying agent employed is air or oxygen, gasification is like combustion process. In general, heat is generated during combustion, whereas the main objective of gasification is to create valuable gaseous products that can be used directly for combustion or be stored for other applications. In addition, due to lower emissions of toxic gases, gasification is the most promising renewable and CO_2 neutral treatment for biomass conversion. Gasification can be considered as a special form of pyrolysis, taking place at higher temperatures to achieve higher gas yields [55]. However, in the pyrolysis and gasification of biomass, some unwanted by-products, and contaminants such as fly ash, NO_x, SO_x, H_2S, NH_3, HCl and tars are unavoidable. Among them, the formation of tars represents one of the main drawbacks for the commercialization of pyrolysis or gasification process. The tars could condense or polymerize at room temperature and block downstream pipelines and foul engines and turbines, which can lead to a decrease in the efficiency and an increase in the cost of the process [50,56-59].

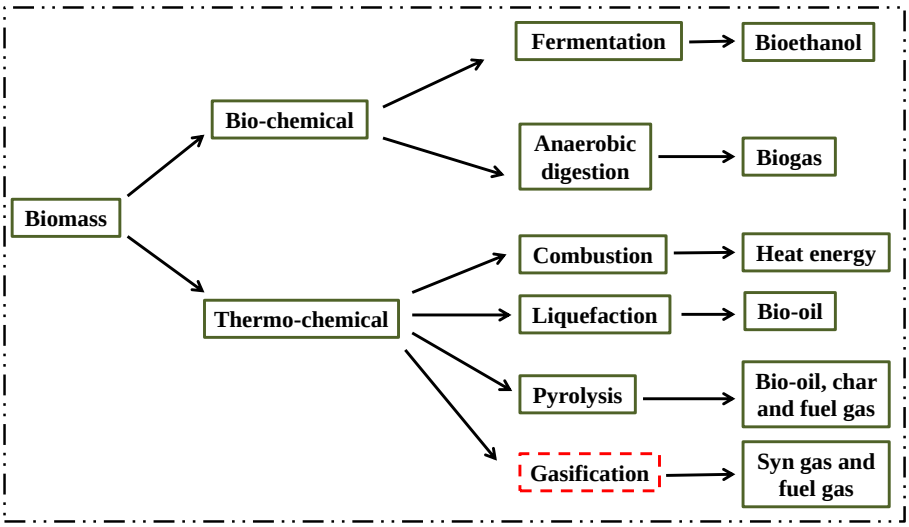

Figure 1.3. Different types of biomass conversion processes, adapted from [48].

1.5. Tars formation during biomass gasification process

Dealing with the tars formation during biomass gasification process is one of the major issues. Tars are complex mixtures of condensable hydrocarbons, including between 1- to 5-ring aromatic compounds along with other oxygenated compounds and complex polycyclic aromatic hydrocarbons (PAHs) [58,60]. In addition, tars can be defined as refractory substances that evolve during smoldering, coking, or gasifying of organic compounds like wood. They have a semifluid (highly viscous), brownish to deep black appearance with a pungent smell [61].

1.5.1. Tars classification and chemical composition

Tars can be classified into four major groups: primary, secondary, alkyl tertiary and condensed tertiary, according to the process conditions [62,63]. Primary tars compounds are produced during pyrolysis stage of gasification process by breakdown of biomass building blocks (cellulose, hemicellulose, and lignin components) and consist of acids, sugars, alcohols, ketones, aldehydes, phenols, catechols, guaiacols, syringols, furans and oxygenates. As the temperature inside the gasifier rises above 500 °C, secondary tars are formed because of primary tars rearrangement, forming non-condensable light gases (CO, CO_2, and H_2O) and heavier molecules such as phenols and olefins. Tars alkyl tertiary products include methyl derivatives of aromatic compounds, such as methylacenaphthylene, methylnaphthalene, toluene, and indene, formed at higher temperature. However, condensed tertiary aromatics form PAHs series without substituent atoms such as benzene, naphthalene, acenaphthylene, anthracene, phenanthrene and pyrene. This type of tertiary tars is also produced from primary tars. In addition, tars are classified in a similar way by other researchers [64]. Typical composition of biomass gasification tars is shown in Figure 1.4 [63]. Similar biomass tars composition is found elsewhere in literature [58,65]. On the other hand, based on their solubility and condensability, tars can be divided into five classes. This classification system has been developed by Energy research Center of The Netherlands (ECN), Toegepast Natuurwetenschappelijk Onderzoek (TNO) and University of Twente

(UT) in the framework of the project "Primary measures for the reduction of tar production in fluidized-bed gasifiers", funded by the Dutch Agency for Research in Sustainable Energy (SDE) [66]. The five classes are the following:

1. GC-undetectable, which are very heavy tars.
2. Heterocyclic, which contain heteroatoms and are highly water-soluble tars, such as pyridine, cresol, phenol, quinoline, isoquinoline, dibenzophenol.
3. Light 1-ring aromatic, which usually do not pose problems regarding condensability and solubility, such as toluene, ethylbenzene, xylene, styrene.
4. Light PAH compounds (2-3 rings), which condense at low temperature even at very low concentration, such as indene, naphthalene, methylnaphthalene, biphenyl, acenaphthylene, fluorine, phenanthrene, anthracene.
5. Heavy PAH compounds (4-7 rings), which condense at high temperatures at low concentrations, such as fluoranthene, pyrene, chrysene, perylene, coronene.

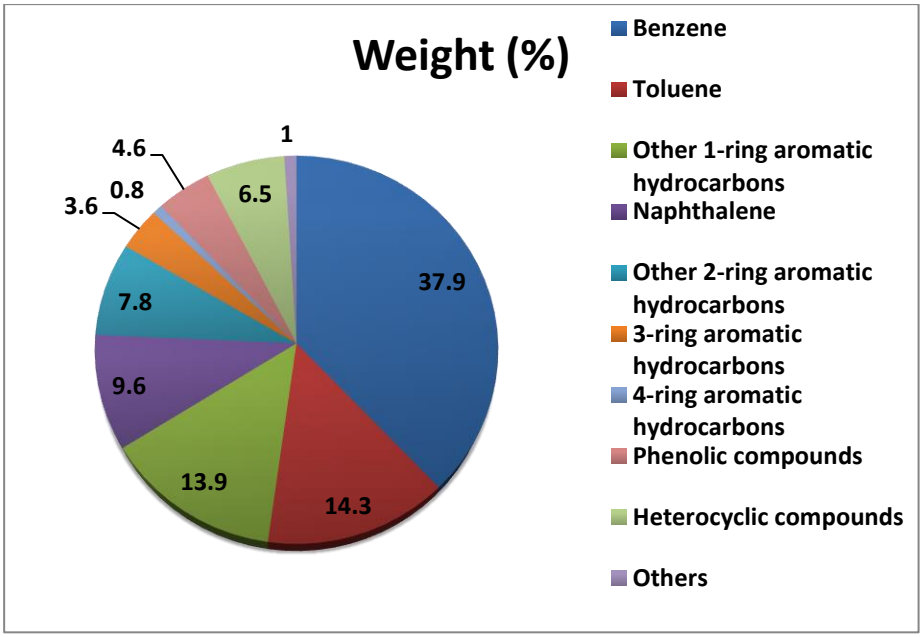

Figure 1.4. Typical biomass tars composition, adapted from [63].

1.5.2. Tars evolution with operation conditions during biomass gasification

The operating conditions play a very important role during biomass gasification in all respects, such as carbon conversion, product gas composition, tars formation and reduction. The most important parameters include temperature, pressure, residence time, gasifying medium and reactor, among others.

1.5.2.1. Temperature

High operating temperature (above 800 °C) is required to reach a high carbon conversion of the biomass and low tars content in the resultant product gas. In general, temperature influences both the

amount and the composition of the tars formed by affecting the chemical reactions occurred in the whole gasification network [57]. Due to the increased reaction temperature, secondary reactions occur in the gas phase. The oxygenated primary tars compounds are converted into light hydrocarbons, aromatics, oxygenates and olefins, which subsequently are transformed into higher hydrocarbons and larger PAHs in tertiary processes [62,63,67-69].

As found in Figure 1.5, primary tars are produced in the pyrolysis step of the gasification process within a temperature range between 200 and 500 °C by decomposition of the dried biomass. Then, with increasing temperature above 500 °C, primary tars start converting to secondary tars. Once the primary tars are nearly destroyed at ≈750 °C, tertiary tars start appearing with increasing temperature, and secondary tars begin to decrease. Thus, high temperatures destroy the primary and secondary tars but not the tertiary tars products [62,63]. As seen in Figure 1.6, a tars maturation scheme is proposed by Elliott et al [70].

It was found in the literature [71-73] that the quantity of detectable tars species decreased with an increase in the temperature. The formation of oxygen-containing compounds such as phenol, cresol and benzofuran is significant only at temperature below 800 °C, and then strongly decreases with increasing temperature. Furthermore, the amount of 1- and 2-ring aromatics with substituents decreases, but 3- and 4-ring aromatics are rapidly formed. Also, the formation of aromatic compounds without substituent group (like benzene,

naphthalene, phenanthrene, among others) is favoured at higher temperature.

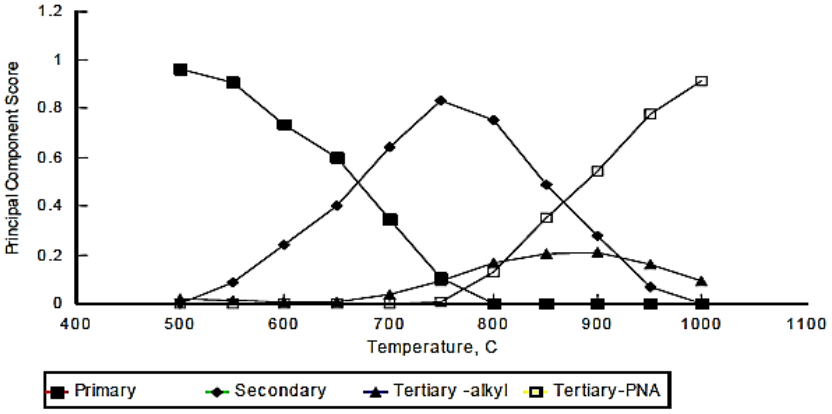

Figure 1.5. Evolution of primary, secondary, and tertiary tars products with temperature for 0.3 s residence time [62,63].

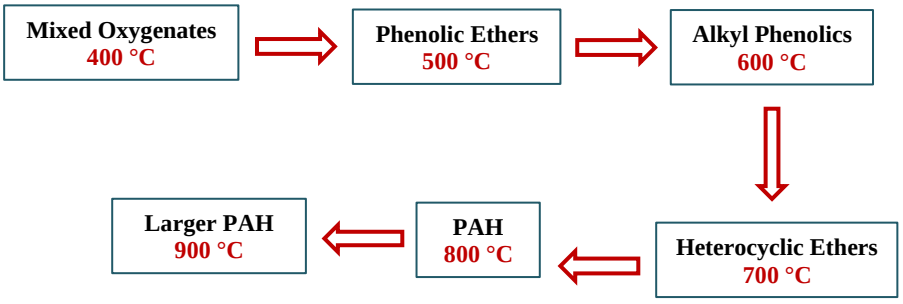

Figure 1.6. Tars maturation scheme adapted from Elliott et al [70].

1.5.2.2. Pressure

When the system pressure for biomass gasification increases, almost complete elimination of phenols is detected, the amount of total tars decreases, while the fraction of PAH increases [74].

1.5.2.3. Residence time

Residence time slightly affects the tars yield but has an important influence on the tars composition. The yield of oxygen-containing compounds, together with 1- and 2-ring compounds (except benzene and naphthalene) tends to decrease with increasing residence time, whereas that of 3- and 4-ring compounds increases in the total tars fraction. Residence time increase allows higher exposure of tars compounds to oxidizing medium, which results in tars reduction [71].

1.5.2.4. Gasifying agent: air, steam, steam-oxygen, and CO_2 gasification

Gasifying agents such as air (and oxygen), steam, carbon dioxide, and steam-oxygen mixture, which are typically used for gasification, may affect the tars formation and conversion. The ratio of fuel to gasification agent is an important parameter that influences the product of gasification, including tars. This parameter is expressed differently for different mediums. For example, for air gasification, the parameter is the equivalence ratio (ER); for steam gasification, it is the steam-to-biomass ratio (S/B); and for steam-oxygen gasification, it is the gasifying ratio. As shown in Table 1.1, the amount of tars generated

in steam gasification is greater than that in steam-oxygen gasification. Among different gasifying agents, air gasification is the lowest tars producer [75].

- Air gasification

Air is the most common agent for gasification because it is abundant in nature and simple to employ. The performance of air gasification heavily depends on the temperature and the equivalence ratio (ER). However, some drawbacks are found in air gasification because of the high nitrogen loading in air (up to 79%), leading to the dilution of the produced gas and lowering its heating value, which increases the cost of gas separation [76]. The ER ratio strongly affects the gasification products type mainly at higher temperature.

According to several studies, it was found that when ER increases, the tars yield decreases [71,77,78], due to the high amount of oxygen that reacts with volatiles in the flaming pyrolysis zone [71]. Besides, the decrease in total tars concentration is greater at higher temperature. At an ER of 0.27, phenols are almost totally converted, and the fraction of PAH, benzene, naphthalene, 3- and 4-ring aromatic compounds increases [71].

- Steam gasification

When steam reacts with biomass, it generates high amount of hydrogen with higher heating value compared with air and oxygen. In this sense, steam reforming reaction promotes tars reduction into

hydrogen and carbon monoxide. Afterwards, the presence of steam generates CO_2 and more H_2 from CO via Water Gas Shift (WGS) reaction. According to literature, an increase in the steam-to-biomass ratio S/B leads to a decrease in the tars yield [75,79,80]. The catalytic steam gasification leads to further tars reduction, promoting tars reforming reaction [81].

- Steam-Oxygen gasification

Because steam gasification is an endothermic reaction, it sometimes requires complex design for heat supply in the process. Moreover, additional amount of oxygen in the gasifying medium can provide the necessary heat for gasification, and then the gasifier is considered as an auto-thermal reactor. In view of that, steam-oxygen mixture for biomass gasification has been studied by many researchers. The tars yield is reduced with increasing the gasifying ratio GR [82,83].

- CO_2 gasification

The use of CO_2 as gasifying agent is promising due to its presence in the gasification atmosphere. Besides, tars can be reformed by dry reforming reactions of CO_2 [84].

Table 1.1. Effect of gasification medium on tars yield and heat properties, adapted from Gil et al [75].

Medium	Operating conditions	Tars yield (g/Nm^3)	LHV (MJ/Nm^3 dry)
Air	ER=0.3 H/C=2.2	2-20	4.5-6.5
Steam	S/B=0.9	30-80	12.7-13.3
Steam-oxygen	GR=0.9 H_2O/O_2=3	4-30	12.5-13.0

1.5.2.5. Gasifier design

Gasifiers are the reactors in which gasification process takes place. Based on the types of reactions, a typical gasifier can be divided into four process zones: the drying zone (100-200 °C), where water present in biomass is evaporated and converted into steam; the pyrolysis zone (200-500 °C), in which dry biomass is converted into volatile gases, liquid tars, and char; the combustion zone (1000-1200 °C), a region where volatile gases, liquid tars, char and hydrogen present in biomass are partially or totally oxidized to generate CO, CO_2 and steam; and the reduction zone (800-1000 °C), in which combustible products such as CO, CO_2, CH_4 and H_2 are produced depending on the gasifying agent via Boudouard reaction ($C + CO_2 \rightarrow 2CO$), water gas reaction ($C + H_2O \rightarrow CO + H_2$), water gas shift reaction ($CO + H_2O \rightarrow CO_2 + H_2$), methanation ($C + 2H_2 \rightarrow CH_4$), steam reforming (tars + $H_2O \rightarrow CO + H_2$), and dry reforming (tars + $CO_2 \rightarrow CO + H_2$) [32,39,50,59].

There are four main types of typical gasifiers utilized for biomass gasification: fixed bed (updraft and downdraft), fluidized bed (bubbling and circulating), entrained flow and plasma gasifiers. The gasifier design can affect the amount of tars in the product gas.

- Fixed bed gasifier: Updraft and downdraft

For updraft gasifier, biomass is fed from the top and the gasifying medium from the bottom, and they move in a countercurrent direction. Since primary tars are obtained at lower temperature (200-500 °C) and move upward through cooler regions without reaching the combustion zone, therefore their conversion into gases and secondary tars are reduced. Thus, updraft gasifier produces high amount of tars (50 g/Nm^3) [39,59].

Downdraft gasifier is a co-current reactor where both gas and biomass move downward. For instance, while passing through the combustion zone and as temperature increases, primary tars can convert into non-condensable gases. For this reason, low tars content (<20 g/Nm^3) is generated [39,59].

- Fluidized gasifier

In a typical fluidized bed (bubbling or circulating), feedstock is fed from the side or the top, while the gasifying agent enters from the bottom. In either case, the moving bed is mixed with the biomass feed. Thus, biomass is highly converted into fuel gases. Generally, the amount of tars generated in a fluidized-bed gasifier is between 5-20

g/Nm^3 and 1-5 g/Nm^3 for bubbling and circulating fluidized bed, respectively [39,59].

- Entrained flow gasifier

In an entrained flow gasifier, biomass and gasifying medium move in a co-current direction. In addition, tars generation is negligible due to the extreme operating conditions (high pressures 2-7 MPa and temperatures > 1000 °C) [39,59].

- Plasma gasifier

Plasma gasification is a relatively new technique, in which high temperatures (3000 °C), or even higher (up to 15000 °C) can be achieved. Under such extremely high temperatures, biomass feedstock is converted within milliseconds into syngas containing very little amount of tars. This technology presents some disadvantages such as high electricity consumption for plasma operation, high investment costs, among others [39,85].

To conclude, updraft gasifiers generate the highest amount of tars, whereas the tars formation with entrained flow and plasma gasifiers is almost negligible.

1.6. Tars removal

The presence of tars in the syngas is generally considered unwanted, leading to low gasification efficiency and additional operational difficulty for syngas cleanup. Thus, tars removal remains an

essential part of the development and design of biomass gasifiers. Several approaches are available for tars reduction, and they are classified into two categories: (1) primary methods (in-situ); and (2) secondary methods (post-gasification), for which the hot gas cleanup is conducted outside the gasifier. As the primary methods are carried out inside the gasifier, the product gas quality can be affected, while being unaffected in the post-gasification process.

1.6.1. Primary methods

Primary methods can be defined as all the measures taken inside the gasifier itself to avoid or convert tars produced. These measures include the proper selection of the operating conditions (already discussed in section 1.5.2), the addition of catalysts or alternative bed additives during gasification process, and finally the modification of the gasifier design [39,56,58,59].

The use of heterogeneous catalysts can be considered in both primary and secondary methods. For instance, catalytic cracking (steam reforming and dry reforming), hydrotreating and hydrocracking are the main catalytic processes used for tars upgrading. These processes will be discussed in detail in section 1.7.

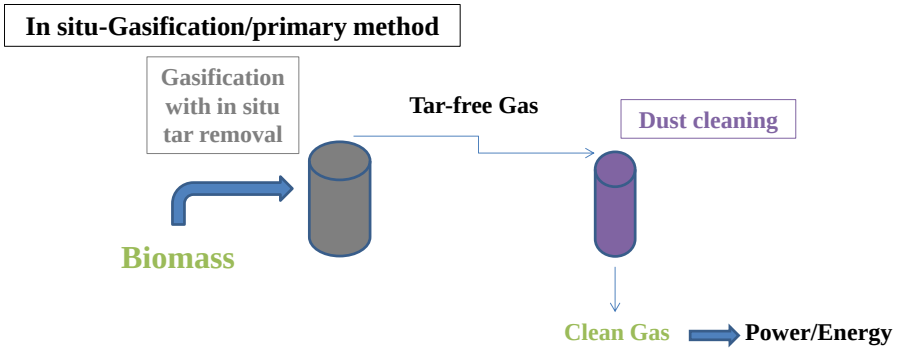

Figure 1.7. In-situ tars reduction.

1.6.2. Secondary methods

Secondary methods use a separate reactor to convert and reduce the tars present in the hot gas product up to acceptable level. They include physical and chemical (will be discussed in the following section) treatments. A substantial amount of tars can be removed from the gas in a post-gasification cleanup section.

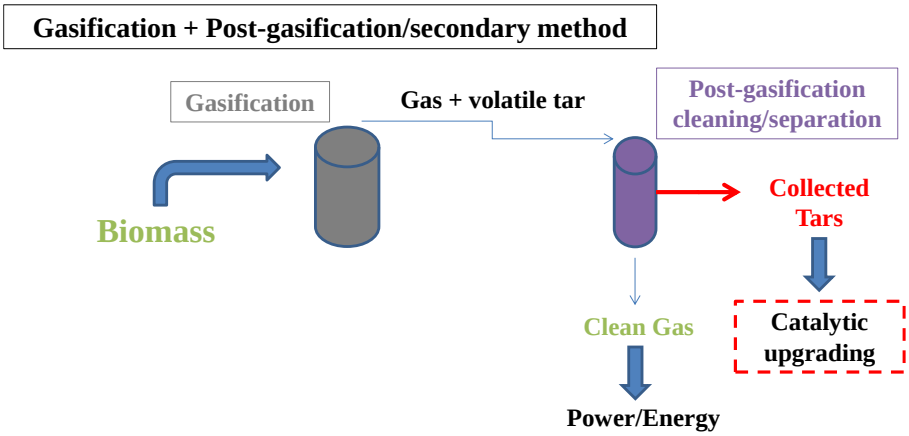

Figure 1.8. Post-gasification tars reduction.

Several mechanical/physical gas cleanup systems are available for removal of both particulates and tars from gases generated during biomass gasification. Based on application, mechanical/physical methods are further divided into two categories: dry (hot) and wet gas cleaning. Dry or hot gas cleaning is usually used at temperatures between 200-500 °C even at 600-800 °C and even at temperatures higher than 1300 °C, while wet or cold gas cleaning is carried out after the gas cooling and typically at 20–60 °C (near ambient conditions) [50,56-59,63,86,87]. Physical and mechanical cleaning approaches are mainly used to capture particles, but they are also used to capture tars in a condensed form.

- Dry (or hot) gas cleaning

On one hand, cyclone, rotating particle separators (RPS), fabric filters, ceramic filters, activated carbon based adsorbers, and sand bed filters can be used to capture tars from producer gas. Several related studies are found elsewhere in the literature [86-89]. On the other hand, catalytic filter can also be incorporated inside the gasifier. This technique combines the filtration for particles removal and catalytic cracking of tars from producer gas in one step. Therefore, a hot and clean gas is obtained at the outlet of the gasifier [90-93].

- Wet (or cold) gas cleaning

Wet gas cleaning consists of wet electrostatic precipitators (ESP), wet scrubbers, wet cyclones, among others. It can be considered as an effective technique to remove particles and condensable tars

droplets from producer gas. In this sense, wet scrubber is an important device in wet gas cleaning. The wet scrubber uses water scrubbing to condense the tars from the producer gas and simultaneously removing the particulates. The most common types of wet scrubber are packed column scrubber (spray tower), venturi scrubber, packed bed scrubber, and impingement scrubber [50,56,86,87]. Several publications have reported the use of these types of wet scrubbers [94-96].

The scrubbing process, also referred to as gas absorption process, is a method in which one or more contaminants present in the gas stream are selectively absorbed into an absorbent. Theoretically, the contaminant in the gas phase must be soluble in the scrubbing liquid. The use of water as a washing medium may be not ideal because it shows important disadvantages including the low or no water solubility of hydrocarbon compounds present in tars, surface tension effects, clogging of apparatus and the economic cost of wastewater treatment. Therefore, use of hydrophobic absorbents should be more practical for tars absorption [87]. In this sense, several kinds of scrubbing mediums such as water, diesel fuel, biodiesel fuel, vegetable oils and engine oils are investigated for tars absorption. In the water scrubber, tars are condensed as a separate liquid on the water surface. Due to the solubility of tars, the change of the absorption liquid from water to an oily material can be expected to improve tars removal performance. The absorption efficiency for light PAHs can be ranked in the following order: diesel fuel > vegetable oil > biodiesel fuel > engine oil > water. However, the amount of tars increases for diesel and biodiesel fuel scrubbers due to

their easy evaporation. Thus, higher tars removal efficiency is obtained while using vegetable oil, and therefore it is considered as the most recommended absorbent to be used in gasification systems [97].

In general, barrier filters (including fabric filters) and cyclone separators are not adequate for tars removal since the tars aerosol particles are less than 1 μm in size and are sticky, thus their removal from the walls of the cyclone and filter is difficult. Equipment like Electrostatic precipitator (ESP) and wet scrubbers are more efficient and can remove most of the tars, but they are more expensive [50].

- Offline methods

In order to reduce in adequate manner the concentration of the tars present in the producer gas from gasification, different methods (online and offline methods) have been used by researchers to arrive at the required values. One of the offline methods is based on using solvents for cold trapping of tars. Acetone, dichloromethane, ice water, methoxy benzene, among others are used to condense and collect tars obtained from biomass gasification [50]. In addition, isopropyl alcohol and n-hexane are used as solvents for tars condensation and collecting [98]. Nevertheless, the use of solvents for tars removal or reduction is expensive and possesses disadvantages in terms of safety and sustainability of the process.

1.7. Catalytic tars upgrading

The tars can undergo thermal destruction by means of thermal cracking, but this typically requires temperatures greater than 1000 °C, and these harsh conditions cause rapid equipment deterioration, affect the cost involved in the process by increasing the energy consumption, produce soot, and decrease the overall energy conversion efficiency of biomass gasification [99]. For this reason, it is desirable to remove tars at lower temperature, requiring the use of catalysts. In this sense, catalysts play an important role in increasing the reaction rate at low-temperature conditions. The presence of catalysts can significantly reduce the energy demand for breaking down chemical bonds in tars-type molecules. As above-mentioned, catalytic processes such as catalytic tars reforming can be applied inside the gasifier (in situ/primary method), or outside the gasifier (post-gasification/secondary method), whereas catalytic hydrotreatment (hydrotreating and hydrocracking) must be applied outside the gasifier as post-gasification treatment once the tars are collected and separated from the gas product.

Since tars produced during biomass gasification process have some similar characteristics and properties with some petroleum fractions, a secondary post-gasification catalytic process will take part of our interest, and a common way to treat these fractions/residues is required. Other heavy residues derived from petroleum such as Vacuum Residue and heavy oils are mainly composed by saturates, aromatics, resins and asphaltenes, containing impurities such as nitrogen, oxygen,

sulphur, nickel, vanadium, among others [11], which are more complex than tars generated from biomass gasification.

The unfavourable properties of tars such as high acidity, viscosity, low thermal instability, and low heating value (LHV) present many obstacles to the substitution of fossil derived fuels. So, an upgrading process is required before its application. Catalytic processes such as steam reforming (with H_2O), dry reforming (with CO_2), hydro-treating, and hydrocracking are usually applied for tars upgrading.

1.7.1. Tars reforming

Catalytic reforming is considered as a catalytic cracking technique, it generally involves passing the dirty gas over catalysts. Two types of reactive processes can occur: steam (with H_2O) and dry (with CO_2) reforming. Catalytic reforming is usually carried out at high temperatures in the range 600-900 °C. For tars reforming, mostly research focuses on biomass gasification tars control, mainly applying steam reforming. Hydrogen (H_2) and carbon monoxide (CO) are the main products obtained in tars reforming. However, when steam is applied, the yields of H_2 and CO_2 are enhanced according to the water gas shift reaction converting CO to H_2 and CO_2. Due to the complexity of tars consisting in complex mixtures of different compounds, phenol, toluene, benzene, and naphthalene are usually used as tars model compounds.

Several reviews have been published on different catalysts for tars conversion, including natural minerals (dolomite, olivine, and

shell), alkali metal catalysts, zeolites, silica-based materials, metal oxides and mixed oxides, carbon materials, char as by-product from biomass gasification, perovskites, Ni-based catalysts, noble metal-based catalysts, among others [27,28,100-102]. Natural minerals such as dolomite and olivine (activity improved when calcined), which are cheap disposable catalysts have been widely used in biomass tars treatment. Świerczyński et al. and Michel et al. studied the activity of Ni/olivine catalyst for tars reforming using toluene and α-methylnaphthalene as model compounds, respectively [103,104]. Similar effect is found when using Fe/olivine compared with olivine alone [105]. The addition of Ni to olivine has been found to significantly improve the activity towards tars conversion, the selectivity to H_2 and CO decreasing the carbon deposition. Noble metals such as Rh, Pt, Pd and Ru have shown excellent performance in terms of activity, stability, selectivity, and carbon deposition, but their use is limited due to the high cost [106,107]. Nickel-based catalysts, used extensively in the petrochemical industry, have shown high activities for tars reforming/decomposition in coal and biomass gasification. Ni/Al_2O_3 is one of the main catalysts used in tars reforming [108-110]. Ni-based catalysts have been widely applied in the steam reforming of biomass tars due to their low cost, high activity for tars destruction (C-C, C-O, C-H and O-H bonds cleavage), easy regeneration and better performance in terms of H_2 production (via water gas shift reaction) [109]. However, their catalytic activity is limited because of the easy deactivation caused by sintering, carbon (coke) deposition and the poisoning of sulphur in biomass gasification [111]. To improve the

catalytic performance of Ni catalysts in steam reforming of tars, several ways are being employed, such as changing the support and/or adding promoters. Improvement in metallic dispersion is an important factor to constrain metal sintering which generally occurs at high temperature reforming activities. In view of this, alloying or bimetallic catalyst synthesis can effectually enhance resistance to metal sintering. In this sense, Fe, Co, Cu, noble metals, among others are the most common and promising elements forming alloys with Ni. These alloys can be used in steam reforming of biomass tars due to their high catalytic activity and coke resistance resulting from the synergistic effect [112-119].

Alumina (especially γ-alumina) is one of the most used catalyst support for tars reforming reaction, because of its good mechanical strength and chemical/physical stability, and availability in dispersion of the active metal phase. One of the major disadvantages is coke deposition and metal sintering, due to its high acidity. The doping of Al_2O_3 (or other catalyst) with various base metal oxides such as CeO_2, ZrO_2, MgO, CaO, among others neutralizes the Lewis acidic centers, which helps to decrease the carbon formation. Particularly, doping Al_2O_3 with metal oxides (CeO_2, ZrO_2) having redox and high oxygen storage properties helps to improve the oxygen vacancy and mobile oxygen species in the support, thereby enhances the activation of steam in steam reforming reaction to produce hydroxyls OH and O. In addition, the transport and supply of oxygen to the active sites is increased, thus promoting the C-C bond breaking in the hydrocarbon,

oxidizing active carbon species to CO, and preventing the carbon deposition. Several related studies can be found in the literature [120-123]. Similar effect of addition of CeO_2 to Ni/olivine and Ni/zeolites is studied [124-126]. Further, the addition of alkaline earth metal oxides (MgO and CaO) is reported, and their presence neutralizes the acidity of the catalyst and reduces coke deposition [125,127,128]. Besides oxygen mobility, basicity is an important property having the same function for coke reduction. MgO and CaO can be added in the form of hydrotalcite precursor [129-131] or dolomite promoter [132]. The calcination of hydrotalcites above 450 °C forms mixed metal oxides having various advantageous properties for catalytic applications such as basicity and large surface area allowing higher metal dispersion and minimizing coke formation.

In addition, hexaaluminate compounds are good candidates to be used as catalytic supports, due to their high surface areas and resistance to sintering and deactivation in high-steam environments [133,134].

1.7.2. Tars hydrotreatment

As above-mentioned, tars produced during biomass gasification process share some similar properties with petroleum fractions having polycyclic aromatic hydrocarbons (PAHs) of diesel boiling point range produced as by-products in oil refining and petrochemical plants.

The catalytic hydrotreatment of petroleum fractions such as LCO and PFO (including model compounds like naphthalene and

methylnaphthalene, among others) is well described in the literature. Hence, as seen in Figure 1.9, LCO (and PFO) can be upgraded to high-value products such as liquid fuels (diesel and gasoline with high cetane and octane numbers, respectively) by applying hydrocracking (known in this specific case as aromatic saturation followed by selective ring opening) [13,17,135-146]. In addition, as represented in Figure 1.10, LCO (and PFO) could be transformed into light aromatic hydrocarbons rich in benzene, toluene, and xylene (BTX) for petrochemical raw materials [13,16,19-24,147-153].

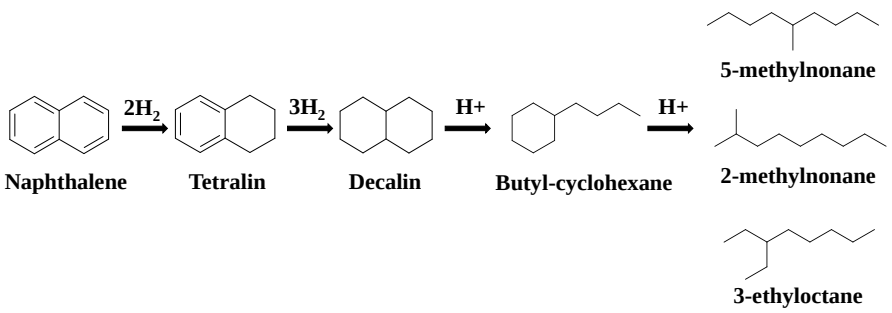

Figure 1.9. Catalytic upgrading of naphthalene as a model molecule representative of tars into high-cetane number diesel products, adapted from [21].

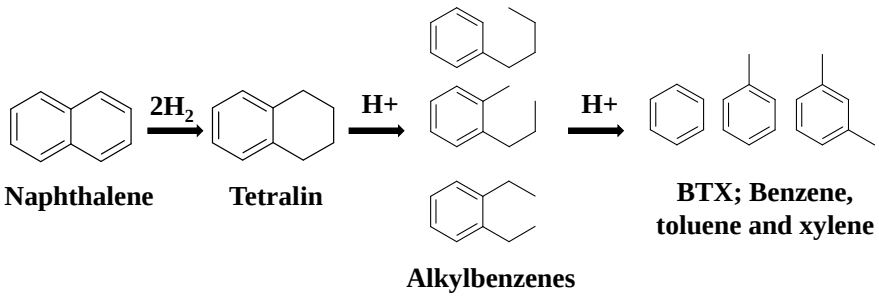

Figure 1.10. Catalytic upgrading of naphthalene as a model molecule representative of tars into BTX products, adapted from [21].

1.7.2.1. Catalytic hydrotreating

Because of the high amount of sulphur, nitrogen and aromatics, a combination of hydrotreating and hydrocracking is required for the treatment of medium-to-heavy oil fractions (i.e., LCO). In this sense, hydrotreating is catalytic chemical technology used to remove sulphur (hydrodesulphurization HDS), nitrogen (hydrodenitrogenation HDN), and to selectively hydrogenate naphthalenes to obtain the corresponding tetralins derivatives (hydrodearomatization). The most used catalysts for hydrotreating are conventional promoted molybdenum sulfides NiMoS and CoMoS supported on γ-Al_2O_3 [154-156]. For instance, Oh et al. studied the catalytic activity of NiWS, CoMoS and NiMoS supported on γ-Al_2O_3 for LCO hydrotreating in the range of 330-400 °C and 60 bar of H_2, prior to its further transformation to BTX products via hydrocracking [22]. The most relevant results were attained with NiMoS/Al_2O_3, where highly selective hydrogenation of two or more ring aromatics into mono-aromatics was achieved, along with minimal loss of aromatics at high HDN conversion rates. In addition, Betancourt et al. investigated the effect of incorporating Vanadium to NiMoS/Al_2O_3 for LCO hydrotreating at 340 °C and ≈50 bar of H_2 [157]. In this sense, the addition of Vanadium highly improved the HDS and HDN activity of LCO hydrotreating. Interestingly, transition metal phosphides such as Ni_2P supported on SiO_2, and MCM-41 were also encountered to be active in the hydrotreating (HDS and HDN) of a model liquid feed containing S- and N-compounds at 31 bar of H_2 and 300-370 ºC [158-160]. For instance, these catalysts showed higher

activity than the commercial $NiMoS/Al_2O_3$ catalyst, being more resistant to S- and N-compounds, as well.

1.7.2.2. Catalytic hydrocracking

Hydrocracking is one of the main catalytic processes in petroleum refinery for the transformation of a wide range of low-value heavy feedstocks into high-quality products, such as low boiling point products (BTX as petrochemical feedstocks), or middle distillates (transportation fuels) [161-165]. Hydrocracking catalysts are commonly bifunctional catalytic systems composed by a hydrogenation/dehydrogenation site and an acidic cracking function. In principle, hydrogenation reaction is exothermic while cracking reaction is endothermic [11]. In some catalysts, the hydrogenation function consists of noble metals (e.g., Pd, Pt), which possess high hydrogenation activity but low resistance to sulphur poisoning, thus limiting their industrial application. In other catalysts, hydrogenation function consists of an association of a sulfided phase of a group VI element (Ni or Co) and a group VIII element (Mo or W) of the periodic table. Usually, the latter ones are preferred for industrial application due to their sulphur and nitrogen resistance, along with their lower price [164-167]. The acidic function consists of alumina, amorphous silica-alumina, zeolite, as well as their composites [20,147,161,164-167]. The most widely used zeolites in commercial hydrocracking units are the ultrastable Y (USY) [164,165]. Due to their higher acidity, zeolites-based catalysts are more active for hydrocracking than amorphous silica-alumina-based ones, however they are less selective to middle

distillates [168]. For instance, the activity and selectivity of a catalyst and products distribution (gases, naphtha, kerosene, diesel) are evaluated by the balance between acid and hydrogenation functions. In this sense, catalysts with higher acidic sites but weak hydrogenation activity produce light products such as naphtha and gases, whereas middle distillates are usually generated with catalysts having lower acidity and enhanced hydrogenation activity [161,169]. One of the main disadvantages of using zeolites for hydrocracking is the microporous character of the solid material, which leads to diffusion limitations resulting in high coke formation and secondary cracking of primary products [170]. Thus, an increase in the average pore size of zeolites aiming at obtaining mesoporous materials, along with appropriate acidity are needed to improve their hydrocracking activity [161,171,172].

According to some reported researches, Ni/H-Beta zeolite [19], NiMoS/BZ zeolite [21] (where BZ represents a physical mixture of H-Beta and H-ZSM-5 zeolites), MoS/BZ [22], MoS/BYZ [23] (where BYZ is a mixture of H-Beta, mesoporous H-Y and H-ZSM-5), CoMo/Beta zeolite [24], Ni_2P/Beta zeolite [148,152,153], NiMoS/alumina-coated USY [149], W/Beta zeolite [150] are commonly applied as bifunctional catalysts for the hydrocracking of hydrotreated LCO (and PFO), along with the model compounds (including naphthalene, methylnaphthalene and tetralin) into light aromatic hydrocarbons such as BTX products. In this sense, large amounts of hydrogen (arriving up to 80 bar) are consumed working at

high temperatures (arriving up to 450 °C). In general, transportation fuels of diesel boiling range production demands more hydrogen than BTX production [21]. All that could lead to serious drawbacks, such as catalyst deactivation and has important impact on the economics of hydrotreatment units.

1.8. References

[1] M.J. Hutzler, S. Sitzer, P.D. Holtberg, J. Conti, J.M. Kendell, A.S. Kydes, Annual Energy Outlook 2003 with projection to 2025, 205, 85, The United States Energy Information Administration, US Department of Energy, Washington, DC, 2003p. 267.

[2]https://www.nationalgeographic.com/environment/energy/reference/fossil-fuels/.

[3] P. McKendry, Bioresource Technology 83 (2002) 37–46.

[4] T. Kaufmann, A. Kaldor, G. Stuntz, M. Kerby, L. Ansell, Catalysis Today 62 (2000) 77.

[5] J. Chang, N. Tsubaki, K. Fujimoto, Fuel 80 (2001) 1639.

[6] R. Yoshida, M. Miyazawa, H. Ishiguro, S. Ito, K. Haraguchi, H. Nagaishi, H. Narita, T. Yoshida, Y. Maekawa, Y. Mitarai, Fuel Processing Technology 51 (1997) 195.

[7] Bauquis PR. A reappraisal of energy supply and demand in 2050. The Institute of Energy Economics, Japan, July (http://eneken.ieej.or.jp/en/outlook/).

[8] G.W. Huber, A. Corma, Angewandte Chemie International Edition 46 (2007) 7184-7201.

[9] S. Dehkissia, F. Larachi, E. Chornet, Fuel 83 (2004) 1323.

[10] A. Matsumura, T. Kondo, S. Sato, I. Saito, Fuel 84 (2005) 411.

[11] R. Sahu, B.J. Song, J.S. Im, Y.-P. Jeon, C.W. Lee, Journal of Industrial and Engineering Chemistry 27 (2015) 12-24.

[12] K. Maniatis, AA.C.M. Beenackers, Biomass Bioenergy 18 (2000) 1–4.

[13] G.C. Laredo, P.M. Vega Merino, P.S. Hernández, Industrial & Engineering Chemistry Research 57 (2018) 7315-7321.

[14] A. Stanislaus, A. Marafi, M.S. Rana, Catalysis Today 153 (2010) 1-68.

[15] G.C. Laredo, Y. Figueroa, J.L. Cano, M.T. Mares, Journal of the Mexican Chemical Society 46 (2002) 115-119.

[16] M. Bouchy, S. Peureux-Denys, P. Dufresne, S. Kasztelan, Industrial & Engineering Chemistry Research 32 (1993) 1592-1602.

[17] V. Calemma, R. Giardino, M. Ferrari, Fuel Processing Technology 91 (2010) 770-776.

[18] J.A. Johnson, S.J. Frey, V.P. Thakkar, NPRA AM-07-40 (2007), 1-16.

[19] Y. Choi, J. Lee, J. Shin, S. Lee, D. Kim, J.K. Lee, Applied Catalysis A: General 492 (2015) 140-150.

[20] J. Lee, Y. Choi, J. Shin, J.K. Lee, Catalysis Today 265 (2016) 144-153.

[21] J. Shin, Y. Oh, Y. Choi, J. Lee, J.K. Lee, Applied Catalysis A: General 547 (2017) 12-21.

[22] Y. Oh, J. Shin, H. Noh, C. Kim, Y.-S. Kim, Y.-K. Lee, J.K. Lee, Applied Catalysis A: General 577 (2019) 86-98.

[23] Y. Oh, H. Noh, H. Park, H. Han, T.-B. Nguyen, J.K. Lee, Catalysis Today 352 (2020) 329-336.

[24] D.P. Upare, S. Park, M.S. Kim, Y.-P. Jeon, J. Kim, D. Lee, J. Lee, H. Chang, S. Choi, W. Choi, Y.-K. Park, C.W. Lee, Journal of Industrial and Engineering Chemistry 46 (2017) 356-363.

[25] www.en.fmsomer.com/?porfolio=tar.

[26] www.ariyancorp.com/light-cycle-oil/.

[27] G. Guan, M. Kaewpanha, X. Hao, A. Abdula, Renewable and Sustainable Energy Reviews 58 (2016) 450-461.

[28] J. Ashok, N. Dewangan, S. Das, P. Hongmanorom, M.H. Wai, K. Tomishige, S. Kawi, Fuel Processing Technology 199 (2020) 106252.

[29] C. Li, K. Suzuki, Resources, Conservation and Recycling 54 (2010) 905–915.

[30] L. Zhu, Y.K. Nugroho, S.R. Shakeel, L. Zhaohua, B. Martinkauppi, E. Hiltunen, Renewable and Sustainable Energy Reviews 78 (2017) 391-400.

[31] A.J. Ragauskas, C.K. Williams, B.H. Davison, G. Britovsek, J. Cairney, C.A. Eckert, et al. Science 311 (2006) 484-489.

[32] S.K. Sansaniwal, K. Pal, M.A. Rosen, S.K. Tyagi, Renewable and Sustainable Energy Reviews 72 (2017) 363-384.

[33] D. Mohan, C.U. Pittman, P.H. Steele, Energy Fuels 20 (2006) 848-889.

[34] S. Yaman, Energy Conversion and Management 45 (2004) 651-671.

[35] E. Bolyos, D. Lawrence, A. Nordin (http://www.ep.liu.se/ecp/009/003/ecp030903.pdf)

[36] J. Lee, Biotechnology 56 (1997) 1-24.

[37] Y. Lin, S. Tanaka, Applied Microbiology and Biotechnology 69 (2006) 627-642.

[38] A.J. Ward, D.M. Lewis, F.B. Green, Algal Research 5 (2014) 204-214.

[39] L. Zhang, C. Xu, P. Champagne, Energy Conversion and Management 51 (2010) 969-982.

[40] B.M. Jenkins, L.L. Baxter, T.R. Miles Jr, T.R. Miles, Fuel Processing Technology 54 (1998) 17-46.

[41] A. Demirbas, Energy Sources Part A 29 (2007) 303–312.

[42] K. Liu, W. Xie, D. Li, W.-P. Pan, J.T. Riley, A. Riga, Energy Fuels 14 (2000) 963-972.

[43] K. Davidsson, L.-E. Amand, B. Leckner, Energy Fuels 21 (2007) 71-81.

[44] K. Ericsson, Energy 32 (2007) 1838-1847.

[45] A. Demirbas, Energy Conversion and Management 41 (2000) 633-646.

[46] A. Demirbas, Energy Conversion and Management 42 (2001) 1357-1378.

[47] G. Maschio, C. Koufopanos, A. Lucchesi, Bioresource Technology 42 (1992) 219-231.

[48] A. Sharma, V. Pareek, D. Zhang, Renewable and Sustainable Energy Reviews 50 (2015) 1081-1096.

[49] M.I. Jahirul, M.G. Rasul, A.A. Chowdhury, N. Ashwath, Energies 5 (2012) 4952-5001.

[50] Rakesh N, S. Dasappa, Renewable and Sustainable Energy Reviews 91 (2018) 1045-1064.

[51] A.M. Shivapuji, S. Dasappa, International Journal of Hydrogen Energy 40 (2015) 10308-10328.

[52] H.V. Sridhar, G. Sridhar, S. Dasappa, P.J. Paul, H.S. Mukunda, 15th Eur biomass Conference Exhib. Berlin (2007) 964-967.

[53] M. Sharma, Rakesh N, S. Dasappa, Renewable and Sustainable Energy Reviews 60 (2016) 450-463.

[54] S.S. Ail, S. Dasappa, Renewable and Sustainable Energy Reviews 58 (2016) 267-286.

[55] J. Rezaiyan, N.P. Cheremisinoff, Boca Raton (FL): CRC Press Taylor & Francis Groups; 2005.

[56] S. Anis, Z.A. Zainal, Renewable and Sustainable Energy Reviews 15 (2011) 2355-2377.

[57] C. Li, K. Suzuki, Renewable and Sustainable Energy Reviews 13 (2009) 594-604.

[58] L. Devi, K.J. Ptasinski, F.J.J.G. Janssen, Biomass and Bioenergy 24 (2003) 125-140.

[59] M.L.V. Rios, A.M. González, E.D.S. Lora, O.A.A. del Olmo, Biomass and Bioenergy 108 (2018) 345-370.

[60] L. Devi, K.J. Ptasinski, F.J.J.G. Janssen, S.V.B. van Paasen, P.C.A. Bergman, J.H.A. Kiel, Renewable Energy 30 (2005) 565-587.

[61] Knoef HAM, editor. Handbook - Biomass gasification. 2nd ed.BTG Biomass Technology Group BV; 2012.

[62] R.J. Evans, T.A. Milne, Developments in Thermochemical Biomass Conversion, Vol. 2. Edited by A.V. Bridgwater and D.G.B. Boocock. London: Blackie Academic & Professional, (1997) 803–816.

[63] T.A. Milne, R.J. Evans, N. Abatzoglou, Report no. NREL/TP-570-25357, NREL, Golden, Colorado, USA; 1998.

[64] D. Feng, Y. Zhao, Y. Zhang, S. Sun, Int. J. Hydrogen Energy 42 (2017) 13070–13084.

[65] G. Guan, M. Kaewpanha, X. Hao, A. Abudula, Renewable and Sustainable Energy Reviews 58 (2016) 450–461.

[66] N. Padban, Progress Report SDE Project Primary Measures for Reduction of Tars during Fluidized Bed Gasification of Biomass. 2001, Department of Thermal Engineering, University of Twente: Enschede, The Netherlands.

[67] P. Morf, P. Hasler, T. Nussbaumer, Fuel 81 (2002) 843–853.

[68] T. Hosoya, H. Kawamoto, S. Saka, Journal of Analytical and Applied Pyrolysis 83 (2008) 78–87.

[69] T. Hosoya, H. Kawamoto, S. Saka, Journal of Analytical and Applied Pyrolysis 78 (2007) 328–336.

[70] D.C. Elliott, Book: Pyrolysis Oils from Biomass chap 6, ACS Symposium Series 376 (1988) 55–65.

[71] C.M. Kinoshita, Y. Wang, J. Zhou, Journal of Analytical and Applied Pyrolysis 29 (1994) 169–181.

[72] Q. Yu, C. Brage, G. Chen, K. Sjöström, Journal of Analytical and Applied Pyrolysis (1997) 40–41:481–489.

[73] C. Brage, Q. Yu, G. Chen, K. Sjöström, Biomass and Bioenergy 18 (2000) 87–91.

[74] R.A. Knight, Biomass and Bioenergy 18 (2000) 67–77.

[75] J. Gil, J. Corella, M. Aznar, M.A. Caballero, Biomass and Bioenergy 17 (1999) 389–403.

[76] J. Watson, Y. Zhang, B. Si, W.-T. Chen, R. de Souza, Renewable and Sustainable Energy Reviews 83 (2018) 1-17.

[77] I. Narváez, A. Orío, M.P. Aznar, J. Corella, Industrial & Engineering Chemistry Research 35 (1996) 2110–2120.

[78] M.M.A. Mohammed, A. Salmiaton, W.A.K.G. Wan Azlina, M.S. Mohammad Amran, A. Fakhru'l-Razi, Energy Conversion and Management 52 (2011) 1555-1561.

[79] J. Herguido, J. Corella, J. GonzPalez-Saiz, Industrial & Engineering Chemistry Research 31 (1992) 1274–1282.

[80] S. Rapagnà, N. Jand, A. Kiennemann, P.U. Foscolo, Biomass and Bioenergy 19 (2000) 187-197.

[81] L. García, M.L. Salvador, J. Arauzo, R. Bilbao, Energy and Fuels 13 (1999) 851–859.

[82] M.P. Aznar, J. Corella, J. Gil, J.A. Martín, M.A. Caballero, A. Olivares, P. Pérez, E. Francés, Developments in thermochemical biomass conversion. London: Blackie (1997) 1194–1208.

[83] J. Gil, M.P. Aznar, M.A. Caballero, E. Francés, J. Corella, Energy and Fuels 11 (1997) 1109–1118.

[84] L. García, M.L. Salvador, J. Arauzo, R. Bilbao, Fuel Processing Technology 69 (2001) 157–174.

[85] M. Hlína, M. Hrabovský, V. Kopecký, M. Konrád, T. Kavka, S. Skoblja, Czechoslovak Journal of Physics 56 (2006) B1179–B1184.

[86] P.J. Woolcock, R.C. Brown, Biomass and Bioenergy 52 (2013) 54–84.

[87] Y. Shen, K. Yoshikawa, Renewable and Sustainable Energy Reviews 21 (2013) 371-392.

[88] P. Hasler, T. Nussbaumer, Biomass and Bioenergy 16 (1999) 385–395.

[89] W. de Jong, O. Unal, J. Andries, K.R.G. Hein, H. Spliethoff, Biomass and Bioenergy 25 (2003) 59–83.

[90] H. Zhao, D.J. Draelants, G.V. Baron, Industrial & Engineering Chemistry Research 39 (2000) 3195–3201.

[91] K. Engelen, Y. Zhang, D.J. Draelants, G.V. Baron, Chemical Engineering Science 58 (2003) 665–670.

[92] L. Ma, H. Verelst, G.V. Baron, Catalysis Today 105 (2005) 729–734.

[93] L. Ma, G.V. Baron, Powder Technology 180 (2008) 21–29.

[94] A.G. Bhave, D.K. Vyas, J.B. Patel, Renewable Energy 33 (2008) 1716–1720.

[95] S. Viswanathan, N.V. Ananthanarayanan, B.J. Azzopardi, The Canadian Journal of Chemical Engineering 83 (2005) 194–203.

[96] D. Khummongkol, C. Tangsathitkulchai, Energy 14 (1989) 113–121.

[97] T. Phuphuakrat, T. Namioka, K. Yoshikawa, Bioresource Technology 102 (2011) 543–549.

[98] D. Prando, S. Shivananda Ail, D. Chiaramonti, M. Baratieri, S. Dasappa, Fuel 181 (2016) 566–572.

[99] G.W. Huber, S. Iborra, A. Corma, Chemical Reviews 106 (2006) 4044–4098.

[100] D. Sutton, B. Kelleher, J.R.H. Ross, Fuel Processing Technology 73 (2001) 155-173.

[101] C. Xu, J. Donald, E. Byambajav, Y. Ohtsuka, Fuel 89 (2010) 1784–1795.

[102] Z. Abu El-Rub, E.A. Bramer, G. Brem, Industrial & Engineering Chemistry Research 43 (2004) 6911–6919.

[103] D. Świerczyński, S. Libs, C. Courson, A. Kiennemann, Applied Catalysis B: Environmental 74 (2007) 211–222.

[104] R. Michel, A. Lamacz, A. Krzton, G. Djéga-Mariadassou, P. Burg, C. Courson, R. Gruber, Fuel 109 (2013) 653-660.

[105] M. Virginie, C. Courson, D. Niznansky, N. Chaoui, A. Kiennemann, Applied Catalysis B: Environmental 101 (2010) 90-100.

[106] K. Tomishige, T. Miyazawa, M. Asadullah, S.-I. Ito, K. Kunimori, Green Chemistry 5 (2003) 399-403.

[107] T. Furusawa, K. Saito, Y. Kori, Y. Miura, M. Sato, N. Suzuki, Fuel 103 (2013) 111-121.

[108] M. Artetxe, M.A. Nahil, M. Olazar, P.T. Williams, Fuel 184 (2016) 629-636.

[109] M. Artetxe, J. Alvarez, M.A. Nahil, M. Olazar, P.T. Williams, Energy Conversion and Management 136 (2017) 119-126.

[110] S. Vivanpatarakij, D. Rulerk, S. Assabumrungrat, Chemical Engineering Transactions 37 (2014) 205-210.

[111] Z. Zhang, L. Liu, B. Shen, C. Wu, Renewable and Sustainable Energy Reviews 94 (2018) 1086-1109.

[112] L. Wang, D. Li, M. Koike, S. Koso, Y. Nakagawa, Y. Xu, K. Tomishige, Applied Catalysis A: General 392 (2011) 248–255.

[113] U. Oemar, P.S. Ang, K. Hidajat, S. Kawi, International Journal of Hydrogen Energy 38 (2013) 5525-5534.

[114] L. Wang, D. Li, M. Koike, H. Watanabe, Y. Xu, Y. Nakagawa, K. Tomishige, Fuel 112 (2013) 654–661.

[115] D. Li, M. Koike, J. Chen, Y. Nakagawa, K. Tomishige, International Journal of Hydrogen Energy 39 (2014) 10959–10970.

[116] D. Li, M. Lu, K. Aragaki, M. Koike, Y. Nakagawa, K. Tomishige, Applied Catalysis B: Environmental 192 (2016) 171–181.

[117] J. Chen, M. Tamura, Y. Nakagawa, K. Okumura, K. Tomishige, Applied Catalysis B: Environmental 179 (2015) 412-421.

[118] P. Chaiprasert, T. Vitidsant, Korean Journal of Chemical Engineering 26 (2009) 1545–1549.

[119] G. Oh, S.Y. Park, M.W. Seo, Y.K. Kim, H.W. Ra, J.-G. Lee, S.J. Yoon, Renewable Energy 86 (2016) 841-847.

[120] K. Tomishige, T. Kimura, J. Nishikawa, T. Miyazawa, K. Kunimori, Catalysis Communications 8 (2007) 1074-1079.

[121] S. Adamu, Q. Xiong, I.A. Bakare, M.M. Hossain, International Journal of Hydrogen Energy 44 (2019) 15811-15822.

[122] T.P. de Castro, E.B. Silveira, R.C. Rabelo-Neto, L.E.P. Borges, F.B. Noronha, Catalysis Today 299 (2018) 251-262.

[123] T.P. de Castro, R.P.S Penguin, R.C. Rabelo-Neto, L.E.P. Borges, F.B. Noronha, Topics in Catalysis 59 (2016) 292-302.

[124] R. Zhang, Y. Wang, R.C. Brown, Energy Conversion and Management 48 (2007) 68-77.

[125] R. Zhang, H. Wang, X. Hou, Chemosphere 97 (2014) 40-46.

[126] M. Inaba, K. Murata, M. Saito, I. Takahara, Energy Fuels 20 (2006) 432-438.

[127] A.A. Rownaghi, R.L. Huhnke, ACS Sustainable Chemical Engineering 1 (2013) 80-86.

[128] J. Ashok, S. Kawi, Applied Catalysis A: General 490 (2015) 24-35.

[129] D. Li, L. Wang, M. Koike, Y. Nakagawa, K. Tomishige, Applied Catalysis B: Environmental 102 (2011) 528–538.

[130] J. Ashok, Y. Kathiraser, M.L. Ang, S. Kawi, Applied Catalysis B: Environmental 172-173 (2015) 116-128.

[131] F.M. Josuinkas, C.P.B. Quitete, N.F.P. Ribeiro, M.M.V.M. Souza, Fuel Processing Technology 121 (2014) 76-82.

[132] R.S. Tan, T.A.T. Abdullah, S.A. Mahmud, R.M. Zin, K.M. Isa, International Journal of Hydrogen Energy 44 (2019) 21303-21314.

[133] M. Machida, T. Teshima, K. Eguch, H. Arai, Chemistry Letters 134 (1991) 231–234.

[134] C.P.B. Quitete, R.C.P. Bittencourt, M.M.V.M. Souza, Applied Catalysis A: General 478 (2014) 234-240.

[135] A. Stanislaus, B.H. Cooper, Science and Engineering 36 (1994) 75-123.

[136] K. Sato, Y. Iwata, Y. Miki, H. Shimada, Journal of Catalysis 186 (1999) 45-56.

[137] R. Contreras, J. Ramírez, R. Cuevas-García, A. Gutiérrez-Alejandre, P. Castillo-Villalón, G. Macías, I. Puente-Lee, Catalysis Today 148 (2009) 49-54.

[138] A. Corma, V. Gonzáalez-Alfaro, A.V. Orchillés, Journal of Catalysis 200 (2001) 34-44.

[139] H. Ma, X. Yang, G. Wen, G. Tian, L. Wang, Y. Xu, B. Wang, Z. Tian, L. Lin, Catalysis Letters 116 (2007) 149-154.

[140] K. Chandra Mouli, V. Sundaramurthy, A.K. Dalai, Journal of Molecular Catalysis A: Chemical 304 (2009) 77-84.

[141] S.G.A. Ferraz, B.M. Santos, F.M.Z. Zotin, L.R.R. Araujo, J.L. Zotin, Industrial and Engineering Chemistry Research 54 (2015) 2646-2656.

[142] A. Galadima, O. Muraza, Fuel 181 (2016) 618-629.

[143] A. Gutiérrez, J.M. Arandes, P. Castaño, M. Olazar, J. Bilbao, Fuel Processing Technology 101 (2012) 64-72.

[144] N. Jin, G. Wang, L. Yao, M. Hu, J. Gao, Industrial & Engineering Chemistry Research 55 (2016) 5108-5115.

[145] V. Calemma, M. Ferrari, S. Rabal, S. Weitkamp, Fuel 111 (2013) 763-770.

[146] A. Gutiérrez, J.M. Arandes, P. Castaño, M. Olazar, J. Bilbao, Fuel 94 (2012) 504-515.

[147] J.-I. Park, J.-K. Lee, J. Miyawaki, Y.-K. Kim, S.-H. Yoon, I. Mochida, Fuel 90 (2011) 182-189.

[148] Y.-S. Kim, G.-N. Yun, Y.-K. Lee, Catalysis Communications 45 (2014) 133-138.

[149] J.-I. Park, S.A. Ali, K. Alhooshani, N. Azizi, J. Miyawaki, T. Kim, Y. Lee, H.-S. Kim, S.-H. Yoon, I. Mochida, Journal of Industrial and Engineering Chemistry 19 (2013) 627-632.

[150] T. Wu, S.-L. Chen, G.-m. Yuan, J. Xu, L.-x. Huang, Y.-q. Cao, T.-t. Fan, Fuel 234 (2018) 1015-1025.

[151] G.C. Laredo, P. Pérez-Romo, J. Escobar, J.L. Garcia-Guitierrez, P.M. Vega-Merino, Industrial & Engineering Chemistry Research 56 (2017) 10939-10948.

[152] Y.-S. Kim, K.-S. Cho, Y.-K. Lee, Journal of Catalysis 351 (2017) 67-78.

[153] Y.-S. Kim, K.-S. Cho, Y.-K. Lee, Catalysts 10 (2020) 47.

[154] R. Prins, V.H.J. De Beer, G.A. Somorjai, Catalysis Reviews 31 (1989) 1-41.

[155] H. Topse, B.S. Clausen, Catalysis Reviews 26 (1984) 395-420.

[156] P. Grange, X. Vanhaeren, Catalysis Today 36 (1997) 375-391.

[157] P. Betancourt, S. Marrero, S. Pinto-Castilla, Fuel Processing Technology 114 (2013) 21-25.

[158] S.T. Oyama, X. Wang, Y.-K. Lee, K. Bando, F.G. Requejo, Journal of Catalysis 210 (2002) 207-217.

[159] Y.-K. Lee, S.T. Oyama, Journal of Catalysis 239 (2006) 376-389.

[160] Y.-K. Lee, S.T. Oyama, Applied Catalysis A:General 548 (2017) 103-113.

[161] J.W. Ward, Fuel Processing Technology 35 (1993) 55-85.

[162] J. Scherzer, A.J. Gruia, Hydrocracking Science and Technology, Marcel Dekker, New York (1996).

[163] J.G. Speight, The Refinery of the Future (2011) 275-313.

[164] A. Corma, A. Martínez, Studies in Surface Science and Catalysis 157 (2005).

[165] C. Martínez, A. Corma, Coordination Chemistry Reviews 255 (2011) 1558-1580.

[166] I.E. Maxwell, Catalysis Today 1 (1987) 385-413.

[167] P.P. Dik, I.G. Danilova, I.S. Golubev, M.O. Kazakov, K.A. Nadeina, S.V. Budukva, V.Yu. Pereyma, O.V. Klimov, I.P. Prosvirin, E.Yu. Gerasimov, T.O. Bok, I.V. Dobryakova, E.E. Knyazeva, I.I. Ivanova, A.S. Noskov, Fuel 237 (2019) 178-190.

[168] A. Corma, A. Martínez, V. Martínez-Soria, Journal of Catalysis 200 (2001) 259-269.

[169] M.O. Kazakov, K.A. Nadeina, I.G. Danilova, P.P. Dik, O.V. Klimov, V.Yu. Pereyma, E.Yu. Gerasimov, I.V. Dobryakova, E.E. Knyazeva, I.I. Ivanova, A.S. Noskov, Catalysis Today 305 (2018) 117-125.

[170] A. Corma, M.J. Díaz-Cabañas, C. López, A. Martínez, Studies in Surface Science and Catalysis 154 (2004) 2380-2386.

[171] R. Chal, C. Gérardin, M. Bulut, S. van Donk, ChemCatChem 3 (2011) 67-81.

[172] J. Francis, E. Guillon, N. Bats, C. Pichon, A. Corma, L.J. Simon, Applied Catalysis A: General 409-410 (2011) 140-147.

CHAPTER 2.

OBJECTIVES

2.1. Main objectives

Tars are considered as an alternative source to fossil fuels to produce energy, fuels, and chemicals. Tars derived from biomass gasification process and from petroleum refining (or distillation) are liquid dense mixtures (semi-viscous) mainly composed by mono-aromatics, di-aromatics, and poly-aromatics (PAHs). These feedstocks are highly required to be upgraded, and they can be converted into light aromatic hydrocarbons (BTX) and transportation fuels (in the range of diesel and gasoline) by means of catalytic hydrocracking. However, the latter process suggests the use of severe reaction conditions to achieve tars conversion.

The design of new catalytic hydrotreatment process is a need for the valorization of these tars. In this sense, the main objective of this research work is the development of heterogeneous catalysts having moderate acidity, to avoid cracking reactions, good hydrogenation function and good stability. These solid catalysts can upgrade a model mixture composed by poly-aromatics representative of real feedstocks of tars generated from both biomass gasification and petroleum refining under mild operative conditions (<300°C and 30 bar of H_2), aiming at producing partially hydrogenated products with improved H/C ratio and density, applied as jet fuel improvements or additives. In addition, the application scope of the developed catalysts could be extended to other hydrogenation processes of industrial interest.

2.2. Specific objectives

- Development and study of simple metal oxides-supported Pd catalysts in the mild hydrotreatment of a mixture of poly-aromatics (representative of tars). The activity, selectivity to the partially hydrogenated products and stability of the catalysts will be studied and compared to some commercial catalysts.
- Development of TiO_2-Al_2O_3 mixed oxide prepared by co-precipitation method studying synthesis parameters and its use as catalyst support. The activity of the TiO_2-Al_2O_3-supported Pd will be evaluated in the mild hydrotreatment of tars-type compounds, and its application scope is extended to other demanding hydrogenation reactions (i.e., reductive amination).
- Development of Ni supported on different simple and mixed oxides catalysts and investigation of their catalytic application in the mild hydrotreatment of tars-type compounds, along with the selective hydrogenation of fatty acids.

CHAPTER 3.
EXPERIMENTAL PROCEDURE

3.1. Reactants and commercial catalysts

Different reagent-grade chemicals were used during the development of this thesis, their purity and the corresponding suppliers are detailed in Table 3.1. The reactants were purchased from Sigma-Aldrich, Alfa Aesar, Acros Organics and TCI Europe. All the reactants and solvents were directly used without any pre-treatment or purification.

Table 3.1.a. Organic reactants and solvents used during this investigation for the mild hydrotreatment of tars-type compounds.

N^0	Reactant	Purity	Supplier
1	Naphthalene	99%	Sigma-Aldrich
2	Phenanthrene	98%	Sigma-Aldrich
3	Acenaphthylene	>90%	TCI Europe
4	1-methylnaphthalene	96%	Alfa Aesar
5	Acenaphthene	97%	Sigma-Aldrich
6	Tetralin	>97%	Sigma-Aldrich
7	n-Hexadecane anhydrous	99%	Acros Organics
8	Decane	99%	Sigma-Aldrich
9	Tetrahydrofuran	99%	Sigma-Aldrich
10	2-propanol	>99.5%	Sigma-Aldrich

Table 3.1.b. Organic reactants and solvents used during this investigation for the selective hydrogenation of fatty acids.

N^0	Reactant	Purity	Supplier
1	Oleic acid	90%	Sigma-Aldrich
2	Stearic acid	95%	Sigma-Aldrich
3	Stearyl alcohol (1-octadecanol)	99%	Sigma-Aldrich
4	n-Heptadecane	99%	Sigma-Aldrich
5	n-Octadecane	99%	Sigma-Aldrich
6	Stearyl stearate	98%	Sigma-Aldrich
7	Decalin	98%	Sigma-Aldrich
8	1,2,4-butanetriol	96%	Alfa Aesar
9	Pyridine	>99%	Sigma-Aldrich
10	Toluene	99.98%	Scharlau
11	N-methyl-N-(trimethylsilyl)-trifluoroacetamide (MSTFA)	>98.5%	Sigma-Aldrich

Table 3.1.c. Organic reactants and solvents used for the reductive amination of acetol with ethylenediamine.

N^0	Reactant	Purity	Supplier
1	Hydroxyacetone (acetol)	90%	Sigma-Aldrich
2	Ethylenediamine	99%	Sigma-Aldrich
3	Methanol	99.5%	Scharlau
4	Chlorobenzene	99.9%	Sigma-Aldrich

In addition, many different catalysts were prepared in this work. Metal precursors and inorganic reactants employed for their synthesis are listed in Table 3.2.

Table 3.2.a. Inorganic reactants used for metal incorporation in catalysts synthesis.

N⁰	Reactant	Purity	Supplier
1	Tetraamminepalladium (II) chloride monohydrate	>99.99%	Sigma-Aldrich
2	Palladium (II) nitrate dihydrate	40% Pd basis	Sigma-Aldrich
3	Tetraamminepalladium (II) nitrate	10wt% in H_2O	Sigma-Aldrich
4	Tetraammineplatinum (II) chloride hydrate▪	99.99%	Sigma-Aldrich
5	Tetraammineplatinum (II) nitrate•	99.995%	Sigma-Aldrich
6	Nickel (II) nitrate hexahydrate	97%	Sigma-Aldrich
7	Iron (III) nitrate nonahydrate	>98%	Sigma-Aldrich
8	Gallium (III) nitrate hydrate	99.9%	Sigma-Aldrich
9	Lanthanum (III) nitrate hexahydrate	99.9%	Sigma-Aldrich
10	Copper (II) nitrate trihydrate	99.999%	Sigma-Aldrich

▪ Used in Chapter 4.

• Used in Chapter 6.

Table 3.2.b. Inorganic reactants used for mixed metal oxides preparations.

N^0	**Reactant**	**Purity**	**Supplier**
1	Titanium (IV) oxychloride-HCl acid solution	15% Ti basis, 38-42% HCl basis	Sigma-Aldrich
2	Titanium (IV) isopropoxide	97%	Sigma-Aldrich
3	Zirconyl chloride octahydrate	98%	Sigma-Aldrich
4	Sodium metasilicate	n.d	Sigma-Aldrich
5	Aluminium (III) nitrate nonahydrate	99.99%	Sigma-Aldrich
6	Ammonia	NH_3 25%	ITW Reagents

In addition, as supports for the synthesis of metal-based catalysts tested during this work, a series of commercial simple metallic oxides was used, and their main physico-chemical properties are listed in Table 3.3.

Table 3.3. Different commercial metallic oxides used as supports for the preparation of catalysts and their main textural properties.

N^0	Metal oxide	Provider	Surface area (m^2/g)	Pore volume (cm^3/g)
1	TiO_2 nanoactive	Nanoscale Corporation	162	0.18
2	TiO_2 aeroxide P25	Sigma-Aldrich	50	0.25
3	TiO_2 anatase	Sigma-Aldrich	11	0.01
4	TiO_2 rutile	Sigma-Aldrich	2	0.00
5	γ-Al_2O_3▪	Abcr	250	0.48
6	γ-Al_2O_3•	Sigma-Aldrich	138	-
7	ZrO_2 monoclinic	CHEMPURE	105	0.22
8	SiO_2 nanopowder	Sigma-Aldrich	505	0.25
9	MgO nanoactive	Nanoscale Corporation	382	0.31

▪ Used in tars mild hydrotreatment and selective hydrogenation of fatty acids.

• Used in the reductive amination of acetol with ethylenediamine (section 5.7).

In general, the commercial materials were softly treated at 100 °C to remove adsorbed water, prior to their use as supports for metal incorporation.

Metal supported on Carbon commercial catalysts (5wt%Pd/C, 5wt%Pt/C, and 5wt%Ru/C) were provided by Sigma-Aldrich and used for preliminary tests in the mild hydrotreatment of tars-type compounds in Chapter 4. In addition, metal supported on alumina commercial catalysts (1wt% Pd/Al_2O_3 and 1wt% Pt/Al_2O_3) were purchased from

Sigma-Aldrich. Further, commercial zeolite H-USY (CBV 720 with Si/Al = 15), purchased from Zeolyst International, was used as support for Pd and Pt incorporation. Zeolite H-USY was calcined under air atmosphere as follows: 1) 150 min to reach 350 °C, 2) 120 min at 350 °C, 3) 150 min to reach 500 °C, 4) 180 min at 500 °C and 5) cooling down under air. In addition, industrial hydrotreating catalysts $NiMoS/Al_2O_3$ and $CoMoS/SiO_2$-Al_2O_3 were employed in this work. Their physic-chemical properties are detailed in Table 3.4. For instance, Al_2O_3-supported Pd and Pt, zeolite-supported Pd and Pt, along with the industrial hydrotreating catalysts were used as references for comparative purpose (Chapter 4).

Table 3.4. Main physico-chemical properties of the industrial hydrotreating catalysts used in this thesis.

Nº	**Catalyst**	**Ni or Co wt%**	**Mo wt%**	**Surface area (m^2/g)**	**Pore volume (cm^3/g)**
1	$NiMoS/Al_2O_3$	3.3	12.0	190	0.41
2	$CoMoS/SiO_2$-Al_2O_3	2.8	8.0	265	0.56

Sulfidation process: The two industrial catalysts above-described were treated prior to their use in catalytic test via sulfidation process in a fix-bed reactor using a mixture of 10% of H_2S in H_2 at a flow of 100 mL/min during 5 h at 400 °C with a heating ramp of 10 °C/min.

3.2. Catalysts preparation

3.2.1. Mixed oxides via co-precipitation method

Co-precipitation procedure adapted from [1] was used to synthesize the mixed oxides employed during this thesis. In this sense, appropriate amounts of metallic precursors were dissolved in milliQ water (300 mL) and kept under stirring during 10 min. Afterwards, a 25vol% NH_4OH aqueous solution was added dropwise (1000 mL/h) until pH = 9 was reached and the solution was kept under stirring during 15 min. Then, the solution was kept at 60 ºC during 12 h before the solids were separated by filtration, washed with distilled water, and dried at 100 ºC during 24 h. Finally, obtained materials were calcined in air at 500 ºC during 3 h with a heating rate of 2 ºC/min. This procedure has been used for mixed oxides employed in Chapter 5 and 6 (Ti-Al, Ti-Zr, Zr-Al, Ti-Si and Si-Al). Information about metal precursors can be found in Table 3.2.b. Titanium (IV) oxychloride, HCl acid solution (15% Ti) was used as Ti precursor in this method.

Concerning Ti-Al materials, the effect of Ti/Al molar ratio, ammonia speed addition, pH during the synthesis and aging time were evaluated in Chapter 5. For instance, Ti-Al-O mixed oxides of different Ti/Al molar compositions were prepared, and the corresponding amounts of metal precursors employed in each case are detailed in table 3.5.

Table 3.5. Amount of Ti and Al precursors used in co-precipitation method.

Ti/Al molar ratio	Ti precursor (mmol)	Al precursor (mmol)
0.4	20.0	40.0
0.8	30.0	30.0
1.3	36.0	24.0
2.2	45.0	15.0
3.0	48.0	12.0

3.2.2. Mixed oxides (TiO_2/Al_2O_3 and TiO_2/ZrO_2) via incipient wetness impregnation

Titanium (IV) isopropoxide was used as Ti precursor in this method, by dissolving a calculated amount of Ti to obtain ≈12wt% in ethanol. The volume of necessary ethanol was previously calculated for each support. Then, the solution was added dropwise to the support. After that, the material was dried at 100 °C during 3 h, and finally calcined in air at 500 °C during 3 h, with a heating rate of 2 °C/min. This method has been used for mixed oxides employed in Chapter 5 (TiO_2/Al_2O_3) and Chapter 6 (TiO_2/Al_2O_3 and TiO_2/ZrO_2). Information about Ti precursor and commercial supports is listed in Tables 3.2.b and 3.3, respectively.

3.2.3. Synthesis of Palladium- (and Platinum) based catalysts via incipient wetness impregnation

Typically, an adequate amount of Pd (and Pt) was dissolved in water milliQ. Afterwards, this solution was added dropwise to the support. Then the material was dried at 100 °C during 3 h, and then reduced at 400 °C during 2 h under a H_2 flow of 100 mL/min with a heating rate of 3 °C/min (4 h in total) and cooled down in N_2 atmosphere. This method has been used for catalysts tested in Chapter 4, Chapter 5, and Chapter 6. The metal precursors employed are listed in Table 3.2.a.

3.2.4. Synthesis of bimetallic Palladium-metal based catalysts via incipient wetness impregnation

An adequate amount of the second metal precursor was dissolved in water milliQ. Afterwards, this solution was added dropwise onto the support. Then, the solid material was dried at 100 °C during 3 h. The next step was the addition of an aqueous solution containing $Pd(NH_3)_4Cl_2.H_2O$ to the solid, and then drying the material at 100 °C during 3 h. Afterwards, the solid material was reduced at 400 °C during 2 h under a H_2 flow of 100 mL/min with a heating rate of 3 °C/min (4 h in total), and finally cooled down in N_2 atmosphere. This method has been used in Chapter 4 to study the effect of addition of another metal to Pd on the catalytic activity in the mild hydrotreatment reaction. The metal precursors used are listed in Table 3.2.a.

3.2.5. Synthesis of Nickel based catalysts via incipient wetness impregnation

Typically, an adequate amount of $Ni(NO_3)_2.6H_2O$ was dissolved in water mQ. Afterwards, this solution was added dropwise to the support. Then the material was dried at 100 °C during 3 h, and then reduced at 450 °C during 2 h under a H_2 flow of 100 mL/min with a heating rate of 3.75 °C/min (4 h in total) and cooled down in N_2 atmosphere. This method has been used for catalysts tested in Chapter 6. Information about Ni precursor can be found in Table 3.2.a.

3.2.6. Synthesis of bimetallic Nickel-Platinum based catalysts via incipient wetness impregnation

An adequate amount of $Ni(NO_3)_2.6H_2O$ was dissolved in water milliQ. Afterwards, this solution was added dropwise to the support. Then, the material was dried at 100 °C during 3 h. The next step requires the addition of an aqueous solution containing $Pt(NH_3)_4(NO_3)_2$, and then drying the material at 100 °C during 3 h. Afterwards, the solid material was reduced at 450 °C during 2 h under a H_2 flow of 100 mL/min with a heating rate of 3.75 °C/min (4 h in total), and finally cooled down in N_2 atmosphere. This method has been used in Chapter 6 to study the effect of addition of Pt to Ni on the catalytic activity in the selective hydrogenation of fatty acids to produce hydrocarbons and alcohols. Data about metal precursors can be found in Table 3.2.a.

3.3. Catalysts analysis and characterization

In this section, the fundamental principles of the different characterization techniques used during this work are discussed.

3.3.1. Inductively Coupled Plasma Atomic Emission Spectroscopy (ICP-AES) [2,3]

This analytical technique is used to detect and quantify chemical elements. It is an emission spectroscopy technique, where excited atoms and ions are produced by a given plasma energy from outside, followed by the emission of an electromagnetic radiation (spectrum rays) at given photon wavelengths characteristic of each element. The intensity of the energy emitted is proportional to the amount (concentration) of that element in the analyzed sample. ICP-AES analysis requires sample dissolution. In this sense, solid supports or catalysts (30-50 mg) were dissolved in a 5 mL mixture of acids HF:HNO_3:HCl (proportion in volume 1:1:3), which afterwards was diluted in 50 mL of distilled water. The composition of solid supports and catalysts has been measured in an ICP-AES Varian 715-ES equipment.

Solution sample is introduced into the nebulizer through a peristaltic pump. This nebulizer produces an aerosol mist, while an argon gas current, along with the sample are injected into the chamber. The large mist particles settle down, whereas the fine particles (1-2%) are later carried into the torch. A radio frequency-generated Ar plasma is formed, causing the excitation of the electrons. When the latters return to the ground state, they emit energy at peculiar wavelengths,

which corresponds to the sample´s elemental composition. The light emitted is focused through lenses and multipliers to the spectrometer. Reference standards are usually used for comparative purpose (background corrections). This system comes up with flexible and rapid analysis of solid materials and catalysts composition.

3.3.2. X-Ray Diffraction (XRD)

X-ray diffraction is a non-destructive analytical technique commonly used for the determination of the atomic and molecular structure of a finely ground crystal (solid). It is also used for the identification of the crystalline phases present in a material in term to obtain information about its chemical composition. X-ray wavelength interval varies between 10 and 100 Å, being in a similar order of magnitude to interplanar spacing in most of crystalline structures. Crystalline materials are characterized by the orderly periodic arrays of atoms, which can diffract X-rays (light). In this sense, diffraction takes place when monochromatic beam of X-rays (light) is scattered by a periodic array with long-range order, resulting in a constructive interference at specific angles. The produced diffraction pattern (XRD peak) brings information about the periodic atomic arrangement in each crystal, thus elucidating the crystalline structure of a sample. The peak intensity is determined by the atomic positions within the lattice planes. However, amorphous materials, which do not consist of periodic array with long-range order, do not show any significant diffraction pattern [4]. The interaction between the incident X-ray beam and the given

solid generates reflected X-rays by constructive interference when conditions assure Bragg's Law. Bragg's Law can be defined as [5]:

$$2d * \sin \theta = n \lambda \qquad \text{(Equation 3.1)}$$

Where d is the spacing between diffraction planes, θ is the incident angle of the beam (diffraction angle), n is any integer and λ is the X-ray wavelength.

In crystallography, the ordered arrangement of atoms, ions or molecules in a crystalline material leads to a specific crystal structure [6]. For instance, ordered structures create symmetric patterns that repeat along the three-dimensional space directions. Crystal structures are expressed in terms of the geometrical arrangement of the particles present in the unit cell, which is defined as the smallest repeating entity (basic building block) having the full symmetry of the crystal structure [7]. In this sense, vectors and planes in a crystal lattice are identified by the three-value Miller index notation (hkl). All crystalline materials fit in one of the 14 Bravais lattices, where interplanar spacing (d) between adjacent (hkl) planes is given by known equations depending on the catalyst structure (i.e., cubic, tetragonal, hexagonal).

In addition, interplanar spacing can be determined using Bragg's Law as follow: $2d_{hkl} * \sin \theta_{hkl} = n \lambda$, if λ is experimentally known and (hkl) and θ are known for a specific lattice plane. Moreover, information about crystallite size (D) can be given by XRD using Scherrer's equation written as [8]:

$$D = K \lambda / B \cos \theta \qquad \text{(Equation 3.2)}$$

Where K is a constant (usually equal to 1), λ is the X-ray wavelength, B is the FWHM (Full Width at Half Maximum), and θ is the Bragg (diffraction) angle.

In our case, XRD patterns of powder solids were performed on a PANalytical Cubix diffractometer equipped with a PANalytical X-Celerator detector, using Cu Kα radiation (λ1 = 1.5406 Å, λ2 = 1.5444 Å, I2/I1 = 0.5) and a graphite monochromator.

3.3.3. Textural analysis. N_2 adsorption isotherms

This gas adsorption method provides information about textural properties of solid materials from gas-solid adsorption and desorption processes. For instance, information about surface area, pore size and pore volume can be reached from the interpretation of adsorption-desorption isotherms. In this sense, Brunauer-Emmett-Teller (BET) theory describes the physical adsorption of gas molecules on a solid surface and has been typically used as an analytical technique to measure the specific surface area of solids [9]. Generally, the most employed gaseous adsorbate for surface area calculation is Nitrogen (at 77 K). The concept of this theory is an extension of the Langmuir theory, where liquid-phase N_2 monolayer molecular adsorption takes place. The resulting BET equation is:

$$\frac{P}{V(P^0-P)} = \frac{1}{V_m*C} + \frac{(C-1)}{V_m*C} * \frac{P}{P^0} \qquad \text{(Equation 3.3)}$$

Where V is the adsorbed gas quantity, V_m is the monolayer adsorbed gas quantity, C is the BET constant related to the heat of

adsorption for the first layer and P and P^0 are the equilibrium and the saturation pressure of adsorbates at the temperature of adsorption (P/P^0 is the relative pressure).

BET surface area (S_{BET}) is defined as:

$$S_{BET} = \frac{V_m}{M} * L * A_m \qquad \text{(Equation 3.4)}$$

Where V_m is the monolayer adsorbed gas quantity, L is Avogadro's number, A_m is the volume of each adsorbed molecule (0.162 nm^2) and finally M is the molar volume of the adsorbate gas. An adsorption isotherm is represented by the adsorbed gas quantity (V) versus relative pressure P/P^0 (at fix temperature conditions). The IUPAC classification of adsorption isotherms [10] is provided in Figure 3.1. The six types of isotherms are characteristic of adsorbents that are microporous (type I), nonporous or macroporous (II, III and VI) or mesoporous materials (types IV and V). Data about pore size distribution, pore geometry and connectivity of mesoporous materials can be given from different shape of adsorption hysteresis (IV and V).

In this work, experiments were performed in Micrometrics ASAP 2000 equipment in term to collect N_2 adsorption isotherms. Samples (200-300 mg with a granulometry between 0.4-0.8 mm) were degassed in vacuum overnight at a temperature of 350 ºC (below their calcination temperature). BET method was used to calculate surface areas, and Barrett-Joyner-Halenda (BJH) method to obtain data about pore size distribution and pore volumes.

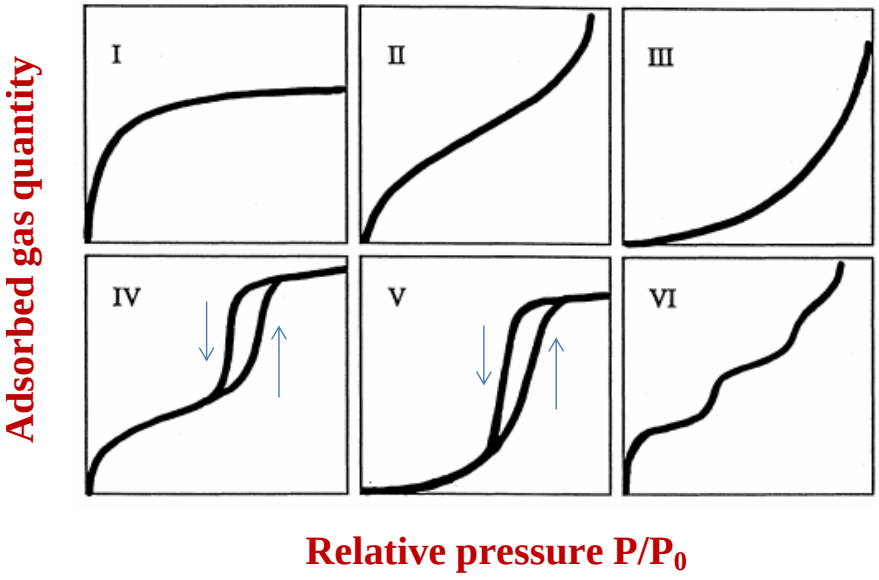

Figure 3.1. IUPAC classification of adsorption isotherms, adapted from [10].

3.3.4. Elemental Analysis (EA)

Elemental analysis (EA) is a technique used to determine the content of carbon, hydrogen, nitrogen, and sulphur in a solid sample. An oxidation process occurs, and it is accomplished by a combustion analysis. The sample is instantaneously burned in an excess of oxygen and the corresponding gas combustion products released are in-situ reduced to produce N_2, SO_x, CO_2, and H_2O. Afterwards, these products will be separated in a chromatographic column and quantified in a TCD detector. Elemental analysis (EA) measurements were performed on a Fisons EA1108CHN-S apparatus aiming at determining organic matter deposition (Cwt%) on the catalysts after their use in catalytic reactions.

3.3.5. Temperature-Programmed Desorption (TPD) of ammonia

Temperature-Programmed Desorption (TPD) of ammonia is a common characterization technique to evaluate surface acid properties (total amount of acid sites) in solid catalysts. In this context, a gas is chemisorbed on the solid surface, and then desorbed with a controlled increasing in the temperature. Different probe molecules can be used for this kind of adsorption measurements. In this sense, NH_3 can behave as a Brönsted/Lewis molecule [11]. Then, NH_3 molecules are chemisorbed due to the interaction with acid centers. Afterwards, when temperature increased, NH_3 molecule is progressively desorbed from the surface and is measured in a TCD detector and a mass spectrometer. Therefore, this method analyzes total acid sites (both Lewis and Brönsted acid sites). Moreover, the strength of these acid centers can be evaluated, as the peaks of NH_3 desorption of stronger acid sites may be shifted to higher temperatures.

Temperature-programmed desorption of ammonia (NH_3-TPD) experiments were carried out on a Micromeritics TPD/2900 apparatus. Typically, 100 mg of the sample (with a granulometry between 0.4-0.8 mm) were pre-treated in an Ar stream at 450 ºC during 1 h to remove the adsorbed contaminants and the volatile species, which can interfere during the gas desorption analysis. Afterwards, NH_3 was chemisorbed by pulses at 100 ºC until equilibrium was attained. Then, the sample was fluxed with helium stream during 15 min to remove the excess of NH_3, prior to raise the temperature up to 500 ºC in a 100 mL/min of He stream with a heating rate of 10 ºC/min. NH_3 desorption was monitored

with a thermal conductivity detector (TCD) and a mass spectrometer. Total volumes of adsorbed ammonia are measured under the standard conditions of pressure and temperature. Finally, the ideal gas law can be used to calculate the total moles of adsorbed NH_3 (equivalent to the total moles of acid sites).

3.3.6. Temperature-Programmed Reduction (TPR)

The thermo-programmed reduction technique (TPR) with hydrogen is usually employed to investigate the reducibility of metallic oxides, either in their mass form or dispersed on a support. This analysis gives information about the number and type of species present in the solid, which are susceptible to reduction. In addition, the reduction temperature of these species can be provided [12]. This method was used to study the reducibility of the different metals (Pd, Pt, and Ni) deposited on simple and mixed metal oxides.

TPR (Temperature-Programmed Reduction) experiments were carried out on Micrometrics Autochem 2910 equipment. Calcined catalysts (50 mg with a granulometry between 0.4-0.8 mm) were initially flushed with 30 mL/min of Ar at room temperature for 30 min, and then a mixture of 10 vol% of H_2 in Ar was passed through the catalyst at a total flow rate of 50 mL/min while the temperature was being raised up to 800 °C at a heating rate of 10 °C/min. The H_2 consumption was monitored in a thermal conductivity detector (TCD) previously calibrated using the reduction of CuO as reference.

3.3.7. CO and H_2 Chemisorption

Chemisorption or chemical adsorption consists of a chemical bond that involves sharing electrons between the adsorbate and the adsorbent, leading to the formation of surface compound. Due to the bond strength, chemisorption is irreversible. Typically, it is considered as single-layer process. For instance, chemisorption provides information about the number of accessible active sites, active surface area, metal dispersion and finally active particle (crystallite) size.

In our work, CO chemisorption was performed on Quantachrome Autosorb-1C equipment by using 300 mg of solid sample (0.4-0.8 mm). Prior to adsorption, the sample was reduced under a H_2 flow by using the same reduction temperature applied for the catalysts (400 ºC) for 2 h. Afterwards, sample was degassed at 1333 x 10^{-3} Pa during 2 h at 400 ºC, and temperature was then decreased at 35 ºC. Next, pure CO was admitted and the first adsorption isotherm (i.e. the total CO uptake) was measured. After evacuation at 35 ºC, the second isotherm (i.e. the reversible CO uptake) was taken. The amount of chemisorbed CO was determined by subtracting the two isotherms. The pressure range studied was 0.5-11 x 10^4 Pa. Pd dispersion was calculated from the amount of irreversibly adsorbed CO, supposing a stoichiometry Pd/CO = 1.

In addition, H_2 chemisorption using the double isotherm method was carried out on a Quantachrome Autosorb-1C equipment. Prior to adsorption, the samples were reduced in situ at 450ºC for 2 h (4 ºC/min).

After reduction, the samples were degassed at $1333x10^{-3}$ Pa for 2 h at the reduction temperature, and then temperature lowered at 30 ºC. Then, pure H_2 was admitted, and the first adsorption isotherm was measured. After evacuation at 30ºC, the second isotherm was measured. The amount of chemisorbed H_2 was then obtained by subtracting the two isotherms. The pressure range studied was 1-11 x 10^4 Pa. The dispersion of Ni was calculated from the amount of irreversibly adsorbed H_2 assuming a stoichiometry of Ni/H=1.

3.3.8. Scanning Electron Microscope with Energy Dispersive X-ray spectroscopy (SEM-EDX)

Information about the morphology of the catalysts and their textural characteristics can be provided by Electron Microscope technique. Especially, SEM (Scanning Electron Microscopy) is used to observe materials at a nano- (nm) and micro-metric (μm) scale [13]. Sample images result by scanning the surface with a focused beam of electrons (2-50 kV). Afterwards, various signals that contain information about sample´s surface and composition are generated due to the interaction between electrons and atoms in the material. Back-scattered electrons (BSE) and secondary electrons (SE) emitted by atoms are detected, thus producing the corresponding image. On one hand, the number of back-scattered electrons (BSE) is determined as result of the interaction between the electrons and the atomic nucleus, and the elemental composition is then provided. On the other hand, secondary electrons (SE) result from the interaction of incident and back-scattered electrons with other electrons that exist in the outer

orbital shell of an atom. Data about catalyst morphology can be given from secondary electrons (SE).

Moreover, Energy Dispersive X-ray spectroscopy (EDS-EDX) can be combined with Scanning Electron Microscopy (SEM-EDX). The basis of this method is detecting the emitted X-ray after radiating the samples with a focused beam of electrons. X-ray energy radiation is characteristic of each element. Then, the wavelength of the emitted radiation (qualitative analysis) and the intensity of each signal (quantitative analysis) bring information about elemental composition. Elemental mapping of catalysts can be also achieved aiming at studying metal dispersion on the support and mixed oxides homogeneity.

X-ray energy-dispersive spectroscopic measurements were performed using a JEOL 6300 scanning electron microscope, equipped with an Oxford LINK ISIS detector connected. An adhesive mounted rigidly to a carbon sample holder was used for samples dispersion, and afterwards, a thin carbon layer is deposited over them. A focused beam of electrons (20 kV) and a counting time of 50-100 s were required to obtain the corresponding images.

3.3.9. Transmission Electron Microscopy (TEM) and High-Resolution Transmission Electron Microscopy (HR-TEM)

In these techniques, the electron beam is transmitted through a specimen to form the corresponding image. This sample is most frequently an ultrathin section less than 100 nm suspended on a metallic grid. The interaction of the electrons with the sample (as the beam is

transmitted through the specimen) forms the image. The differential absorption of electrons by different element composition (or thickness of the material) creates TEM image contrast. Then, the image is magnified and focused onto an imaging device such as fluorescent screen, a layer of photographic film, among others. Because of the smaller wavelength of electrons (high-energy electron beams >200 KeV), TEM and HR-TEM microscopes provide images at significantly higher resolution than Scanning Electron Microscopy (SEM) images.

TEM micrographs were realized using JEOL JEM-1010 instrument operating at 200 KV, equipped with a digital camera MegaView III and image acquisition software AnalySIS. HR-TEM measurements of the selected catalysts were carried out on a Jeol JEM-2100F equipment, working at a voltage of 200 kV. The HR micrograph analysis, lattice spacing, First Fourier Transform (FFT) and phase interpretation, were realized with the Gatan Digital Micrograph software (Gatan Inc.) and the Java version of the Electron Microscope Software (JEM).

3.3.10. X-Ray Photoelectron Spectroscopy (XPS)

X-ray Photoelectron Spectroscopy technique brings quantitative and qualitative information about chemical species in the surface of solid catalysts [14]. To illustrate, data about surface elemental composition, surface structure, chemical and electronic state of the elements, which exist in the outer 6 nm layer of a material, can be identified.

Based on the photoelectric effect, the sample surface is radiated by a monochromatic X-ray beam. Due to the interaction of X-ray photons with elements in the surface, electrons move to internal energy bands and therefore they are emitted. Additionally, XPS detectors must be employed under ultrahigh vacuum conditions aiming at counting the number of electrons during the acquisition of a spectrum. Then, a typical XPS spectrum can be defined as a plot of the number of electrons detected versus their binding energy. Then, electron binding energy can be determined when both, photon radiation energy and the ejected photo-emitted electron kinetic energy are well recognized. A characteristic set of XPS peaks at characteristic binding energy values is generated for each element, which identifies each one existing on the surface, along with its chemical and electronic state.

In our work, this technique was used to analyze elemental composition and electronic states of Palladium species supported on TiO_2, before and after several reuses, also after regeneration with H_2 (Chapter 4). In addition, composition, and electronic states of Nickel species in the case of Ni and PtNi supported on TiO_2/Al_2O_3 catalysts were evaluated (Chapter 6). X-ray photoelectron spectroscopy (XPS) data were obtained from a SPECS spectrometer equipped with a 150-MCD-9 detector and employing a non-monochromatic Al K_α (1486.6 eV) X-ray source. Spectra were recorded at 200 ºC, using an analyzer pass energy of 30 eV, a X-ray power of 50 W and under 10^{-9} mbar of pressure. With respect to data processing of the XPS spectra, binding energy (BE) values were referenced to the C*1s* signal for Pd samples

and Al*2s* for Ni and PtNi samples. Finally, spectra has been treated using the CASA software.

3.4. Catalytic tests

3.4.1. Catalytic mild hydrotreatment of tars-type molecules

Catalytic hydrotreatment reactions were carried out in a 12 mL autoclave-type reactor with PEEK (Polyether ether ketone)-graphite interior, equipped with a magnetic bar, pressure control and a valve for either liquid or gas extraction. Reactor was placed over a steel jacket individual support equipped with temperature control system.

Typically, 0.5 g of a model mixture representative of tars composed by naphthalene (0.125 g), phenanthrene (0.125 g), acenaphthylene (0.125 g) and 1-methylnaphthalene (0.125 g) dissolved in 4.0 g of n-hexadecane, and 0.2 g of catalyst were introduced in the autoclave-type reactor. The reactor was hermetically closed, purged with N_2, pressurized at 10-36 bar of H_2 and heated at 250-300 °C, under continuous stirring (1000 rpm), and the reaction continued during 7 h. These conditions were selected to maintain all the reactants in the liquid phase to avoid mass transfer limitations. Liquid samples were collected from reactor, and then analyzed by gas chromatography techniques to follow the evolution of reaction.

3.4.1.1. Re-uses of the catalyst

Catalytic recycling experiments were carried out by using the catalysts in consecutive runs. After reaction, the solid catalyst was separated from the liquids by centrifugation, washed three times with 2-propanol, and then dried at 100 °C during 1 h, prior to its next reuse in the mild hydrotreatment of tars-type compounds under the same reaction operating conditions. Solid catalyst recovered from re-uses was also analyzed by different solid characterization techniques above mentioned in this Chapter.

3.4.2. Catalytic selective hydrogenation of fatty acids done at ITQ

Catalytic hydrogenation reactions were performed in the same type of reactor employed for the mild hydrotreatment of tars-type compounds and previously described in section 3.4.1. These experiments were preliminary performed at ITQ to select the adequate catalysts for the more in-depth study carried out by means of high-throughput reactor system of REALCAT platform at Lille, France (see next section).

Typically, 3.0 g of 15wt% oleic acid/decalin solution and 0.05 g of catalyst were introduced in the autoclave-type reactor. The reactor was hermetically closed, purged with N_2, pressurized at 30 bar of H_2 and heated at 220-275 °C, under continuous stirring (1000 rpm), and the reaction continued during 4 h. Liquid samples were collected from reactor, and then analyzed by gas chromatography techniques to follow the evolution of reaction.

3.4.3. Catalytic selective hydrogenation of fatty acids done at REALCAT platform (Lille-FRANCE)

The catalytic tests were performed in Screening Pressure Reactor (SPR) equipment, from Freeslate, which is an automated high-throughput reactors system. The Freeslate SPR is equipped with 24 stainless steel 6 mL reactors that allow carrying out up to 24 experiments per run with operational conditions up to 400 °C and pressure up to 50 bar. Temperature, pressure, and flow profiles are automatically controlled based on a user-defined recipe. Good solid/liquid/gas contacting is achieved, and mass transfer problems are limited by the high intensity orbital agitation (up to 800 rpm).

Typically, 1.56 mL of 15wt% oleic acid/decalin solution and 5-50 mg of catalyst were introduced into the reactors. Filled reactors were placed in the SPR and purged with N_2. Afterwards, the reactors were purged with H_2 and the H_2 pressure was set to 30-45 bar. After that, the catalytic test started along with the agitation (800 rpm), and the temperature was increased to 225-275 °C and kept during 3 h.

Liquid samples were collected from reactor, and then analyzed by gas chromatography techniques to follow the evolution of reaction.

3.4.4. Reductive amination of acetol to 2-methylpiperazine

Reductive cycle-amination reactions were performed in a 6 mL “batch” type micro-reactor equipped with a magnetic bar, a probe and valve for liquid extraction, and a pressure control.

Typically, 0.325 g of acetol, 0.227 g of ethylenediamine, 1.250 g of methanol (as solvent), and 0.011 g of catalyst were introduced in the batch reactor (with slow addition of acetol at an addition rate of 100 μL/h). The reactor was purged with N_2, pressurized at 13 bar of H_2 and heated at 90 °C, under continuous stirring (800 rpm), and the reaction continued during 3 h. The H_2 pressure was kept practically constant by recharging every 30 minutes). Liquid samples were collected from reactor, and then analyzed by gas chromatography techniques to follow the evolution of reaction.

3.5. Analysis of reactions mixtures

Gas chromatography (GC) has been employed for reactants and products separation and analysis during catalytic experiments. In gas chromatography, a micro-syringe installed in an auto-sampler is used to inject a known volume of sample into the injector section. This sample is then vaporized along with a carrier gas that forms the mobile phase, which enters the capillary column. Then, the gases formed interact with the walls of the column coated with the stationary phase. The capillary column is placed inside an oven, where temperature can be modified. These factors lead to compounds elution at different times (retention time). The compounds exit at the end of the column and are detected by means of detector device. An electronic signal corresponding to each compound is finally produced.

3.5.1. Catalytic mild hydrotreatment of tars-type molecules

Small liquid aliquots (100 µL) were collected at different time intervals during reaction, diluted with 0.4-0.5 g of tetrahydrofuran solution containing 1wt% of n-decane as external standard, and then filtered off to remove the catalyst prior to GC injection. Liquid samples were analyzed by an Agilent Technologies 7890A GC system equipped with a flame ionization detector (FID) working at 300 °C, along with a HP-5 MS capillary column (30 m x 250 µm x 0.25 µm). N_2 was employed as a carried gas. The injector is working at 250 °C with a split mode. The oven temperature begun at 40 °C, then increased to 150 °C with a heating rate of 5 °C/min (hold time: 5 min), and finally increased to 250 °C with a heating rate of 5 °C/min.

Reactants and products are quantified from response factors, which are determined by using n-decane as chromatographic standard.

The products were identified by Agilent 6890 N GC system coupled with an Agilent 5973 N mass detector and equipped with a HP-5 MS capillary column (30 m x 250 µm x 0.25 µm), also in comparison to commercial reference chemicals when available.

3.5.2. Catalytic selective hydrogenation of fatty acids done at ITQ

Small liquid aliquots (50 µL) were collected at different time intervals in a glass vial, diluted with 2 mL of toluene. Then, 0.4 g of a solution prepared of 1,2,4-butanetriol (as external standard) in pyridine (1 mg/mL) were added. Afterwards, the sample was treated via

silylation (or derivatization) with 0.3 g of N-methyl-N-(trimethylsilyl)-trifluoroacetamide (MSTFA). Then, the mixture was shaken vigorously and kept at room temperature during 15 min prior to GC analysis.

Liquid sample analysis was done by means of Agilent Technologies 7890A GC system equipped with a FID detector working at 390 °C, along with a GC capillary column (Agilent J&W GC columns – Select Biodiesel for Glycerides Ultimetal – 10 m x 0.32 mm x 0.10 µm, P/N: CP9077). N_2 was employed as a carrier gas. The injector is working with a track oven mode at 250 °C, and on column. The oven temperature begun at 50 °C (hold time: 2 min), then increased to 140 °C with a heating rate of 20 °C/min, and finally increased to 280 °C with a heating rate of 15 °C/min (hold time: 15 min).

3.5.3. Catalytic selective hydrogenation of fatty acids done at REALCAT platform (Lille-FRANCE)

Small liquid aliquots (50 µL) were collected at the end of the reaction in a glass vial and diluted with 2 mL of toluene. Then, 400 µL of a solution prepared of 1,2,4-butanetriol (as external standard) in pyridine (1 mg/mL) were added. Afterwards, a silylation (derivatization) treatment was carried out by adding 300 µL of N-methyl-N-(trimethylsilyl)-trifluoroacetamide (MSTFA). Then, the mixture was shaken vigorously and kept at 60 °C during 1 h prior to GC injection.

Liquid samples were analyzed by a GC-FID-MS-QP2010 Ultra SHIMADZU equipped with a GC capillary column (Agilent J&W GC

columns - Select Biodiesel for Glycerides Ultimetal - 10 m x 0.32 mm x 0.10 µm, P/N: CP9077). H_2 was employed as a carrier gas. The injector is working with a split mode at 300 °C. The oven temperature begun at 40 °C (hold time: 1 min), then increased to 140 °C with a heating rate of 20 °C/min, then to 230 °C with a heating rate of 15 °C/min, and finally increased to 300 °C with a heating rate of 20 °C/min (hold time: 5 min).

Reactants and products are quantified from response factors, which are determined by using 1,2,4-butanetriol as chromatographic standard.

3.5.4. Reductive amination of acetol to 2-methylpiperazine

Small liquid aliquots were collected, diluted with 0.4 g of methanol solution containing 1wt% of chlorobenzene as external standard, and then filtered off to remove the catalyst prior to GC injection. Liquid samples were analyzed by a 3900-Varian GC system equipped with a FID detector and a capillary column (HP-5, 30 m length). The products were identified by Agilent 6890 N GC system coupled with an Agilent 5973 N mass detector and equipped with a HP-5 MS capillary column (30 m x 250 µm x 0.25 µm).

Reactants and products are quantified from response factors, which are determined by using chlorobenzene as chromatographic standard.

3.6. Calculations

The catalytic activity of the different catalysts along this work is discussed in terms of reactant conversion and products selectivity (and yield). The following formulas have been employed:

- **For tars mild hydrotreatment reaction**

$$\boldsymbol{Conversion}\ (\boldsymbol{mol}\%) = \frac{(\boldsymbol{Reactant_x\ moles\ at\ t_0 - Reactant_x\ moles\ at\ t})}{\boldsymbol{Reactant_x\ moles\ at\ t_0}} \times \mathbf{100}$$

$$\boldsymbol{Selectivity}\ (\boldsymbol{mol}\%) = \frac{\boldsymbol{Product_x\ moles\ at\ t}}{(\boldsymbol{Reactant_x\ moles\ at\ t_0 - \ Reactant_x\ moles\ at\ t})} \times \mathbf{100}$$

$$\boldsymbol{Yield}\ (\boldsymbol{mol}\%) = \boldsymbol{Selectivity\ X\ Conversion}$$

$$\boldsymbol{Turn\ Over\ Number}\ (\boldsymbol{TON}) = \frac{\boldsymbol{Total\ products\ moles\ at\ t}}{\boldsymbol{Metal\ moles\ in\ catalyst}}$$

- **For fatty acids selective hydrogenation reaction**

$$\boldsymbol{Conversion}\ (\boldsymbol{wt}\%) = \frac{(\boldsymbol{Reactant_x\ mass\ at\ t_0 - Reactant_x\ mass\ at\ t})}{\boldsymbol{Reactant_x\ mass\ at\ t_0}} \times \mathbf{100}$$

$$\boldsymbol{Selectivity}\ (\boldsymbol{wt}\%)\ = \frac{\boldsymbol{Product_x\ mass\ at\ t}}{(\boldsymbol{Reactant_x\ mass\ at\ t_0 - \ Reactant_x\ mass\ at\ t})} \times \mathbf{100}$$

$$\boldsymbol{Selectivity\ in\ liquids}\ (\boldsymbol{wt}\%) = \frac{\boldsymbol{Product_x\ mass\ at\ t}}{\boldsymbol{Total\ products\ mass\ at\ t}} \times \mathbf{100}$$

$$\boldsymbol{Yield}\ (\boldsymbol{wt}\%) = \boldsymbol{Selectivity\ X\ Conversion}$$

- **For both above-mentioned reactions**

$$\textbf{\textit{Mass balance}}\ (\%) = \frac{\textbf{\textit{mass}}\ (\textbf{\textit{products}} + \textbf{\textit{reactants at t}})}{\textbf{\textit{reactants mass at}}\ t_0} \times \mathbf{100}$$

- **For reductive amination reaction**

$$\textbf{\textit{Conversion}}\ (\textbf{\textit{mol}}\%) = \frac{(\textbf{\textit{Reactant}}_x\ \textbf{\textit{moles at}}\ t_0 - \textbf{\textit{Reactant}}_x\ \textbf{\textit{moles at t}})}{\textbf{\textit{Reactant}}_x\ \textbf{\textit{moles at}}\ t_0} \times \mathbf{100}$$

$$\textbf{\textit{Selectivity in liquids}}\ (\textbf{\textit{mol}}\%) = \frac{\textbf{\textit{Product}}_x\ \textbf{\textit{moles at t}}}{\textbf{\textit{Total products moles at t}}} \times \mathbf{100}$$

$$\textbf{\textit{Yield}}\ (\textbf{\textit{mol}}\%) = \textbf{\textit{Selectivity X Conversion}}$$

Total conversion, selectivities and yields of the different products, were calculated through GC analysis, taking ethylenediamine as the reference reactant.

3.7. References

[1] X. Zhang, T. Wang, L. Ma, Q. Zhang, X. Huang, Y. Yu, Applied Energy 112 (2013) 533-538.

[2] V.A. Fassel, R.N. Kniseley, Analytical Chemistry 46 (1974) 1110A-1120a.

[3] J. Nölte, ICP Emission Spectrometry: A Practical Guide, Wiley-VCH Verlag BmbH & Co (2003).

[4] A. Chauhan, P. Chauhan, Journal of Analytical & Bioanalytical Techniques 5 (2014).

[5] N.W. Gregory, Journal of the American Chemical Society 79 (1957) 1773-1774.

[6] J.R. Hook, H.E. Hall, Solid State Physics. Manchester Physics Series (2nd ed.). John Wiley & Sons (2010).

[7] A.R. West, Basic Solid State Chemistry (2nd ed.). Wiley. p.1 (1999).

[8] U. Holzwarth, N. Gibson, Nature Nanotechnology 6 (2011) 534.

[9] S. Brunauer, P.H. Emmett, E.J. Teller, Journal of the American Chemical Society 60 (1938) 309-319.

[10] M.D. Donohue, G.L. Aranovich, Advances in Colloid and Interface Science 76-77 (1998) 137-152.

[11] G.I. Kapustin, T.R. Brueva, A.L. Klyachko, S. Beran, B. Wichterlova, Applied Catalysis 42 (1988) 239-246.

[12] G. Leofanti, G. Tozzala, M. Padovan, G. Petrini, S. Bordiga, A. Zecchina, Catalysis Today 34 (1997) 307-327.

[13] W. Zhou, R. Apkarian, Z.L. Wang, D. Joy, Scanning Microscopy for Nanotechnology: Techniques and Applications (2007) 1-40.

[14] H. Bubert, J.C. Rivière, W.S.M. Werner, X-Ray Photoelectron Spectroscopy. Surface and Thin Film Analysis (2011).

CHAPTER 4.

TITANIUM OXIDE-SUPPORTED PD AS AN EFFICIENT AND STABLE CATALYST FOR THE MILD HYDROTREATMENT OF TARS-TYPE COMPOUNDS

4.1. Introduction

In the last years, due to the continuous depletion of conventional fossil sources and the increasing interest and demand for energy and transportation fuels, the less attended energy sources such as oils sources (bitumen, oils sands, wood oils, among others), light (LCO) and heavy petroleum fractions (with high contents of tars) have been explored and processed as alternative energy sources [1,2]. The light tars are one of these possible fuel sources.

Light tars are liquid dense mixtures formed during petroleum distillation and/or refining. In addition, they could be produced during the pyrolysis or gasification of coal or biomass [3]. In all the cases, these unwanted tars are commonly condensed and accumulated in the reactors and pipelines, and they must be removed to prevent blockages, their treatment being a challenge. These fractions contain different compounds, mainly monoromatics such as benzenes, toluenes, among others, along with low-value poly-aromatics compounds, such as naphthalenes, acenaphthylenes, phenanthrenes, anthracenes, pyrenes, among others. Additionally, as already mentioned in Chapter 1, any hydrocarbon with molecular weight higher than benzene could be considered as tars [4].

In addition, hydrotreatment processes mentioned in Chapter 1 (hydrotreating and hydrocracking) require high temperature and H_2 pressure, with increasing energy consumptions, while catalyst deactivation becomes problematic. In this sense, the processing of light tars feedstocks via catalytic hydrotreatment at lower H_2 pressure

and moderate temperature is highly recommended. In this way, heavier feedstocks having high boiling points are upgraded into more valuable medium to low boiling point products with higher H/C ratio and higher heating value.

With the aforesaid reasons in mind, the use of metal supported catalysts for tars hydrotreatment, where the support is less acidic than zeolites, could be adequate to decrease the level of cracking reactions, thus increasing the amount of medium molecular weight products and avoiding the excessive production of gases and light gasoline-type compounds during the process. With this purpose, highly and homogeneously dispersed Pd nanoparticles supported on TiO_2 material will be prepared and characterized in this work, and then applied as efficient catalyst for the upgrading of a mixture of poly-aromatic hydrocarbons representative of real feedstocks of tars (derived from petroleum distillation or biomass gasification) under moderate H_2 pressure and temperature (at <300 °C and ≈30 bar of H_2). Particularly, special attention will be paid on the catalytic stability and post-reaction physico-chemical characterization, even after consecutive catalyst recycling. This tars representative mixture processing will allow obtaining intermediate products partially hydrogenated in the range of C9-C15 cyclic hydrocarbons, by partially keeping the structure of the starting reactants. Afterwards, these intermediates could be applied as jet fuel components (or boosters), as well as valuable chemical products (i.e., solvents, reaction intermediates, etc.).

In order to facilitate reaction mixtures analysis and results discussions, the liquid products obtained will be grouped as depicted in Figure 4.1. The different groups are as follows: MonoAr "monoaromatics and/or alkylmonoaromatics", tetralin "tetralin and methyltetralin", decalin "cis/trans decalin and methyldecalin", Ace " Acenaphthene", HAce-1 " 1 hydrogenated ring of acenaphthene", HPhe-1 "1 hydrogenated ring of phenanthrene (1,2,3,4-tetrahydrophenanthrene TetHPhe and 9,10-dihydrophenanthrene DiHPhe", HPhe-2 "2 hydrogenated rings of phenanthrene (1,2,3,4,4a,9,10,10a-octahydrophenanthrene asymOHPhe and 1,2,3,4,5,6,7,8-octahydrophenanthrene symOHPhe", and HAce-2/HPhe-3 "totally hydrogenated products of acenaphthylene and phenanthrene (perhydrophenanthrene)".

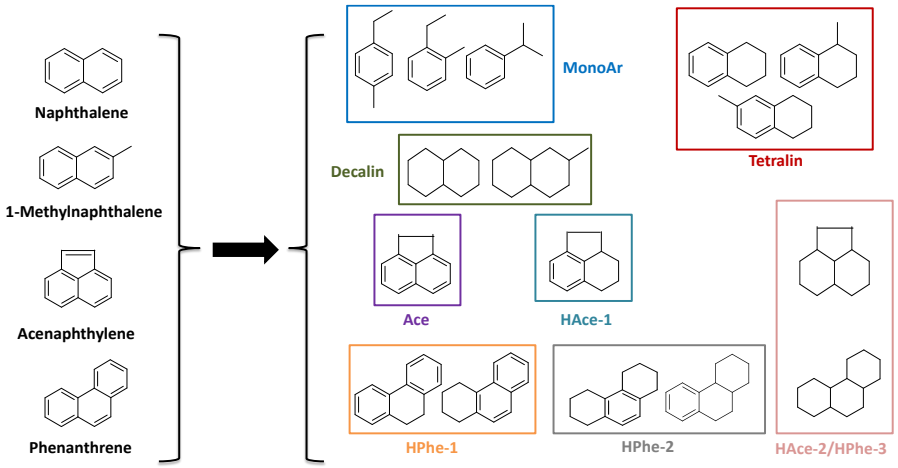

Figure 4.1. Chemical structure of the reactants and the different groups of obtained products.

4.2. Preliminary experiments with Pd-, Pt- and Ru-based commercial catalysts

In a preliminary approach, and in order to assess the adequate metal selection to be used as catalyst for tars mild hydrotreatment, different metal supported on Carbon commercial catalysts (5wt%Ru/C, 5wt%Pt/C, and 5wt%Pd/C) were tested in the reaction. As shown in Table 4.1, these preliminary results showed that Pd/C catalyst achieved better levels of conversion of tars-type reactants. For instance, the conversion of tars-type molecules at 7 h was 71%, 55% and 52%, for Pd, Pt and Ru based catalysts, respectively. In addition, Pd/C catalyst presented more hydrogenation activity than the analogous Ru and Pt supported on Carbon materials, being more selective to HAce-1. For instance, Ace was easily obtained in all the cases and rapidly converted to HAce-1 for Pd/C catalyst. Consequently, Pd was selected as the appropriate active metal phase for the mild hydrotreatment of tars-type compounds.

Table 4.1. Catalytic activity (Conversion and selectivity to the different groups of products) of carbon-supported Pd, Pt and Ru commercial catalysts (comparison at 50-60% of conversion).[a]

Catalyst	Conv. (mol%)	TON [b]	Product selectivity (mol%) [c]							
			Mono Ar	Tetralin	Decalin	Ace	HAce -1	HPhe -1	HPhe -2	HAce-2/HPhe-3
Pd/C	71	21	2.0	32.2	0.0	4.2	42.3	17.8	1.6	0.0
Pt/C	55	30	2.2	29.1	0.0	34.2	12.8	21.1	0.6	0.0
Ru/C	52	15	2.2	31.7	0.0	35.6	14.2	15.8	0.7	0.0

[a] Reaction conditions: 0.5 g of tars-type compounds, 4.0 g of n-hexadecane, 0.2 g of catalyst, 250 ºC, 30 bar of H_2 during 7 h. [b] TON = mols of products/mols of metal. [c] Liquid phase composition; Selectivity = mols of product (t) x 100/total mols of identified products (t).

4.3. Catalytic screening of Pd supported on different simple metal oxides

Afterwards, different Pd nanoparticles based materials were prepared by depositing ≈2wt% Pd (through incipient wetness impregnation method) onto different commercial metal oxides, such as TiO_2, γ-Al_2O_3, MgO and SiO_2 (X-rays diffraction patterns of Pd-based catalysts in Figure A4.1 in Annex). The main physico-chemical and textural properties of the Pd catalysts and their attained catalytic results are listed in Table 4.2. The Pd-based catalysts were screened in the mild hydrotreatment of tars-type molecules at 250 °C and 30 bar of H_2 pressure during 7 h. As can be seen in Table 4.2 and Figure 4.2, the highest both conversion (89%) and TON (67) were achieved with Pd/TiO_2 Nano catalyst. In spite of the lower surface area of TiO_2 Nano compared with the rest of used supports, the Pd/TiO_2 Nano catalyst showed better activity than Pd/γ-Al_2O_3 catalyst, and much better than Pd/MgO and Pd/SiO_2 (with 74%, 63% and 54% conversion, respectively). The selectivity towards the different groups of products detected in the reaction mixture is presented in Figure 4.3. In general, the more active catalyst is expected to show higher selectivity to tetralin, decalin, HPhe-2 and HAce-2/HPhe-3 type of products, and lower selectivity to monoAr, Ace and HPhe-1, respectively. In this sense, a rationalized reaction scheme for this model tars-compounds mild hydrotreatment is proposed in Figure 4.4. For instance, when selectivity of all the Pd-based catalysts of Table 4.2 was compared in the range of 54-57% of conversion, Pd/TiO_2 Nano, Pd/Al_2O_3 and

Pd/MgO offered quite similar selectivities to the different groups of products, whereas Pd/SiO_2 was encountered to be slightly less selective to tetralin and more selective to acenaphthene (Ace). In addition, the corresponding selectivities to the different groups of hydrogenated products at different reaction times of the selected Pd catalysts are listed in Tables 4.3, 4.4, 4.5 and 4.6.

Taking into consideration all the above-mentioned, Pd/TiO_2 Nano was encountered as the most efficient catalyst in the mild hydrotreatment of tars-type compounds, and it was selected for further studies.

Table 4.2. Physico-chemical properties of metal oxides-supported Pd catalysts and their catalytic performance in tars-type compounds mild hydrotreatment.[a]

Catalyst	Pd (wt%)[b]	Support surface area (m^2/g)[c]	Conversion (mol%)	TON[d]
Pd/TiO_2 Nano	2.3	162	89	67
Pd/γ-Al_2O_3	2.3	250	74	46
Pd/MgO	1.7	382	63	54
Pd/SiO_2	2.0	505	54	35

[a] Reaction conditions: 0.5 g of tars-type compounds, 4.0 g of n-hexadecane, 0.2 g of catalyst, 250 °C, 30 bar of H_2 during 7 h. [b] Pd loading measured by ICP. [c] Calculated from N_2 adsorption isotherms (BET method). [d] TON = mols of products/mols of metal.

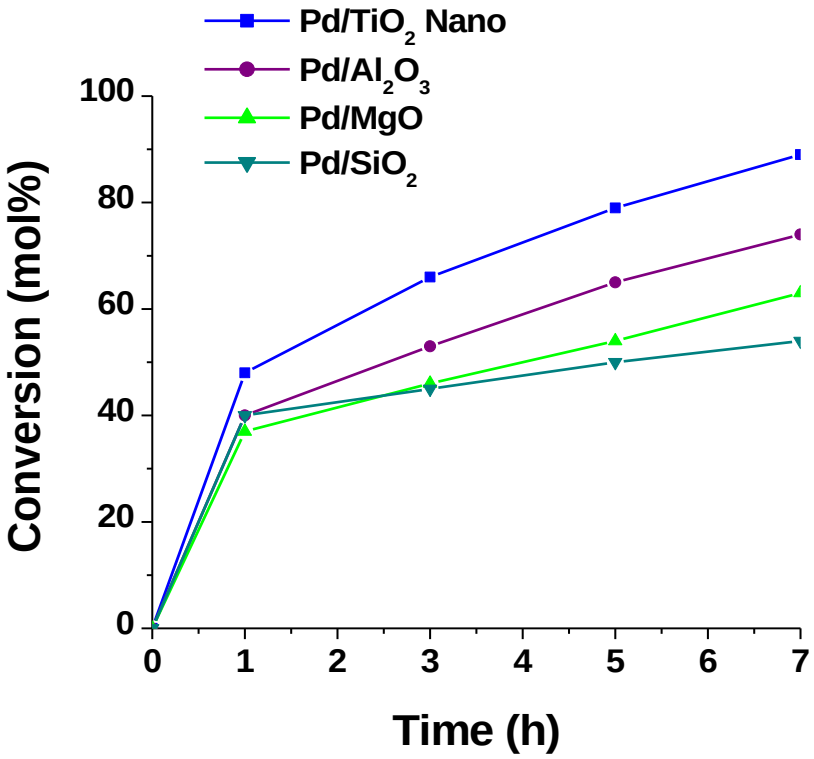

Figure 4.2. Conversion vs Time of different metal oxides-supported Pd catalysts in the tars mild hydrotreatment. Reaction conditions: 0.5 g of tars-type compounds, 4.0 g of n-hexadecane, 0.2 g of catalyst, 250 °C, 30 bar of H_2 during 7h.

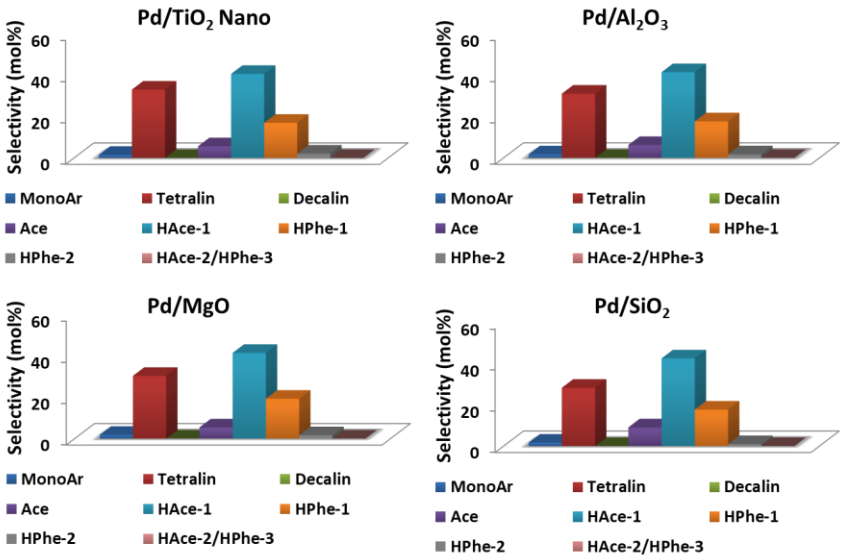

Figure 4.3. Selectivity to the different groups of products for metal oxides-supported Pd catalysts (compared at 54-57% of conversion). <u>Reaction conditions</u>: 0.5 g of tars-type compounds, 4.0 g of n-hexadecane, 0.2 g of catalyst, 250 °C, 30 bar of H_2.

Table 4.3. Selectivity to the different products groups for 2.2wt%Pd/TiO_2 Nano at 250 °C and 30 bar of H_2.

Time (h)	Conv. (mol%)	Product selectivity (mol%)							
		Mono Ar	Tetralin	Decalin	Ace	HAce-1	HPhe-1	HPhe-2	HAce-2/HPhe-3
0	0	0.0	0.0	0.0	0.0	0.0	0.0	0.0	0.0
1	48	1.6	25.9	0.0	10.7	43.6	17.3	0.9	0.0
3	66	1.4	40.3	0.1	0.6	37.7	16.7	3.3	0.0
5	79	1.3	48.8	0.1	0.0	31.8	12.9	5.3	0.0
7	89	1.1	51.8	0.2	0.0	26.2	7.9	7.5	0.1

Table 4.4. Selectivity to the different products groups for 2.3wt%Pd/γ-Al_2O_3 at 250 °C and 30 bar of H_2.

Time (h)	Conv. (mol%)	Product selectivity (mol%)							
		Mono Ar	Tetralin	Decalin	Ace	HAce-1	HPhe-1	HPhe-2	HAce-2/HPhe-3
0	0	0.0	0.0	0.0	0.0	0.0	0.0	0.0	0.0
1	40	1.8	18.8	0.0	26.9	36.9	15.2	0.4	0.0
3	53	1.7	31.1	0.0	6.2	41.5	17.7	1.7	0.0
5	65	1.6	39.8	0.0	0.0	39.2	16.4	3.0	0.0
7	74	1.5	46.4	0.0	0.0	34.6	13.1	4.4	0.0

Table 4.5. Selectivity to the different products groups for 1.7wt%Pd/MgO at 250 °C and 30 bar of H_2.

Time (h)	Conv. (mol%)	Product selectivity (mol%)							
		Mono Ar	Tetralin	Decalin	Ace	HAce-1	HPhe-1	HPhe-2	HAce-2/HPhe-3
0	0	0.0	0.0	0.0	0.0	0.0	0.0	0.0	0.0
1	37	1.9	15.0	0.0	40.4	29.2	13.2	0.3	0.0
3	46	1.9	24.0	0.0	16.5	39.1	17.7	0.8	0.0
5	54	1.8	30.4	0.0	5.4	41.5	18.6	1.6	0.0
7	63	1.8	36.6	0.0	0.8	40.1	18.4	2.3	0.0

Table 4.6. Selectivity to the different products groups for 2.0wt%Pd/SiO_2 at 250 °C and 30 bar of H_2.

Time (h)	Conv. (mol%)	Product selectivity (mol%)							
		Mono Ar	Tetralin	Decalin	Ace	HAce-1	HPhe-1	HPhe-2	HAce-2/HPhe-3
0	0	0.0	0.0	0.0	0.0	0.0	0.0	0.0	0.0
1	40	1.4	14.9	0.0	41.7	30.8	11.3	0.0	0.0
3	45	1.5	20.6	0.0	24.8	37.9	14.8	0.4	0.0
5	50	1.6	24.7	0.0	15.1	41.2	16.7	0.7	0.0
7	54	1.7	28.3	0.0	9.0	42.5	17.7	0.9	0.0

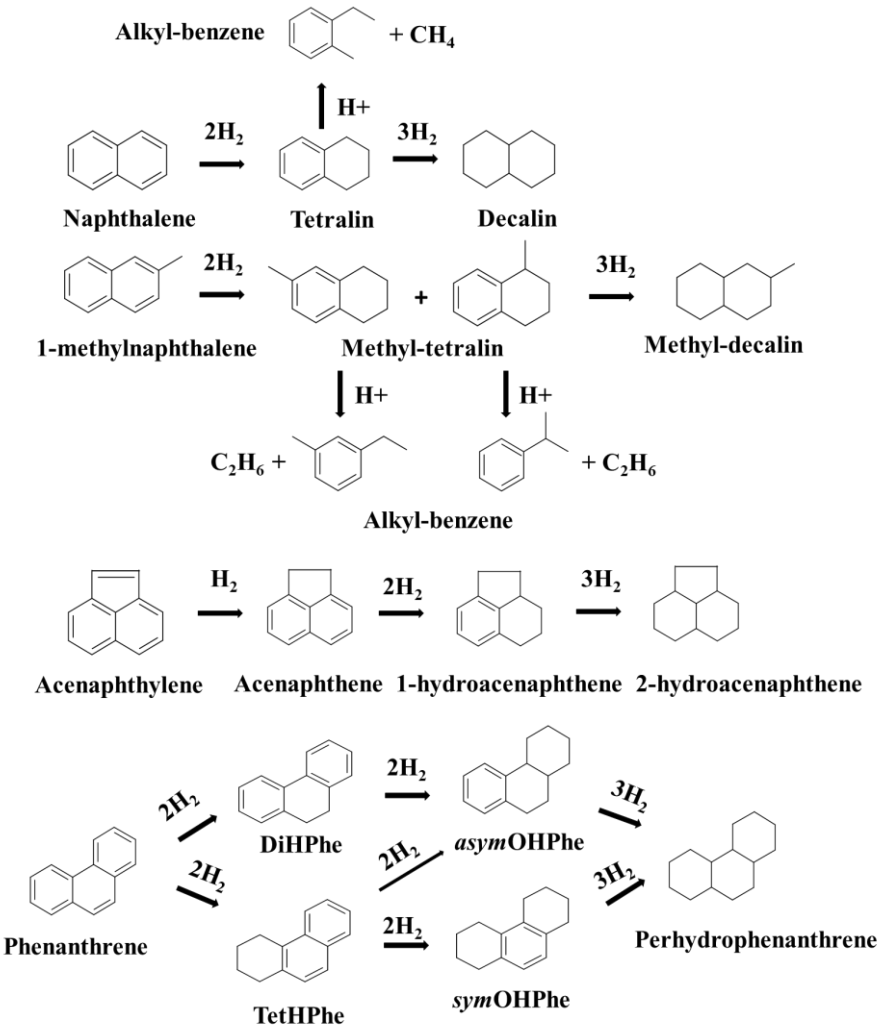

Figure 4.4. Proposed reaction scheme for the mild hydrotreatment of tars-type compounds.

4.4. Effect of Pd content and Pd precursor

Pd/TiO_2 Nano catalysts with different metal content (0.8wt%, 1.3wt% and 2.2wt%, respectively) were prepared and characterized by different techniques (ICP, XRD, TEM), and then tested in the mild

hydrotreatment of tars-type molecules to ascertain the optimal Pd loading needed in the solid catalyst.

X-ray diffraction (XRD) patterns of the various Pd supported on TiO_2 Nano catalysts (Figure 4.5) predominantly showed the presence of anatase phase and a small amount of brookite. In addition, the intensity of the diffraction peaks attributed to Pd^0 species increased when increasing the Pd content in the sample from 0.8wt% to 2.2wt%Pd. This tendency is also in agreement with the increase in the Pd nanoparticle sizes (from 4-7 to 12 nm) observed when increasing the Pd loadings in the catalysts (Figure A4.2).

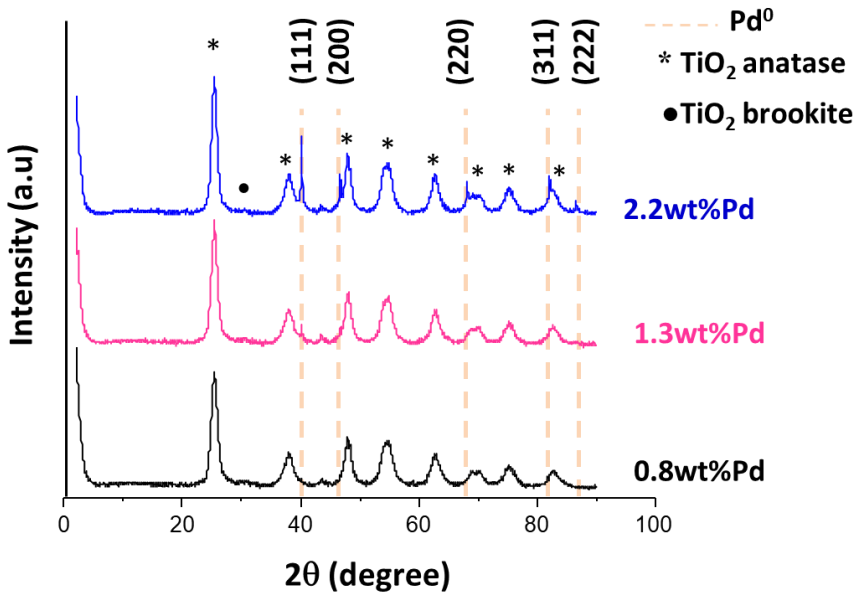

Figure 4.5. X-ray diffraction patterns for different TiO_2 Nano-supported Pd catalysts.

The Pd/TiO_2 Nano catalysts were evaluated in the mild hydrotreatment of tars compounds (at 250 °C and P_{H2} = 30 bar with 0.2 g of catalyst during 7 h), and the results regarding attained tars conversion and calculated TON are summarized in Figures 4.6 and 4.7. As can be seen, the highest tars conversion (≈90% at 7 h) was encountered for 2.2wt%Pd/TiO_2 sample followed by 1.3wt%Pd/TiO_2 (Conv. ≈75%) and 0.8wt%Pd/TiO_2 (Conv. ≈63%) catalysts, respectively. On the contrary, calculated TON values followed the reverse order: 0.8wt%Pd/TiO_2 (TON = 117) > 1.3wt%Pd/TiO_2 (TON = 91) > 2.2wt%Pd/TiO_2 (TON = 67). For the two latter Pd-catalysts, a quite similar selectivity to the different groups of products was encountered at 63-65% range of conversion, while 0.8wt%Pd/TiO_2 catalyst showed a slightly lower selectivity to tetralin and HPhe-2 hydrogenated products (Figure 4.8). The corresponding selectivities to the different groups of products at different reaction times of the selected Pd-based catalysts are listed in Tables 4.3, 4.7, and 4.8 for 2.2wt%Pd/TiO_2, 1.3wt%Pd/TiO_2 and 0.8wt%Pd/TiO_2, respectively.

From these results, it can be concluded that 1.3wt%Pd/TiO_2 Nano material presents a good compromise between Pd loading, catalytic activity (tars conversion and TON) and selectivity to the different groups of products. Consequently, the 1.3wt%Pd loaded TiO_2 material was selected for further studies.

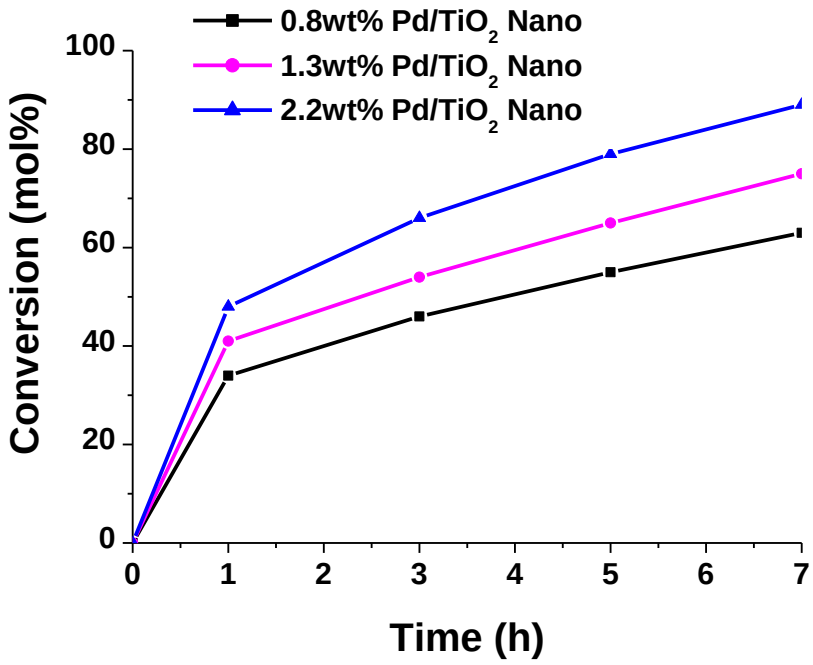

Figure 4.6. Conversion vs time for different TiO_2 Nano-supported Pd catalysts in tars mild hydrotreatment. Reaction conditions: 0.5 g of tars-type compounds, 4.0 g of n-hexadecane, 0.2 g of catalyst, 250 °C, 30 bar of H_2 during 7 h.

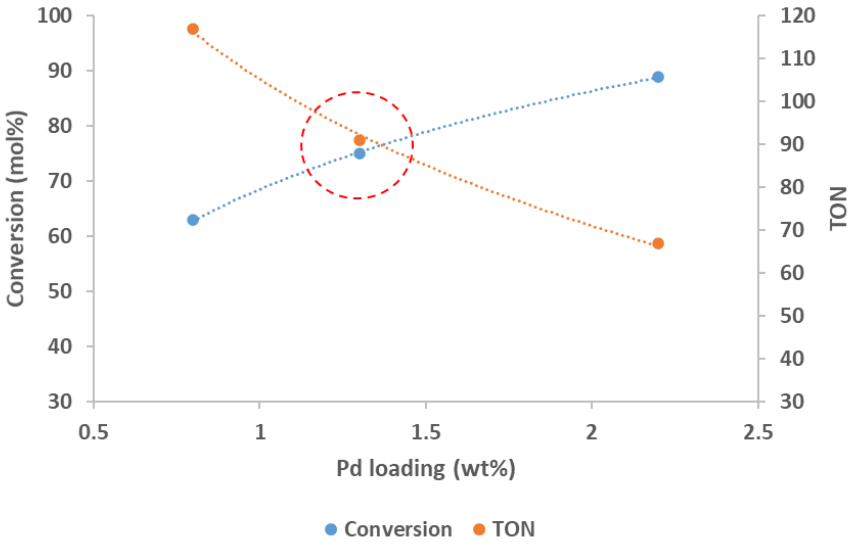

Figure 4.7. Conversion and TON vs Pd loading of different TiO_2 Nano-supported Pd catalysts in tars mild hydrotreatment. Reaction conditions: 0.5 g of tars-type compounds, 4.0 g of n-hexadecane, 0.2 g of catalyst, 250 °C, 30 bar of H_2 during 7 h.

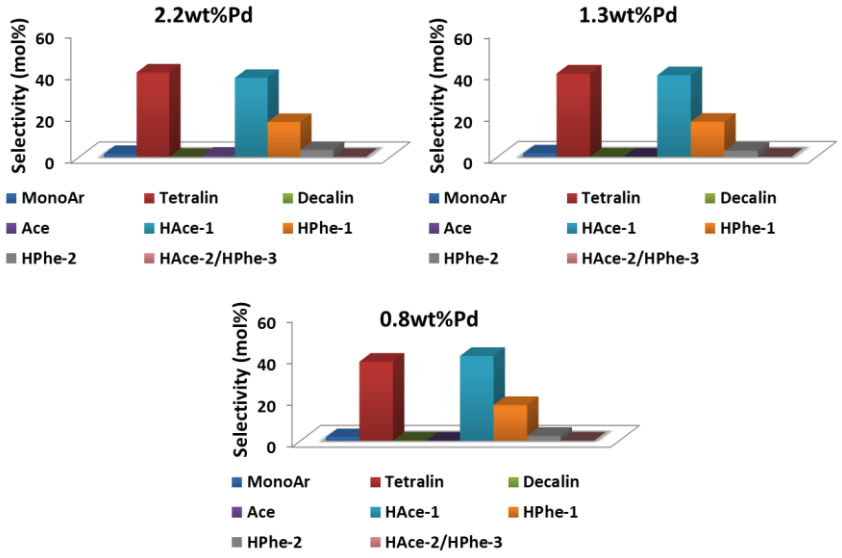

Figure 4.8. Selectivity to the different groups of products for TiO_2-supported Pd catalysts (compared at 63-65% of conversion). Reaction conditions: 0.5 g of tars-type compounds, 4.0 g of n-hexadecane, 0.2 g of catalyst, 250 °C, 30 bar of H_2 during 7 h.

Table 4.7. Selectivity to the different products groups for 1.3wt%Pd/TiO_2 Nano at 250 °C and 30 bar of H_2.

Time (h)	Conv. (mol%)	Product selectivity (mol%)							
		Mono Ar	Tetralin	Decalin	Ace	HAce-1	HPhe-1	HPhe-2	HAce-2/HPhe-3
0	0	0.0	0.0	0.0	0.0	0.0	0.0	0.0	0.0
1	41	1.7	20.1	0.0	26.7	37.7	13.4	0.4	0.0
3	54	1.6	31.4	0.0	6.3	42.1	16.9	1.7	0.0
5	65	1.5	39.8	0.1	0.0	39.1	16.7	2.9	0.0
7	75	1.3	43.1	0.1	0.0	31.5	13.1	3.9	0.0

Table 4.8. Selectivity to the different products groups for 0.8wt%Pd/TiO_2 Nano at 250 °C and 30 bar of H_2.

Time (h)	Conv. (mol%)	Product selectivity (mol%)							
		Mono Ar	Tetralin	Decalin	Ace	HAce-1	HPhe-1	HPhe-2	HAce-2/HPhe-3
0	0	0.0	0.0	0.0	0.0	0.0	0.0	0.0	0.0
1	34	1.4	12.4	0.0	55.1	23.6	7.5	0.0	0.0
3	46	1.7	25.3	0.0	18.5	39.4	14.4	0.8	0.0
5	55	1.7	32.6	0.0	4.8	42.5	16.9	1.6	0.0
7	63	1.6	37.8	0.0	0.0	40.6	17.0	2.3	0.0

Additionally, the effect of using different Pd precursors during the synthesis of Pd/TiO_2 Nano material was assessed. Noticeably, the catalytic activity of these Pd-based catalysts remained practically unchangeable or suffered just minor variations when other Pd precursors were used for their preparation (Table 4.9). These results evidenced that the Pd precursor was not a key point for the catalysts preparation. In any case, $Pd(NH_3)_4Cl_2.H_2O$ compound was preferred as the Pd precursor used for Pd catalysts preparation in this study.

Table 4.9. Pd/TiO_2 Nano impregnated by different Pd precursors and their catalytic results in the mild hydrotreatment of tars-type molecules.[a]

Pd Precursor	Pd (wt%)[b]	Conversion (mol%)	TON[c]
$Pd(NH_3)_4Cl_2.H_2O$	1.3	75	91
$Pd(NO_3)_2.2H_2O$	1.3	79	90
$Pd(NO_3)_2.4NH_3$	0.8	68	127
$Pd(NH_3)_4Cl_2.H_2O$	0.8	63	117

[a] Reaction conditions: 0.5 g of tars-type compounds, 4.0 g of n-hexadecane, 250 °C, 30 bar of H_2, 0.2 g catalyst during 7 h. [b] Values measured by ICP. [c] TON = mols of products/mols of metal.

4.5. Effect of TiO_2 crystalline phase used as support

Different titanium oxide samples presenting different crystalline phases, such as TiO_2 Nano, TiO_2 P25, TiO_2 Anatase and TiO_2 Rutile were used for the preparation of Pd/TiO_2 type catalysts (XRD patterns in Figure 4.9) to check the effect of support crystalline phases on the catalytic performance of the catalysts in the mild hydrotreatment of tars. Commercial TiO_2 Nano is high surface area nanocrystalline sample majorly composed by anatase phase of titania, while TiO_2 P25 is a widely used titanium oxide sample composed by a mixture of anatase and rutile phases of titania. In addition, TiO_2 Anatase and TiO_2 Rutile are pure commercial samples of titania anatase and rutile phases, respectively. As can be seen in Figure 4.9, Pd(111) diffraction peak was detected in all Pd-based catalysts. Table 4.10 shows the main textural and physico-chemical properties, as well

as the catalytic performance of the above-mentioned ≈1.3wt%Pd/TiO_2 materials (see also Figure 4.10). As can be seen, catalytic activity order in terms of both tars conversion and TON encountered for these samples was: Pd/TiO_2 Nano > Pd/TiO_2 P25 > Pd/TiO_2 Anatase > Pd/TiO_2 Rutile. This tendency correlates with the surface areas measured for each one of the supports, as well as with the metal dispersion and metal particle size determined by CO chemisorption (see Table 4.10). Thus, Pd supported onto TiO_2 Nano material possesses the smallest Pd particle size (13 nm), the highest Pd dispersion (also Pd/TiO_2 P25), along with the highest catalytic activity (Conv. ≈75%) towards tars conversion in the mild hydrotreatment process in comparison with the other TiO_2 supports. For instance, Pd/TiO_2 Nano demonstrated to be more active and more selective catalyst towards hydrogenated products, for example tetralin group, compared with the other Ti-based catalysts (see Figure 4.11, selectivity to different products at 35-40% of conversion). Interestingly, the selectivity to hydroacenaphthene (HAce-1), which is a more hydrogenated secondary product derived from primary product acenaphthene (Ace), increased in the following order: Pd/TiO_2 Rutile (18%) < Pd/TiO_2 Anatase (23%) < Pd/TiO_2 P25 (32%) < Pd/TiO_2 Nano (38%). This clearly suggests that Pd/TiO_2 Nano was more active to hydrogenate the ring of Ace to obtain HAce-1 than the other TiO_2-type catalysts. In addition, the selectivities to the different groups of products at different reaction times are listed in Tables 4.7, 4.11, 4.12 and 4.13 for Pd/TiO_2 Nano, Pd/TiO_2 P25, Pd/TiO_2 Anatase and Pd/TiO_2 Rutile catalysts, respectively. Therefore, these data let us to

conclude that Pd/TiO_2 Nano catalyst is the more active and selective towards the hydrogenated products among the different TiO_2-supported Pd catalysts here tested.

Table 4.10. Main textural and physico-chemical properties and catalytic performance in tars mild hydrotreatment for different titanium oxides-supported Pd catalysts.[a]

Catalyst	Pd (wt%) [b]	S_{BET} Support (m^2/g)[c]	Particle dispersion (%)[d]	Particle size (nm)[d]	Conv. (mol%)	TON [e]
Pd/TiO_2 Nano	1.3	162	8.1	13	75	91
Pd/TiO_2 P25	1.4	50	8.9	13	66	67
Pd/TiO_2 Anatase	1.4	11	2.3	49	44	46
Pd/TiO_2 Rutile	1.3	2	1.1	103	35	38

[a] Reaction conditions: 0.5 g of tars-type compounds, 4.0 g of n-hexadecane, 250 °C, 30 bar of H_2, 0.2 g catalyst during 7 h. [b] Values measured by ICP. [c] Calculated values from N_2 adsorption isotherms (BET method); [d] Average diameter of Pd nanoparticles and Pd dispersion calculated by CO chemisorption, with the stoichiometry being Pd:CO = 1:1. [e] TON = mols of products/mols of metal.

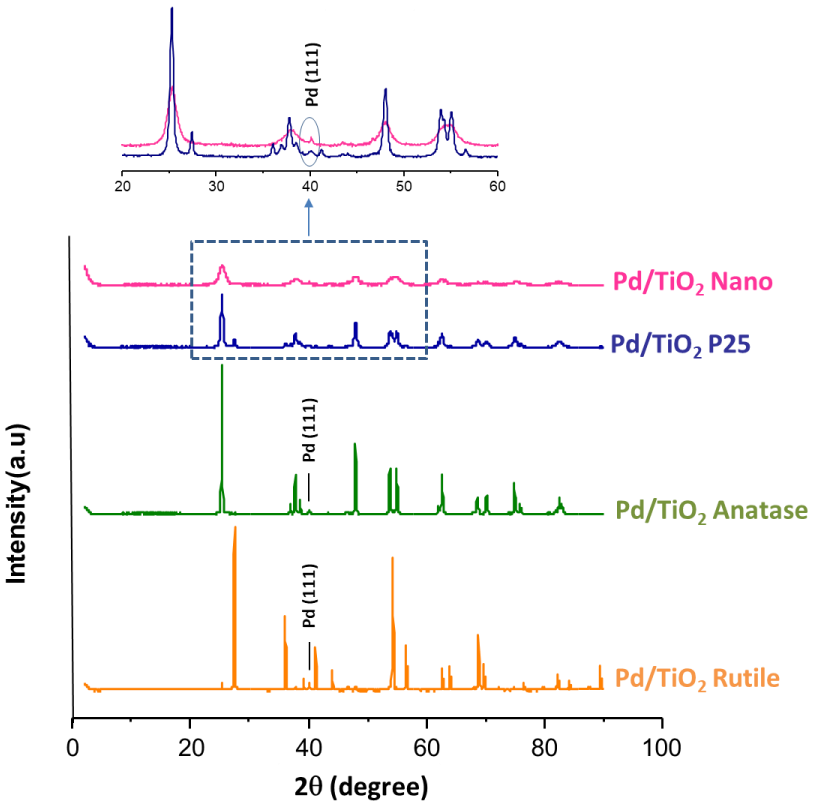

Figure 4.9. X-ray diffraction patterns of different TiO_2-supported Pd catalysts (Inset showing a zoom of 20-60 º region for Pd/TiO_2 Nano and Pd/TiO_2 P25).

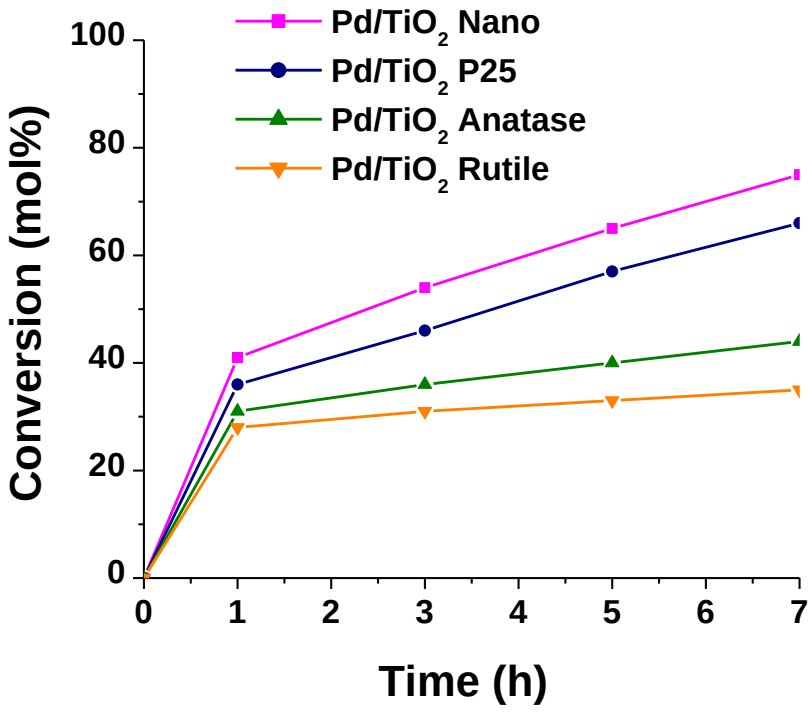

Figure 4.10. Conversion vs time for different TiO_2-supported Pd catalysts in mild hydrotreatment of tars. Reaction conditions: 0.5 g of tars-type compounds, 4.0 g of n-hexadecane, 0.2 g of catalyst, 250 °C, 30 bar of H_2 during 7 h.

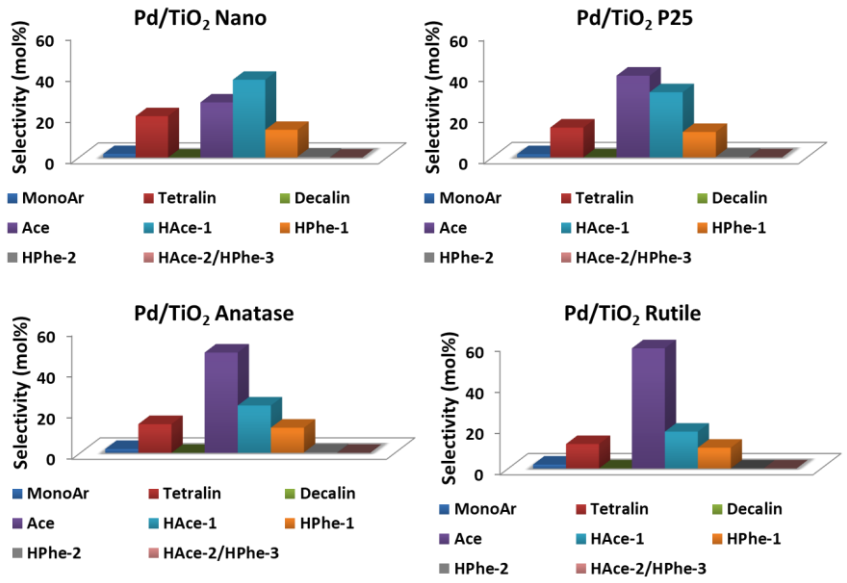

Figure 4.11. Selectivity to the different groups of products for TiO_2-supported Pd catalysts (at 35-40% of conversion). Reaction conditions: 0.5 g of tars-type compounds, 4.0 g of n-hexadecane, 0.2 g of catalyst, 250 °C, 30 bar of H_2 during 7 h.

Table 4.11. Selectivity to the different products groups for 1.4wt%Pd/TiO_2 P25 at 250 °C and 30 bar of H_2.

Time (h)	Conv. (mol%)	Product selectivity (mol%)							
		MonoAr	Tetralin	Decalin	Ace	HAce-1	HPhe-1	HPhe-2	HAce-2/HPhe-3
0	0	0.0	0.0	0.0	0.0	0.0	0.0	0.0	0.0
1	36	1.5	14.5	0.0	39.7	31.7	12.4	0.3	0.0
3	46	1.6	24.3	0.0	14.1	41.5	17.6	0.9	0.0
5	57	1.6	33.0	0.0	2.4	42.0	18.9	2.2	0.0
7	66	1.5	37.6	0.0	0.0	37.8	17.1	2.9	0.0

Table 4.12. Selectivity to the different products groups for 1.4wt%Pd/TiO_2 Anatase at 250 °C and 30 bar of H_2.

Time (h)	Conv. (mol%)	Product selectivity (mol%)							
		MonoAr	Tetralin	Decalin	Ace	HAce-1	HPhe-1	HPhe-2	HAce-2/HPhe-3
0	0	0.0	0.0	0.0	0.0	0.0	0.0	0.0	0.0
1	31	1.4	8.9	0.0	68.5	13.6	7.6	0.0	0.0
3	36	1.9	14.0	0.0	48.7	23.0	12.2	0.2	0.0
5	40	2.0	17.9	0.0	35.0	29.3	15.4	0.4	0.0
7	44	2.0	19.4	0.0	24.5	30.7	16.1	0.5	0.0

Table 4.13. Selectivity to the different products groups for 1.3wt%Pd/TiO_2 Rutile at 250 °C and 30 bar of H_2.

Time (h)	Conv. (mol%)	Product selectivity (mol%)							
		MonoAr	Tetralin	Decalin	Ace	HAce-1	HPhe-1	HPhe-2	HAce-2/HPhe-3
0	0	0.0	0.0	0.0	0.0	0.0	0.0	0.0	0.0
1	28	1.0	5.8	0.0	81.4	7.7	4.2	0.0	0.0
3	31	1.4	7.5	0.0	74.3	10.8	6.0	0.0	0.0
5	33	1.6	9.8	0.0	65.8	14.7	8.1	0.0	0.0
7	35	1.9	11.9	0.0	58.4	17.9	10.1	0.0	0.0

With the aim of establishing structure-activity relationships of the here selected TiO_2-supported Pd catalysts, their acidic properties were studied through NH_3-TPD, and the amounts of adsorbed ammonia representing the total amount of acid sites determined for each sample are listed in Table 4.14. For instance, the total amounts of acid sites encountered for Pd/TiO_2 Nano and Pd/TiO_2 P25 were 367 and 200 µmol/g, respectively. Both catalytic samples presented a broad distribution of the ammonia adsorption-desorption peak from

100-500 °C. Thus, whereas Pd/TiO_2 P25 showed only one broad peak at 250 °C, Pd/TiO_2 Nano showed two peaks at 250 °C and 350 °C, respectively (see Figure 4.12). Noticeably, these two peaks for Pd/TiO_2 Nano were distributed in two regions, related to weaker acid sites for the peak at lower temperature (250 °C) and stronger acid sites for the peak at higher temperature (350 °C). However, very low interaction of ammonia with Pd/TiO_2 Anatase and Pd/TiO_2 Rutile was detected (practically no peaks observed in Figure 4.12), this leading to low values of total amounts of acid sites appearing in Table 4.14 (43 and 23 μmol/g, respectively). Summarizing, TiO_2 Nano and TiO_2 P25 were found as the more acidic samples, also having the higher surface areas, both combined properties improved their catalytic properties for the conversion of tars-type compounds. Thus, the higher conversion was observed for Pd/TiO_2 Nano followed by TiO_2 P25 catalyst. More importantly, the higher selectivities towards the more hydrogenated products (i.e., tetralin, HAce-1, etc.) were also observed with these two catalysts (see Figure 4.11).

Additionally, and aiming at investigating the reducibility of Pd species, H_2-TPR measurements of the different TiO_2-supported Pd catalysts were performed and the total amount of adsorbed H_2 in each case is reported in Table 4.14 (see also H_2-TPR profiles in Figure 4.13). For Pd/TiO_2 Nano and Pd/TiO_2 P25, a band with the maximum centered at 378 °C and 392 °C, respectively, was identified and their corresponding H_2 uptakes (193 and 115 μmol/g, respectively) were calculated. On the contrary, practically no H_2 adsorption peaks were

detected for Pd/TiO_2 Rutile and Pd/TiO_2 Anatase. Therefore, negligible hydrogen consumption occurred in both Pd/TiO_2 Anatase and Pd/TiO_2 Rutile samples. TPR profiles (Figure 4.13) showed a negative peak at 63 ºC for all the samples, although the intensity of this peak changed depending on the support type. This peak corresponds to H_2 desorption from Pd hydrides PdH_x species, which are produced through H_2 adsorption/diffusion in the Pd^0 crystallites at lower temperature [5]. For instance, the intensity of this negative peak for the Pd/TiO_2 catalysts here studied increased in this order: Pd/TiO_2 Nano < Pd/TiO_2 P25 < Pd/TiO_2 Anatase < Pd/TiO_2 Rutile. From H_2-TPR data, Pd/TiO_2 Nano, followed by Pd/TiO_2 P25, appeared to have higher capability for adsorbing and dissociating H_2 at the catalyst surface than the other Pd/TiO_2 catalysts.

Table 4.14. Quantitative data for NH_3-TPD and H_2-TPR measurements of TiO_2-supported Pd catalysts.

Catalyst	Total amount of acid sites (μmol/g)	Total amount of adsorbed H_2 (μmol/g)
Pd/TiO_2 Nano	367	193
Pd/TiO_2 P25	200	115
Pd/TiO_2 Anatase	43	<1
Pd/TiO_2 Rutile	23	<1

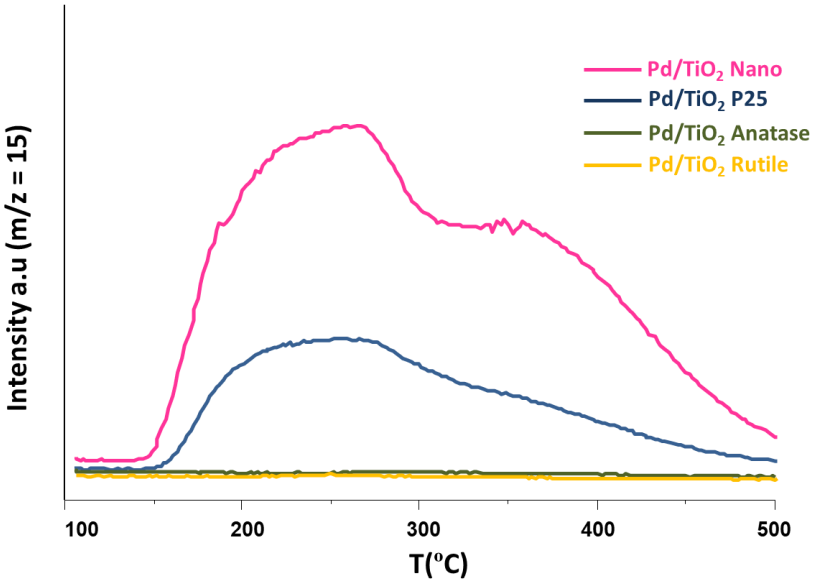

Figure 4.12. NH_3-TPD profiles for different TiO_2-supported Pd catalysts.

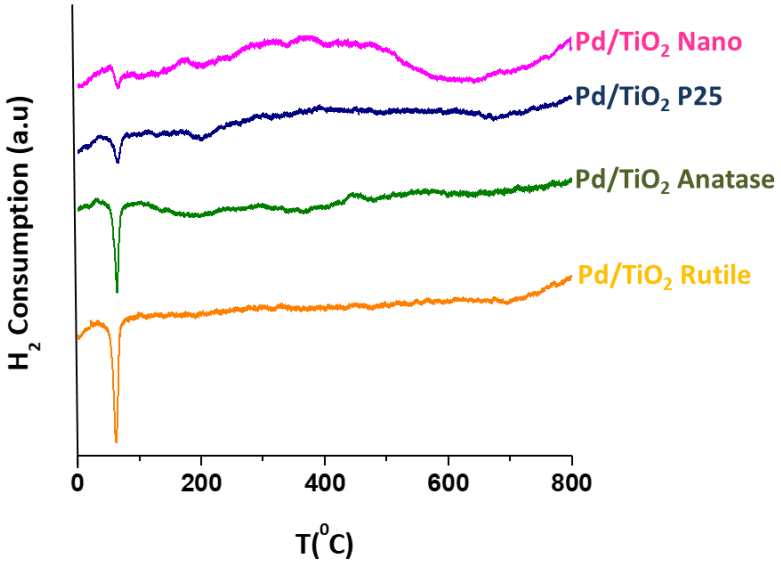

Figure 4.13. H_2-TPR profiles for different TiO_2-supported Pd catalysts.

In light of all the above-mentioned, and mainly taking into consideration the most relevant textural and physico-chemical (acidity, surface area, Pd nanoparticles sizes, etc.) properties, together with the catalytic properties up to now evidenced, Pd/TiO_2 Nano was selected as the adequate catalyst for the mild hydrotreatment of tars-type compounds, and further studies were performed aiming at optimizing its usage in this process.

4.6. Effect of reaction conditions for Pd/TiO_2 Nano catalyst

Optimization of the operational conditions in tars mild hydrotreatment for 1.3wt%Pd/TiO_2 Nano catalyst was performed by studying the effect of reaction parameters such as temperature, H_2 pressure and catalyst loading on both tars-type compounds conversion and selectivity towards the more hydrogenated products. On one hand, reactions at 250 °C, 275 °C and 300 °C were carried out to evaluate the influence of temperature on the catalytic activity of Pd/TiO_2 Nano catalyst. As shown in Figure 4.14A, the conversion increased from 75% at 250 °C to ≈90% at 275 °C, and no significant difference was detected with further increasing the temperature till 300 °C. Meanwhile, as depicted in Figure 4.15, from moderate to high selectivity to tetralin and other more hydrogenated products groups (i.e., HPhe-2) was found when increasing the temperature from 250 °C to 275 °C (and 300 °C). In addition, the selectivities to the different groups of products at different reaction times of Pd/TiO_2 Nano

catalyst working at different temperatures are listed in Tables 4.7, 4.15 and 4.16, respectively at 250 ºC, 275 ºC and 300 ºC.

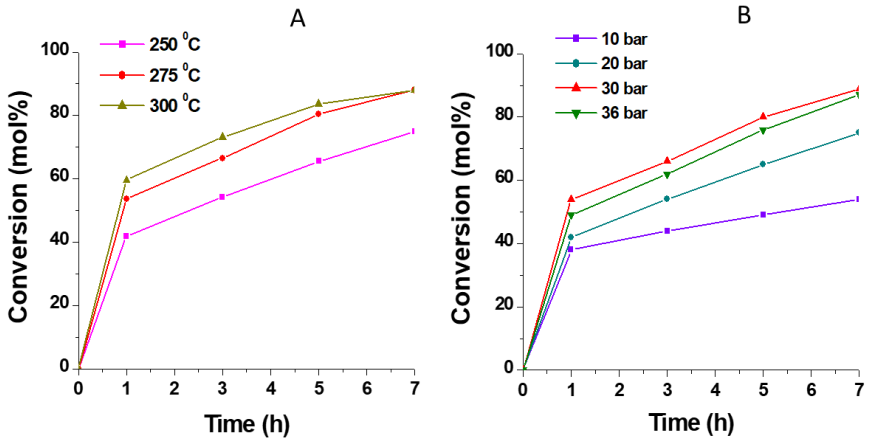

Figure 4.14. Conversion vs time for 1.3wt%Pd/TiO_2 Nano in tars mild hydrotreatment: (A) At 30 bar of H_2, 0.2 g catalyst, during 7 h ; (B) At 275 °C, 0.2 g catalyst, during 7 h.

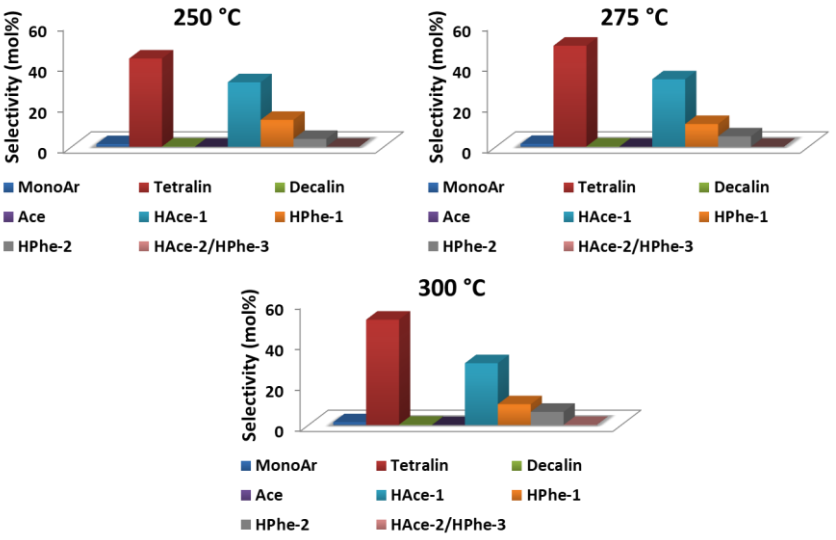

Figure 4.15. Selectivity to the different groups of products for 1.3wt%Pd/TiO_2 Nano (compared at ≈75% of conversion) at different temperatures. Reaction conditions: 0.5 g of tars-type compounds, 4.0 g of n-hexadecane, 0.2 g of catalyst, 30 bar of H_2 during 7 h.

Table 4.15. Selectivity to the different products groups for 1.3wt%Pd/TiO_2 Nano, 275 °C, 30 bar of H_2.

Time (h)	Conv. (mol%)	Product selectivity (mol%)							
		MonoAr	Tetralin	Decalin	Ace	HAce-1	HPhe-1	HPhe-2	HAce-2/HPhe-3
0	0	0.0	0.0	0.0	0.0	0.0	0.0	0.0	0.0
1	53	1.6	34.1	0.0	4.1	43.0	15.5	1.7	0.0
3	66	1.5	45.1	0.0	0.3	36.3	13.0	3.8	0.0
5	80	1.3	53.0	0.3	0.0	29.7	9.2	6.4	0.1
7	88	1.2	55.2	0.5	0.0	25.3	6.0	9.0	0.3

Table 4.16. Selectivity to the different products groups for 1.3wt%Pd/TiO_2 Nano, 300 °C, 30 bar of H_2.

Time (h)	Conv. (mol%)	Product selectivity (mol%)							
		MonoAr	Tetralin	Decalin	Ace	HAce-1	HPhe-1	HPhe-2	HAce-2/HPhe-3
0	0	0.0	0.0	0.0	0.0	0.0	0.0	0.0	0.0
1	59	1.6	42.1	0.0	1.7	36.9	14.4	3.3	0.0
3	73	1.4	51.5	0.2	0.2	30.2	10.2	6.5	0.1
5	84	1.3	56.6	0.4	0.0	25.6	7.3	9.3	0.3
7	88	1.2	56.7	0.4	0.0	22.2	6.4	10.5	0.4

On the other hand, the influence of the H_2 pressure on the catalytic performance of the 1.3wt%Pd/TiO_2 Nano was investigated at 275 °C using 0.2 g of catalyst during 7 h. The reactions were carried out at 10, 20, 30 and 36 bar of H_2. As shown in Figure 4.14B, the conversion increased from 54% to ≈90% when increasing the H_2 pressure from 10 to 30 bar, while practically similar conversions were observed at both 30 and 36 bar of H_2; this probably due to the limitations of H_2 solubility in the n-hexadecane under the reaction conditions and the autoclave-type reactor here used (see section 3.4.1). In addition, as seen in Figure 4.16, similar selectivities to the different groups of products (compared at the same level of conversion), were found when working at 275 °C and H_2 pressure ≥20 bar. However, the catalyst showed higher selectivity to the less hydrogenated primary product acenaphthene (Ace) when working at 10 bar of H_2. Moreover, the selectivities to the different groups of products at different reaction times of Pd/TiO_2 Nano catalyst working at 275 ºC and different H_2

pressures are listed in Tables 4.15 (30 bar), 4.17 (10 bar), 4.18 (20 bar) and 4.19 (36 bar).

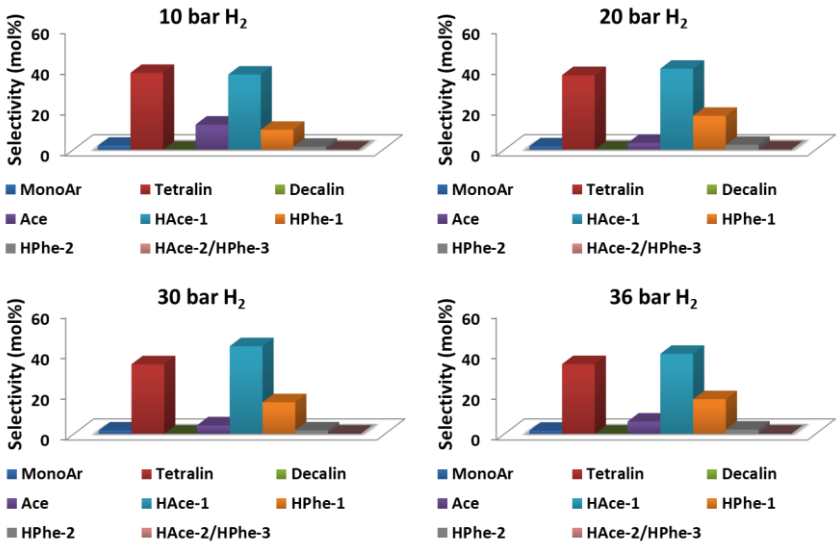

Figure 4.16. Selectivity to the different groups of products for 1.3wt%Pd/TiO_2 Nano (at ≈53% of conversion) at different H_2 pressures. <u>*Reaction conditions*</u>*: 0.5 g of tars-type compounds, 4.0 g of n-hexadecane, 0.2 g of catalyst, 275 °C during 7 h.*

Table 4.17. Selectivity to the different products groups for 1.3wt%Pd/TiO_2 Nano, 275 °C, 10 bar of H_2.

Time (h)	Conv. (mol%)	Product selectivity (mol%)							
		MonoAr	Tetralin	Decalin	Ace	HAce-1	HPhe-1	HPhe-2	HAce-2/HPhe-3
0	0	0.0	0.0	0.0	0.0	0.0	0.0	0.0	0.0
1	38	1.8	15.5	0.0	49.4	25.3	8.1	0.0	0.0
3	44	2.1	25.2	0.0	26.8	35.1	10.2	0.5	0.0
5	49	1.9	30.4	0.0	18.1	38.0	10.7	0.9	0.0
7	54	1.9	37.7	0.0	12.3	36.9	9.7	1.4	0.0

Table 4.18. Selectivity to the different products groups for 1.3wt%Pd/TiO_2 Nano, 275 °C, 20 bar of H_2.

Time (h)	Conv. (mol%)	Product selectivity (mol%)							
		MonoAr	Tetralin	Decalin	Ace	HAce-1	HPhe-1	HPhe-2	HAce-2/HPhe-3
0	0	0.0	0.0	0.0	0.0	0.0	0.0	0.0	0.0
1	42	1.8	23.4	0.0	21.0	39.8	13.6	0.4	0.0
3	45	1.6	32.6	0.0	6.4	41.0	16.6	1.8	0.0
5	64	1.5	40.5	0.0	0.0	38.5	16.6	2.9	0.0
7	75	1.4	53.3	0.2	0.0	29.6	8.4	6.0	0.0

Table 4.19. Selectivity to the different products groups for 1.3wt%Pd/TiO_2 Nano, 275 °C, 36 bar of H_2.

Time (h)	Conv. (mol%)	Product selectivity (mol%)							
		MonoAr	Tetralin	Decalin	Ace	HAce-1	HPhe-1	HPhe-2	HAce-2/HPhe-3
0	0	0.0	0.0	0.0	0.0	0.0	0.0	0.0	0.0
1	49	1.6	28.3	0.0	10.3	41.6	17.2	1.0	0.0
3	63	1.4	40.1	0.0	1.7	36.9	16.8	3.1	0.0
5	77	1.3	49.5	0.1	0.0	30.9	13.2	5.1	0.0
7	87	1.1	50.1	0.2	0.0	24.5	8.5	6.7	0.1

From all these achieved results, the optimal operational conditions to carry out the tars mild hydrotreatment over 1.3wt%Pd/TiO_2 Nano were 275 °C and 30 bar of H_2 pressure. Under these reactions conditions, catalyst loading was also optimized by performing experiments with catalyst ranging from 0.05 to 0.25 g (see Figure 4.17), the maximum conversion being achieved by working with 0.2 g of 1.3wt%Pd/TiO_2 Nano catalyst.

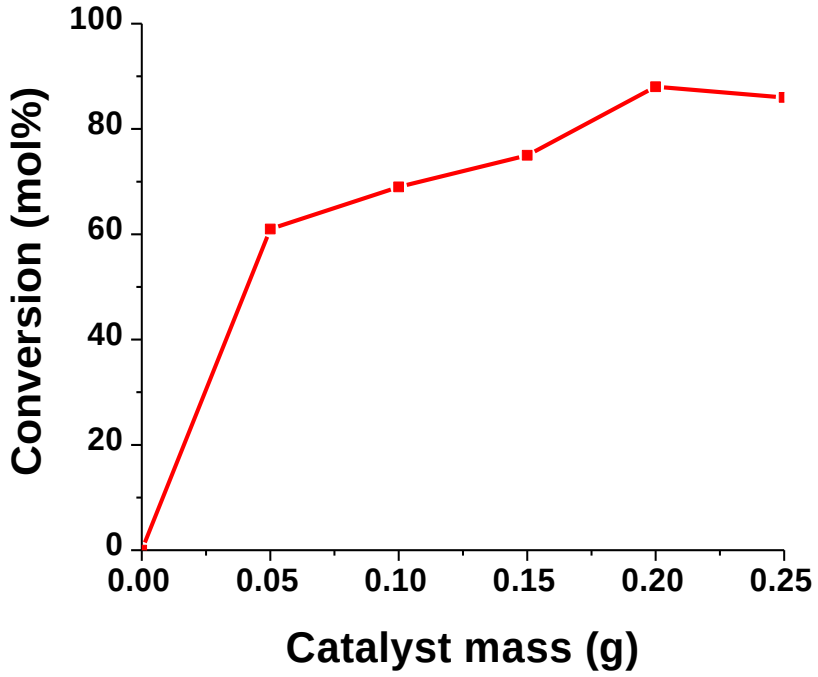

Figure 4.17. Catalyst loading optimization in tars mild hydrotreatment over 1.3wt%Pd/TiO_2 Nano. Reaction conditions: 0.5 g of tars-type compounds, 4.0 g of n-hexadecane, 275 °C, 30 bar of H_2 during 7 h.

4.7. Energy and Hydrogen consumption in function of the temperature using AspenPlus®

In a complementary work done during the investigation of tars-type mild hydrotreatment in our group [6], energy and hydrogen consumption in function of the reaction temperature of the process were evaluated by using AspenPlus®, and results are shown in Figure 4.18. As can be seen, energy consumption increased when increasing the temperature of the process from 250 ºC to 300 ºC. However, this tendency was not found to be the same in the case of hydrogen consumption. In this sense, a slightly lower hydrogen consumption was calculated when the process works at 275 ºC.

Summarizing, operational conditions of the mild hydrotreatment of the tars-type molecules could be adjusted to work at 275 ºC to minimize H_2 consumption, also attaining acceptable energy target. These results are in agreement and justify the optimal reaction conditions selected in previous sections, thus adjusting the atomic economy and the energy efficiency of the process as much as possible.

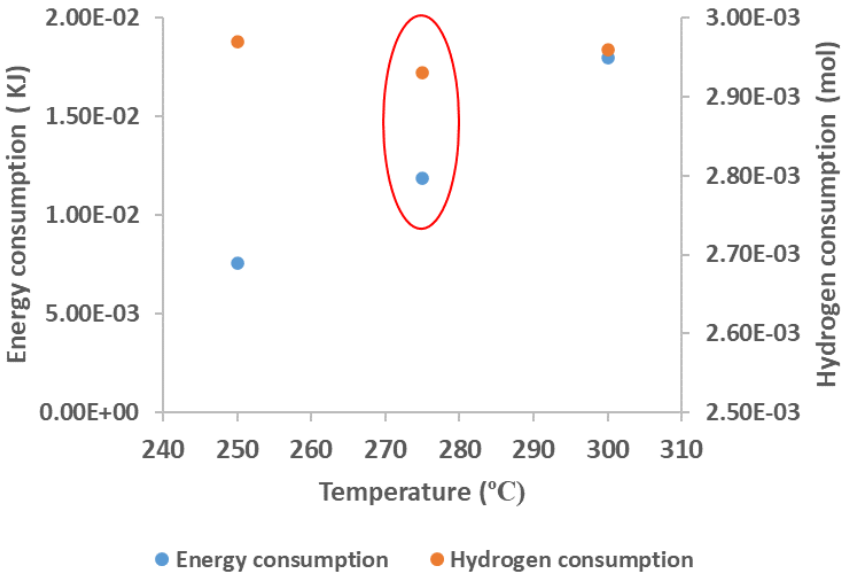

Figure 4.18. Energy and hydrogen consumption in function of the temperature for tars mild hydrotreatment.

4.8. Reusability tests

In general, one important point in the usage of metal-supported type catalysts for the mild hydrotreatment of tars-type molecules depends on the possibility of recycling the solid catalyst several times. In order to evaluate the stability of the here studied 1.3wt%Pd/TiO_2 Nano catalyst under reaction conditions and its remaining activity after several reuses, a set of experiments was performed in which the Pd-based catalyst used in a first reaction was recovered and then recycled at least three more times. Everytime, the spent catalyst recovered from the reaction mixture at the end of the experiment by centrifugation, was then washed with 2-propanol and dried at 100 °C

during 1 h, before its use in a new catalytic experiment (see section 3.4.1.1). Results obtained from reusability tests for Pd-supported on TiO_2 Nano catalysts in tars mild hydrotreatment are summarized in Figure 4.19 and Table 4.20.

As can be seen, the catalytic activity evaluated in terms of tars-type compounds conversion at three different reaction times (1, 3 and 7 h) did not suffer any decay even after four consecutive uses of the catalyst (Figure 4.19). However, after the first use, few amount of carbon was deposited on the catalyst surface, and its percentage increased after three more uses, without affecting the catalytic activity. It is worth to note that after regeneration of the catalyst at 400 ºC under H_2 flow, the carbon deposition strongly decreased (from ≈1.5 to ≈0.6, see Table 4.20). In addition, any Pd leaching was detected after several reuses (Table 4.20).

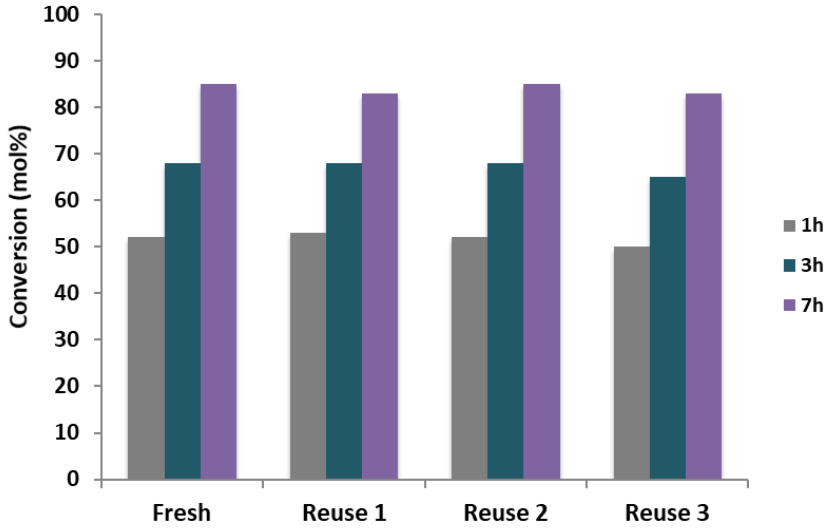

Figure 4.19. Reusability test for 1.3wt%Pd/TiO_2 Nano in mild hydrotreatment of tars. Reaction conditions: 0.5 g of tars-type compounds, 4.0 g of n-hexadecane, 0.2 g of catalyst, 275 °C, 30 bar of H_2.

Table 4.20 Effect of reusability and regeneration with H_2 on carbon deposition over Pd/TiO_2 Nano catalyst in tars mild hydrotreatment.

Pd/TiO_2 Nano	% N[a]	% C[a]	% H[a]	Pd (wt%)[b]	Pd Particle size (nm)[c]
Fresh	0.000	0.085	0.434	1.3	2.7
First use	0.000	0.753	0.368	1.3	-
Third reuse	0.118	1.492	0.280	1.3	2.3
Regeneration	0.078	0.599	0.241	-	2.0

[a] Results from elemental analysis (EA). [b] Values measured by ICP. [c] Average diameter of Pd nanoparticles calculated from TEM measurements of, at least, 100 particles.

HR-TEM measurements of fresh, reused and regenerated Pd/TiO_2 Nano catalysts were performed, and images are shown in

Figures 4.20 and 4.21, where the presence of Pd metallic species can be appreciated. In fact, small particle size was encountered, with average diameter around 2 nm for Pd/TiO_2 fresh, reused and regenerated catalysts (see Table 4.20 and Figure 4.22). In this sense, although the fresh catalyst showed most of Pd particle sizes between 1.0-1.5 nm, there was a certain number of particles with sizes higher than 2 nm, this leading to an average particle size of around 2.7 nm for the fresh material, which evidences that no increase in the particle size occurred after several reuses. This can also be observed from the TEM images of Figure 4.20, where practically no changes in Pd particles sizes and their distribution were observed between fresh, used and regenerated samples.

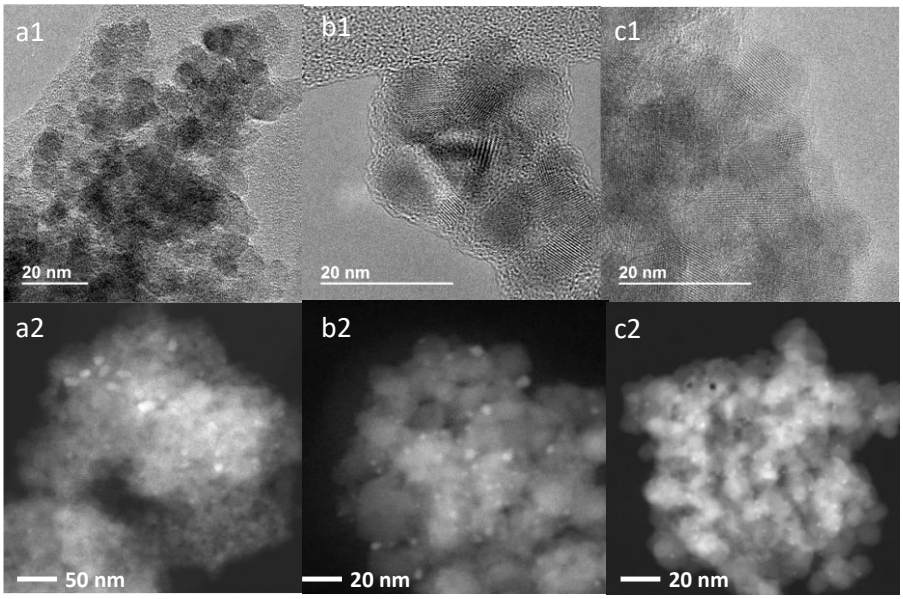

Figure 4.20. HR-TEM (1) and HR-STEM (2) images of a) fresh, b) reused and c) regenerated (with H_2) Pd/TiO_2 Nano catalyst.

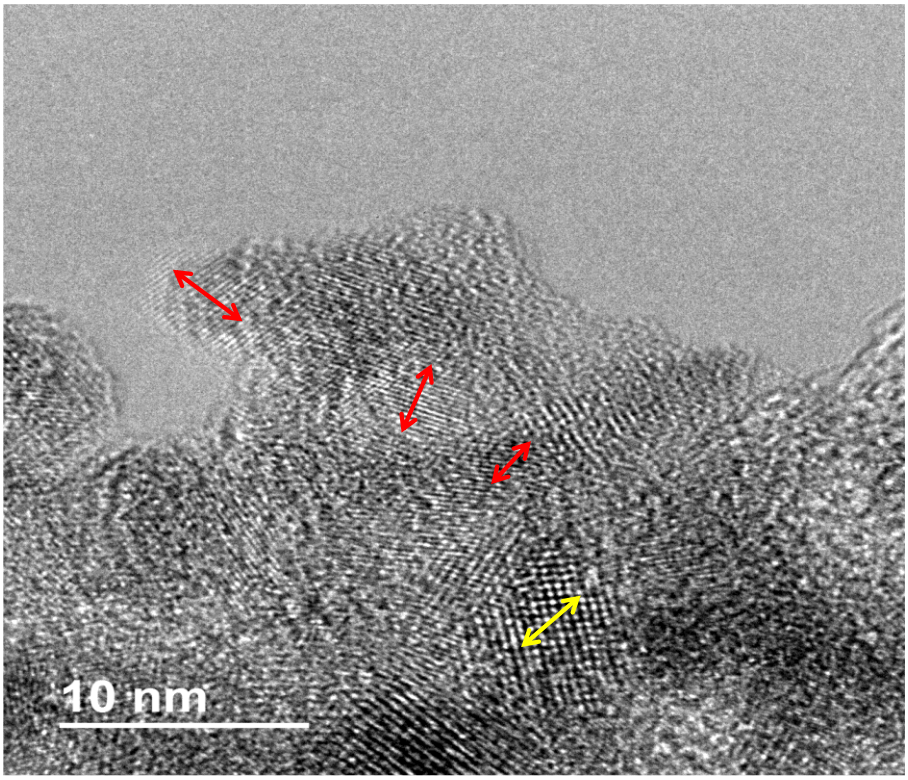

Figure 4.21. HR-TEM image of fresh Pd/TiO_2 Nano catalyst (red: Pd (111) d≈0.22 nm and yellow: Ti (101) d≈0.35 nm).

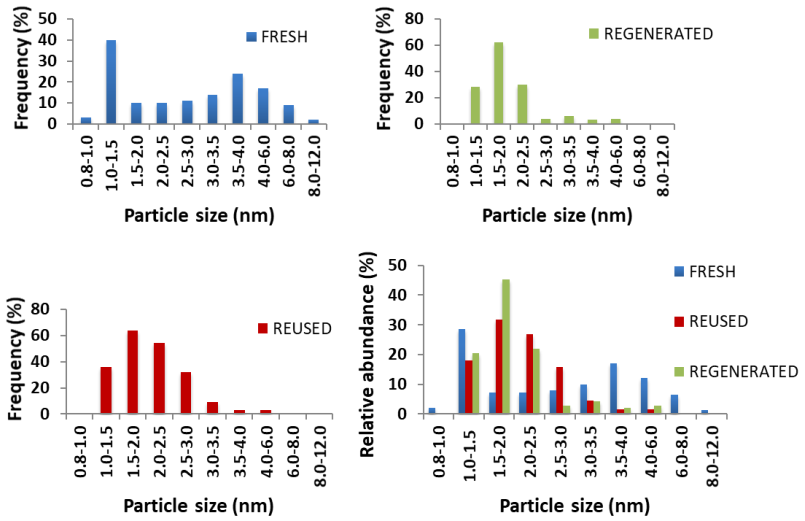

Figure 4.22. Pd particle size distribution of fresh, reused and regenerated samples of Pd/TiO_2 Nano catalyst.

The X-ray diffractions patterns after first use and third reuse of the Pd/TiO_2 Nano catalyst (Figure 4.23) practically showed identical signals for all the measured catalytic samples, with only a small shift in the peak placed at $2\theta = 40^{o}$ assigned to Pd (111), probably due to the transformation of Pd^{0} into Pd^{2+} species. This meaning that the structure of the catalyst remained practically unaltered and just few changes in the Pd species state take place during the hydrotreatment process.

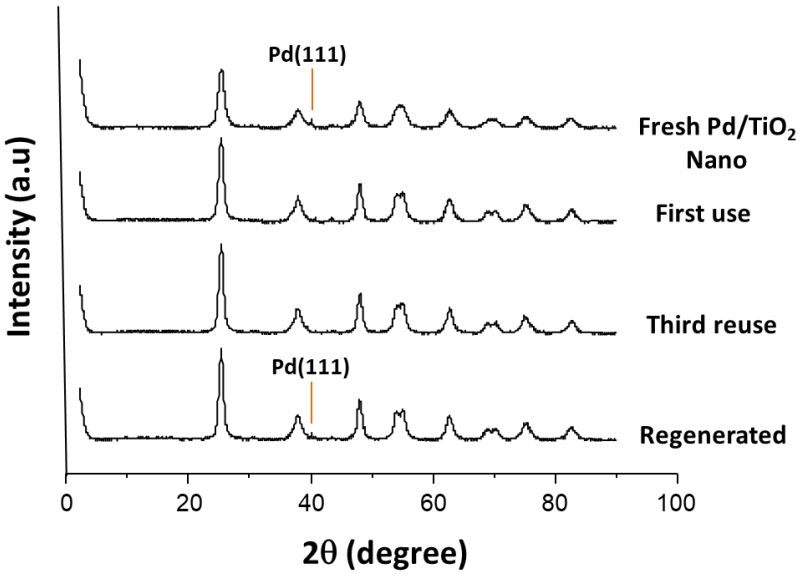

Figure 4.23. X-ray diffraction patterns of fresh, used and regenerated (with H_2) Pd/TiO_2 Nano catalyst.

In order to gain new insights in the role of Pd species in the catalyst and aiming at understanding what was occurring on the solid surface during the reaction, X-ray photoelectron spectroscopy (XPS) analysis was employed to evaluate the electronic properties and the nature of Pd species present before and after reuses in Pd/TiO_2 Nano catalyst. Results of XPS measurements carried out over fresh, reused and regenerated (with H_2) catalyst are presented in Figure 4.24 and Table 4.21a. It was found that Pd 3d spectra of the fresh catalyst can be divided into four components located at 334.64 eV (Pd^0 $3d_{5/2}$), 336.48 eV (Pd^{2+} $3d_{5/2}$), 339.87 eV (Pd^0 $3d_{3/2}$) and 341.84 eV (Pd^{2+} $3d_{3/2}$). For the reused sample, two components were found located at

335.71 eV (Pd^{2+} $3d_{5/2}$) and 340.96 eV (Pd^{2+} $3d_{3/2}$), respectively. And finally, again four components located at 335.07 eV (Pd^0 $3d_{5/2}$), 337.05 eV (Pd^{2+} $3d_{5/2}$), 340.35 eV (Pd^0 $3d_{3/2}$) and 342.05 eV (Pd^{2+} $3d_{3/2}$) were encountered in the Pd 3d spectra of the regenerated catalyst. From these data, the corresponding relative abundance of Pd species present in the catalytic samples was calculated and the results are exposed in Table 4.21b. As can be seen, the fresh catalyst presented a Pd^0/Pd^{2+} species ratio of around 80/20, while after the catalyst usage in the reaction only the presence of Pd^{2+} species (100%) was detected in the solid. Nevertheless, after regeneration with H_2 of the Pd/TiO_2 Nano catalyst, the Pd^0 species are recovered and the Pd^0/Pd^{2+} species ratio is reestablished. In fact, this Pd^0/Pd^{2+} ratio was higher in the regenerated catalyst than in the fresh material.

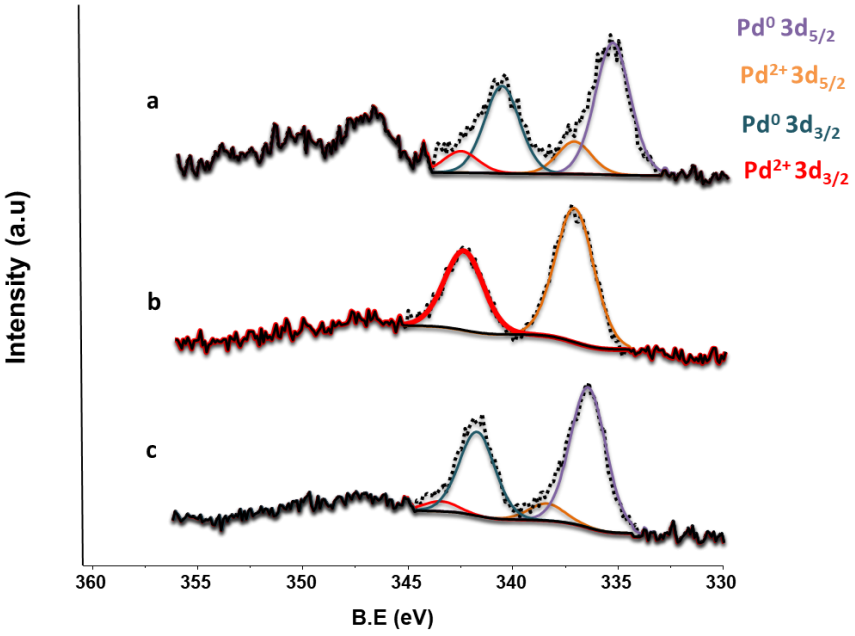

Figure 4.24. X-ray photoelectron spectroscopy (XPS) patterns of Pd 3d for a) fresh, b) after 3 reuses and c) after regeneration with H_2 of Pd/TiO_2 Nano catalyst.

Table 4.21a. X-ray photoelectron spectroscopy (XPS) values of binding energies for the fresh, reused and regenerated (with H_2) Pd/TiO_2 Nano catalyst.

Pd/TiO_2 Nano	Pd $3d_{5/2}$		Pd $3d_{3/2}$	
	Pd^0	Pd^{2+}	Pd^0	Pd^{2+}
Fresh	334.64	336.48	339.87	341.84
Reused	-	335.71	-	340.96
Regenerated	335.07	337.05	340.35	342.05

Table 4.21b. X-ray photoelectron spectroscopy (XPS) values of the percentage of Pd 3d species for the fresh, reused and regenerated (with H_2) Pd/TiO_2 Nano catalyst.

Pd/TiO_2 Nano	% Pd^0 $3d_{5/2}$	% Pd^{2+} $3d_{5/2}$	Pd^0/Pd^{2+}
Fresh	80.98	19.02	4.26
Reused	-	100	-
Regenerated	89.23	10.77	8.29

All these evidences let us to conclude that initially the Pd^0 species present in the Pd/TiO_2 Nano catalyst are responsible for the catalytic activity demonstrated in the hydrotreatment process. Nevertheless, these Pd^0 species are transformed into Pd^{2+} species during the process, the latter species being the only ones present in the used catalyst. Therefore, in order to answer the question of how the used catalyst is capable to maintain its catalytic activity after several reuses, an experiment of tars mild hydrotreatment was performed by using an especially prepared PdO/TiO_2 Nano catalyst by working at 275 °C and 30 bar of H_2 (optimal conditions). The attained results were very similar to those obtained with the Pd/TiO_2 Nano catalyst reduced (activated under H_2 flow) prior to the reaction. This meaning that the catalyst is able to be activated or *"in situ"* reduced under reaction conditions. This fact could explain the maintained catalytic activity after reuses, where the catalyst was *"in situ"* reactivated with H_2 and Pd^{2+} species formed during hydrotreatment process were

transformed into Pd^0 (redox cycle) under these reaction conditions, which confirmed the stability and the reusability of the catalyst.

Summarizing, all these data revealed the remarkable stability of the Pd/TiO_2 Nano catalyst in the tars mild hydrotreatment, which can be efficiently reused several times with practically no changes in TiO_2 structure, quite low carbon deposition, any Pd leaching detected and maintaining both small Pd particle size and their adequate distribution, even after regeneration of the catalyst.

4.9. Comparison with commercial catalysts and previously reported catalysts

Up to now, the Pd/TiO_2 Nano material here studied has demonstrated to be an efficient and stable catalyst in the tars-type compounds mild hydrotreatment for obtaining hydrogenated and partially hydrogenated hydrocarbons in the C9-C15 range. Of course, a wide range of metal-supported catalysts have been used for the hydrotreatment of tars molecules. Therefore, comparison of our Pd/TiO_2 Nano material with some selected and previously reported hydrotreatment catalysts under the reaction conditions employed in this work was done, and the achieved results are summarized in Table 4.22 (see also Table A4.1 in Annex). As can be seen, our Pd/TiO_2 Nano catalyst was more active (higher conversion and comparable TONs) than Pd/Al_2O_3 and Pt/Al_2O_3 catalysts, also showing better selectivity to the more hydrogenated products (tetralin and others). With respect to CoMo- and NiMo-based commercial catalysts,

Pd/TiO_2 Nano showed higher conversion than that of $CoMoS/SiO_2$-Al_2O_3 and comparable to that observed with $NiMoS/Al_2O_3$; however, Pd/TiO_2 Nano was encountered to be more active having higher TON (103) than the one calculated for both NiMo- and CoMo-based samples (TON = 7), along with less carbon deposition on the catalyst surface after reaction. In addition, although the conversion achieved with Pd and Pt supported on zeolite USY was higher than in the case of Pd/TiO_2 Nano, significant difference in the mass balance values and carbon deposition was detected. In the same way, zeolite-supported materials showed different selectivity in comparison with Pd/TiO_2 Nano and $NiMoS/Al_2O_3$, which were encountered to be selective to the same type of hydrogenated or partially hydrogenated products. For instance, as mentioned in Table 4.22, Pd/USY and Pt/USY showed higher selectivity to monoaromatics (including BTXs in this case) than Pd/TiO_2 Nano, and lower selectivity to the hydrogenated or partially hydrogenated products such as tetralin, HPhe-1 and HPhe-2. In addition, from the values of mass balance and the higher selectivity to some cracked products, it could be concluded that higher amounts of gases were produced over Pd/USY and Pt/USY, along with some other by-products (i.e., alkylated and dialkylated aromatics), which do not form part of our interest in this specific study. Thus, in spite of the higher activity of metal supported on zeolites (mainly due to their hydrocracking properties), the high production of gases and coke (deposited on the catalyst surface), along with the low production of hydrogenated products become important

disadvantages when the production of partially hydrogenated C9-C15 range hydrocarbons are the targeted products.

Table 4.22. Catalytic activity comparison between Pd/TiO_2 Nano and other commercial catalysts in the tars mild hydrotreatment.[a]

Catalyst	Conv. (mol%)	TON[d]	Mass balance (%)	Product selectivity (mol%)			% C
				MonoAr	Tetralin	HPhe-1/HPhe-2	
Pd/TiO_2 Nano	88	103	98	1.2	55.2	6.0/9.0	0.8
Pd/Al_2O_3[b]	69	97	91	1.4	37.4	11.9/3.1	0.9
Pt/Al_2O_3[b]	57	143	91	2.2	27.1	14.9/0.0	0.7
NiMoS/Al_2O_3[c]	93	7	94	1.3	54.3	5.2/9.1	2.0
CoMoS/SiAl[c]	73	7	90	1.8	42.2	10.4/3.0	1.7
Pd/USY[b]	98	85	54	5.5	33.6	1.3/3.4	10.0
Pt/USY[b]	98	144	54	5.0	36.7	1.1/4.2	15.7

[a] Reaction conditions: 0.5 g of tars-type compounds, 4 g of n-hexadecane, at 275 °C and 30 bar of H_2 during 7 h. [b] For Pd- and Pt-based catalysts, metal content ≈1.0wt%, except for Pd/TiO_2 Nano (1.3wt%). [c] In NiMoS/Al_2O_3, Ni content = 3.3wt% and Mo content = 12.0wt%; and in CoMoS/SiO_2-Al_2O_3, Co content = 2.8wt%; and Mo content = 8.0wt%. [d] TON = mols of products / mols of Metal in catalyst.

4.10. Effect of Pd doping with another metal

After achieving good results with Pd supported on TiO_2 Nano catalyst, the influence of adding another metal along with Pd was investigated. For this purpose, different metal-doped Pd/TiO_2 Nano materials were prepared by incorporating small amounts of metals such as Pt, Ga, Fe, La, Ni, and Cu together with Pd onto the TiO_2 support via incipient wetness impregnation method (see section 3.2.4, Chapter 3). The Pd(Metal)/TiO_2 Nano catalysts thus prepared were screened in the mild hydrotreatment of tars-type compounds and their catalytic activity was compared with that of the non-doped Pd/TiO_2 Nano catalyst. The obtained results in terms of tars conversion and yields to the different products groups are summarized in Tables 4.23 and 4.24, respectively.

As can be seen in Table 4.23, the catalytic activity of the metal-doped Pd catalysts was not improved compared with non-doped Pd catalyst in most of the cases, except for Pd-Pt doped sample which showed similar activity compared to non-doped Pd material. Additionally, as can be seen in Table 4.24, the yield of Tetralin, HAce-1 and HPhe-2 products groups (more hydrogenated products) decreased when the conversion of tars molecules decreased for the metal-doped Pd catalysts. Simultaneously, the yield of Ace (less hydrogenated product) increased in these cases, this showing the lower hydrogenating activity of the metal-doped Pd catalysts, and evidencing the superior catalytic performance of the non-doped Pd/TiO_2 Nano catalyst for the mild hydrotreatment of tars.

Table 4.23. Catalytic activity comparison between metal-doped PdM/TiO_2 Nano and non-doped Pd/TiO_2 Nano catalysts (M = Metal).[a]

Catalyst	Pd (wt%)[b]	Metal (wt%)[b]	Conversion (mol%)	TON[c]
Pd/TiO_2	1.3	-	88	103
PdPt/TiO_2	1.2	0.4	89	100
PdGa/TiO_2	1.5	0.4	65	53
PdFe/TiO_2	1.5	0.6	64	39
PdCu/TiO_2	1.4	0.6	52	32
PdLa/TiO_2	1.5	0.7	44	37
PdNi/TiO_2	1.5	0.5	39	22

[a] Reaction conditions: 0.5 g of tars-type compounds, 4.0 g of n-hexadecane, at 275 °C and 30 bar of H_2 during 7 h. [b] Values measured by ICP. [c] TON = mols of products / mols of metal in catalyst.

Table 4.24. Yields of the different groups of products for metal-doped PdM/TiO_2 Nano and non-doped Pd/TiO_2 Nano catalysts.[a]

Catalyst	Conv. (mol%)	Product yield (mol%)							
		Mono Ar	Tetralin	Decalin	Ace	HAce-1	HPhe-1	HPhe-2	HAce-2/HPhe-3
Pd/TiO_2	88	1.0	49.3	0.4	0.0	22.6	5.4	8.0	0.2
PdPt/TiO_2	89	1.1	49.4	0.6	0.0	22.0	5.3	7.0	0.1
PdGa/TiO_2	65	1.0	27.1	0.0	0.8	22.5	8.3	2.3	0.0
PdFe/TiO_2	64	0.6	24.6	0.0	1.0	22.1	7.5	2.1	0.0
PdCu/TiO_2	52	0.8	15.0	0.0	6.1	16.6	6.0	0.5	0.0
PdLa/TiO_2	44	1.0	9.8	0.0	9.7	14.6	7.2	0.4	0.0
PdNi/TiO_2	39	1.2	5.1	0.0	15.5	5.4	2.7	0.2	0.0

[a] Reaction conditions: 0.5 g of tars-type compounds, 4.0 g of n-hexadecane, at 275 °C and 30 bar of H_2 during 7 h.

4.11. Conclusions

- The mild hydrotreatment of a model mixture of tars-type compounds (i.e., naphthalene, 1-methylnaphthalene, acenaphthylene and phenanthrene) simulating those produced from petroleum distillation or from biomass gasification, into hydrogenated and partially hydrogenated products in the range of C9-C15 was studied over Pd supported on TiO_2 catalysts.
- The hydrotreatment activity and selectivity towards the desired hydrogenated products (i.e., tetralin and others) were strongly dependent on the amount of acid sites and the surface area of the catalysts, together with Pd particle size and their proper distribution. Thus, the increase in both acidity and surface area of the catalyst, along with the presence of small and well distributed Pd nanoparticles, lead to an improvement in the activity for the mild hydrotreatment of tars. Among different TiO_2 crystalline phases used as supports, TiO_2 Nano possessing majorly titania Anatase phase was found as the more adequate to accommodate small Pd nanoparticles.
- For the optimized 1.3wt%Pd/TiO_2 Nano catalyst, the operational conditions encountered to maximize both conversion and selectivity to the desired products were: 275 °C, 30 bar of H_2 and 0.2 g of catalyst during 7 h.
- More interestingly, after consecutive reuses, Pd/TiO_2 Nano catalyst remained active and stable, with very low carbon deposition, any Pd leaching detected, and practically no changes in

the Pd nanoparticle size, even after regeneration (with H_2) of the used catalyst. Thus, although Pd^0 active species were transformed into Pd^{2+} species during the hydrotreatment process, the Pd metallic species were recovered when the used catalyst was added to the reaction medium for a new test via an "in situ" reduction, similarly to what could be achieved by "ex situ" regeneration under H_2 flow.

- Finally, the activity of Pd/TiO_2 Nano catalyst in the tars mild hydrotreatment was discussed in comparison with other previously reported hydrotreating catalysts, such as $CoMoS/SiO_2$-Al_2O_3 and $NiMoS/Al_2O_3$, as well as metal supported on alumina and zeolite H-USY. For instance, Pd/TiO_2 Nano catalyst demonstrated to be more active and selective than metal supported on alumina and CoMo-based catalysts, with conversion values comparable to those of $NiMoS/Al_2O_3$ but having much higher TON and less carbon deposition. Additionally, other types of products (higher amounts of gases, light hydrocarbons and monoaromatics) were generated with Pd/USY as catalyst, along with high carbon deposition on the catalyst surface.
- The catalytic activity of Pd/TiO_2 Nano catalyst was not improved by doping with metal along with Pd, the metal-doped Pd catalysts showing lower hydrogenating capacity compared with the non-doped Pd/TiO_2 Nano sample.
- In summary, Pd/TiO_2 Nano catalyst was encountered as an efficient and stable catalyst for the mild hydrotreatment of tars-type compounds for obtaining hydrogenated and partially

hydrogenated C9-C15 hydrocarbon products that could be applied as fuels components or additives (i.e., jet-fuel improvers) or as chemicals and solvents for industry.

4.12. References

[1] D. P. Upare, S. Park, M. S. Kim, Y.- P. Jeon, J. Kim, D. Lee, J. Lee, H. Chang, S. Choi, W. Choi, Y.-K. Park, C. W. Lee, Journal of Industrial and Engineering Chemistry 46 (2017) 356-363.

[2] T. Kaufmann, A. Kaldor, G. Stuntz, M. Kerby, L. Ansell, Catalysis Today 62 (2000) 77.

[3] C. Li, K. Suzuki, Resources, Conservation and Recycling 54 (2010) 905–915.

[4] K. Maniatis, A.A.C.M. Beenackers, Biomass and Bioenergy 18 (2000) 1–4.

[5] V.A. de la Peña O'Shea, M.C. Alvarez-Galván, J.L.G. Fierro, P.L. Arias, Applied Catalysis B: Environmental 57 (2005) 191-199.

[6] Master thesis of Fernando Llerena Corral entitled "Estudio teórico de procesos de hidrotratamiento catalítico de alquitranes y derivados de biomasa", 2019-2020.

CHAPTER 5.

TITANIA-ALUMINA-SUPPORTED PD CATALYSTS FOR THE MILD HYDROTREATMENT OF TARS-TYPE COMPOUNDS

5.1. Introduction

In continuation of our previous study on the preparation of metal supported catalyst for the mild hydrotreatment of tars-type compounds, and after the interesting results achieved with Pd supported on TiO_2 Nano material (see Chapter 4), the work is focused on the development of novel Pd supported on mixed metal oxide catalysts. Ideally, these Pd-based catalysts will optimize the catalytic performance for tars-type compounds transformation or at least achieve similar catalytic results compared to Pd/TiO_2 Nano material, but by decreasing the amount of Ti in the material. For instance, mixed metal oxides can be easily synthesized in wide range of metal composition via cheap and easy scale-up processes such as co-precipitation method (section 3.2.1), leading to mixed metal oxides with high surface areas.

In this context, and as starting point for this part of the work, mixed metal oxides with different metal composition, such as TiO_2-Al_2O_3, TiO_2-ZrO_2, TiO_2-SiO_2, ZrO_2-Al_2O_3 and SiO_2-Al_2O_3 have been prepared by co-precipitation method. Afterwards, Pd nanoparticles have been supported onto these different mixed metal oxides via incipient wetness impregnation method (section 3.2.3). The catalytic activity of these here prepared Pd-catalysts is evaluated in the mild hydrotreatment of tars-type compounds by working at 250 ºC and 30 bar of H_2 (section 3.4.1). Among the different mixed metal oxides, TiO_2-Al_2O_3 has been selected and considered as the most adequate support for Pd nanoparticles. In addition, synthesis parameters such as

Ti/Al molar ratio, pH during co-precipitation, addition rate of ammonia solution, along with the aging time are investigated in this work.

One important point to be addressed during the study of the selected Pd supported on TiO_2-Al_2O_3 catalyst relays on its reusability and resistance to carbon deposition after consecutive reuses, also comparing its catalytic activity with Pd supported on simple metal oxides, such as Al_2O_3 and TiO_2 Nano already used in Chapter 4.

In addition, a TiO_2/γ-Al_2O_3 novel material has been prepared via incipient wetness impregnation method (section 3.2.2) and used as support for Pd nanoparticles deposition on its surface. The catalytic performance of the latter material has also been studied and compared to that of Pd supported on both TiO_2 Nano and TiO_2-Al_2O_3 materials. Although the catalytic activity for these three Pd-based materials could be quite similar, in general, the Pd/TiO_2/γ-Al_2O_3 catalyst can offer some advantages over the other two Pd catalysts, taking into consideration its cost and the easier way to synthesize it.

Finally, the application scope of the Pd supported on TiO_2-Al_2O_3 catalyst is extended to other types of hydrogenation reactions. Thus, apart from studying its efficiency as catalyst in the mild hydrotreatment of tars-type compounds, its efficacy as catalyst in the reductive amination of bio-derived acetol to produce 2-methylpiperazine is also assessed in this study.

5.2. Catalytic screening of different mixed metal oxides compositions

In a first attempt, different materials with different metal oxides compositions, such as TiO_2-Al_2O_3, TiO_2-ZrO_2, TiO_2-SiO_2, ZrO_2-Al_2O_3 and SiO_2-Al_2O_3 were prepared by means of co-precipitation method. Afterwards, Pd nanoparticles were incorporated onto the above-mentioned materials via incipient wetness impregnation method. The main textural and physico-chemical properties of the materials, including surface area and pore volume of the supports, and the metal composition of the mixed metal oxides, along with the Pd loadings of the final Pd-based catalysts are listed in Table 5.1. As can be seen, Pd loadings were between 1.7-2.0wt% for all the materials prepared, close to the theoretical value (2.0wt%). Metals combination in mixed metal oxides ranged from 0.7 (for Si-Al mixed oxide) to 1.3 (for Ti-Al mixed oxide), close to the expected/theoretical value (≈1.0). Finally, supports surface areas were ≥200 m^2/g (except for Si-Al mixed oxide), while a wide range of pore volumes were found for the different samples here studied.

Table 5.1. Main textural and physico-chemical properties of the mixed metal oxides-supported Pd catalysts.

Catalyst	Pd (wt%)[a]	Molar ratio[b]	Support S_{BET} (m^2/g)[c]	Support Vp (cm^3/g)[c]
Pd/TiO_2-Al_2O_3	1.8	Ti/Al=1.3	280	0.24
Pd/TiO_2-ZrO_2	2.0	Ti/Zr=1.0	270	0.16
Pd/TiO_2-SiO_2	1.7	Ti/Si=1.1	200	0.15
Pd/ZrO_2-Al_2O_3	1.8	Zr/Al=0.8	247	0.08
Pd/SiO_2-Al_2O_3	1.9	Si/Al=0.7	146	0.14

[a,b] Values measured by ICP. [c] Calculated values from N_2 adsorption isotherms.

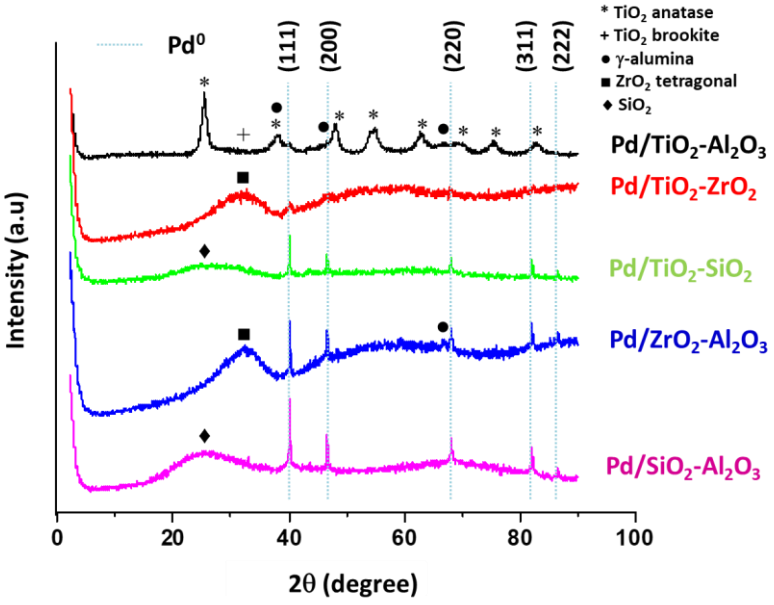

Figure 5.1. X-ray diffraction (XRD) patterns of the mixed metal oxides-supported Pd catalysts.

X-ray diffraction (XRD) patterns of the mixed metal oxides-supported Pd catalysts are shown in Figure 5.1. As can be seen, the TiO_2-Al_2O_3 material presented the peaks of the TiO_2 anatase crystalline phase diluted in an amorphous alumina. However, the other mixed metal oxides materials showed an amorphous structure, where some of the characteristic metallic oxide phases are weekly detected. In addition, the Pd peak intensity increased following this order: Pd/TiO_2-Al_2O_3 < Pd/TiO_2-ZrO_2 < Pd/TiO_2-SiO_2 < Pd/ZrO_2-Al_2O_3 < Pd/SiO_2-Al_2O_3. This could suggest that the Pd nanoparticles were better dispersed onto TiO_2-Al_2O_3 than on the other mixed metal oxides, also having smaller particle size. In this sense, as can be seen in Figure 5.2, HRTEM measurements of Pd/TiO_2-Al_2O_3, Pd/TiO_2-SiO_2 and Pd/ZrO_2-Al_2O_3 catalysts were performed, and the presence of Pd nanoparticles was recognized. In addition, the calculated Pd particle size average values were as follows: 4-5 nm, 5-6 nm and 6-8 nm, respectively for Pd/TiO_2-Al_2O_3, Pd/TiO_2-SiO_2 and Pd/ZrO_2-Al_2O_3 materials, which is consistent with the results obtained from XRD patterns. For instance, Pd particle size distribution of both Pd/TiO_2-SiO_2 and Pd/ZrO_2-Al_2O_3 (mainly of the latter) shifted towards slightly higher values, compared with Pd/TiO_2-Al_2O_3 sample (Figure 5.3).

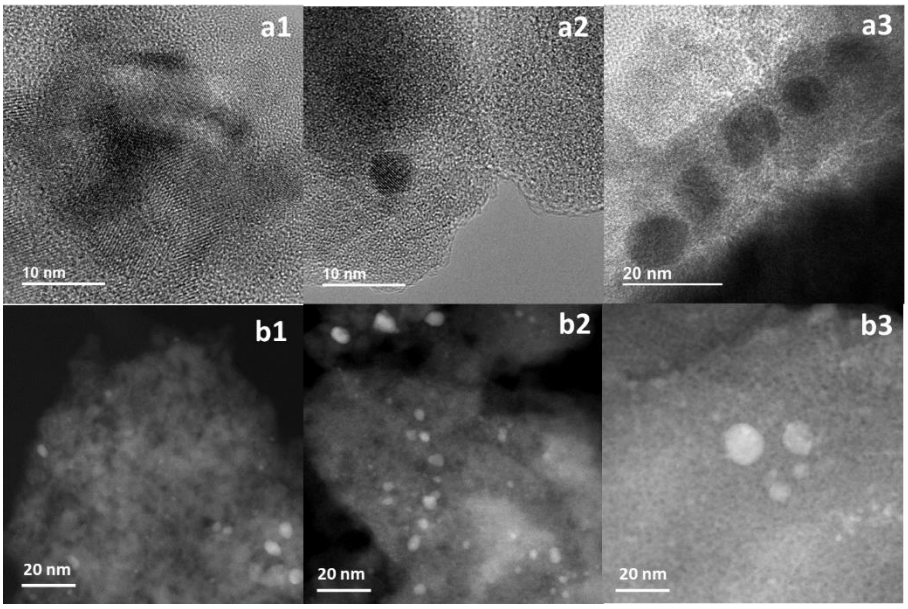

Figure 5.2. (a) HRTEM and (b) STEM images of: (1) Pd/TiO_2-Al_2O_3, (2) Pd/TiO_2-SiO_2 and (3) Pd/ZrO_2-Al_2O_3 catalysts.

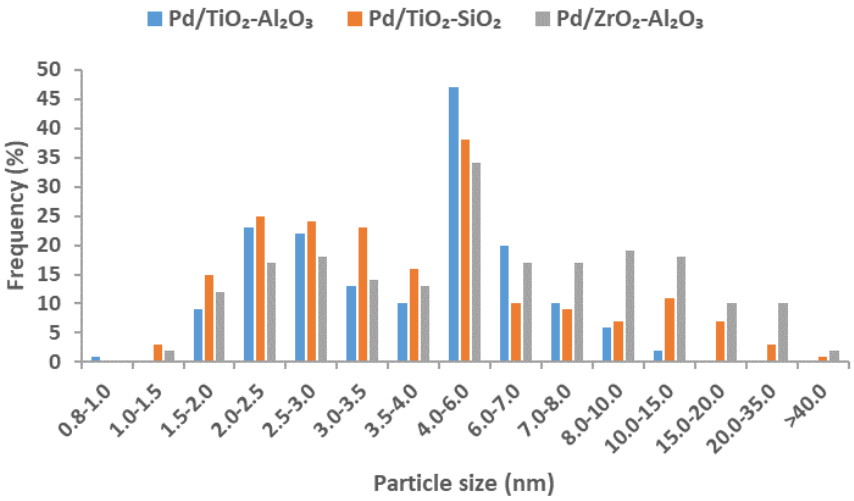

Figure 5.3. Pd nanoparticle size distribution of Pd-based catalysts.

The Pd supported on mixed metal oxides materials were tested as catalysts in the tars mild hydrotreatment using a model mixture (i.e., naphthalene, 1-methylnaphthalene, acenaphthylene and phenanthrene) of tars-type compounds by working at 250 ºC and 30 bar of H_2 during 7 h, and the attained results in terms of tars conversion and products selectivity are drawn in Figures 5.4 and 5.5, respectively.

Tars conversion data of Figure 5.4 clearly showed that Pd/TiO_2-Al_2O_3 was the most active catalyst (90% conversion at 7 h), followed by Pd/TiO_2-ZrO_2 (76% conv.), Pd/TiO_2-SiO_2 (69% conv.), Pd/ZrO_2-Al_2O_3 (58% conv.) and Pd/SiO_2-Al_2O_3 (54% conv.), with calculated TON (mols prod / mol Pd) values for each one of the catalysts of 73, 61, 58, 46 and 38, respectively. With respect to the selectivity observed for the here studied Pd-catalysts, the general trends were found quite similar for all the samples essayed when selectivity to the desired groups of hydrogenated products are compared at 51-55% of tars conversion (Figure 5.5). In addition, the corresponding selectivities to the different groups of hydrogenated products at different reaction times of the selected catalysts are listed in Tables 5.2, 5.3, 5.4, 5.5 and 5.6, respectively. Thus, it is important to note that Pd/TiO_2-Al_2O_3 showed higher selectivity to the more hydrogenated product (i.e., tetralin) than Pd/TiO_2-ZrO_2 and Pd/TiO_2-SiO_2 samples, and much higher in comparison with values reached for Pd/ZrO_2-Al_2O_3 and Pd/SiO_2-Al_2O_3 materials, respectively.

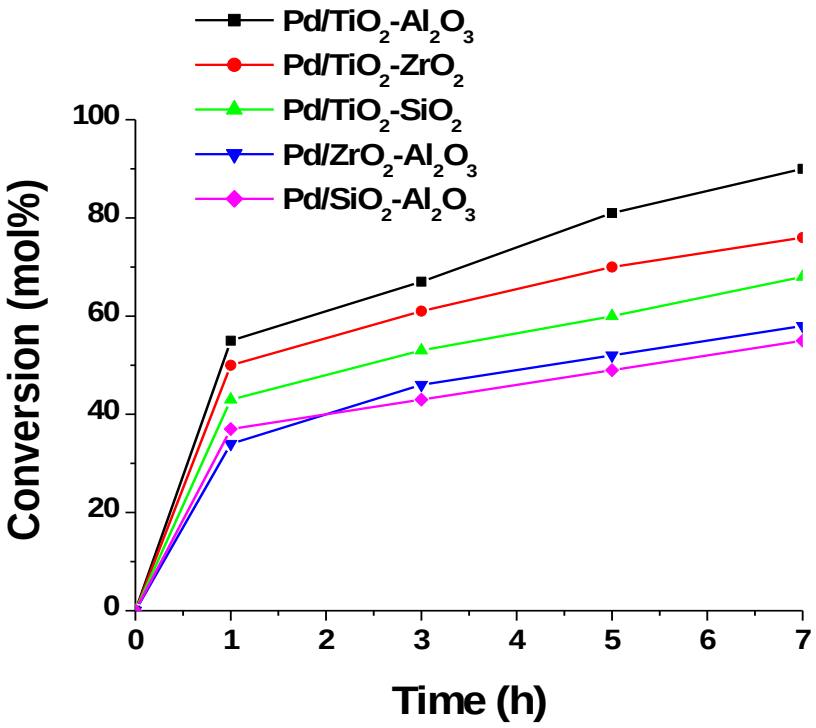

Figure 5.4. Conversion of tars-type compounds over Pd/mixed metal oxides catalysts in tars mild hydrotreatment. Reaction conditions: 0.5 g of tars-type compounds, 4.0 g of n-hexadecane, 0.2 g of catalyst, 30 bar of H_2, 250 °C, during 7 h.

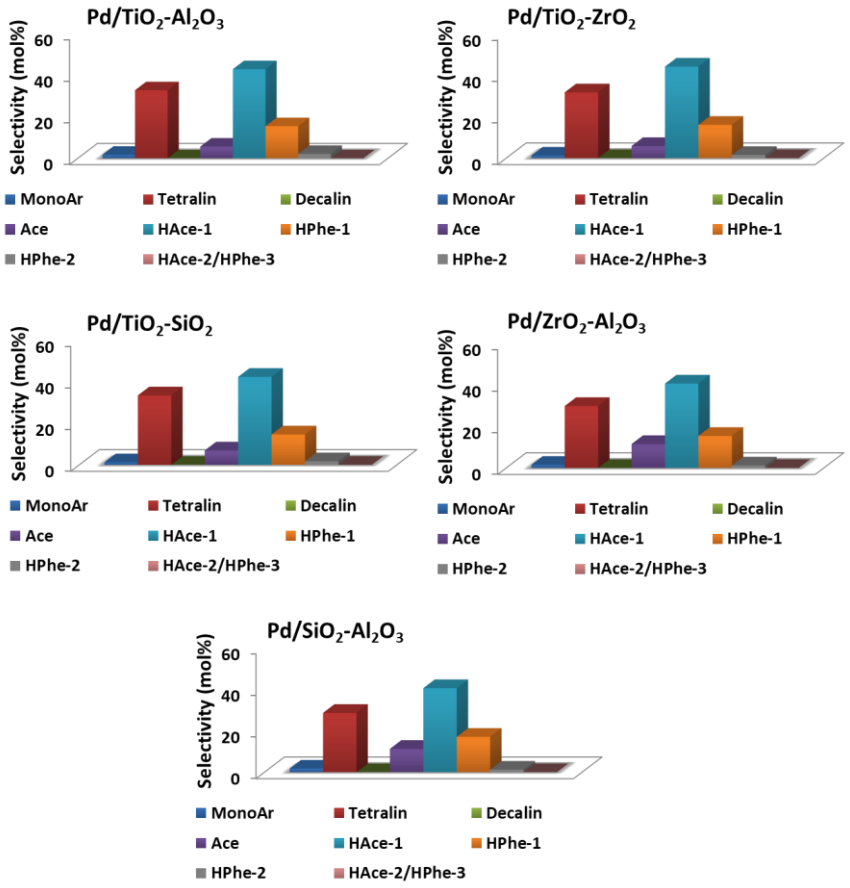

Figure 5.5. Selectivity to the different groups of products for different Pd/mixed metal oxides at 51-55% of conversion. Reaction conditions: 0.5 g of tars-type compounds, 4.0 g of n-hexadecane, 0.2 g of catalyst, 250 °C, 30 bar of H_2.

Table 5.2. Selectivity to the different products groups for 1.8wt%Pd/TiO_2-Al_2O_3 at 250 °C and 30 bar of H_2.

Time (h)	Conv (mol%)	Product selectivity (mol%)							
		Mono Ar	Tetralin	Decalin	Ace	HAce-1	HPhe-1	HPhe-2	HAce-2/HPhe-3
0	0	0.0	0.0	0.0	0.0	0.0	0.0	0.0	0.0
1	**55**	**1.7**	**32.6**	**0.0**	**5.6**	**42.7**	**15.4**	**2.1**	**0.0**
3	67	1.5	41.2	0.0	0.5	38.0	14.9	3.8	0.0
5	81	1.3	49.2	0.1	0.0	31.9	12.0	5.5	0.0
7	90	1.2	54.4	0.3	0.0	28.2	8.4	7.6	0.0

Table 5.3. Selectivity to the different products groups for 2.0wt%Pd/TiO_2-ZrO_2 at 250 °C and 30 bar of H_2.

Time (h)	Conv (mol%)	Product selectivity (mol%)							
		Mono Ar	Tetralin	Decalin	Ace	HAce-1	HPhe-1	HPhe-2	HAce-2/HPhe-3
0	0	0.0	0.0	0.0	0.0	0.0	0.0	0.0	0.0
1	**51**	**1.2**	**31.6**	**0.0**	**5.8**	**44.0**	**16.0**	**1.5**	**0.0**
3	61	1.1	37.8	0.0	1.3	40.8	16.3	2.8	0.0
5	70	1.0	43.2	0.0	0.0	36.7	15.3	3.8	0.0
7	76	1.0	46.9	0.0	0.0	33.6	13.9	4.6	0.0

Table 5.4. Selectivity to the different products groups for 1.7wt%Pd/TiO_2-SiO_2 at 250 °C and 30 bar of H_2.

Time (h)	Conv (mol%)	Product selectivity (mol%)							
		Mono Ar	Tetralin	Decalin	Ace	HAce-1	HPhe-1	HPhe-2	HAce-2/HPhe-3
0	0	0.0	0.0	0.0	0.0	0.0	0.0	0.0	0.0
1	43	1.2	26.0	0.0	19.6	40.1	12.1	1.0	0.0
3	**53**	**1.2**	**33.4**	**0.0**	**6.9**	**42.3**	**14.6**	**1.7**	**0.0**
5	61	1.3	38.7	0.0	3.5	39.5	14.6	2.7	0.0
7	69	1.3	44.0	0.0	0.0	36.7	14.5	3.6	0.0

Table 5.5. Selectivity to the different products groups for 1.8wt%Pd/ZrO_2-Al_2O_3 at 250 °C and 30 bar of H_2.

Time (h)	Conv (mol%)	Product selectivity (mol%)							
		Mono Ar	Tetralin	Decalin	Ace	HAce-1	HPhe-1	HPhe-2	HAce-2/HPhe-3
0	0	0.0	0.0	0.0	0.0	0.0	0.0	0.0	0.0
1	34	1.4	20.7	0.0	39.8	31.3	9.0	0.6	0.0
3	46	1.4	24.8	0.0	24.5	36.4	12.1	0.8	0.0
5	**52**	**1.5**	**29.8**	**0.0**	**11.5**	**40.6**	**15.4**	**1.2**	**0.0**
7	57	1.5	33.6	0.0	5.4	41.5	16.5	1.5	0.0

Table 5.6. Selectivity to the different products groups for 1.9wt%Pd/SiO_2-Al_2O_3 at 250 °C and 30 bar of H_2.

Time (h)	Conv (mol%)	Product selectivity (mol%)							
		Mono Ar	Tetralin	Decalin	Ace	HAce-1	HPhe-1	HPhe-2	HAce-2/HPhe-3
0	0	0.0	0.0	0.0	0.0	0.0	0.0	0.0	0.0
1	37	1.2	15.2	0.0	51.0	23.3	8.9	0.4	0.0
3	43	1.4	20.3	0.0	33.6	31.6	12.3	0.7	0.0
5	49	1.7	25.1	0.0	19.0	38.0	15.4	1.0	0.0
7	**54**	**1.7**	**28.5**	**0.0**	**11.2**	**40.4**	**17.0**	**1.2**	**0.0**

Summarizing, Pd/TiO_2-Al_2O_3 showed better catalytic performance than other mixed metal oxides-supported Pd catalysts here tested in the tars mild hydrotreatment. Therefore, TiO_2-Al_2O_3 mixed metal oxide was selected for further improvements as the most adequate support for Pd nanoparticles in these types of hydrotreatment catalysts.

5.3. Optimization of TiO_2-Al_2O_3 synthesis

Once Pd supported on TiO_2-Al_2O_3 material was selected as the most efficient catalyst for the mild hydrotreatment of tars-type compounds, different parameters of the mixed metal oxide synthesis were studied, this aims to optimize the final catalytic performance of the Pd-based material. In this sense, the effect of changing the Ti/Al molar ratio, the pH value, the aging time used and the addition rate of the ammonia solution (precipitating agent) during the synthesis of mixed metal oxide were investigated, and the attained results are discussed in the following sections.

5.3.1. Effect of changing Ti/Al molar ratio

First, the effect of varying Ti/Al molar ratio was studied. In this sense, Ti/Al molar ratio was increased from 0.4 to 3.0. The main textural and physico-chemical properties of the supports, including the Ti/Al molar ratio, along with the Pd loading are listed in Table 5.7. As can be seen from data, when Ti/Al molar ratio increased from 0.4 to 2.2, the specific surface area of the material decreased (from 354 to 226 m^2/g), along with its pore volume (from 0.37 to 0.15 cm^3/g); whereas when Ti/Al molar ratio was further increased from 2.2 to 3.0, no significant differences were encountered in both the surface areas and pore volumes values. This could be explained from the XRD patterns (Figure 5.6), where the crystallinity of the material (TiO_2 anatase phase) increased when increasing Ti/Al molar ratio from 0.4

to 2.2, while remained practically similar when Ti/Al ratio was further increased from 2.2 to 3.0.

In addition, the acidic properties of the TiO_2-Al_2O_3 materials having different Ti/Al molar ratios were evaluated through NH_3-TPD measurements. The corresponding desorption profiles of the here studied TiO_2-Al_2O_3 materials can be found in Figure A5.1. The total amount of ammonia adsorbed for each one of the materials is shown in Table 5.7. As can be seen, the total acidity measured decreased from 397 to 240 μmol/g when increasing Ti/Al molar ratio from 0.4 to 3.0.

Table 5.7. Main textural and physico-chemical properties of Pd/TiO_2-Al_2O_3 catalysts with different Ti/Al molar ratio.[a]

Sample (Ti/Al molar ratio)[b]	Support S_{BET} (m^2/g)[c]	Support Vp (cm^3/g)[c]	Support acidity (μmol/g)[d]	Pd (wt%)[e]
Pd/TiO_2-Al_2O_3 (Ti/Al = 0.4)	354	0.37	397	2.0
Pd/TiO_2-Al_2O_3 (Ti/Al = 0.8)	350	0.26	-	2.0
Pd/TiO_2-Al_2O_3 (Ti/Al = 1.3)	280	0.24	345	1.8
Pd/TiO_2-Al_2O_3 (Ti/Al = 2.2)	226	0.15	276	1.7
Pd/TiO_2-Al_2O_3 (Ti/Al = 3.0)	188	0.17	240	1.9

[a] Synthesis parameters: 1000 mL/h NH_3 addition rate, pH = 9, aging time = 12 h at 60 °C. [b,e] Values measured by ICP. [c] Calculated values from N_2 adsorption isotherms. [d] Total amount of acid sites calculated from NH_3-TPD measurements.

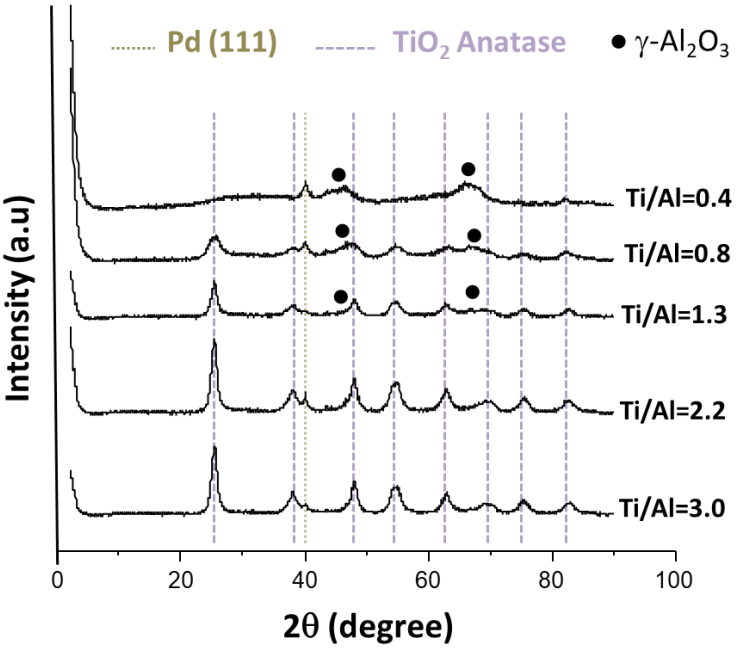

Figure 5.6. X-ray diffraction (XRD) patterns of Pd/TiO_2-Al_2O_3 catalysts with different Ti/Al molar ratio.

The Pd/TiO_2-Al_2O_3 samples possessing different Ti/Al molar ratio were tested in the mild hydrotreatment of tars-type compounds at 250 °C and 30 bar of H_2 during 7 h, and the tars conversion obtained in function of the Ti/Al composition and the total acidity of supports for the different Pd-catalysts here studied are represented in Figure 5.7. As can be seen, the total acidity of the supports increased with the increase in Al content of the samples, although the maximum conversion (90%) was achieved when working with the catalyst having Ti/Al molar ratio equal to (or close to) 1.3. In addition, as seen in Figure 5.8, the here studied Pd catalysts showed similar selectivity

to the different groups of products, compared at 67-70% of tars conversion in all the cases.

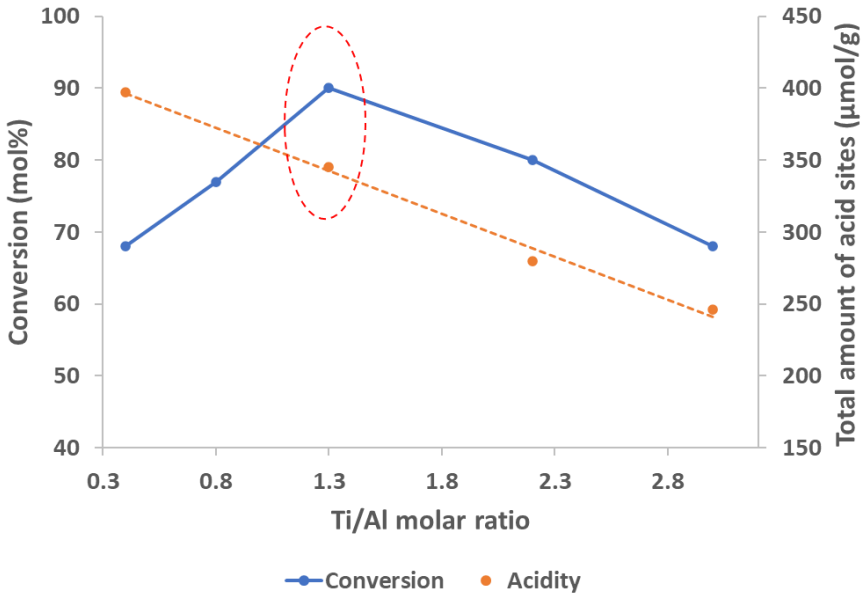

Figure 5.7. Tars conversion in function of Ti/Al molar ratio and total acidity for different Pd/TiO_2-Al_2O_3 catalysts. Reaction conditions: 0.5 g of tars-type compounds, 4.0 g of n-hexadecane, 0.2 g of catalyst, 250 ºC, 30 bar of H_2, during 7 h.

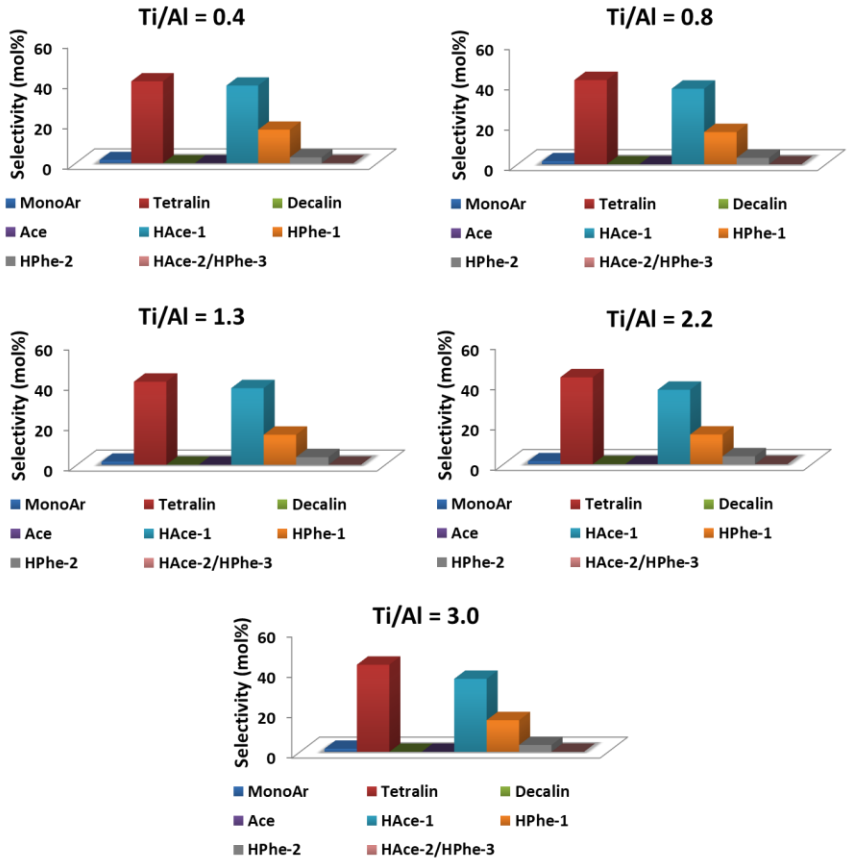

Figure 5.8. Selectivity to the different groups of products for different Pd/TiO_2-Al_2O_3 with different Ti/Al molar ratio at 67-70% of conversion. Reaction conditions: 0.5 g of tars-type compounds, 4.0 g of n-hexadecane, 0.2 g of catalyst, 250 °C, 30 bar of H_2.

In light of all the above-mentioned, TiO_2-Al_2O_3 having Ti/Al molar ratio of 1.3 was selected as the most adequate support to accommodate Pd nanoparticles, mainly taking into consideration the high surface area reported by the support, this allowing having well dispersed metal nanoparticles with small particle sizes. In addition,

high catalytic activity was achieved with this Pd-based material. Apparently, a moderate TiO_2 anatase crystalline phase diluted in an amorphous alumina matrix, combined with a moderate to high acidity are needed to achieve good performance in the tars mild hydrotreatment reaction.

5.3.2. Effect of pH during synthesis

After selecting the optimal Ti/Al molar ratio (≈1.3) for the synthesis of TiO_2-Al_2O_3 material, the effect of pH during mixed oxide co-precipitation was evaluated. For this purpose, three different preparations were done by increasing the pH of the synthetic mixture from 5 to 9. Then, 1.3wt% of Pd was incorporated (by incipient wetness impregnation) onto the synthesized TiO_2-Al_2O_3 materials. The main textural properties of the supports obtained at different pH values during synthesis, along with the Pd loadings for each of the samples are listed in Table 5.8. Apparently, there is not much difference observed in the textural properties of the titania-alumina supports obtained at different pHs, although maximum both surface area and pore volume were achieved by making the mixed oxide synthesis at pH = 7.8. Nevertheless, and as can be seen from Figure 5.9, when increasing the acidity of the medium during the titania-alumina co-precipitation, the structure of the material changed from amorphous at pH = 5.1 and 7.8 to crystalline at pH = 9.2. In addition, due to the absence of the diffraction peaks corresponding to Pd (111) at 40°, the Pd species seemed to have good dispersion onto the different TiO_2-

Al_2O_3 mixed metal oxides here studied, independently of the pH used for the synthesis.

Table 5.8. Main textural and physico-chemical properties of Pd/TiO_2-Al_2O_3 catalysts with supports synthesized at different pHs.[a]

Sample	Support S_{BET} (m^2/g)[b]	Support V_p (cm^3/g)[b]	Pd (wt%)[c]
Pd/TiO_2-Al_2O_3 (pH = 5.1)	284	0.27	1.3
Pd/TiO_2-Al_2O_3 (pH = 7.8)	336	0.29	1.3
Pd/TiO_2-Al_2O_3 (pH = 9.2)	280	0.24	1.3

[a] Synthesis parameters: Ti/Al ≈ 1.3, 1000 mL/h NH_3 addition rate, aging time = 12 h at 60 °C. [b] Calculated values from N_2 adsorption isotherms. [c] Values measured by ICP.

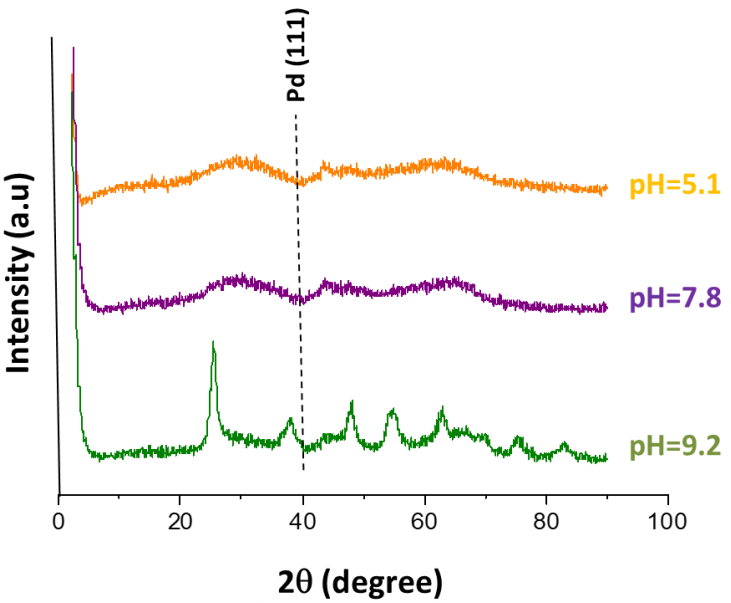

Figure 5.9. X-ray diffraction (XRD) patterns of Pd/TiO_2-Al_2O_3 catalysts with supports synthesized at different pHs.

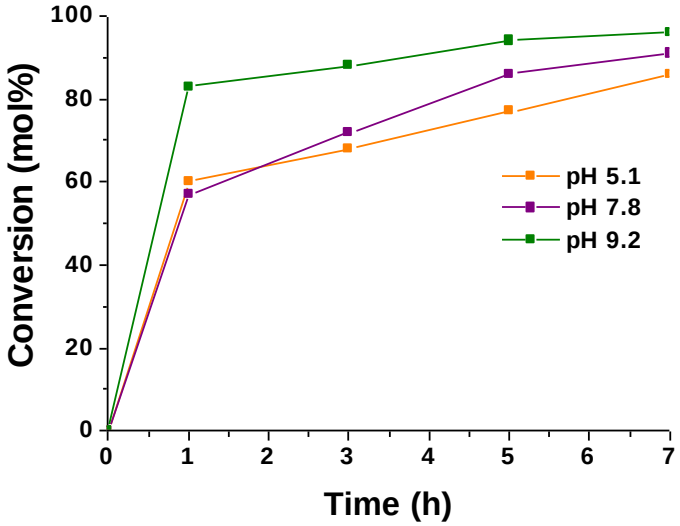

Figure 5.10. Conversion of tars-type compounds over Pd/TiO_2-Al_2O_3 catalysts with supports synthesized at different pHs. Reaction conditions: 0.5 g of tars-type compounds, 4.0 g of n-hexadecane, 0.2 g of catalyst, 275 ºC, 30 bar of H_2, during 7 h.

As can be seen in Figure 5.10, the selected Pd catalysts were evaluated in the tars mild hydrotreatment reaction at 275 °C and 30 bar of H_2. It was found that the conversion of tars-type molecules was higher when mixed oxide precursor was prepared at the highest pH (9.2) in comparison with the other lower pHs studied. Particularly, the differences in the catalytic activity were higher at shorter reaction times (i.e., after 1 h of reaction), where 83% of tars conversion (and TON = 105) was achieved for the material synthesized at pH = 9.2, while conversion values ≤60% (and TON <70) were encountered for the other Pd catalysts with supports prepared at lower pHs. In addition, selectivity to the desired groups of hydrogenated products

(Figure 5.11) showed that the selected catalysts presented quite similar selectivity values (compared at 83-86% conversion of tars-type compounds). Tables 5.9, 5.10 and 5.11 showed the corresponding selectivity values to the different groups of hydrogenated products at different reaction times for the three Pd-based catalysts here studied.

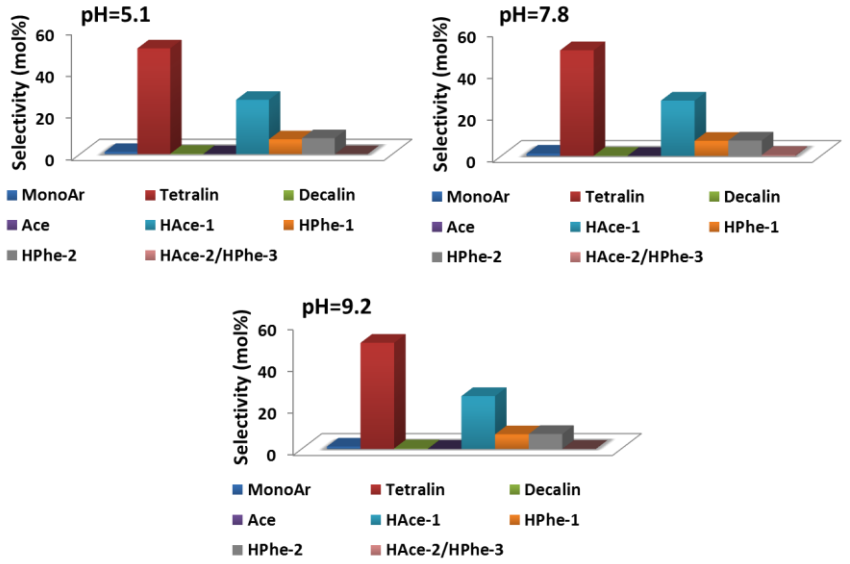

Figure 5.11. Selectivity to the different groups of products for different Pd/TiO_2-Al_2O_3 catalysts at 83-86% of conversion. Reaction conditions: 0.5 g of tars-type compounds, 4.0 g of n-hexadecane, 0.2 g of catalyst, 275 °C, 30 bar of H_2.

Table 5.9. Selectivity to the different products groups for 1.3wt%Pd/TiO_2-Al_2O_3 (pH = 5.1) at 275 °C and 30 bar of H_2.

Time (h)	Conv (mol%)	Product selectivity (mol%)							
		Mono Ar	Tetralin	Decalin	Ace	HAce-1	HPhe-1	HPhe-2	HAce-2/HPhe-3
0	0	0.0	0.0	0.0	0.0	0.0	0.0	0.0	0.0
1	60	1.2	35.8	0.0	1.8	34.7	12.0	2.5	0.0
3	68	1.3	47.6	0.0	0.0	34.2	11.9	5.2	0.0
5	77	1.2	49.0	0.0	0.0	30.1	9.5	6.4	0.0
7	**86**	**1.1**	**50.5**	**0.2**	**0.0**	**26.0**	**7.1**	**7.6**	**0.0**

Table 5.10. Selectivity to the different products groups for 1.3wt%Pd/TiO_2-Al_2O_3 (pH = 7.8) at 275 °C and 30 bar of H_2.

Time (h)	Conv (mol%)	Product selectivity (mol%)							
		Mono Ar	Tetralin	Decalin	Ace	HAce-1	HPhe-1	HPhe-2	HAce-2/HPhe-3
0	0	0.0	0.0	0.0	0.0	0.0	0.0	0.0	0.0
1	57	1.2	31.6	0.0	3.2	35.7	12.7	1.8	0.0
3	72	1.1	43.8	0.0	0.0	31.0	10.3	4.6	0.0
5	**86**	**1.1**	**50.6**	**0.1**	**0.0**	**26.5**	**7.2**	**7.4**	**0.5**
7	91	1.0	54.2	0.4	0.0	25.0	5.3	10.0	0.6

Table 5.11. Selectivity to the different products groups for 1.3wt%Pd/TiO_2-Al_2O_3 (pH = 9.2) at 275 °C and 30 bar of H_2.

Time (h)	Conv (mol%)	Product selectivity (mol%)							
		Mono Ar	Tetralin	Decalin	Ace	HAce-1	HPhe-1	HPhe-2	HAce-2/HPhe-3
0	0	0.0	0.0	0.0	0.0	0.0	0.0	0.0	0.0
1	**83**	**1.1**	**50.8**	**0.2**	**0.0**	**25.3**	**7.0**	**7.1**	**0.0**
3	88	1.1	54.0	0.6	0.0	25.9	5.9	10.4	0.7
5	94	1.0	57.3	1.0	0.0	24.1	4.3	12.7	0.9
7	96	1.0	57.4	2.0	0.0	22.6	3.4	13.8	1.2

For all the above-mentioned, Pd/TiO_2-Al_2O_3 with the support prepared at pH around 9, possessing adequate surface area (280 m^2/g), and presenting titania anatase crystalline phase in moderate extent and diluted in amorphous γ-alumina, was selected as the most active catalyst for the mild hydrotreatment of tars-type compounds here studied.

5.3.3. Effect of the rate of ammonia solution addition

In this section, the effect of the rate of addition of ammonia solution used as precipitating agent for titania-alumina synthesis was studied after selecting the optimal Ti/Al molar ratio (1.3) and the pH during mixed oxide co-precipitation. For instance, 80 mL/h, 160 mL/h, 500 mL/h and 1000 mL/h are the four different rates that will be evaluated in the synthesis of TiO_2-Al_2O_3 materials. As in the previous section, 1.3wt% of Pd was incorporated (by incipient wetness impregnation) onto the supports thus synthesized. The main textural properties of the supports obtained with different precipitating agent addition rates, along with the Pd loadings for each one of the catalytic samples prepared are listed in Table 5.12. As can be seen, a decrease in the surface area of the supports was observed by increasing the addition rate of the ammonia solution from 80 mL/h (339 m^2/g) to 1000 mL/h (280 m^2/g), although this change in the addition rate did not significantly affect the pore volume values attained. In addition, and as shown in Figure 5.12, where the XRD patterns of the different Pd/TiO_2-Al_2O_3 materials are presented, when adding the ammonia solution at 80 mL/h, the structure of the resultant material was found

to be amorphous. However, the titania-alumina material started to get some crystallinity at NH_3 addition rate of 160 mL/h, where a signal at 25° corresponding to the TiO_2 anatase crystalline phase (101) can be observed. Finally, when increasing the addition rate of ammonia solution from 160 to 1000 mL/h, the titania-alumina material obtained was more crystalline, presenting the characteristic peaks of titania anatase phase. With respect to the presence of Pd metallic species, no diffraction peaks were detected in any of the samples here studied, this suggesting that Pd nanoparticles were well dispersed onto the TiO_2-Al_2O_3 mixed oxides, and probably having small particle size.

Table 5.12. Main textural and physico-chemical properties of Pd/TiO_2-Al_2O_3 catalysts studying the effect of ammonia solution addition rate.[a]

Sample (Addition rate)	Support S_{BET} (m^2/g)[b]	Support V_p (cm^3/g)[b]	Pd (wt%)[c]
Pd/TiO_2-Al_2O_3 (80 mL/h)	339	0.26	1.3
Pd/TiO_2-Al_2O_3 (160 mL/h)	325	0.27	1.3
Pd/TiO_2-Al_2O_3 (500 mL/h)	303	0.24	1.3
Pd/TiO_2-Al_2O_3 (1000 mL/h)	280	0.24	1.3

[a] Synthesis parameters: Ti/Al ≈ 1.3, pH 9, aging time = 12 h at 60 °C. [b] Calculated values from N_2 adsorption isotherms. [c] Values measured by ICP.

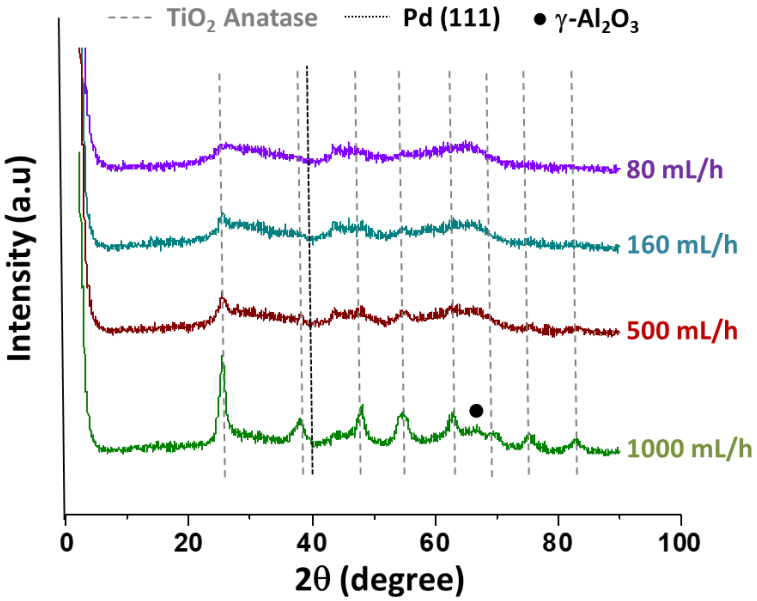

Figure 5.12. X-ray diffraction (XRD) patterns of Pd/TiO_2-Al_2O_3 catalysts at different ammonia solution addition rates.

The catalytic activity of the selected Pd catalysts was evaluated in the tars mild hydrotreatment reaction at 275 °C and 30 bar of H_2. It was found (see Figure 5.13) that the conversion of tars-type compounds was higher when ammonia solution was added at the highest rate (1000 mL/h) in comparison with the other lower addition rates studied. Particularly, the differences in the catalytic activity were higher at shorter reaction times (i.e., after 1 h of reaction), where 83% of tars conversion (and TON = 105) was achieved for the material synthesized using 1000 mL/h NH_3 addition rate, while conversion values ≤70% (and TON <80) were encountered for the other Pd catalysts with supports prepared at lower addition rates of NH_3.

Furthermore, selectivity to the desired groups of hydrogenated products in Figure 5.14 showed that the selected catalysts presented quite similar selectivity values (compared at 83% conversion of tars-type compounds). Tables 5.13, 5.14, 5.15 and 5.16 showed the corresponding selectivity values to the different groups of hydrogenated products at different reaction times for the four Pd-based catalysts here studied.

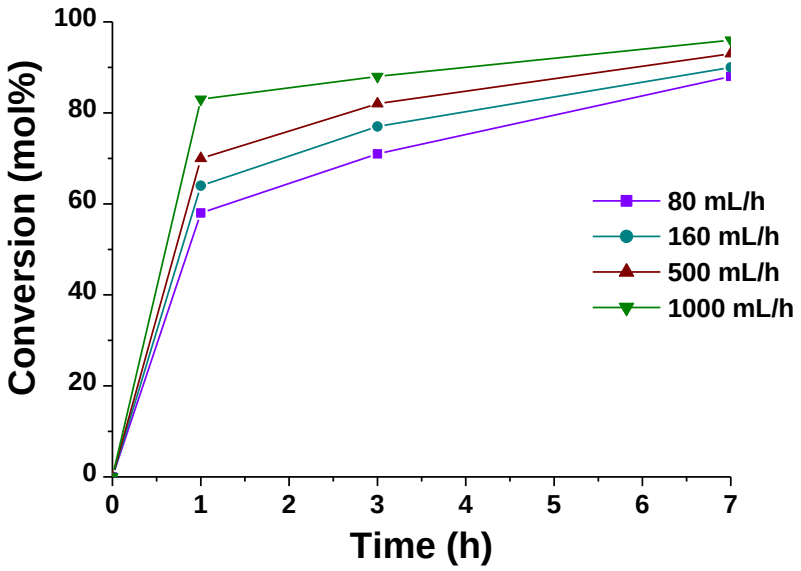

Figure 5.13. Conversion of tars-type compounds over Pd/TiO_2-Al_2O_3 catalysts changing the ammonia addition rate during synthesis. Reaction conditions: 0.5 g of tars-type compounds, 4.0 g of n-hexadecane, 0.2 g of catalyst, 275 ºC, 30 bar of H_2, during 7 h.

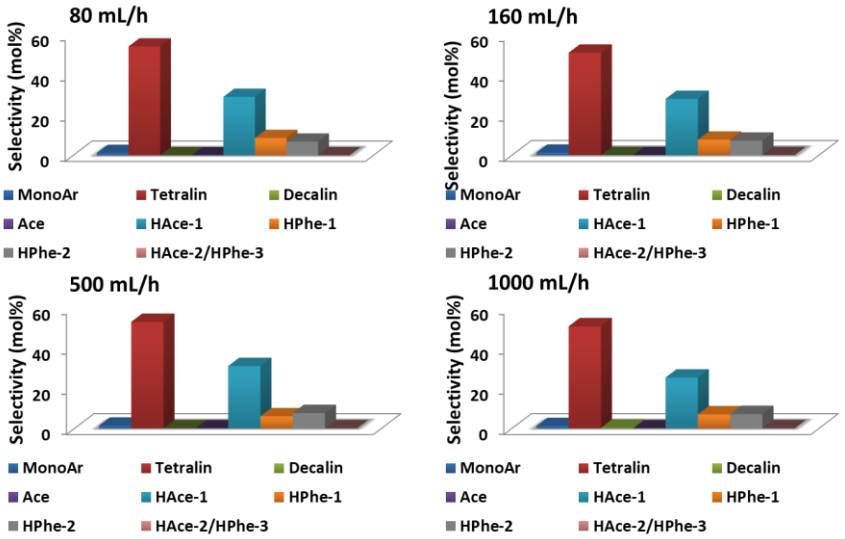

Figure 5.14. Selectivity to the different groups of products for Pd/TiO_2-Al_2O_3 at 82-83% of conversion. Reaction conditions: 0.5 g of tars-type compounds, 4.0 g of n-hexadecane, 0.2 g of catalyst, 275 °C, 30 bar of H_2.

Table 5.13. Selectivity to the different products groups for 1.3wt%Pd/TiO_2-Al_2O_3 (NH_3 addition rate: 80 mL/h).

Time (h)	Conv (mol%)	Product selectivity (mol%)							
		Mono Ar	Tetralin	Decalin	Ace	HAce-1	HPhe-1	HPhe-2	HAce-2/HPhe-3
0	0	0.0	0.0	0.0	0.0	0.0	0.0	0.0	0.0
1	58	1.5	37.8	0.0	2.0	41.7	14.8	1.8	0.0
3	72	1.4	48.2	0.0	0.0	34.4	11.6	4.4	0.0
5	**83**	**1.2**	**54.0**	**0.0**	**0.0**	**29.3**	**8.6**	**6.8**	**0.0**
7	88	1.2	53.0	0.3	0.0	25.2	6.3	8.1	0.0

Table 5.14. Selectivity to the different products groups for 1.3wt%Pd/TiO_2-Al_2O_3 (NH_3 addition rate: 160 mL/h).

Time (h)	Conv (mol%)	Product selectivity (mol%)							
		Mono Ar	Tetralin	Decalin	Ace	HAce-1	HPhe-1	HPhe-2	HAce-2/HPhe-3
0	0	0.0	0.0	0.0	0.0	0.0	0.0	0.0	0.0
1	64	1.5	41.7	0.0	0.4	39.6	13.8	3.0	0.0
3	76	1.3	50.5	0.0	0.0	32.3	10.1	5.2	0.0
5	**83**	**1.2**	**51.0**	**0.2**	**0.0**	**28.1**	**7.7**	**7.2**	**0.0**
7	90	1.1	51.5	0.4	0.0	23.9	5.3	9.1	0.0

Table 5.15. Selectivity to the different products groups for 1.3wt%Pd/TiO_2-Al_2O_3 (NH_3 addition rate: 500 mL/h).

Time (h)	Conv (mol%)	Product selectivity (mol%)							
		Mono Ar	Tetralin	Decalin	Ace	HAce-1	HPhe-1	HPhe-2	HAce-2/HPhe-3
0	0	0.0	0.0	0.0	0.0	0.0	0.0	0.0	0.0
1	70	1.3	47.2	0.2	0.0	36.8	8.8	5.2	0.0
3	**82**	**1.3**	**53.1**	**0.4**	**0.0**	**31.0**	**6.0**	**7.6**	**0.0**
5	87	1.2	52.6	0.6	0.0	27.2	4.5	9.3	0.0
7	93	1.1	52.1	0.8	0.0	23.4	2.9	11.0	0.8

Table 5.16. Selectivity to the different products groups for 1.3wt%Pd/TiO_2-Al_2O_3 (NH_3 addition rate: 1000 mL/h).

Time (h)	Conv (mol%)	Product selectivity (mol%)							
		Mono Ar	Tetralin	Decalin	Ace	HAce-1	HPhe-1	HPhe-2	HAce-2/HPhe-3
0	0	0.0	0.0	0.0	0.0	0.0	0.0	0.0	0.0
1	**83**	**1.1**	**50.8**	**0.2**	**0.0**	**25.3**	**7.0**	**7.1**	**0.0**
3	88	1.1	54.0	0.6	0.0	26.0	5.9	10.4	0.7
5	94	1.0	57.3	1.0	0.0	24.1	4.3	12.7	0.9
7	96	1.0	57.4	2.0	0.0	22.6	3.4	13.8	1.2

Summarizing, Pd/TiO_2-Al_2O_3 with the support prepared at 1000 mL/h of ammonia solution addition rate demonstrated to be the

most efficient catalyst for the mild hydrotreatment of tars-type compounds. Apparently, the presence of an appropriate amount of TiO_2 anatase crystalline phase in the mixed metal oxide used as support seems to play an important role in this type of hydrotreatment reaction.

5.3.4. Effect of aging time

Once the parameters such as Ti/Al molar ratio, pH of the synthesis medium, and the ammonia solution addition rate were established and optimized during the mixed metal oxide co-precipitation method, the next step was focused on investigating the effect of aging time at 60 °C. For instance, four different aging times (0 h, 6 h, 12 h and 24 h) were studied in the TiO_2-Al_2O_3 material preparation. As usually, 1.3wt% of Pd was impregnated onto the supports thus synthesized. The main textural properties of the attained supports, along with the Pd loadings for each one of the catalytic samples are shown in Table 5.17. As can be seen, when increasing the aging time after co-precipitation from 0 to 24 h, the specific surface area of the TiO_2-Al_2O_3 mixed oxide decreased from 383 to 246 m^2/g. Nevertheless, and except for the TiO_2-Al_2O_3 prepared without aging (aging time = 0 h), practically no variations are observed in the pore volume values for the different mixed oxides samples. Moreover, XRD patterns obtained for the different Pd supported on TiO_2-Al_2O_3 samples (Figure 5.15) confirmed that without aging and when the aging time during the support synthesis was 6 h, the material structure resulted in an amorphous solid. However, when the aging time during

the mixed oxide synthesis was increased to 12 h, the attained material showed a crystalline structure with diffraction peaks corresponding to those of TiO_2 anatase crystalline phase. With further increase in the aging time to 24 h, some additional crystallinity in the resultant material was detected. Finally, and concerning the Pd metallic species, no diffraction peaks were found in most of the samples or they were rather difficult to detect, this suggesting that Pd nanoparticles were well dispersed onto the surface of TiO_2-Al_2O_3 support, and probably with small particle size.

Table 5.17. Main textural and physico-chemical properties of Pd/TiO_2-Al_2O_3 catalysts with supports prepared by changing the aging time.[a]

Sample (Aging time)	Support S_{BET} (m^2/g)[b]	Support V_p (cm^3/g)[b]	Pd (wt%)[c]
Pd/TiO_2-Al_2O_3 (0 h)	383	0.28	1.3
Pd/TiO_2-Al_2O_3 (6 h)	313	0.25	1.3
Pd/TiO_2-Al_2O_3 (12 h)	280	0.24	1.3
Pd/TiO_2-Al_2O_3 (24 h)	246	0.25	1.4

[a] Synthesis parameters: Ti/Al ≈ 1.3, pH = 9, 1000 mL/h NH_3 addition rate, aging at 60 °C. [b] Calculated values from N_2 adsorption isotherms, [c] Values measured by ICP.

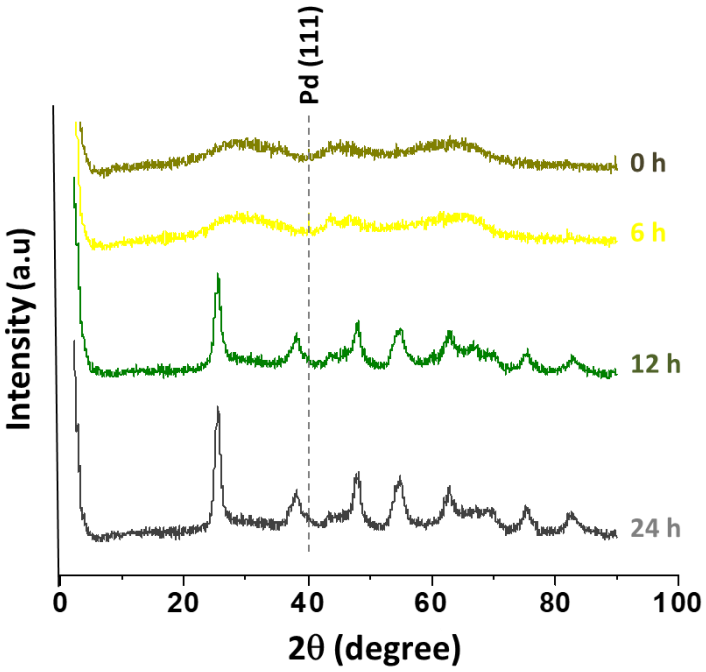

Figure 5.15. X-ray diffraction (XRD) patterns of Pd/TiO_2-Al_2O_3 catalysts with supports prepared at different aging times.

The catalytic activity of the different Pd catalysts was evaluated in the mild hydrotreatment of tars-type compounds at 275 °C and 30 bar of H_2 (Figure 5.16). For instance, it was found that the tars conversion was higher for the sample at 12 h aging time (83% and 96% conversion after 1 h and 7 h, respectively), in comparison with the other samples prepared at different aging times. Moreover, the calculated TON followed the same trend observed for tars conversion, with a maximum value (TON = 130 at 7 h) when the aging time used for support synthesis was 12 h. Therefore, the catalytic performance in the mild hydrotreatment of tars-type compounds of the Pd/TiO_2-Al_2O_3

appeared to be improved and optimized when the aging time used for the mixed oxide precursor synthesis was 12 h.

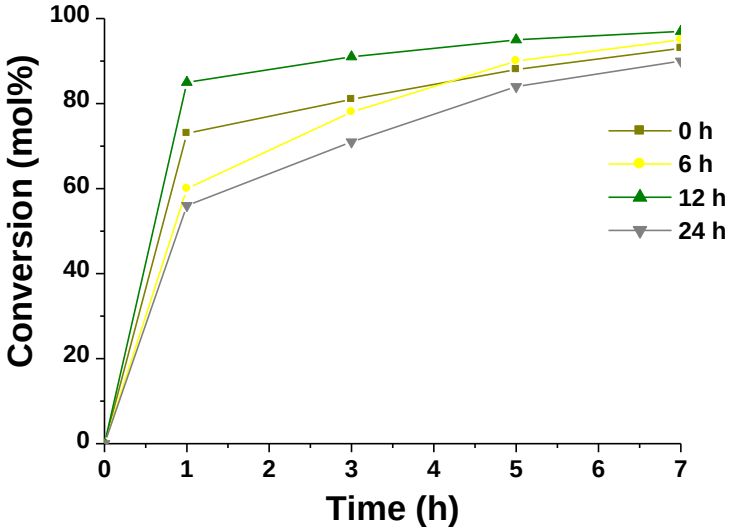

Figure 5.16. Conversion of tars-type compounds over Pd/TiO_2-Al_2O_3 catalysts with supports prepared by changing the aging time during synthesis. Reaction conditions: 0.5 g of tars-type compounds, 4.0 g of n-hexadecane, 0.2 g of catalyst, 275 ºC, 30 bar of H_2, during 7 h.

In addition, with respect to the selectivity to the desired groups of hydrogenated products shown in Figure 5.17, similar selectivity levels to tetralin, HAce-1, HPhe-1 and HPhe-2 main products were found for all the here studied catalysts (comparison made at 90% of tars-type compounds conversion). The selectivities to the different groups of hydrogenated products at different reaction times for the

different Pd-based catalysts essayed are detailed in Tables 5.18, 5.19, 5.20 and 5.21, respectively.

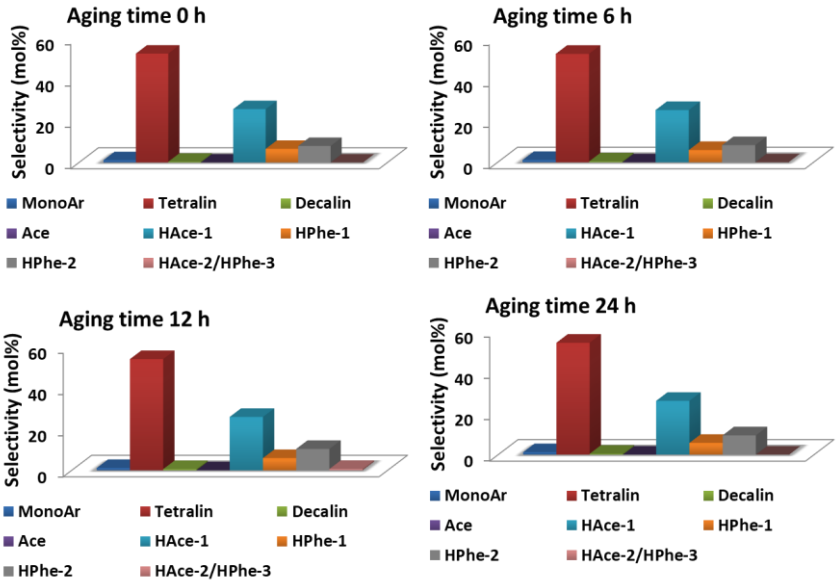

Figure 5.17. Selectivity to the different groups of products for different Pd/TiO_2-Al_2O_3 at 90% of conversion. Reaction conditions: 0.5 g of tars-type compounds, 4.0 g of n-hexadecane, 0.2 g of catalyst, 275 °C, 30 bar of H_2.

Table 5.18. Selectivity to the different products groups for 1.3wt%Pd/TiO_2-Al_2O_3 (without aging) at 275 °C and 30 bar of H_2.

Time (h)	Conv (mol%)	Product selectivity (mol%)							
		Mono Ar	Tetralin	Decalin	Ace	HAce-1	HPhe-1	HPhe-2	HAce-2/HPhe-3
0	0	0.0	0.0	0.0	0.0	0.0	0.0	0.0	0.0
1	73	1.2	46.1	0.0	0.1	30.8	9.6	4.7	0.0
3	81	1.1	48.3	0.2	0.0	27.8	8.4	6.0	0.0
5	**89**	**1.1**	**52.5**	**0.4**	**0.0**	**25.7**	**6.6**	**8.0**	**0.0**
7	93	1.1	54.0	0.6	0.0	24.1	5.0	9.5	0.1

Table 5.19. Selectivity to the different products groups for 1.3wt%Pd/TiO_2-Al_2O_3 (aging time = 6 h) at 275 °C and 30 bar of H_2.

Time (h)	Conv (mol%)	Product selectivity (mol%)							
		Mono Ar	Tetralin	Decalin	Ace	HAce-1	HPhe-1	HPhe-2	HAce-2/HPhe-3
0	0	0.0	0.0	0.0	0.0	0.0	0.0	0.0	0.0
1	60	1.3	38.6	0.0	3.0	43.9	10.7	2.0	0.0
3	78	1.2	46.0	0.2	0.0	29.7	9.3	5.3	0.0
5	**90**	**1.1**	**52.5**	**0.4**	**0.0**	**25.3**	**5.9**	**8.3**	**0.0**
7	95	1.1	54.8	0.9	0.0	23.7	2.3	11.3	0.9

Table 5.20. Selectivity to the different products groups for 1.3wt%Pd/TiO_2-Al_2O_3 (aging time = 12 h) at 275 °C and 30 bar of H_2.

Time (h)	Conv (mol%)	Product selectivity (mol%)							
		Mono Ar	Tetralin	Decalin	Ace	HAce-1	HPhe-1	HPhe-2	HAce-2/HPhe-3
0	0	0.0	0.0	0.0	0.0	0.0	0.0	0.0	0.0
1	83	1.1	50.8	0.2	0.0	25.3	7.0	7.1	0.0
3	**88**	**1.1**	**54.0**	**0.6**	**0.0**	**26.0**	**5.9**	**10.4**	**0.7**
5	94	1.0	57.3	1.0	0.0	24.1	4.3	12.7	0.9
7	96	1.0	57.4	2.0	0.0	22.6	3.4	13.8	1.2

Table 5.21. Selectivity to the different products groups for 1.3wt%Pd/TiO_2-Al_2O_3 (aging time = 24 h) at 275 °C and 30 bar of H_2.

Time (h)	Conv (mol%)	Product selectivity (mol%)							
		Mono Ar	Tetralin	Decalin	Ace	HAce-1	HPhe-1	HPhe-2	HAce-2/HPhe-3
0	0	0.0	0.0	0.0	0.0	0.0	0.0	0.0	0.0
1	56	1.4	35.5	0.0	4.1	35.5	13.0	2.0	0.0
3	71	1.2	42.3	0.0	0.0	31.4	10.6	4.6	0.0
5	84	1.1	48.1	0.2	0.0	26.7	7.5	6.9	0.0
7	**90**	**1.2**	**54.2**	**0.4**	**0.0**	**26.0**	**5.7**	**9.3**	**0.0**

To highlight, and after the study and optimization of the synthesis methodology for the titania-alumina mixed oxide precursor

of the Pd-based catalyst for tars mild hydrotreatment, Pd supported on TiO_2-Al_2O_3 with the support having Ti/Al molar ratio ≈ 1.3, synthesized at pH = 9, with ammonia solution addition rate of 1000 mL/h, and being precipitated during 12 h (aging time) at 60 ºC, was considered as the most efficient catalyst for the mild hydrotreatment of tars-type compounds. According to the above-mentioned parameters, it can be concluded that a TiO_2-Al_2O_3 support having high surface area and moderate TiO_2 anatase crystalline phase contained in an amorphous alumina material, plays a crucial role in the mild hydrotreatment of tars-type molecules, by accomodating well dispersed active Pd metallic nanoparticles in adequate manner onto its large specific surface.

5.4. Reusability tests for Pd supported on TiO_2-Al_2O_3

After optimization of the synthesis parameters of the Pd/TiO_2-Al_2O_3 catalyst, one important point for applying this material as catalyst in the mild hydrotreatment of tars-type compounds relies on the possibility of recycling it several times. In order to investigate the stability of this catalyst under the hydrotreatment reaction conditions (275 °C and 30 bar of H_2), and its remaining activity after several reuses, a set of reactions was carried out in which the Pd/TiO_2-Al_2O_3 catalyst was used in a first reaction, and then recycled four more times (see section 3.4.1.1 in Chapter 3). At the end of every reaction, the solid catalyst was recovered from the reaction mixture by centrifugation, washed with 2-propanol, and dried at 100 °C in an oven during 1 h, before its use in a new catalytic experiment. The

catalytic results (in terms of tars conversion at different reaction times) obtained for consecutive recycling of Pd/TiO_2-Al_2O_3 in the tars mild hydrotreatment are summarized in Figure 5.18.

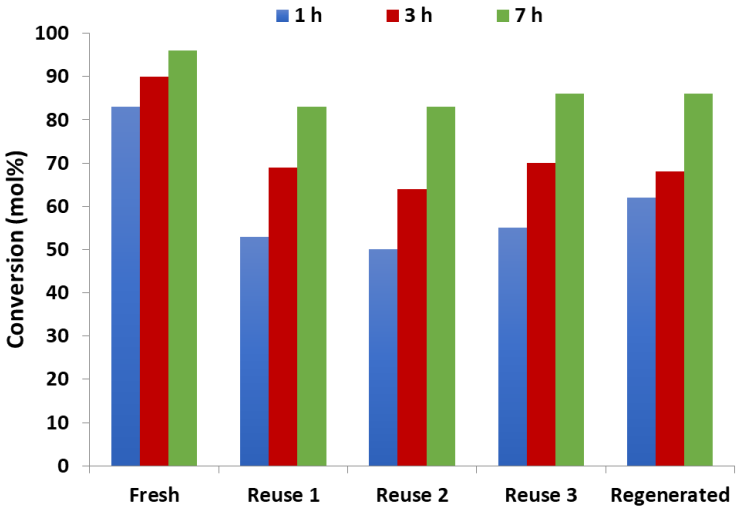

Figure 5.18. Reusability tests for Pd/TiO_2-Al_2O_3 in the tars mild hydrotreatment. Reaction conditions: 0.5 g of tars-type compounds, 4.0 g of n-hexadecane, 0.2 g of catalyst, 275 °C and 30 bar of H_2.

It can be seen from Figure 5.18 that the catalytic activity achieved with the use of Pd/TiO_2-Al_2O_3 fresh catalyst decreased in the first catalyst reuse. For instance, the conversion of tars-type compounds decreased from 83% to 53% (at 1 h), 90% to 69% (at 3 h), and 96% to 83% (at 7 h), respectively, when comparing data of the fresh and the first reused catalyst (Fig. 5.18). More importantly, the catalytic activity remained practically constant during the following reuses (reuses 2 and 3), and after catalyst regeneration with H_2. Probably, the carbonaceous compounds deposition onto the catalytic

surface could be one of the main reasons explaining the decrease in the catalytic activity occurring during recycling, although other causes could not be ruled out. In order to understand what happened on the catalyst surface during reuses, the effect of catalyst reusability along with its regeneration on the organic matter deposition, metal content and Pd nanoparticle size of the Pd/TiO_2-Al_2O_3 catalyst was systematically studied, and the obtained results are shown in Table 5.22. As can be seen, the carbon deposited on the solid catalyst determined after the first use was 1.35%, while it was increased until 2.62% after four consecutive uses (third reuse). Remarkably, these C values were strongly reduced after catalyst regeneration with H_2. With respect to the Pd loading before and after reuses, no significant difference was detected, thus no Pd leaching occurred after several reuses.

Table 5.22. Effect of reusability and regeneration on carbon deposition, metal loading and Pd nanoparticle size of Pd/TiO_2-Al_2O_3 catalyst.

Pd/TiO_2-Al_2O_3	%C[a]	%H[a]	Pd (wt%)[b]	Pd particle size (nm)[c]
Fresh	0.00	0.89	1.30	2.3
First use	1.35	1.09	-	-
Third reuse	2.62	0.93	1.24	2.5
Regenerated	0.80	0.66	-	2.0

[a] Results from elemental analysis (EA). [b] Pd content measured by ICP. [c] Average diameter of Pd nanoparticles calculated from TEM measurements of, at least, 100 particles.

In addition, the fresh Pd/TiO_2-Al_2O_3 catalyst was analyzed by means of high-resolution transmission electron microscopy (HR-TEM) and scanning electron microscope (SEM-EDX). The images of the catalyst here studied are shown in Figures 5.19, 5.20 and A5.3. It is important to note that the presence of metallic Pd nanoparticles can be recognized in all of them. On one hand, HR-TEM image (Fig. 5.19a) clearly shows small Pd particles mostly presenting Pd (111) phase (red arrows), together with TiO_2 (101) species (yellow arrow). On the other hand, Pd nanoparticles appear to be well dispersed on the titania-alumina support as it is shown in SEM-EDX image (Fig. 5.19c), similarly to what is observed for Ti and Al, which seemed to be homogeneously dispersed on the solid (see Fig. A5.3). All these results are also confirmed by the HRTEM-EDX measurements performed on the Pd/TiO_2-Al_2O_3 fresh catalyst shown in Figure 5.20, where highly dispersed Pd nanoparticles are detected onto an homogeneous Ti-Al-O mixed oxide.

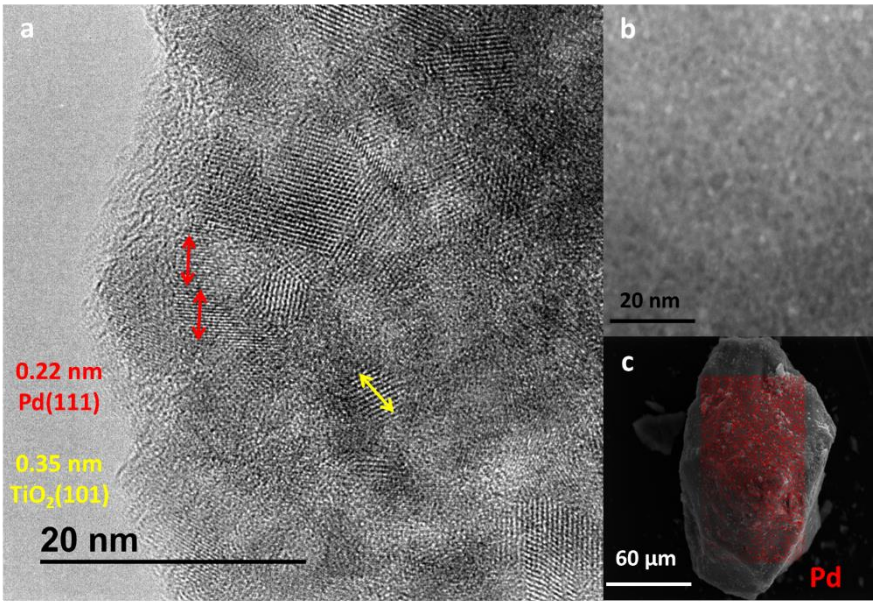

Figure 5.19. (a) HR-TEM, (b) STEM and (c) SEM-EDX mapping of the Pd/TiO_2-Al_2O_3 fresh catalyst.

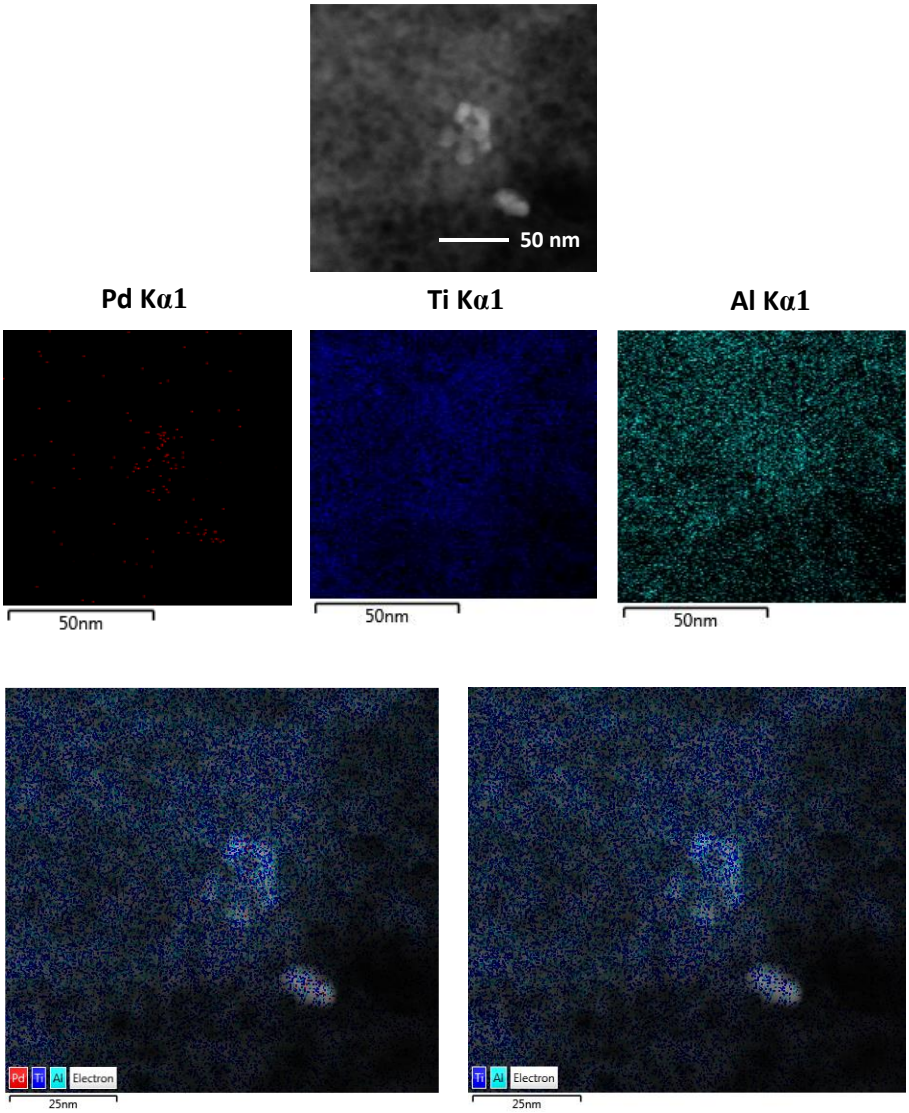

Figure 5.20. HRTEM-EDX mapping of Pd/TiO_2-Al_2O_3 catalyst.

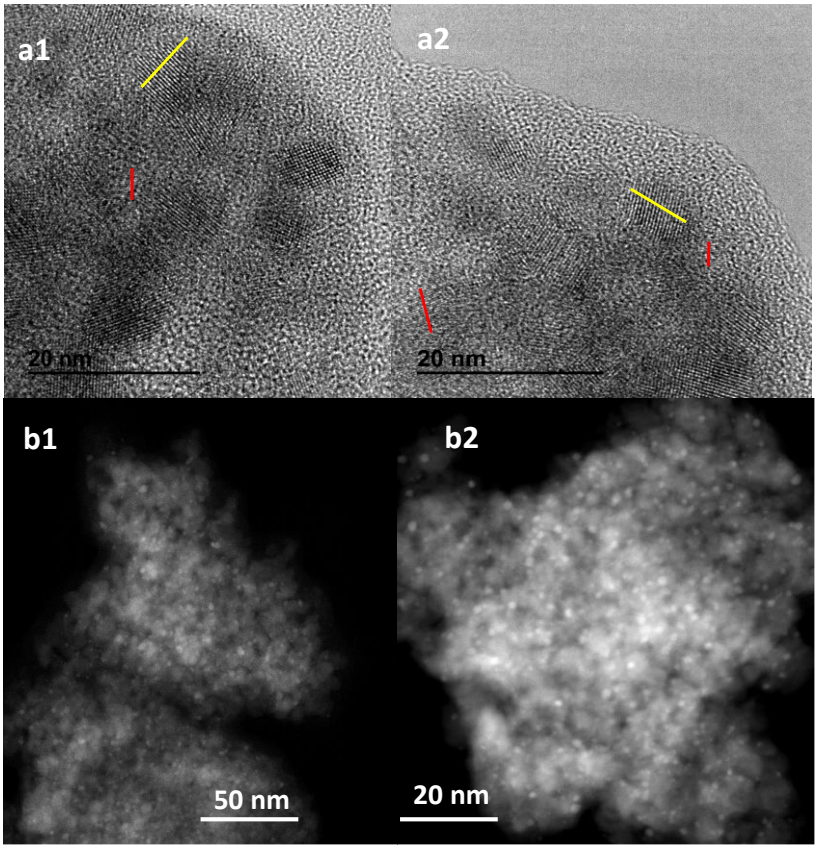

Figure 5.21. (a) HR-TEM, (b) STEM of the Pd/TiO_2-Al_2O_3 (1) reused and (2) regenerated catalysts (red: Pd (111) d≈0.22 nm and yellow: Ti (101) d≈0.35 nm).

Additionally, HR-TEM and STEM measurements of the Pd/TiO_2-Al_2O_3 reused and regenerated catalysts were carried out (Figure 5.21), in which the presence of both Pd (111) (red arrow) and TiO_2 (101) (yellow arrow) species was detected. Apparently, Pd nanoparticle sizes are quite similar for both reused and regenerated catalysts, and they practically did not change compared to the Pd nanoparticle sizes observed for the fresh catalyst. In fact, and as can be

seen in Table 5.22, the average Pd nanoparticle size (calculated from TEM measurements) was around 2 nm in all the cases. Thus, when comparing the particle size distributions obtained from TEM measurements of the catalysts (Figure 5.22), the fresh and the reused catalysts presented Pd nanoparticle sizes centered between 2.0-2.5 nm, while nanoparticle size distributions for the regenerated sample slightly moved towards lower values (between 1.5-2.0 nm). All these observations mean that the Pd nanoparticle size was not affected after several reuses and even after regeneration of the Pd/TiO_2-Al_2O_3 catalyst.

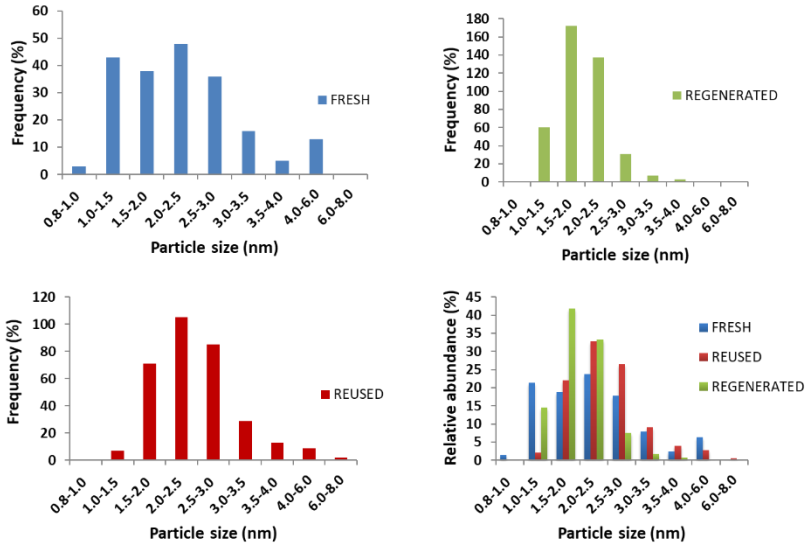

Figure 5.22. Pd nanoparticle size distributions of Pd/TiO_2-Al_2O_3 fresh, reused (third reuse) and regenerated catalysts.

X-ray diffraction patterns of the Pd/TiO_2-Al_2O_3 fresh, reused and regenerated catalysts were also performed in order to check the

stability of the support crystalline structure during consecutive reuses and regeneration of the catalyst. As can be seen in Figure 5.23, no changes in the material structure were detected after several reuses and even after regeneration of the used sample in the presence of H_2, always compared to the crystalline structure of the fresh Pd/TiO_2-Al_2O_3 catalyst.

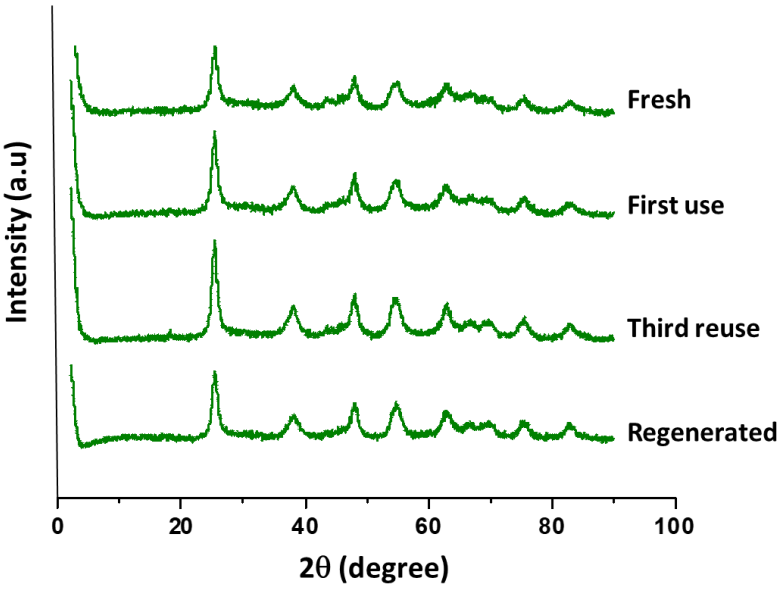

Figure 5.23. X-ray diffraction (XRD) patterns of the fresh, reused and regenerated Pd/TiO_2-Al_2O_3 catalysts.

As described in Chapter 4 in the case of Pd/TiO_2 Nano, we suggest that the Pd^0 species present in the fresh Pd/TiO_2-Al_2O_3 catalyst are responsible for the catalytic activity demonstrated in the hydrotreatment process. However, these Pd^0 species are probably transformed into Pd^{2+} species after reaction. This meaning that the

catalyst could be activated or "in situ" reduced under reaction conditions, explaining the stability of the catalysts after several reuses.

Summarizing, the Pd/TiO_2-Al_2O_3 catalyst demonstrated to be an efficient catalyst for the mild hydrotreatment of tars-type compounds. Although its catalytic performance was slightly decreased after the first use, probably due to the carbon deposition onto the catalyst surface, the activity was stabilized and maintained constant during the following consecutive reuses performed (up to third reuse), while it was slightly increased after regeneration with H_2. Remarkably, the Pd nanoparticle sizes and the crystalline structure of the material did not suffer changes after several reuses and even after regeneration of the catalyst.

5.5. Comparison of Pd supported on γ-Al_2O_3, TiO_2 Nano and TiO_2-Al_2O_3

After optimization of the main parameters for the preparation of Pd/TiO_2-Al_2O_3 catalyst and its stability after several reuses, it is important to establish an adequate comparison of this catalyst with the monometallic oxides-supported Pd catalysts, more specifically Pd/γ-Al_2O_3 and Pd/TiO_2 Nano materials. In this sense, Pd supported on γ-Al_2O_3, TiO_2 Nano and TiO_2-Al_2O_3 catalysts were evaluated in the tars mild hydrotreatment in terms of their catalytic activity, selectivity towards the desired hydrogenated products, reusability and stability, among others. The main textural and physico-chemical properties of the three Pd catalysts, including their corresponding Pd loadings and

Pd particle sizes are listed in Table 5.23. In addition, HR-TEM measurements of Pd supported on γ-Al_2O_3, TiO_2 Nano and TiO_2-Al_2O_3 were performed, and their corresponding images are shown in Figure 5.24.

Table 5.23. Main textural and physico-chemical properties of Pd supported on γ-Al_2O_3, TiO_2 Nano and TiO_2-Al_2O_3.

Catalyst	S_{BET}	Pd	Pd particle size	
	(m^2/g)[a]	(wt%)[b]	TEM[c]	CO[d]
Pd/γ-Al_2O_3	220	1.3	2.4	2.5
Pd/TiO_2	134	1.3	3.0	13.0
Pd/TiO_2-Al_2O_3	278	1.3	2.3	3.7

[a] Calculated values from N_2 adsorption isotherms. [b] Values measured by ICP. [c] Average diameter of Pd nanoparticles calculated from TEM measurements of, at least, 100 particles. [d] Average diameter of Pd nanoparticles calculated by CO chemisorption, with the stoichiometry being Pd:CO = 1:1.

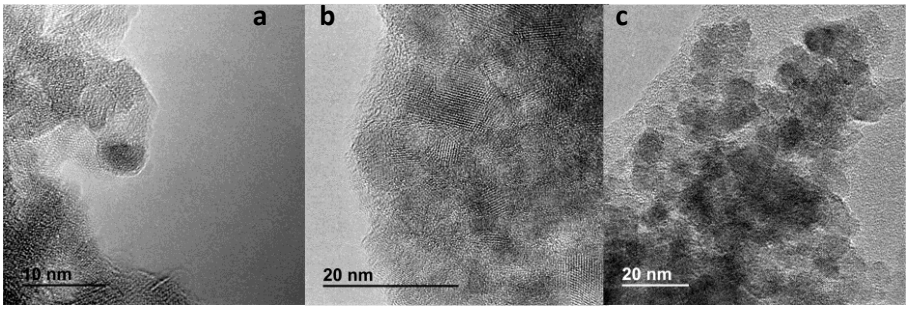

Figure 5.24. HR-TEM images of a) Pd/γ-Al_2O_3, b) Pd/TiO_2 Nano and c) Pd/TiO_2-Al_2O_3 catalysts.

In Figure 5.25, the catalytic activity (tars conversion) in the tars mild hydrotreatment of the Pd supported on γ-Al_2O_3, TiO_2 Nano and TiO_2-Al_2O_3 materials is compared. As can be seen, the tars conversion encountered at 7 h of reaction was higher for Pd/TiO_2-Al_2O_3 (96%), followed by Pd/TiO_2 Nano (88%) and Pd/γ-Al_2O_3 (75%), the differences being more pronounced at shorter reaction times (see for example tars conversion values at 1 h of reaction in Fig. 5.25). However, selectivity to the different groups of hydrogenated products was quite similar for the three Pd-based catalysts here compared (Figure 5.26). The selectivities to the different groups of hydrogenated products at different reaction times for the different Pd-based catalysts essayed are detailed in Tables 5.20, 5.24 and 5.25, respectively.

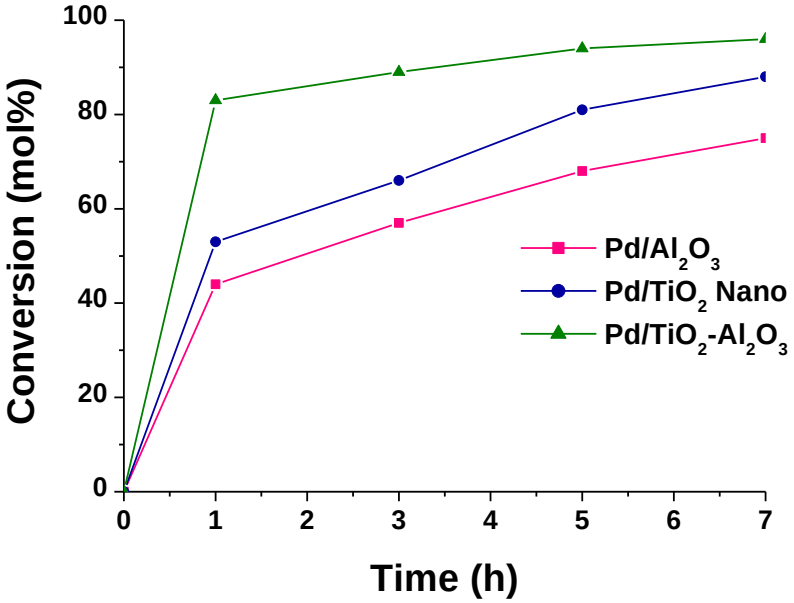

Figure 5.25. Conversion of tars-type compounds over Pd supported on γ-Al_2O_3, TiO_2 Nano and TiO_2-Al_2O_3. Reaction conditions: 0.5 g of tars-type compounds, 4.0 g of n-hexadecane, 0.2 g of catalyst, 275 ºC, 30 bar of H_2, during 7 h.

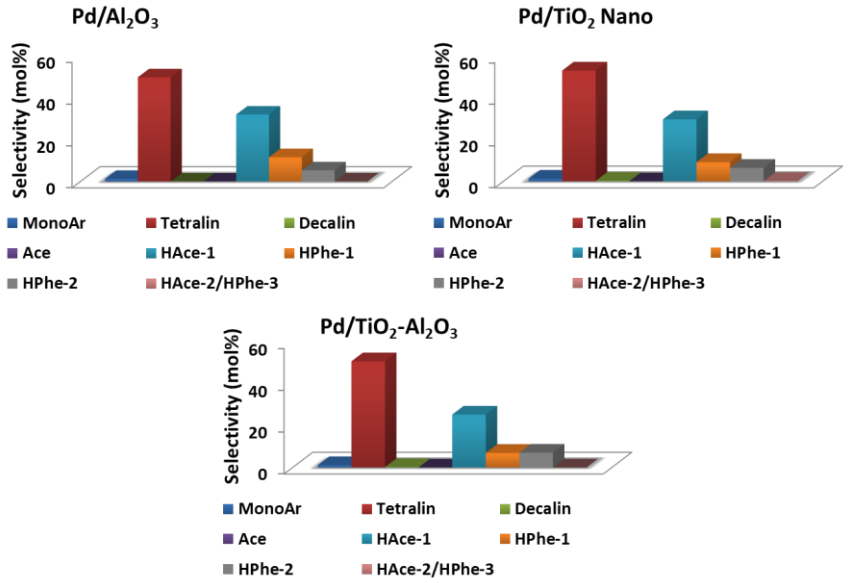

Figure 5.26. Selectivity to the different groups of products for Pd/γ-Al_2O_3, Pd/TiO_2 Nano and Pd/TiO_2-Al_2O_3 at 75-83% of conversion. Reaction conditions: 0.5 g of tars-type compounds, 4.0 g of n-hexadecane, 0.2 g of catalyst, 275 °C, 30 bar of H_2.

Table 5.24. Selectivity to the different products groups for 1.3wt%Pd/γ-Al_2O_3 at 275 °C and 30 bar of H_2.

Time (h)	Conv (mol%)	Product selectivity (mol%)							
		Mono Ar	Tetralin	Decalin	Ace	HAce-1	HPhe-1	HPhe-2	HAce-2/HPhe-3
0	0	0.0	0.0	0.0	0.0	0.0	0.0	0.0	0.0
1	44	1.8	22.4	0.0	18.5	33.6	15.7	0.8	0.0
3	57	1.4	33.4	0.0	4.6	36.3	16.8	2.3	0.0
5	68	1.2	42.3	0.0	0.3	33.9	14.2	3.8	0.0
7	**75**	**1.3**	**49.9**	**0.0**	**0.0**	**32.1**	**11.7**	**5.4**	**0.0**

Table 5.25. Selectivity to the different products groups for 1.3wt%Pd/TiO_2 Nano, 275 °C, 30 bar of H_2.

Time (h)	Conv. (mol%)	Product selectivity (mol%)							
		MonoAr	Tetralin	Decalin	Ace	HAce-1	HPhe-1	HPhe-2	HAce-2/HPhe-3
0	0	0.0	0.0	0.0	0.0	0.0	0.0	0.0	0.0
1	53	1.6	34.1	0.0	4.1	43.0	15.5	1.7	0.0
3	66	1.5	45.1	0.0	0.3	36.3	13.0	3.8	0.0
5	**80**	**1.3**	**53.0**	**0.3**	**0.0**	**29.7**	**9.2**	**6.4**	**0.1**
7	88	1.2	55.2	0.5	0.0	25.3	6.0	9.0	0.3

Another important point for comparing the here selected Pd catalysts was their reusability and stability after several reuses. The catalytic recycling results obtained after 7 h of reaction in each case are shown in Figure 5.27. For instance, the conversion of tars-type compounds decreased from 75% to 59% after three reuses for Pd/γ-Al_2O_3, whereas Pd/TiO_2 Nano was found to be stable during three reuses (conversion around 85%). In the case of Pd/TiO_2-Al_2O_3, and as it was discussed in the previous section of this chapter, the tars conversion decreased from 96% to ≈85% from the first use to the second use, then the activity was maintained mostly constant after the following consecutive reuses. It is important to mention that the catalytic behaviour of Pd/TiO_2-Al_2O_3 after the first use and during the three consecutive reuses was similar compared to Pd/TiO_2 Nano catalyst. In addition, it was constated that no Pd leaching occurred for the three Pd catalysts during the process.

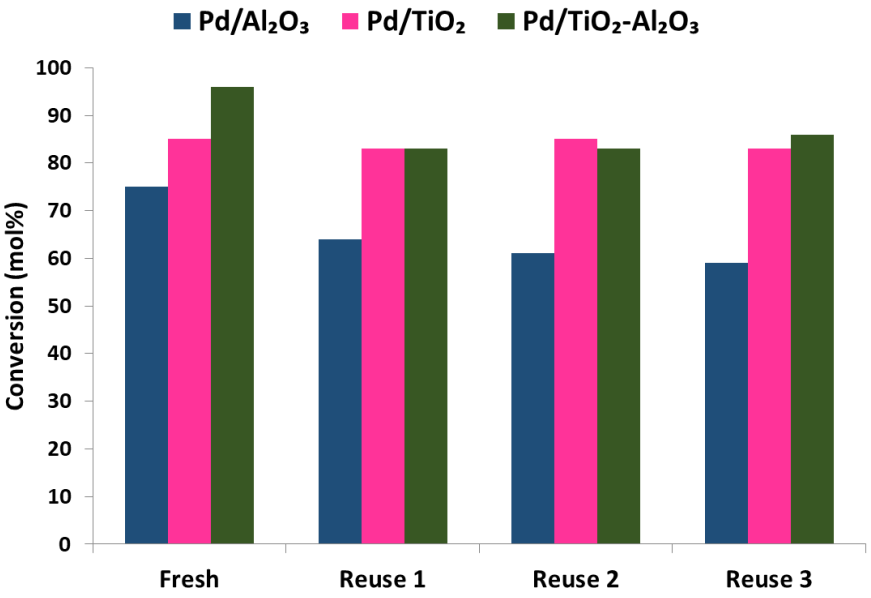

Figure 5.27. Reusability tests for Pd supported on γ-Al_2O_3, TiO_2 Nano and TiO_2-Al_2O_3 in tars mild hydrotreatment. Reaction conditions: 0.5 g of tars-type compounds, 4.0 g of n-hexadecane, 0.2 g of catalyst, 275 °C and 30 bar of H_2, during 7 h.

The organic matter deposition after the first use, third reuse and regeneration of Pd supported on γ-Al_2O_3, TiO_2 Nano and TiO_2-Al_2O_3 catalysts was also studied by means of elemental analysis (see Table 5.26). It can be concluded that Pd/γ-Al_2O_3 accumulated more carbonaceous compounds during reaction and was less resistant to carbon deposition, this explaining why this material was not capable to maintain the catalytic activity along consecutive reuses in comparison with Pd/TiO_2 Nano and Pd/TiO_2-Al_2O_3 catalysts. For instance, in the case of Pd/γ-Al_2O_3, the amount of carbon deposited on the solid was not totally removed after regeneration with H_2. On the

contrary, the amount of C deposited and accumulated onto the solid was much lower in the case of both Pd/TiO_2 Nano and Pd/TiO_2-Al_2O_3 catalysts, being strongly reduced after regeneration with H_2 in both cases. With respect to the Pd particle size behaviour encountered for the three Pd-based catalysts in this study, it can be seen in Table 5.26 and in Figure 5.28, respectively, that an increase in the average Pd particle size was detected after consecutive reuses in the case of Pd/γ-Al_2O_3. In that case, and as can be seen in the Pd particle size distribution (Figure 5.28), particle sizes with values even higher than 8-12 nm were encountered. In general, the Pd particle size values evolution encountered for both Pd/TiO_2 and Pd/TiO_2-Al_2O_3 materials during recycling study was quite similar. In these cases, Pd particle sizes even shifted towards slightly lower values after reuses, and they remain around 2 nm after regeneration with H_2 for the two Pd supported on TiO_2-based catalysts.

Table 5.26. Effect of reusability on carbon deposition and average Pd nanoparticle size of Pd supported on γ-Al_2O_3, TiO_2 Nano and TiO_2-Al_2O_3.

Catalyst	%C[a] [1st use/3rd reuse/regenerated]	Pd particle size[b] (nm) [fresh/3rd reuse/regenerated]
Pd/ γ-Al_2O_3	4.00/6.20/2.31	2.4/nd/3.8
Pd/TiO_2 Nano	0.75/1.49/0.59	3.0/2.0/2.0
Pd/TiO_2-Al_2O_3	1.35/2.62/0.80	2.3/2.5/2.0

[a] Results obtained from elemental analyses (EA). [b] Average diameter of Pd nanoparticles calculated from TEM measurements of, at least, 100 particles.

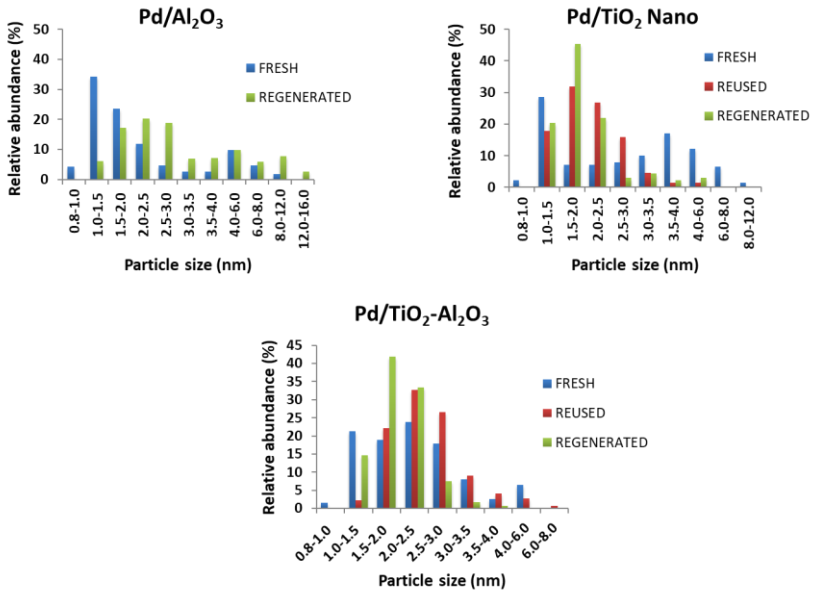

Figure 5.28. Pd nanoparticle size distribution of Pd supported on γ-Al_2O_3, TiO_2 Nano and TiO_2-Al_2O_3 catalysts (fresh, reused and regenerated).

Finally, and with the aim of establishing structure-activity relationships for the three here selected Pd catalysts, a study of their acidic properties was performed through NH_3-TPD measurements. The corresponding desorption profiles of Pd supported on γ-Al_2O_3, TiO_2 Nano and TiO_2-Al_2O_3 can be found in Figure 5.29. In addition, the total amount of ammonia adsorbed for each one of the catalysts is shown in Table 5.27. As can be seen, the total acidity measured can be ordered as follows: Pd/TiO_2-Al_2O_3 ≈ Pd/TiO_2 Nano > Pd/γ-Al_2O_3. This finding might explain the similar catalytic behaviour observed for Pd/TiO_2 Nano and Pd/TiO_2-Al_2O_3, which is superior than Pd/γ-Al_2O_3. Thus, a correlation between catalytic activity and total acidity can be established, where higher acidity results in higher catalytic activity.

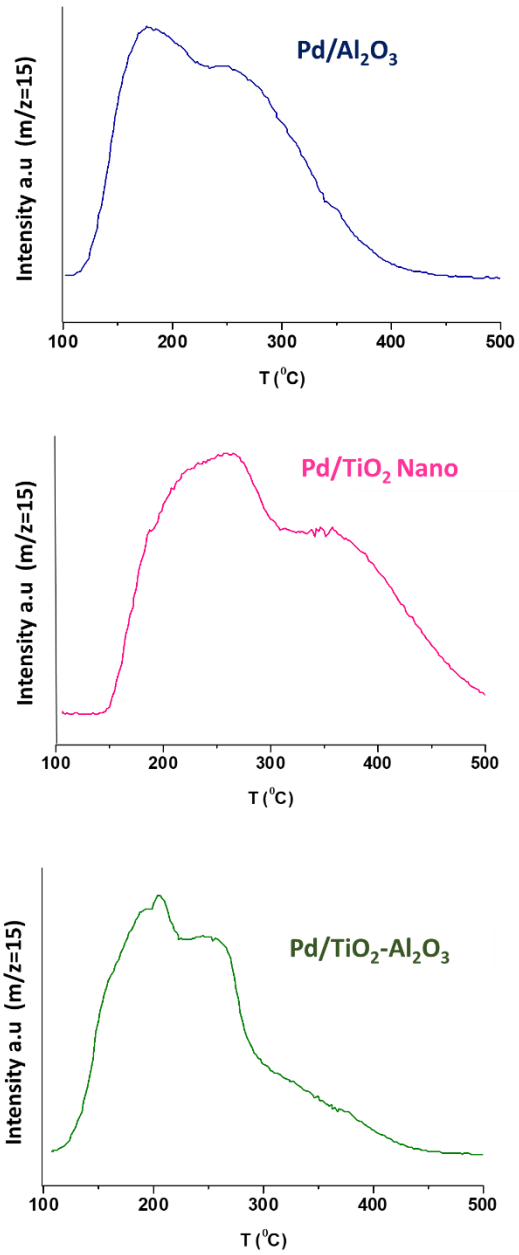

Figure 5.29. NH_3-TPD desorption profiles of Pd supported on γ-Al_2O_3, TiO_2 Nano and TiO_2-Al_2O_3.

Table 5.27. Ammonia adsorption on the different Pd catalysts.

Catalyst	Ammonia adsorbed (μmol/g)
Pd/γ-Al_2O_3	327
Pd/TiO_2 Nano	367
Pd/TiO_2-Al_2O_3	373

5.6. Pd supported on TiO_2/γ-Al_2O_3 as an efficient and cheap catalyst for the mild hydrotreatment of tars-type compounds

After obtaining some interesting results with Pd/TiO_2 Nano and Pd/TiO_2-Al_2O_3 in the mild hydrotreatment of tars-type molecules, another strategy studied was to synthesize a cheaper catalyst by reducing the amount of TiO_2 in the solid material. The idea is to generate a thin layer (or two-three layers) of titania covering the alumina material surface, thus taking advantage of the properties of the titania as support for Pd nanoparticles, but using much less amount of this TiO_2. In this sense, TiO_2/γ-Al_2O_3 was synthesized via incipient wetness impregnation method using Titanium isopropoxide as Ti precursor and ethanol as solvent. The amount of Ti impregnated was around 12wt%. After that, 1.3wt%Pd was supported onto the TiO_2/γ-Al_2O_3, the resultant material having the following main textural properties: surface area of 180 m^2/g and pore volume of 0.34 cm^3/g.

X-ray diffraction patterns of Pd supported on TiO_2/γ-Al_2O_3 are shown in Figure 5.30, and compared to the diffractogram of γ-Al_2O_3 sample. As can be seen, the peaks of TiO_2 anatase phase can be detected in $Pd/TiO_2/\gamma$-Al_2O_3 material, along with the peaks corresponding to gamma alumina. In addition, the very week diffraction peaks corresponding to the presence of Pd (111) metallic species can be observed in the Pd supported sample.

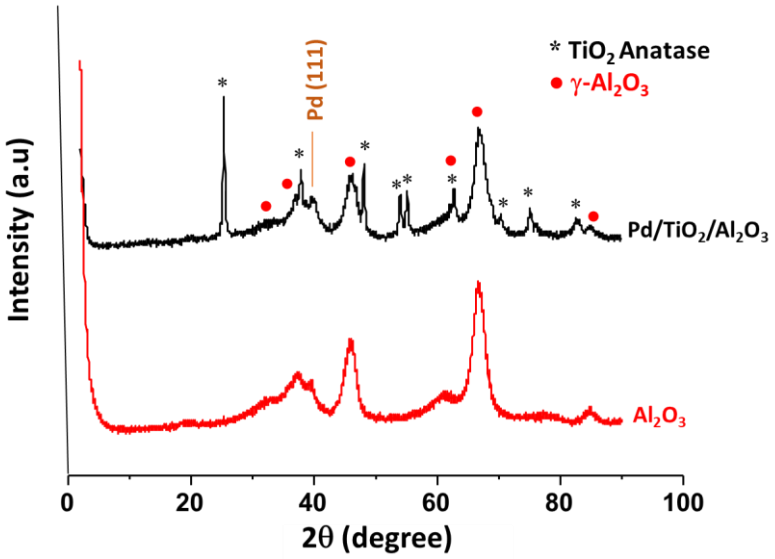

Figure 5.30. X-ray diffraction (XRD) patterns of $Pd/TiO_2/\gamma$-Al_2O_3 and γ-Al_2O_3 samples.

Pd supported on TiO_2/γ-Al_2O_3 catalyst was also analyzed by means of high-resolution transmission electron microscopy (HR-TEM) and scanning electron microscopy-energy dispersive X-ray

spectroscopy (SEM-EDX). The images are shown in Figures 5.31, 5.32 and A5.4. The presence of metallic Pd nanoparticles (red mark) can be clearly distinguished in the image (Fig. 5.31a and c), as well as the presence of TiO_2 phase (yellow mark, Fig. 5.31c). In addition, the Pd nanoparticle size distribution is represented in Figure 5.31d, resulting in an average Pd nanoparticle size around 3.5-4.0 nm, which is bigger than Pd nanoparticles encountered in the case of Pd supported on γ-Al_2O_3, TiO_2 Nano and TiO_2-Al_2O_3. It is worthing to note that, from data of Figure 5.32 and A5.4, both Pd and Ti elements were found to be homogeneously dispersed on the surface of the gamma alumina, this evidencing the adequate deposition of the TiO_2 phase onto the alumina support, and allowing then to properly accommodate the well dispersed Pd nanoparticles.

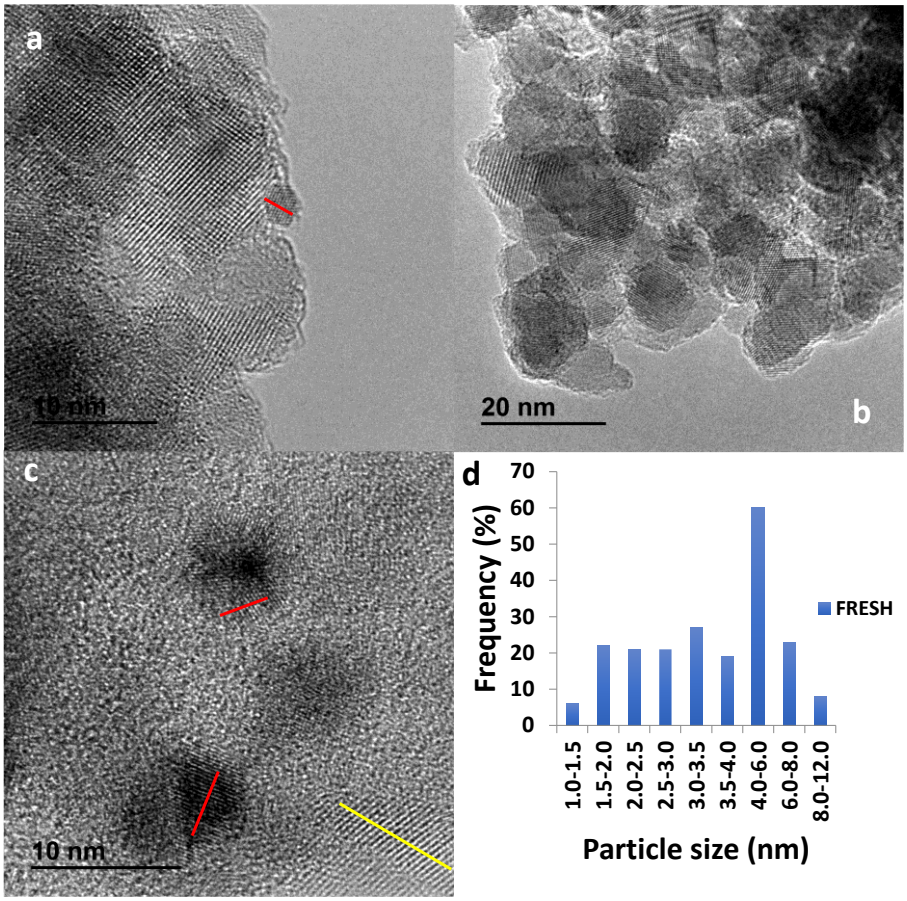

Figure 5.31. (a, b and c) HR-TEM images and (d) particle size distribution of the Pd/TiO_2/γ-Al_2O_3 catalyst (red: Pd (111), d≈0.22 nm and yellow: Ti (101), d≈0.35 nm).

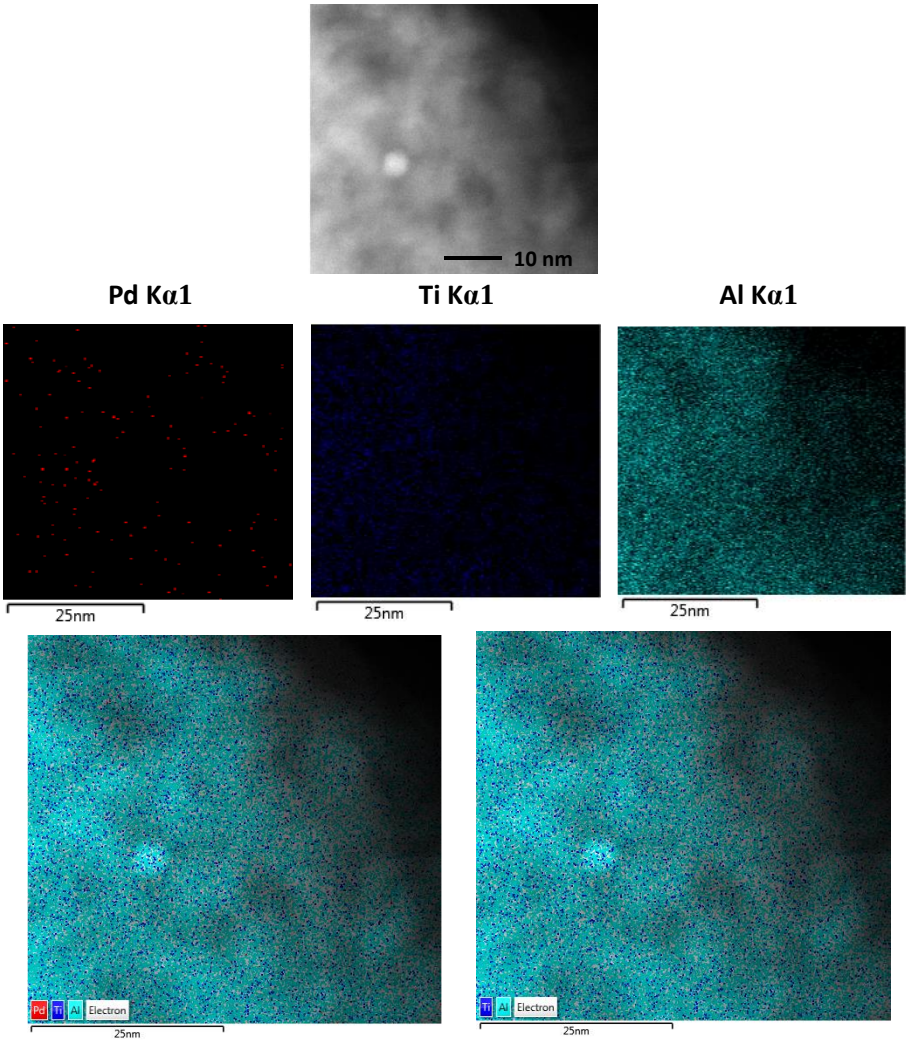

Figure 5.32. HRTEM-EDX mapping of $Pd/TiO_2/\gamma\text{-}Al_2O_3$ catalyst.

The catalytic activity of $Pd/TiO_2/\gamma\text{-}Al_2O_3$ was evaluated in the mild hydrotreatment of tars-type compounds at 275 ºC and 30 bar of H_2 during 7 h, and the attained results in terms of conversion of tars-type compounds and selectivity towards the hydrogenated products are listed in Table 5.28. In addition, its catalytic activity in terms of

conversion of tars-type compounds in a first catalytic test was compared with that of Pd/γ-Al_2O_3, Pd/TiO_2 Nano and Pd/TiO_2-Al_2O_3 catalysts (Figure 5.33). For instance, Pd/TiO_2/γ-Al_2O_3 showed similar tars-type conversion compared to Pd/TiO_2 Nano, higher than Pd/γ-Al_2O_3 and lower than Pd/TiO_2-Al_2O_3. Furthermore, similar selectivity to the different groups of hydrogenated products, compared at 75-83% of conversion, was achieved with all the Pd-based catalysts here studied (Figure 5.34).

Table 5.28. Selectivity to the different products groups for 1.3wt%Pd/TiO_2/γ-Al_2O_3 at 275 °C and 30 bar of H_2.

Time (h)	Conv (mol%)	Product selectivity (mol%)							
		Mono Ar	Tetralin	Decalin	Ace	HAce-1	HPhe-1	HPhe-2	HAce-2/HPhe-3
0	0	0.0	0.0	0.0	0.0	0.0	0.0	0.0	0.0
1	54	1.5	29.3	0.0	5.4	37.3	15.6	1.4	0.0
3	67	1.5	44.3	0.0	0.7	35.7	13.6	4.3	0.0
5	79	1.3	52.3	0.0	0.0	30.7	9.7	6.8	0.0
7	84	1.4	58.7	0.2	0.0	29.3	7.6	9.4	0.0

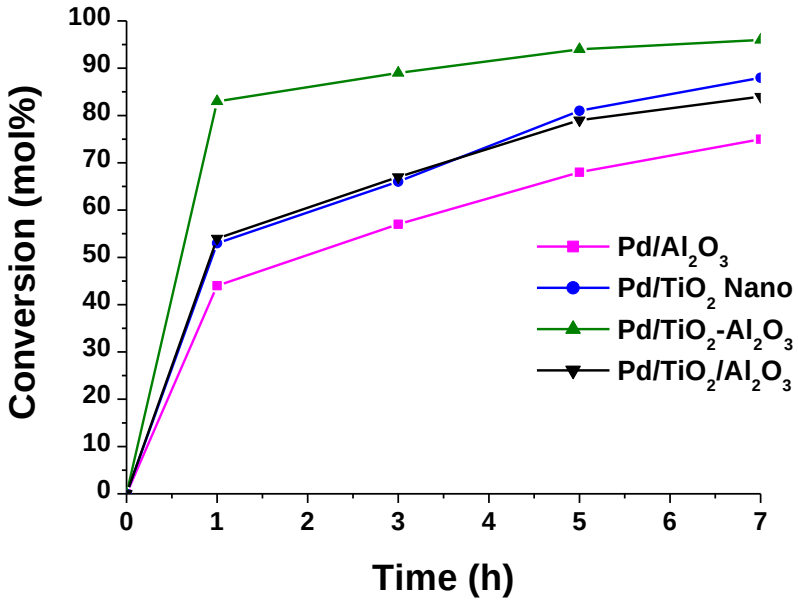

Figure 5.33. Conversion of tars-type compounds over Pd supported on γ-Al_2O_3, TiO_2 Nano, TiO_2-Al_2O_3 and TiO_2/γ-Al_2O_3. Reaction conditions: 0.5 g of tars-type compounds, 4.0 g of n-hexadecane, 0.2 g of catalyst, 275 ºC, 30 bar of H_2, during 7 h.

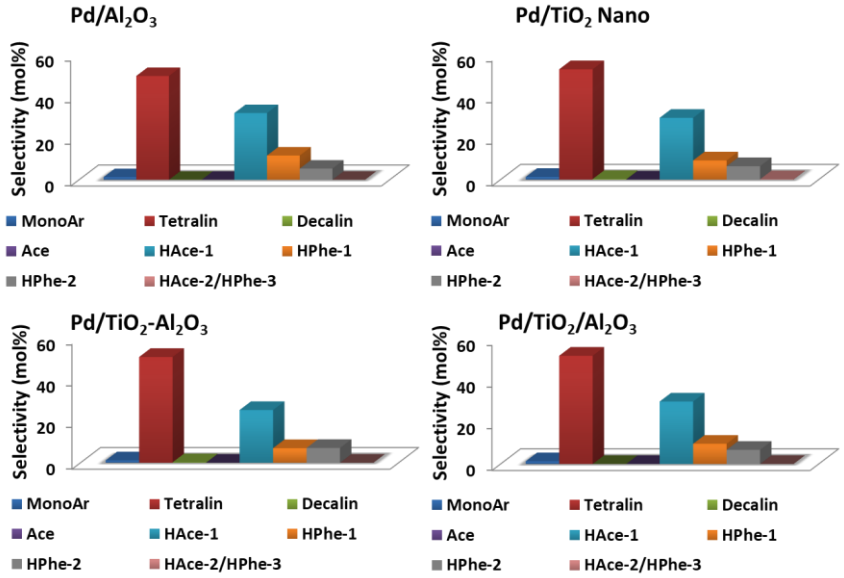

Figure 5.34. Selectivity to the different groups of products for Pd/γ-Al_2O_3, Pd/TiO_2 Nano, Pd/TiO_2-Al_2O_3 and Pd/TiO_2/γ-Al_2O_3 at 75-83% of conversion. Reaction conditions: 0.5 g of tars-type compounds, 4.0 g of n-hexadecane, 0.2 g of catalyst, 275 °C, 30 bar of H_2.

To highlight, Pd/TiO_2/γ-Al_2O_3 catalyst was successfully prepared and tested in the mild hydrotreatment of tars-type compounds. The latter showed similar catalytic activity compared to Pd/TiO_2 Nano. Interestingly, from an economic point of view, Pd/TiO_2/γ-Al_2O_3 material possesses some advantages over the other above-mentioned Pd catalysts, taking into consideration its easier preparation method (impregnation of Ti precursor onto the support) and lower cost (less Ti content over commercial available gamma alumina support).

5.7. Application scope: Pd supported on TiO_2-Al_2O_3 as an efficient catalyst for the reductive amination of bio-derived acetol to 2-methylpiperazine

As already described, Pd/TiO_2-Al_2O_3 catalyst was found to be an efficient catalyst for the mild hydrotreatment of tars-type compounds. Interestingly, its application scope was extended to other demanding hydrogenation reactions. In this sense, Pd/TiO_2-Al_2O_3 catalyst was tested in the reductive amination of hydroxyacetone or acetol, product of the selective dehydration of glycerol, with ethylenediamine to produce high-added value N-heterocycle (2-methylpiperazine, 2-MP) [1]. This study provides a new and sustainable catalytic route to synthesize organo-nitrogen molecules from renewable raw materials (i.e., acetol) as a carbon source. The piperazine can be found as a building block for a large number of drugs with high added value, such as antihistamines and antidepressants, which are highly valued chemicals used as synthesis intermediate in organic chemistry [2].

Reductive cycle-amination reactions were performed in liquid phase in a "batch" type reactor where reactants, such as acetol and ethylenediamine were mixed together with the solid catalyst and methanol as solvent. Experiments were carried out at 90 ºC and 13 bar of H_2 pressure during 3 h, and liquid samples were collected and analyzed by means of gas chromatography (See Experimental Part, Chapter 3). A schematic representation of the reaction pathways occurring during the reductive amination of acetol with

ethylenediamine to mainly form 2-methylpiperazine (2-MP) is given in Figure 5.35.

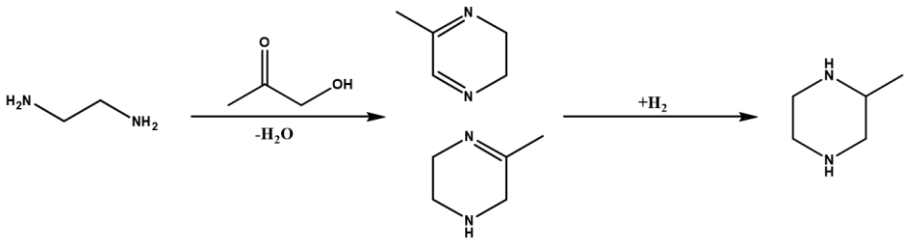

Figure 5.35. Main reaction pathways for the reductive amination of acetol to 2-MP.

In this sense, different Pd supported on simple and mixed metal oxides such as Al_2O_3, ZrO_2, TiO_2 Nano, MgO, TiO_2-ZrO_2, ZrO_2-Al_2O_3 and TiO_2-Al_2O_3 were evaluated in the reductive amination reaction, and in this chapter we focused on comparing the catalytic performance of Pd/TiO_2-Al_2O_3, Pd/TiO_2 Nano and Pd/Al_2O_3 materials. For instance, data of Table 5.29 indicate that Pd/TiO_2-Al_2O_3 catalyst demonstrated the highest catalytic activity among the three selected catalysts (yield of 2-MP = 57%), followed by Pd/TiO_2 Nano (yield of 2-MP = 44%), and Pd/Al_2O_3 (yield of 2-MP = 23%).

Table 5.29. Yield of 2-MP and TON in the reductive cycle-amination of acetol with ethylenediamine.[a]

Catalyst	Pd (wt%)[b]	Yield of 2-MP (mol%)	TON[c]
Pd/Al_2O_3	1.0	23	818
Pd/TiO_2 Nano	1.2	44	1304
Pd/TiO_2-Al_2O_3	1.0	57	2028

[a] Reaction conditions: 0.325 g of acetol, 0.227 g of ethylenediamine, 1.250 g of methanol, 0.011 g of catalyst at 90 ºC and 13 bar of H_2, for 3 h under stirring (800 rpm) and with slow addition of acetol (100 µL/h). [b] Values obtained from ICP. [c] TON = mol 2-MP / mol Pd.

In order to explain the catalytic differences observed between these three Pd-based catalysts, IR spectroscopy with CO adsorption as a probe molecule was performed, being the most relevant technique in this work. In this sense, the surface metal sites (i.e., crystal facets, uncoordinated sites and particle morphology) were analyzed. For instance, and as can be seen in Figure 5.36, IR band of the Pd-CO interaction at 2042 cm^{-1}, which is characteristic of unsaturated sites, was observed in the Pd/TiO_2-Al_2O_3 catalyst. In addition, IR bands at 2092 and 2085 cm^{-1} (characteristics of (111) and (100) facets, respectively), along with IR bands at 1988 and 1925 cm^{-1} (characteristics of bridge CO and 3-fold CO configuration on Pd terraces, respectively) are observed, but being more dominant in the Pd/TiO_2 Nano and Pd/Al_2O_3 samples. Thus, based on the IR-CO results and correlating them with the catalytic data of Table 5.29, it is probably that uncoordinated Pd sites as in the Pd/TiO_2-Al_2O_3 sample

favour imine (C=N) group hydrogenation, as already found in previous work [3].

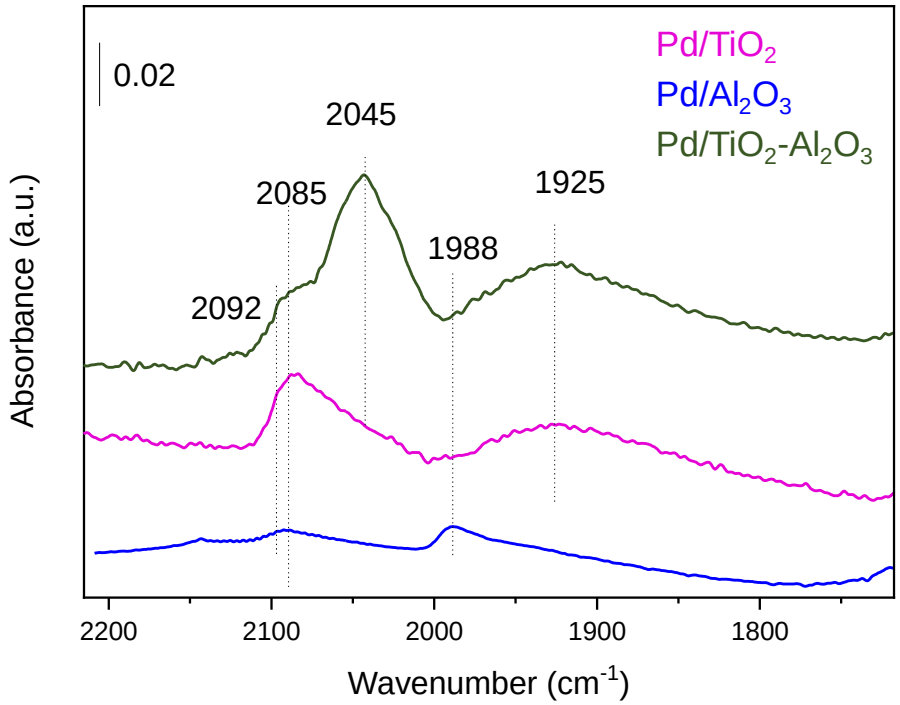

Figure 5.36. IR spectra of CO adsorption at saturation coverage (i.e., 8.5 mbar CO) on Pd-based catalysts.

Summarizing, Pd/TiO_2-Al_2O_3 catalyst demonstrated higher catalytic performance compared with Pd/TiO_2 Nano and Pd/Al_2O_3 materials in the reductive amination of acetol with ethylenediamine, resulting in higher yields of 2-methylpiperazine. For instance, the presence of uncoordinated Pd sites in the Pd supported on mixed oxide catalyst seemed to favour the hydrogenation of imine (C=N) group, thus improving the 2-MP formation.

5.8. Conclusions

- Better catalytic results in the tars mild hydrotreatment are obtained with Pd/TiO_2-Al_2O_3 material compared with Pd supported on other mixed metal oxides with different metal compositions such as TiZr, TiSi, ZrAl and SiAl.
- The synthesis of TiO_2-Al_2O_3 support is optimized, and most relevant results are found when Pd is supported on TiO_2-Al_2O_3 having a Ti/Al molar ratio ≈ 1.3, synthesized at pH = 9, with ammonia solution addition rate of 1000 mL/h, and being precipitated during 12 h (aging time) at 60 ºC. This optimized Pd/TiO_2-Al_2O_3 catalyst shows to be the most efficient catalyst for the mild hydrotreatment of tars-type compounds.
- Pd/TiO_2-Al_2O_3 catalyst is efficient and stable for the tars mild hydrotreatment, even after consecutive reuses. Thus, quite low carbon deposition, any Pd leaching and changes in the Pd particle size (and distribution) are observed after consecutive reuses and regeneration with H_2.
- Pd/TiO_2-Al_2O_3 showed similar catalytic activity compared to Pd/TiO_2 Nano, and better than Pd/γ-Al_2O_3 in the tars mild hydrotreatment. In this sense, Pd/TiO_2-Al_2O_3 and Pd/TiO_2 Nano materials are more resistant to carbon deposition than Pd/γ-Al_2O_3. In addition, bigger Pd particle size (and distribution) is found in the case of Pd/γ-Al_2O_3 after several reuses.
- TiO_2/γ-Al_2O_3 material is successfully synthesized via incipient wetness impregnation method. In addition, the catalytic activity of

$Pd/TiO_2/\gamma\text{-}Al_2O_3$ catalyst is found to be similar to that of Pd/TiO_2 Nano, being cheaper and easier to prepare in comparison with Pd supported on co-precipitated Ti-Al mixed oxide.

- The application scope of $Pd/TiO_2\text{-}Al_2O_3$ catalyst is extended to another demanding hydrogenation reaction, such as the reductive amination of bio-derived acetol with ethylenediamine to produce 2-methylpiperazine (2-MP). In this sense, $Pd/TiO_2\text{-}Al_2O_3$ catalyst showed higher activity compared with Pd supported on Al_2O_3 and TiO_2 Nano samples, probably due to the presence of uncoordinated Pd sites that favour the imine (C=N) group hydrogenation.

5.9. References

[1] J. Mazarío, Z. Raad, P. Concepción, C. Cerdá-Moreno, M.E. Domine, Catalysis Science & Technology 10 (2020) 8049-8063.

[2] R.D. Taylor, M. MacCoss, A.D. Lawson, Journal of Medicinal Chemistry 57 (2014) 5845-5859.

[3] J.D. Vidal, M.J. Climent, P. Concepción, A. Corma, S. Iborra, M.J. Sabater, ACS Catalysis 5 (2015) 5812-5821.

CHAPTER 6.

NI-BASED CATALYSTS FOR HYDROGENATION REACTIONS

6.1. Introduction

After achieving interesting results in the mild hydrotreatment of tars by using Pd supported on mixed metal oxides (TiO_2-Al_2O_3 prepared via co-precipitation method and TiO_2/Al_2O_3 prepared via incipient wetness impregnation method) as catalysts, our focus was to prepare non-noble metal-based catalysts. For this purpose and attending to the reported use of different transition metals in hydrotreatment processes [1-3], Ni was selected as the active phase for the novel catalysts development. In this sense, simple metal oxides such as gamma Al_2O_3, TiO_2 (P25) and ZrO_2 monoclinic, along with mixed metal oxides such as TiO_2-Al_2O_3, TiO_2/Al_2O_3, TiO_2-ZrO_2, TiO_2/ZrO_2 and ZrO_2-Al_2O_3 were employed as supports for Ni incorporation via incipient wetness impregnation method (see section 3.2.5, Chapter 3). As it was done for Pd-based catalysts in previous chapters, the here studied catalysts were tested in the hydrotreatment of tars-type compounds under mild reaction conditions. In addition, the Ni-based catalysts here prepared were used in the selective hydrogenation of fatty acids under mild reaction conditions, mainly for hydrocarbons production, that could be applied as renewable components for automotive fuels.

6.2. Ni-based catalysts for the mild hydrotreatment of tars-type compounds

As above-mentioned, Ni supported on simple metal oxides (gamma Al_2O_3, TiO_2 (P25) and ZrO_2 monoclinic) and mixed metal oxides (TiO_2-Al_2O_3, TiO_2/Al_2O_3, TiO_2-ZrO_2, TiO_2/ZrO_2 and ZrO_2-

Al_2O_3) were prepared and well characterized prior to be tested in the mild hydrotreatment of tars-type compounds. For the mixed metallic oxides synthesized via co-precipitation method, and as it was previously described in Chapter 5, the different metal molar ratios in the samples were as follows: Ti/Al = 1.3, Ti/Zr = 1.0 and Zr/Al = 0.7, respectively. In addition, the amount of Ti impregnated onto Al_2O_3 and ZrO_2 to generate the corresponding TiO_2/Al_2O_3 and TiO_2/ZrO_2 materials was around 12wt%. Ni was incorporated onto the different metal oxides by incipient wetness impregnation to theoretically achieve ≈14-15wt% of Ni in the final solids. The Ni loadings and the main textural properties of the Ni-based catalysts thus obtained are listed in Table 6.1. As can be seen, the Ni loadings obtained ranged between 12.9 and 14.2wt%, the metal contents reached were around 14wt% in the case of simple metal oxides supports, and between 12.9 and 13.8wt% for the other metallic mixed oxides supports. In general, only slight decrease in the surface area of the materials was observed after the Ni incorporation, except for Ni/TiO_2-ZrO_2 where the surface area decay was close to 30%.

Table 6.1. Ni loadings and main textural properties of the Ni-based catalysts.

Catalyst	Ni	Surface area (m^2/g)[b]		Pore volume (cm^3/g)[b]	
	(wt%)[a]	Support	Catalyst	Support	Catalyst
Ni/Al_2O_3	14.2	250	222	0.48	0.30
Ni/TiO_2	14.0	50	78	0.25	0.25
Ni/ZrO_2	13.9	105	90	0.22	0.15
Ni/TiO_2-Al_2O_3	12.9	295	250	0.29	0.24
$Ni/TiO_2/Al_2O_3$	13.8	180	166	0.34	0.26
Ni/TiO_2-ZrO_2	13.6	300	205	0.26	0.14
$Ni/TiO_2/ZrO_2$	13.5	88	80	0.17	0.15
Ni/ZrO_2-Al_2O_3	13.2	230	186	0.10	0.06

[a] Values measured by ICP. [b] Calculated from N_2 adsorption isotherms.

The different Ni-based catalysts here prepared were essayed in the hydrotreatment of tars-type molecules under mild reaction conditions (275 ºC and 30 bar of H_2), and the results in terms of conversion of tars and yields to the different formed products are exposed in Table 6.2. As can be seen, the Ni supported on simple metal oxides achieved good levels of tars conversion (81% for Ni/TiO_2, 82% for Ni/ZrO_2, and 94% for Ni/Al_2O_3, respectively), better than other Ni supported on mixed metallic oxides in the Table 6.2. Nevertheless, the highest conversion of tars molecules (conv. = 98%) after 7 h of reaction was encountered for $Ni/TiO_2/Al_2O_3$ catalyst. The same tendency was observed in terms of products distribution, with more hydrogenated products produced with the $Ni/TiO_2/Al_2O_3$ catalyst, thus operating slightly better than Ni/Al_2O_3 and the other simple metal oxides-based materials, and much better than most of the mixed metallic oxides-based catalysts.

Remarkably, the $Ni/TiO_2/Al_2O_3$ catalyst was capable to reach this tars molecules conversion (98%) with adequate production of more hydrogenated compounds at lower reaction times (see Table 6.3). As can be seen in the Table, the maximum selectivity to the partially hydrogenated products was achieved at 1-2 h of reaction, while totally hydrogenated products, such as decalin and HAce-2/HPhe-3 were slowly and continuously generated at longer reaction times.

Table 6.2. Conversion of tars and yield to different products groups in the tars mild hydrotreatment over different Ni-based catalysts.[a]

Catalyst	Conv. mol%	Product yield (mol%)							
		Mono Ar	Tetralin	Decalin	Ace	HAce-1	HPhe -1	HPhe -2	HAce-2/HPhe-3
$Ni/TiO_2/ZrO_2$	55	1.0	20.2	0.0	4.0	18.9	6.3	1.2	0.0
Ni/ZrO_2-Al_2O_3	59	1.1	22.1	0.0	4.7	17.9	6.8	1.0	0.0
Ni/TiO_2-Al_2O_3	73	1.0	30.9	0.0	0.8	20.8	6.3	3.6	0.0
Ni/TiO_2-ZrO_2	80	0.9	39.6	0.0	0.0	22.2	6.1	5.8	0.0
Ni/TiO_2	81	1.1	42.7	0.0	0.0	23.3	6.5	6.5	0.0
Ni/ZrO_2	82	1.1	45.7	0.0	0.0	23.4	6.7	6.2	0.0
Ni/Al_2O_3	94	1.0	52.0	1.6	0.0	22.7	4.2	11.4	1.2
$Ni/TiO_2/Al_2O_3$	98	1.0	48.9	6.1	0.0	18.8	2.9	14.4	5.2

[a] Reaction conditions: 0.5 g of tars-type compounds, 4.0 g of n-hexadecane, at 275 °C, 30 bar of H_2, 0.2 g of catalyst during 7 h.

Table 6.3. Selectivity to the different products groups in the tars mild hydrotreatment over $Ni/TiO_2/Al_2O_3$ at 275 °C and 30 bar of H_2.

Time (h)	Conv. mol%	Product selectivity (mol%)							
		Mono Ar	Tetralin	Decalin	Ace	HAce-1	HPhe-1	HPhe-2	HAce-2/HPhe-3
0	0	0.0	0.0	0.0	0.0	0.0	0.0	0.0	0.0
1	98	1.1	53.7	2.8	0.0	21.9	2.1	15.6	2.1
3	98	1.0	51.3	4.6	0.0	20.3	2.4	15.3	3.1
5	98	1.0	49.6	5.7	0.0	19.2	2.8	14.8	4.7
7	98	1.0	50.1	6.2	0.0	19.3	3.0	14.7	5.3

Summarizing, the $Ni/TiO_2/Al_2O_3$ catalyst with Ni incorporated onto a γ-Al_2O_3 support containing ≈12wt% Ti (as TiO_2 probably in the form of thin layers) deposited on its surface was encountered to be an efficient catalyst for the mild hydrotreatment of tars-type compounds. Apparently, the strong interaction between Ni and Al_2O_3 is responsible for this excellent catalytic behaviour of Ni supported on Al_2O_3 and TiO_2/Al_2O_3 catalysts. For this reason, the application of these Ni-based catalysts was extended to other hydrogenation reactions, such as selective hydrogenation of fatty acids for hydrocarbons production, as different types of Ni-based catalysts were already reported and well described in the literature for this type of reaction.

6.3. Ni-based catalysts for the selective hydrogenation of fatty acids for hydrocarbons and/or alcohols production

6.3.1. Introduction

As consequence to the expending of fossil resources, and the increased interest and need for energy and transportation fuels, it is important to stress the utilization of alternative and renewable resources, thus developing economical processes to produce sustainable fuels and chemicals. In this sense, biomass feedstock represents the most current available source of renewable carbon and is promising to produce sustainable liquid fuels (biofuels) and chemicals [4,5].

Biodiesel (Fatty Acid Methyl Esters FAMEs), one of the most employed renewable alternatives for substituting fossil fuels, is obtained by transesterification of the triglycerides (or vegetable oils) with methanol in the presence of mainly basic catalysts [4,6]. The raw materials being the source of triglycerides are colza, sunflower, soy, or palm oil, whereas the biodiesel (FAMEs) produced can be directly used as a fuel or mixed with petro-diesel in different ratios [4]. However, FAMEs have demonstrated many drawbacks, such as low energy density and high viscosity compared with fossil derived diesel, thermal and oxidation stability, and tendency to polymerize forming coke [7,8]. In this sense, and for overcoming these disadvantages, novel catalytic processes are being developed and studied to transform fatty acids and fatty esters into hydrocarbons and alcohols useful for both fuel and petrochemical applications.

One alternative that is gaining force in the last years is the production of the called green diesel via hydrodeoxygenation, decarboxylation and decarbonylation of vegetable oils and fats. In all the cases, reactions are performed by using heterogeneous catalysts mainly based on metals supported on inorganic matrix [9-12]. Hydrodeoxygenation (HDO) process requires a large quantity of hydrogen to reduce the oxygenated species present in the fatty acids and fatty esters, and the hydrocarbon produced has the same chain length as the original fatty acid and fatty ester [9]. However, decarboxylation (DCO_2) and decarbonylation (DCO) generate hydrocarbons with one carbon less than the original fatty acid and fatty ester, releasing CO_2 and CO, respectively. In addition, DCO_2 and DCO occurred by using small amount of hydrogen, or even an inert atmosphere [10-13]. In this sense, under inert He atmosphere (15 bar), oleic acid, used as a fatty acid model molecule, was mainly transformed into unsaturated hydrocarbons (i.e., heptadecene), which could be adsorbed on the catalyst surface and block its active centers. In the case of stearic acid, n-heptadecane was mainly produced under He atmosphere via decarboxylation. However, n-heptadecane was the only product detected when working under 10% H_2 in the case of both fatty acids, mainly via decarboxylation of stearic acid [14].

Many studies have reported the production of hydrocarbons from fatty acids and fatty esters. For instance, Li et al. [15] have studied the production of n-heptadecane from oleic acid using Ni/ZrO_2-Al_2O_3 as catalyst at 280 ºC and 30 bar of H_2 during 6 hours, thus yielding

95wt% of n-heptadecane (in liquids) via decarbonylation route. Additionally, it was mentioned that the stearyl stearate, by-product formed by esterification of stearic acid and stearyl alcohol (1-octadecanol) intermediates, was transformed into n-heptadecane via hydrogenolysis [15,16]. Jenišťová et al. [17] have reported the production of n-heptadecane (96wt% yield and 97wt% selectivity, in liquids) by converting stearic acid using 5wt%Ni/Al_2O_3 at 300 ºC and 30 bar of H_2 during 6 hours. The effect of H_2 pressure was also investigated, concluding that the hydrogen is important and crucial for the formation of n-heptadecane (via formation of stearyl alcohol intermediate). This was already confirmed by the early work done by Maier et al. using Pd/SiO_2 at 330 ºC, evidencing that no reaction occurs under nitrogen atmosphere [18]. Further, Li et al. [19] have investigated the chemoselective hydrodeoxygenation HDO of oleic acid to long-chain hydrocarbons using a nitrogen-doped carbon-alumina hybrid supported iron (Fe-N-C@Al_2O_3) as catalyst at 320 ºC and 40 bar of H_2 during 8 hours. The n-octadecane and n-heptadecane yields were as follows: 92mol% and 6mol%, respectively (in liquids).

In light of the above-mentioned considerations, it is possible to convert fatty acids and fatty esters into hydrocarbons via hydrodeoxygenation HDO (n-octadecane or C18 formation) and decarbonylation or decarboxylation (n-heptadecane or C17 formation) processes. In most of the cases, the use of Ni-based catalysts and the presence of hydrogen appear to be crucial for the reaction taking place. For this reason, Ni-based catalysts were prepared in this work and tested

in the selective hydrogenation of fatty acids, mainly for hydrocarbons production.

6.3.2. Catalytic screening of Ni-based catalysts

Prior to the first catalytic test, blank test was carried out at 275 ºC and 30 bar of H_2 for 3 h to accurate the adequate performing of the experiments by determining the quantity of evaporated liquids during the test. The catalytic experiments were carried out in a slurry parallel reactors system (at REALCAT platform, Lille, France, see section 3.4.3, Chapter 3) with the 24 reactors filled with 1.56 mL of 15wt% oleic acid in decalin solution. Indeed, the results obtained from blank experiments (see Table A6.1 in Annex) showed no significant loss (<10%) in the masses of the reactors detected before and after tests, this meaning that the system worked adequately and was ready for the first catalytic screening.

Afterwards, different Ni supported on simple and mixed metal oxides, already prepared and described in the previous section (see Table 6.1), were tested in the selective hydrogenation of oleic acid (model molecule representative of fatty acids feedstocks). The first catalytic screening was carried out at 275 ºC and 30 bar of H_2 during 3 h, with 25 mg of catalyst, and the attained results in terms of selectivity to the different products at total conversion of oleic acid are shown in Figure 6.1. In fact, oleic acid conversion was 100% for all the catalysts tested under these reaction conditions. The main products obtained during the reaction were stearic acid, stearyl alcohol (1-octadecanol),

n-heptadecane (C17), n-octadecane (C18), stearyl stearate and carbon monoxide (CO).

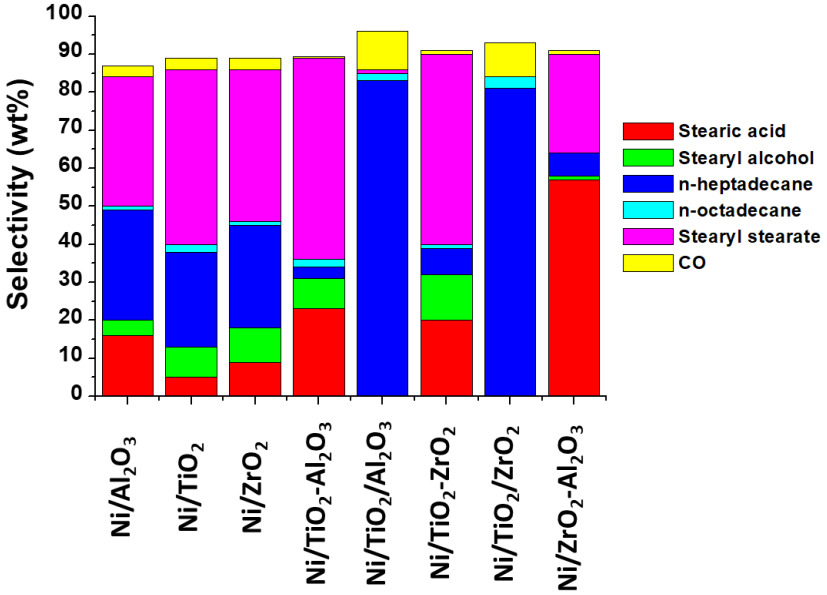

Figure 6.1. Selectivity to the different products in the oleic acid selective hydrogenation over Ni-based catalysts (Conversion = 100%). Reactions conditions: 1.56 mL of 15wt% oleic acid in decalin solution, 25 mg of catalyst, 275 ºC, 30 bar of H_2, during 3 h.

On one hand, and it can be seen from data of Figure 6.1, Ni supported on TiO_2/Al_2O_3 and TiO_2/ZrO_2 were the most selective catalysts to n-heptadecane (C17) with 83% and 81% selectivity, respectively, and with very low selectivity to n-octadecane C18 (2% and 3%, respectively). In both cases, CO was detected as practically the only one gas product of the reaction (together with traces of methane)

by qualitative GC-TCD analysis of extracted gaseous sample from the autoclave reactor. Thus, CO gas selectivity was found to be 10% and 9% for $Ni/TiO_2/Al_2O_3$ and $Ni/TiO_2/ZrO_2$, respectively. For instance, CO selectivity was calculated by estimating the mass of CO from the following equation (n CO = n C17), and the maximum CO selectivity that could be achieved was found to be 10% (using the following formula, Max CO selectivity = 100 x MW CO/MW oleic acid).

On the other hand, the n-heptadecane (C17) selectivity was between 25-29% when using Ni supported on simple metal oxides (i.e., Al_2O_3, TiO_2, and ZrO_2) with very similar products distribution. Thus, the presence of stearic acid (the double bond hydrogenated product of oleic acid) was detected, together with small amounts of stearyl alcohol (intermediate) and large amounts of stearyl stearate. In addition, Ni/TiO_2-Al_2O_3 and Ni/TiO_2-ZrO_2 presented low production of hydrocarbons (n-heptadecane and n-octadecane), whereas the amounts of stearic acid, stearyl stearate and stearyl alcohol were increased (the latter in minor extent). Finally, a very low hydrogenation activity was observed with Ni/ZrO_2-Al_2O_3 catalyst, which mainly produced stearic acid and stearyl stearate accompanied with small amount of n-heptadecane (C17).

Summarizing, Ni supported on TiO_2/Al_2O_3 and TiO_2/ZrO_2 were the most active catalytic systems for n-heptadecane production. Apparently, the presence of thin layers of TiO_2 deposited onto Al_2O_3 and ZrO_2 materials seemed to play an important role in the n-heptadecane (C17) production. These two catalytic systems were

selected for further studies to develop an optimized catalyst for the selective hydrogenation of fatty acids.

6.3.3. Influence of the addition of Pt to Ni supported on TiO_2/Al_2O_3 and TiO_2/ZrO_2 catalysts

In addition to the selection of Ni supported on TiO_2/Al_2O_3 and TiO_2/ZrO_2 as efficient catalysts for the selective hydrogenation of oleic acid for n-heptadecane (C17) production, the effect of incorporating another metal along with Ni was evaluated. In this case, Pt was incorporated as dopant together with Ni onto TiO_2/Al_2O_3 and TiO_2/ZrO_2 materials. In addition, Pt supported on the same mixed metallic oxides materials were prepared for comparative purpose. The main physico-chemical and textural properties of the catalysts thus synthesized are listed in Table 6.4.

Table 6.4. Main physico-chemical and textural properties of the monometallic Ni- and Pt- and bimetallic PtNi-based catalysts.

Catalyst	Ni (wt%)[a]	Pt (wt%)[a]	Surface area (m^2/g)[b]	Pore volume (cm^3/g)[b]
$Ni/TiO_2/Al_2O_3$	13.8	-	166	0.26
$Ni/TiO_2/ZrO_2$	13.5	-	80	0.15
$PtNi/TiO_2/Al_2O_3$	14.2	0.6	192	0.28
$PtNi/TiO_2/ZrO_2$	14.2	0.6	77	0.15
$Pt/TiO_2/Al_2O_3$	-	1.2	182	0.33
$Pt/TiO_2/ZrO_2$	-	1.2	86	0.17

[a] Values measured by ICP. [b] Calculated from N_2 adsorption isotherms.

The catalytic performance of monometallic Ni- and Pt- and bimetallic PtNi-based catalysts was evaluated in the selective hydrogenation of oleic acid at 275 ºC and 30 bar of H_2 during 3 h by means of the 24 slurry parallel reactors system (REALCAT platform). The attained results in terms of selectivity to the different products at 100% conversion level for all the catalysts are shown in Figure 6.2.

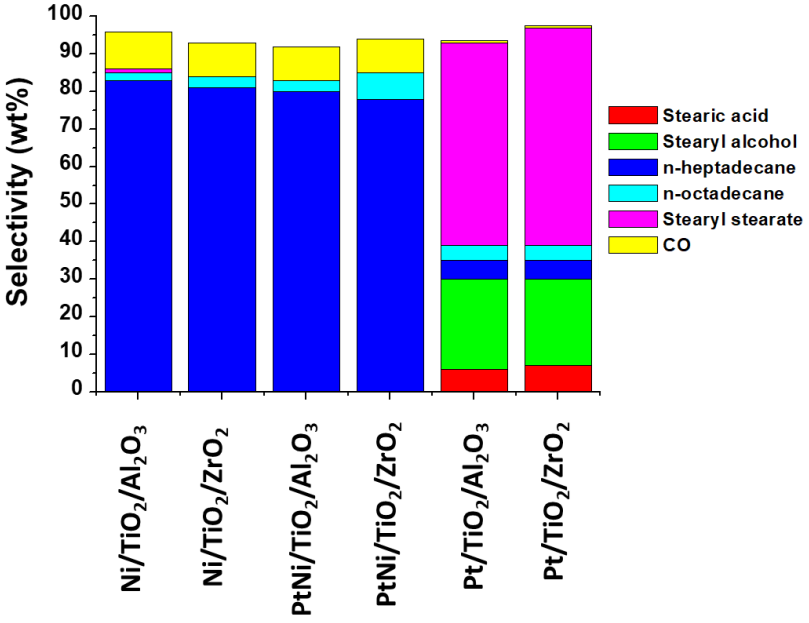

Figure 6.2. Selectivity to the different products for Ni-, PtNi- and Pt-based catalysts in the oleic acid selective hydrogenation (Conversion = 100%). Reactions conditions: 1.56 mL of 15wt% oleic acid in decalin solution, 25 mg of catalyst, 275 ºC, 30 bar of H_2, during 3 h.

As can be seen from Figure 6.2, monometallic Ni and bimetallic PtNi supported on TiO_2/Al_2O_3 and TiO_2/ZrO_2 materials offered quite similar selectivity to n-heptadecane (C17) (around 80% selectivity)

under these reaction conditions, thus achieving the maximum production of n-heptadecane (C17). It is worth to note that the selectivity to n-octadecane (C18) increased from 3% to 7% when adding Pt to Ni supported on TiO_2/ZrO_2 catalyst. However, for monometallic Pt-based catalysts, the n-heptadecane (C17) formation was almost negligible, these Pt-based catalysts being more selective to stearyl alcohol (≈23-24% selectivity). In addition, the stearyl alcohol and mainly stearyl stearate were produced in high extent, with 54% and 58% selectivity for $Pt/TiO_2/Al_2O_3$ and $Pt/TiO_2/ZrO_2$ materials, respectively.

Table 6.5. Values of Mass Balances, total yields of CO, C18 and C17 compared with C18 and C17 yields in liquids.[a]

Catalyst	Mass Balance (wt%)	Yields (wt%)					
	Liquids	Total	CO	Total C18	Total C17	C17 in liquids	C18 in liquids
$Ni/TiO_2/Al_2O_3$	86	96	10	2	83	96	3
$Ni/TiO_2/ZrO_2$	84	94	9	3	81	96	4
$PtNi/TiO_2/Al_2O_3$	83	92	9	3	80	97	3
$PtNi/TiO_2/ZrO_2$	85	94	9	7	78	92	8
$Pt/TiO_2/Al_2O_3$	94	94	<1	4	5	5	5
$Pt/TiO_2/ZrO_2$	98	98	<1	4	5	6	4

[a] Reactions conditions: 1.56 mL of 15wt% oleic acid in decalin solution, 25 mg of catalyst, 275 ºC, 30 bar of H_2, during 3 h.

In Table 6.5, the mass balance of the reactions along with the hydrocarbons (C17 + C18) both total and in liquids yields were listed to discuss and verify experimental results. As above-mentioned, the CO

yield was calculated by estimating the mass of CO from the equation (n CO = n C17). Then, the total mass balance was calculated by adding the mass of CO to the mass of other products. Thus, after estimating the CO mass, the total mass balance was almost closed, which confirmed that the catalytic experiments were adequately performed. With respect to hydrocarbons yields, particularly n-heptadecane (C17) yield, the total C17 yield considering CO formation by decarbonylation during the process was obviously lower than C17 yield in liquids in the case of monometallic Ni and bimetallic PtNi catalysts. In addition, 100% yield of hydrocarbons (C17 and C18) was achieved in liquids, because practically no other products were detected in GC analysis of the liquids. However, in the case of monometallic Pt catalysts, due to the extremely low CO formation, no differences were found in the values of the mass balances and n-heptadecane (C17) yields (considering both total and in liquids).

Considering the latest discussed results, monometallic Ni and bimetallic PtNi supported on TiO_2/Al_2O_3 and TiO_2/ZrO_2 catalysts were considered as efficient catalysts for the selective hydrogenation of oleic acid at 275 ºC and 30 bar of H_2 during 3 h. In addition, when working with 25 mg of catalyst, no significant difference in the results was found for the here studied catalysts. Thus, for a better understanding of the reaction mechanism and evaluation of the catalytic performance of different metal supported on mixed oxides systems, further experiments varying the catalyst loading (mass) in the reaction medium were carried out. Similarly, other relevant operational parameters of the reaction,

such as temperature, H_2 concentration, among others were systematically studied together with catalysts loading. In this sense, experiments were performed at 225 ºC, 250 ºC and 275 ºC by also changing the H_2 concentration at 30 bar of total pressure (20% H_2/80% N_2, 60% H_2/40% N_2 and 100% H_2) using monometallic Ni- and bimetallic PtNi-supported on TiO_2/Al_2O_3 and TiO_2/ZrO_2 catalysts. The most relevant catalytic results are shown and discussed in the following sections of this chapter.

It is important to remark that one set of experiments was carried out at 275 ºC and 30 bar of H_2 during 3 h, by disposing the solid catalyst with and without pre-activation under H_2 atmosphere at 400 ºC during 2 h before the catalytic test. The results indicated that similar catalytic behaviour was achieved with and without catalyst pre-activation (see Table A6.2), this meaning that the active metallic species in the catalyst could be activated or reduced "in situ" in the reactor under the reaction conditions employed. Thus, catalyst pre-activation before the catalytic tests is, in principle, not needed or required.

6.3.4. Evaluation of monometallic Ni and bimetallic PtNi supported on TiO_2/Al_2O_3 and TiO_2/ZrO_2 catalysts by varying the catalyst loading

In order to get new insights in the evolution of the reaction products aiming at comparing the catalytic activity of the here studied monometallic Ni- and bimetallic PtNi-supported on TiO_2/Al_2O_3 and TiO_2/ZrO_2 materials, a series of experiments was performed by varying the mass of catalysts used in the reaction from 5 mg to 25 mg, whereas

the other reaction parameters (temperature, H_2 concentration and pressure, and reaction time) were maintained constant. The catalytic results in terms of selectivity to the different products attained at 100% conversion of oleic acid are depicted in Figure 6.3, and then discussed for each one of the main products obtained in the following paragraphs.

Stearic acid: At lower catalyst loading (5 mg), the stearic acid was detected for all the catalysts, mainly for $Ni/TiO_2/ZrO_2$ (43% selectivity), and when increasing the catalyst mass from 5 mg to 25 mg, the stearic acid was totally disappeared. These results mean that the $Ni/TiO_2/ZrO_2$ appears to be the less active catalyst among the materials here studied.

Stearyl alcohol (C18OH): As in the case of stearic acid, at 5 mg of catalyst, the stearyl alcohol was detected for all the catalysts, especially for $Ni/TiO_2/Al_2O_3$ and $PtNi/TiO_2/ZrO_2$ (with 14% and 19% selectivity, respectively). Moreover, when increasing the catalyst mass from 5 to 20 mg, the stearyl alcohol was totally transformed for practically all the catalysts, except for $Ni/TiO_2/ZrO_2$. Finally, at the highest catalyst loading (25 mg), no stearyl alcohol was detected.

n-heptadecane (C17): For $Ni/TiO_2/Al_2O_3$, the n-heptadecane (C17) selectivity increased from 15% to 83%, when increasing the catalyst mass from 5 to 25 mg, having the maximum C17 production with 20-25 mg of catalyst. In the case of $PtNi/TiO_2/Al_2O_3$, the C17 selectivity increased from 46% to ≈80%, when increasing the catalyst mass from 5 to 25 mg and reached its maximum with only 10 mg of

catalyst. Thus, $PtNi/TiO_2/Al_2O_3$ showed higher activity than the analogous $Ni/TiO_2/Al_2O_3$ material. In the same way, the C17 selectivity observed for $Ni/TiO_2/ZrO_2$ catalyst increased from 3% to ≈80%, having the maximum at 25 mg of catalyst, while for $PtNi/TiO_2/ZrO_2$ the selectivity increased from 16% to 78%, reaching its maximum with only 10 mg of catalyst, as well. Here again, the bimetallic PtNi-based catalyst was more active than the analogous monometallic Ni-based sample, especially when working at lower catalyst loading. In general, the following catalytic reactivity order was found: $PtNi/TiO_2/Al_2O_3$ > $PtNi/TiO_2/ZrO_2$ > $Ni/TiO_2/Al_2O_3$ > $Ni/TiO_2/ZrO_2$.

n-octadecane (C18): In general, the C18 selectivity was quite low for all the catalysts here studied, being slightly higher in the case of $PtNi/TiO_2/ZrO_2$ (8-9%).

Stearyl stearate: At lower catalyst loading (5 mg), the stearyl stearate was highly formed for all the catalysts, and mainly for $PtNi/TiO_2/ZrO_2$ (54% selectivity). Additionally, when increasing the catalyst mass from 5 to 25 mg, no stearyl stearate was produced for the bimetallic PtNi-based catalysts, probably because its further transformation into n-heptadecane (C17). Besides, the selectivity to stearyl stearate decreased and achieved zero for the monometallic Ni-based catalysts.

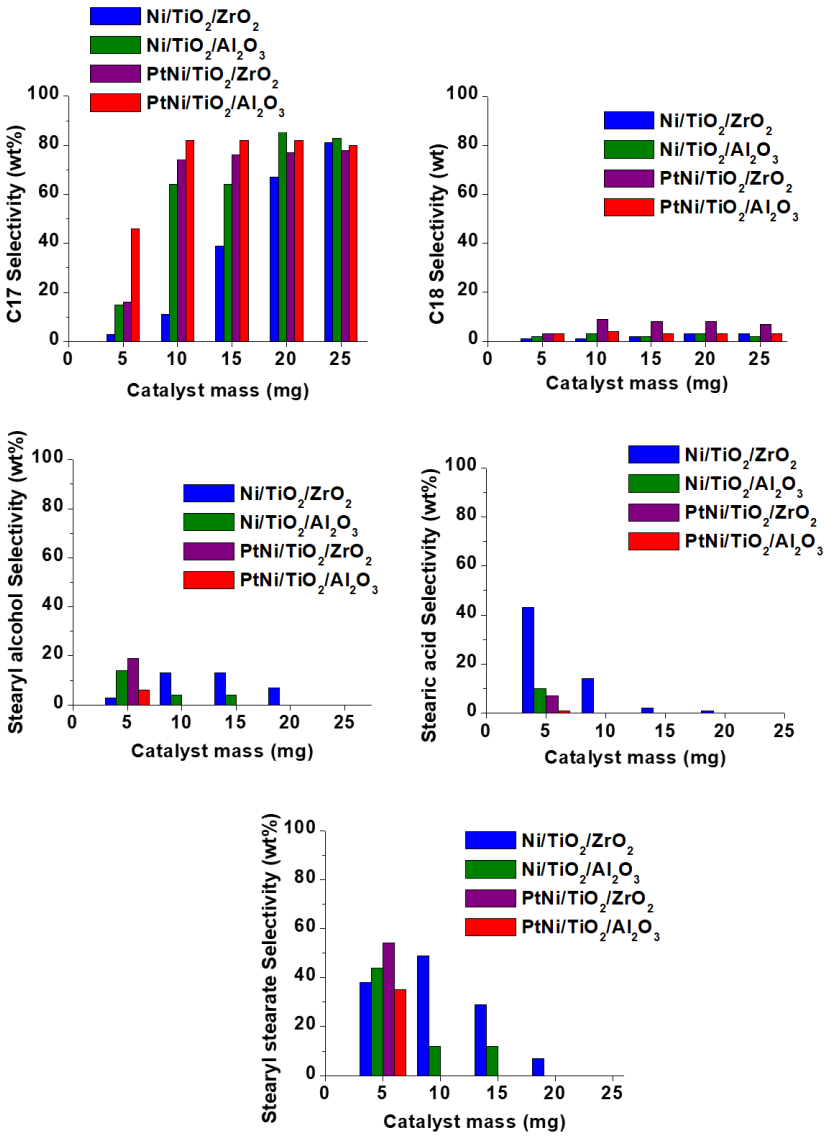

Figure 6.3. Selectivity to the different products obtained in the oleic acid selective hydrogenation over monometallic Ni- and bimetallic PtNi-based catalysts at different catalyst loadings (Conversion = 100%). Reactions conditions: 1.56 mL of 15wt% oleic acid in decalin solution, 275 ºC, 30 bar of H_2, during 3 h.

Summarizing, the TiO_2/Al_2O_3-supported catalysts were found to be more active for the n-heptadecane (C17) production (probably via decarbonylation of stearyl alcohol) than the TiO_2/ZrO_2-supported ones. Moreover, the slight decrease in the n-heptadecane (C17) selectivity values observed for $PtNi/TiO_2/ZrO_2$ compared to $PtNi/TiO_2/Al_2O_3$ was compensated by the higher n-octadecane (C18) formation. In addition, the Pt doping seemed to improve the catalytic activity of the monometallic Ni-based catalysts, and mainly in the case of TiO_2/Al_2O_3-supported catalysts. For the latter materials, it is probably that reaction takes place via decarbonylation of stearyl alcohol (intermediate formed from stearic acid primary product). Nevertheless, more inputs are needed from other reaction parameters studies before proposing any plausible reaction mechanism.

6.3.5. Influence of reaction temperature on the activity of monometallic Ni and bimetallic PtNi supported on TiO_2/Al_2O_3 and TiO_2/ZrO_2 catalysts

The influence of the reaction temperature on the catalytic performance of monometallic Ni- and bimetallic PtNi-based catalysts in the oleic acid selective hydrogenation was studied. In this sense, a series of additional catalytic experiments at 225 ºC and 250 ºC was performed for comparison with those attained at 275 ºC, also varying the amount of catalyst in the reaction medium. In all the cases, the rest of reaction parameters (H_2 concentration and pressure, reaction time, among others) remained unaltered.

The selectivity to n-heptadecane (C17) and stearyl alcohol (C18OH) attained by working at different temperatures with monometallic Ni and bimetallic PtNi supported on TiO_2/Al_2O_3 and TiO_2/ZrO_2 catalysts was compared and summarized in Figures 6.4 and 6.5, respectively.

On one hand, and as can be seen from Figure 6.4, the selectivity to n-heptadecane (C17) increased for both monometallic Ni-based catalysts when increasing the temperature from 225 ºC to 275 ºC. For instance, very high C17 selectivity (83% and 81% for $Ni/TiO_2/Al_2O_3$ and $Ni/TiO_2/ZrO_2$, respectively) was attained with 25 mg of catalyst at 275 ºC, and with 50 mg of $Ni/TiO_2/Al_2O_3$ (86% C17 selectivity) at 250 ºC. Thus, the increase in the reaction temperature improved the n-heptadecane (C17) production, the formation of the latter being almost negligible at 225 ºC. In addition, the n-heptadecane (C17) was more rapidly formed over $Ni/TiO_2/Al_2O_3$ compared with $Ni/TiO_2/ZrO_2$.

On the other hand, and in the case of bimetallic PtNi-based catalysts, the increase in the temperature from 225 ºC to 275 ºC also led to an increase in the n-heptadecane (C17) selectivity. In this sense, very high C17 selectivity was reached with 10 mg of catalyst at 275 ºC (82% and 74% for $PtNi/TiO_2/Al_2O_3$ and $PtNi/TiO_2/ZrO_2$, respectively). Slightly higher values of C17 selectivities were attained with 25 mg of these catalysts by working at 250 ºC (85% and 76% for $PtNi/TiO_2/Al_2O_3$ and $PtNi/TiO_2/ZrO_2$, respectively). On the contrary, it should be noted that C17 was produced in lower extent when working

at 225 ºC, even with 50 mg of these two catalysts (65% and 50% C17 selectivity for $PtNi/TiO_2/Al_2O_3$ and $PtNi/TiO_2/ZrO_2$, respectively).

Finally, and with respect to n-octadecane (C18) (see Figure A6.1), its formation was negligible or very small (<5%) for both monometallic Ni-based catalysts and $PtNi/TiO_2/Al_2O_3$ material. Nevertheless, higher production of C18 was encountered for $PtNi/TiO_2/ZrO_2$ (10-14% C18 selectivity), which compensated the differences observed in the C17 selectivity values for the bimetallic PtNi-based catalysts.

This increase in the n-heptadecane (C17) selectivity was also confirmed by the decrease in the selectivity to stearyl alcohol (Figure 6.5), stearic acid (see Figure A6.2) and stearyl stearate (see Figure A6.3) when increasing the reaction temperature. Apparently, the two transformations leading to n-heptadecane (from stearyl alcohol and stearyl stearate) were highly favoured in the presence of bimetallic PtNi-based catalysts, mainly at temperatures ≥250 ºC. Thus, the rate of decarbonylation of stearyl alcohol (route of C17 formation) was higher in the case of bimetallic PtNi-based catalysts compared with their analogous monometallic Ni-based catalysts, the differences being more easily detected by working at 225 ºC.

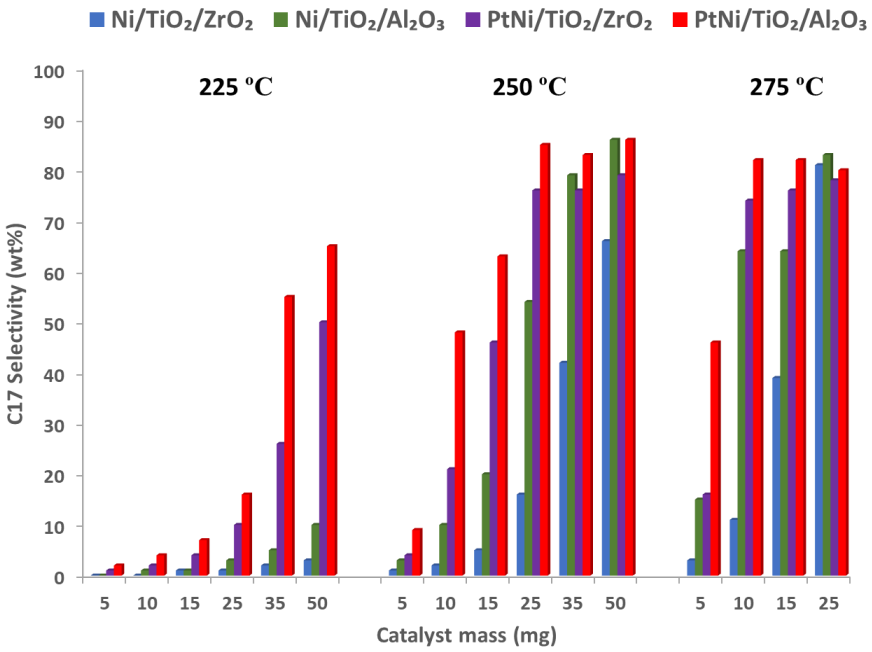

Figure 6.4. Influence of the temperature on the selectivity to n-heptadecane (C17) obtained in the oleic acid selective hydrogenation over monometallic Ni- and bimetallic PtNi-supported catalysts (Conversion = 100%). Reactions conditions: 1.56 mL of 15wt% oleic acid in decalin solution, 30 bar of H_2, during 3 h.

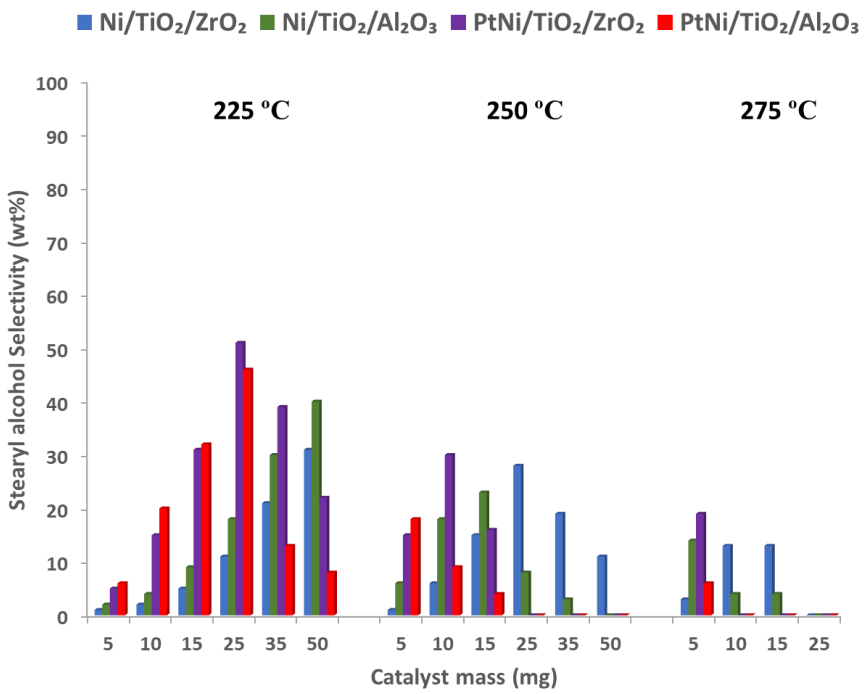

Figure 6.5. Influence of the temperature on the selectivity to stearyl alcohol (C18OH) obtained in the oleic acid selective hydrogenation over monometallic Ni- and bimetallic PtNi-supported catalysts (Conversion = 100%). Reactions conditions: 1.56 mL of 15wt% oleic acid in decalin solution, 30 bar of H_2, during 3 h.

As above-mentioned, the selectivity to stearyl alcohol (C18OH) decreased for all the catalysts when increasing the temperature from 225 ºC to 275 ºC (Figure 6.5). Therefore, when working at 225 ºC and with the adequate amount of catalyst (for example, 25 mg for bimetallic PtNi-based catalysts and 50 mg for monometallic Ni-based catalysts), stearyl alcohol yields were apparently maximized. For instance, for $Ni/TiO_2/Al_2O_3$ and $Ni/TiO_2/ZrO_2$ catalysts the maximum selectivity to

stearyl alcohol was 40% and 31%, respectively. In addition, the maximum C18OH selectivity was 46% and 51% for $PtNi/TiO_2/Al_2O_3$ and $PtNi/TiO_2/ZrO_2$, respectively, whereas with higher loadings of these two catalysts, the consecutive stearyl alcohol (C18OH) transformation into n-heptadecane (C17) was favoured due to the high decarbonylation activity observed with these catalytic systems. In this sense, the amount of catalyst, this meaning the amount of metallic active sites available on the catalytic surface to carry out the hydrogenation reaction, played a key role for the stearyl alcohol production, mainly for the bimetallic PtNi-based catalysts.

From the catalytic data previously discussed, it can be concluded that the adequate reaction temperature to produce n-heptadecane (C17) in high yields during the selective hydrogenation of oleic acid was 275 ºC. In addition, catalyst loading should be maintained ≥25 mg for Ni-based catalysts and ≥10 mg for their analogous PtNi-based materials to attain the good yield of the C17 hydrocarbon.

6.3.6. Influence of hydrogen concentration on the activity of monometallic Ni and bimetallic PtNi supported on TiO_2/Al_2O_3 and TiO_2/ZrO_2 catalysts

From the results up to now attained during oleic acid selective hydrogenation using different monometallic Ni- and bimetallic PtNi-based catalysts, the next steps of this study consisted of evaluating the effect of decreasing the hydrogen concentration by working at 30 bar

of pressure and 275 ºC, aiming at optimizing the n-heptadecane (C17) production. In order to investigate this issue, a series of experiments was performed by varying the H_2 concentrations (20%, 60% and 100% H_2 mixed or diluted with N_2) in the reaction system and always working at 30 bar of pressure. The catalytic results obtained in terms of n-heptadecane (C17) selectivity for the different catalysts here studied are shown in Figure 6.6.

As can be seen in Figure 6.6, the selectivity to n-heptadecane (C17) increased when increasing the H_2 concentration from 20% to 60% for all the selected catalysts, and no significant differences were detected when further increase in the H_2 concentration from 60% till 100% was essayed. In fact, these small differences observed could be due to experimental error. In addition, some small differences in the selectivity to the other products of reaction, such as n-octadecane (C18), stearyl alcohol, stearic acid, and stearyl stearate could be detected when comparing the results attained in the tests performed with 60% and 100% H_2 concentration in the system (Figure A6.4, A6.5, A6.6 and A6.7, respectively).

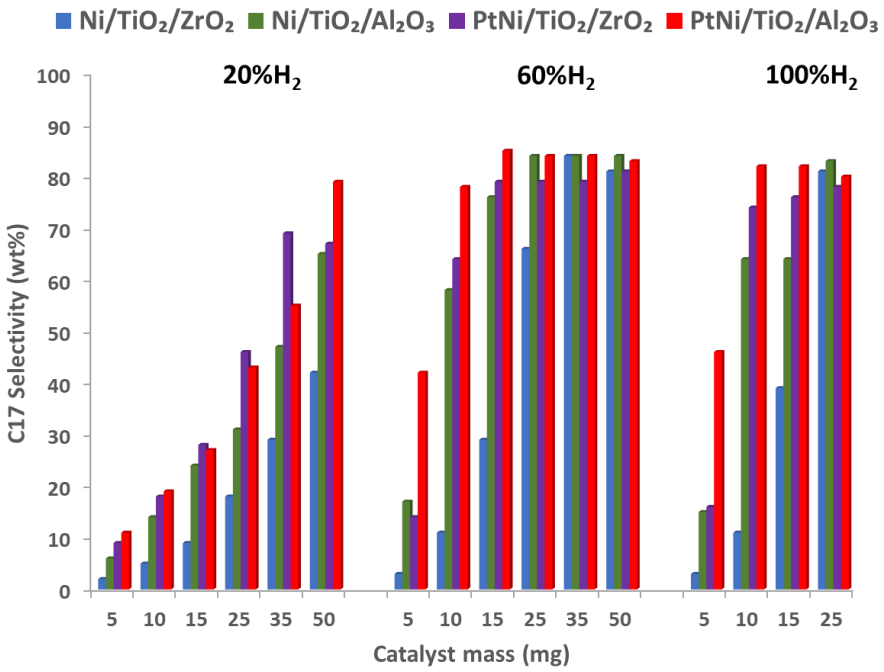

Figure 6.6. Influence of H_2 concentration on the selectivity to n-heptadecane (C17) obtained in the oleic acid selective hydrogenation over monometallic Ni- and bimetallic PtNi-supported catalysts (Conversion = 100%). Reactions conditions: 1.56 mL of 15wt% oleic acid in decalin solution, 275 ºC, 30 bar, during 3 h.

In general, the presence of hydrogen seemed to be crucial for n-heptadecane (C17) formation. Apparently, at lower hydrogen concentration (20% H_2), high amounts of stearic acid and stearyl stearate were present in the products after reaction, along with low amounts of stearyl alcohol (C18OH) and n-heptadecane (C17). On the contrary, at higher hydrogen concentrations (60% H_2 and 100% H_2), higher amounts of n-heptadecane (C17) were obtained. In this case, stearic acid was formed in lower amounts at low catalyst loadings

before its total conversion at higher catalyst loadings. Additionally, higher amounts of stearyl alcohol and stearyl stearate were produced at catalyst loadings from low (5-10 mg) to medium (15-25 mg) before their total transformation at high catalyst loadings (>25 mg). Considering the aforementioned results, it was confirmed that n-heptadecane (C17) was produced from stearyl alcohol (and stearyl stearate) via decarbonylation instead of decarboxylation of stearic acid under these reaction conditions, thus requiring working under hydrogen concentrations able to convert stearic acid into stearyl alcohol.

6.3.7. Comparison of catalytic results of experiments at different reaction temperatures, with changes in hydrogen concentration and catalyst loading

As mentioned in previous sections of this chapter, catalytic experiments for the oleic acid selective hydrogenation using monometallic Ni and bimetallic PtNi supported on TiO_2/Al_2O_3 and TiO_2/ZrO_2 catalysts were performed at different temperatures (225 ºC, 250 ºC and 275 ºC), and with different catalysts loading (from 5 up to 50 mg). In addition, the influence of the hydrogen concentration mixed with nitrogen (20%, 60% and 100% H_2) under 30 bar of pressure was investigated in each one of the cases. The catalytic results attained are summarized and shown in Figure 6.7. As can be seen, the most efficient catalysts in the selective hydrogenation of oleic acid for n-heptadecane (C17) production were the bimetallic $PtNi/TiO_2/Al_2O_3$ and $PtNi/TiO_2/ZrO_2$, these materials being more selective to n-heptadecane (C17) and more active even at lower catalyst loadings (top and left

region of the Figure 6.7). As already discussed, the maximum n-heptadecane (C17) selectivity was attained working with only 10 mg of catalyst at 275 ºC and hydrogen concentration equal or higher than 60%.

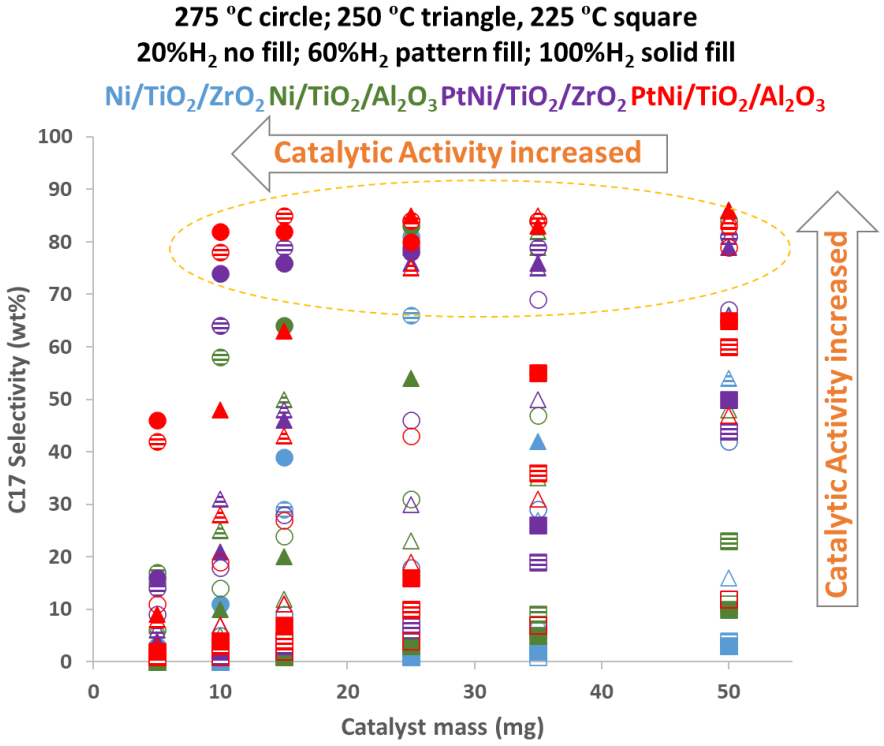

Figure 6.7. Selectivity to n-heptadecane (C17) in function of catalyst loading using monometallic Ni and bimetallic PtNi catalysts (Conversion = 100%). Reactions conditions: 1.56 mL of 15wt% oleic acid in decalin solution, 225-275 ºC, 30 bar of pressure, during 3 h.

In general, no significant differences were encountered in the C17 selectivity values by working at H_2 concentrations of 60% and 100%, these differences could be due to experimental error when

working with high-throughput system, C17 selectivity being sometimes slightly higher at 60% of H_2 compared with the values obtained at 100% H_2.

6.3.8. Influence of the hydrogen concentration (and pressure) on the activity of monometallic Ni and bimetallic PtNi supported catalysts by working at 225 ºC

Along this study, the formation of the intermediate stearyl alcohol (C18OH) was observed as predominant product under some specific reaction conditions when using selected Ni-based catalysts here studied. Therefore, and with the idea of maximizing the production of stearyl alcohol (C18OH), the influence of the hydrogen concentration and pressure was evaluated for the monometallic Ni- and bimetallic PtNi-based catalysts here studied. The attained results for these different catalysts in terms of selectivity to stearyl alcohol (C18OH) are shown in Figure 6.8.

For instance, the selectivity to stearyl alcohol (C18OH) increased when increasing the H_2 concentration from 20% to 60%, and then to 100%, always working at 30 bar of overall pressure for all the catalysts. In addition, the superior activity of bimetallic PtNi-based materials with respect to their analogous monometallic Ni-based catalysts was observed. On one hand, the maximum selectivity values to stearyl alcohol (C18OH) achieved for $Ni/TiO_2/Al_2O_3$ and $Ni/TiO_2/ZrO_2$ catalysts were 40% and 31%, respectively (at 30 bar of 100% H_2) and were 46% and 33%, respectively (at 45 bar of 100% H_2).

In addition, this maximum was achieved for both monometallic Ni-based samples by working with the highest amount of catalyst (50 mg). On the other hand, the maximum selectivity to stearyl alcohol (C18OH) attained for $PtNi/TiO_2/Al_2O_3$ increased from 46% to 51% when increasing the H_2 pressure from 30 to 45 bar (at 100% of H_2). In the same way, the maximum selectivity reached for $PtNi/TiO_2/ZrO_2$ increased from 51% to 55% with the increase of H_2 pressure from 30 to 45 bar. A similar trend was observed for both bimetallic PtNi-based materials and the maximum selectivity to stearyl alcohol (C18OH) was reached when working with 25 mg of catalyst, while the stearyl alcohol production decreased at higher catalyst loadings, mainly due to its further transformation into n-heptadecane (C17).

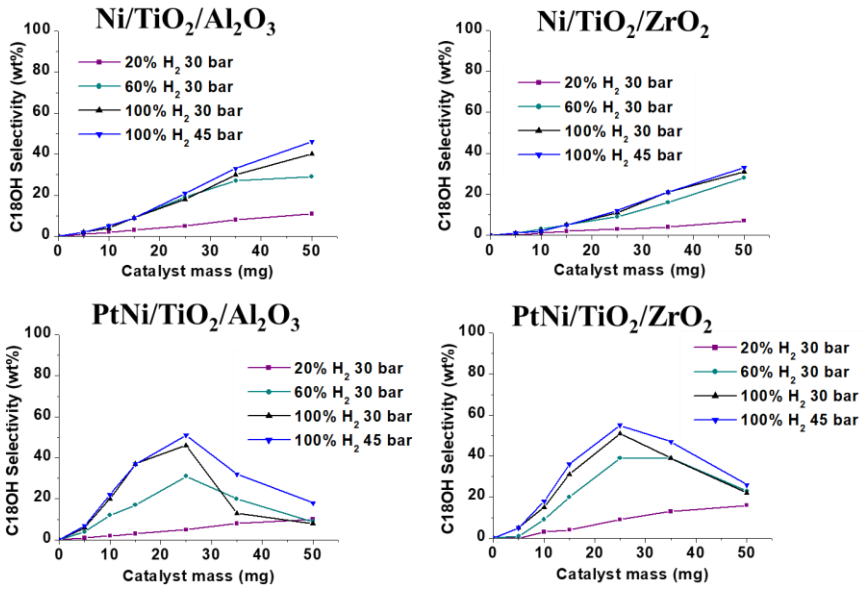

Figure 6.8. Influence of the H_2 concentration (and pressure) on the selectivity to stearyl alcohol (C18OH) over monometallic Ni- and bimetallic PtNi-supported catalysts (Conversion = 100%). Reactions conditions: 1.56 mL of 15wt% oleic acid in decalin solution, 225 ºC, during 3 h.

Summarizing, bimetallic PtNi-based catalysts were found to be more active and selective to the production of stearyl alcohol (C18OH) than their analogous monometallic Ni-based catalysts, when working at lower catalyst loading (25 mg). Thus, the optimal operational conditions for maximizing the stearyl alcohol production in our catalytic system were reached by working with bimetallic PtNi-based catalyst (25 mg of $PtNi/TiO_2/ZrO_2$ being preferred) at 225 ºC and with 100% of H_2 at 45 bar of total pressure. Under these conditions, up to 55% yield (based on liquids) of the corresponding stearyl alcohol (C18OH) was obtained.

6.3.9. Proposed reaction mechanism

With all the catalytic results obtained in this study for the different Ni-based catalytic materials here prepared and after their complete discussion and evaluation, it is possible to construct a reaction network for the transformation of the oleic acid into the different products observed during the selective hydrogenation process. In this sense, the selectivity to different reaction products in function of the catalyst loading, mainly when working at lower temperatures and over $PtNi/TiO_2/Al_2O_3$ catalyst is depicted in Figure 6.9.

As can be seen in the Figure, stearic acid is the first product rapidly formed in the reaction (primary and unstable product), which is then converted into other compounds. Stearyl alcohol and stearyl stearate appear as the main secondary products of the reaction, probably formed from stearic acid. Depending on the reaction conditions, both stearyl alcohol and stearyl stearate are also converted to other products. Finally, hydrocarbons appear as secondary or even tertiary and stable products, which are increased when either more catalyst or more drastic conditions are used.

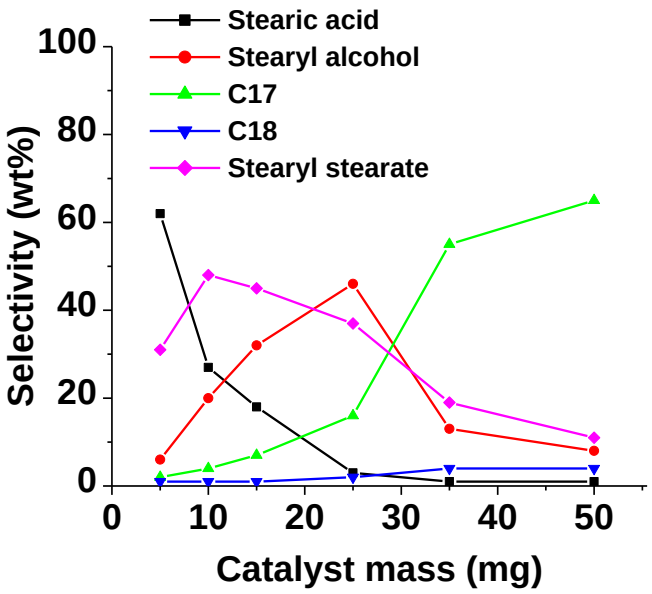

Figure 6.9. Selectivity in function of the catalyst loading in the oleic acid selective hydrogenation over PtNi/TiO_2/Al_2O_3 (Conversion = 100%). Reactions conditions: 1.56 mL of 15wt% oleic acid in decalin solution, 225 ºC, 30 bar of H_2, during 3 h.

Considering all these results, a plausible reaction mechanism for the selective hydrogenation of oleic acid over Ni-based, and preferably PtNi-based catalysts here studied, is proposed, and represented in Figure 6.10.

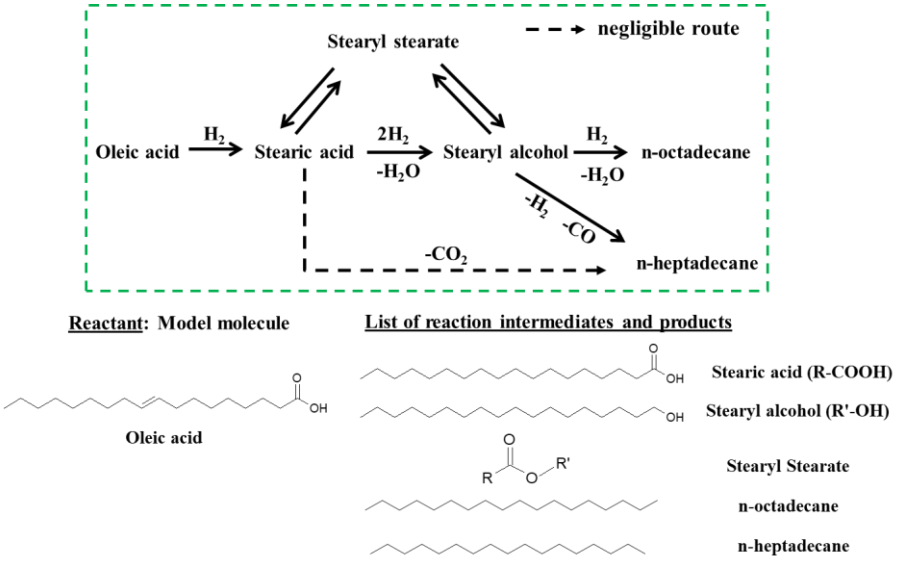

Figure 6.10. Proposed reaction mechanism for the selective hydrogenation of oleic acid over Ni- and PtNi-based catalysts.

First, the double bond present in the oleic acid is hydrogenated to form the stearic acid. Afterwards, the latter acid is selectively hydrogenated to stearyl alcohol (C18OH), and a side reaction between stearic acid and stearyl alcohol occurs giving stearyl stearate as by-product. Then, stearyl alcohol is further transformed into n-heptadecane (C17) via decarbonylation (-CO) or into n-octadecane (C18) via hydrodeoxygenation ($-H_2O$). As previously reported, stearyl alcohol undergoes first a dehydrogenation step forming stearyl aldehyde (intermediate product not detected), which is rapidly decarbonylated to produce n-heptadecane (C17) [15,20,21]. In addition, stearyl alcohol suffers dehydration yielding octadecene, the latter is further hydrogenated leading to n-octadecane (C18) formation [15,20,21]. At the same time, stearyl stearate is probably converted into stearic acid

and stearyl alcohol, which are further transformed to n-heptadecane (C17) and/or n-octadecane (C18).

Two more catalytic experiments were performed in order to confirm the proposed reaction pathways for fatty acids hydrogenation over our Ni-based developed materials. On one hand, an experiment was carried out using stearic acid as reactant and $Ni/TiO_2/Al_2O_3$ as catalyst by working at 275 ºC and 30 bar of N_2, this meaning in the absence of H_2 in the system. As result, negligible amount of n-heptadecane (C17) was detected in the reaction medium. On the other hand, a second catalytic test was performed using stearyl alcohol as reactant and $Ni/TiO_2/Al_2O_3$ as catalyst by working at 275 ºC and 30 bar of H_2, resulting in high n-heptadecane (C17) formation. These experimental evidences confirm that n-heptadecane (C17) is formed during the fatty acid hydrogenation process mainly through decarbonylation of the stearyl alcohol and not via decarboxylation of the stearic acid.

6.3.10. Catalysts characterization

The catalytic materials prepared in this study were systematically characterized by different analytical and spectroscopic techniques for solid materials analysis available at ITQ. As it was previously described and discussed, the main textural and physico-chemical properties of Ni-, PtNi-, and Pt-based catalysts are listed in Tables 6.1 and 6.4. In addition, structural determination for the different

catalysts was performed by means of X-ray diffraction measurements described in the following section.

6.3.10.1. X-ray diffraction (XRD)

X-ray diffraction patterns of the Ni-, PtNi- and Pt-based samples are shown in Figures 6.11 and 6.12. In general, diffraction peaks of the Ni and Pt metals incorporated onto the metal oxides supports are difficult to detect and assign, this probably meaning that the metals are deposited as small and well dispersed nanoparticles. This is a relevant evidence mainly for Ni-based catalysts with relatively high metal contents (>12wt%). For instance, in the case of Ni/Al_2O_3, no Ni peaks were observed, although taking into consideration the high Ni content, Ni (111) and gamma Al_2O_3 peaks could be superposed. In addition, the XRD patterns of Ni/TiO_2 showed Ni (111) and Ni (200) peaks at 44.6 º and 52.2 º, respectively, whereas the peak assigned to Ni (220) and that of the TiO_2 anatase phase (main phase detected for TiO_2 support) could coincide at 76.8 º. In the case of Ni/ZrO_2, peaks assigned to the presence of Ni (111), Ni (200) and Ni (220) phases were not detected, and probably they are superposed with ZrO_2 monoclinic diffractions peaks. Similarly, the peaks of Ni species were not observed in diffraction patterns of $Ni/TiO_2/ZrO_2$ and $PtNi/TiO_2/ZrO_2$ samples. In addition, Ni (111) peak could be superposed with gamma Al_2O_3 peak at 44.6 º for $Ni/TiO_2/Al_2O_3$ and $PtNi/TiO_2/Al_2O_3$ materials. On the contrary, Ni/TiO_2-ZrO_2 and Ni/ZrO_2-Al_2O_3 catalysts showed three peaks at 44.6, 52.2 and 76.8 º, corresponding to Ni (111), Ni (200) and Ni (220) phases, respectively. Moreover, the peak of Ni (111) phase was clearly

detected for Ni/TiO_2-Al_2O_3, whereas Ni (200) and Ni (220) peaks probably coincide with TiO_2 anatase peaks in this material. Finally, and with respect to Pt diffraction peaks, monometallic Pt-based catalysts showed a very week peak of Pt (111) phase located at 39.7 º, whereas no Pt peak was detected for bimetallic PtNi-based materials. The latter fact could be due to lower Pt loading, also suggesting that Pt is well dispersed on the supports and forming small nanoparticles.

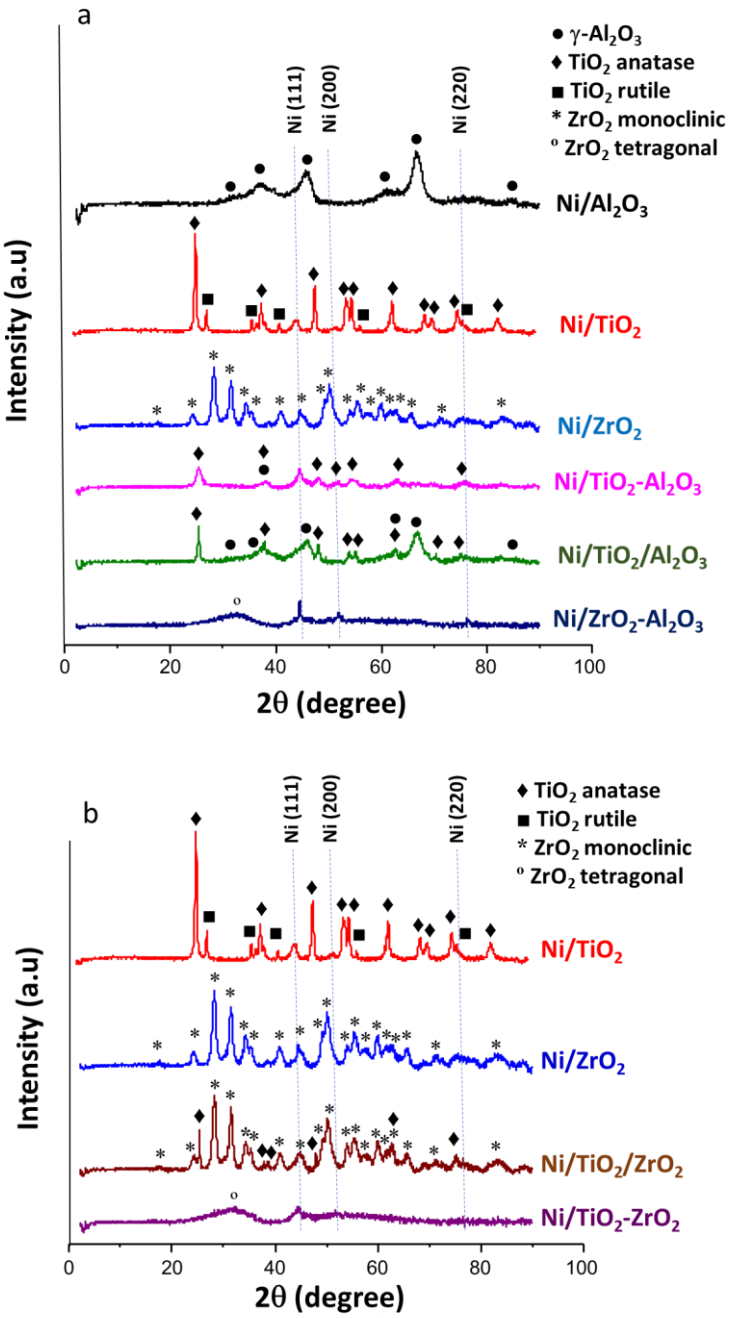

Figure 6.11. X-ray diffraction patterns of monometallic Ni-based catalysts containing a) Al_2O_3 and b) TiO_2 and ZrO_2.

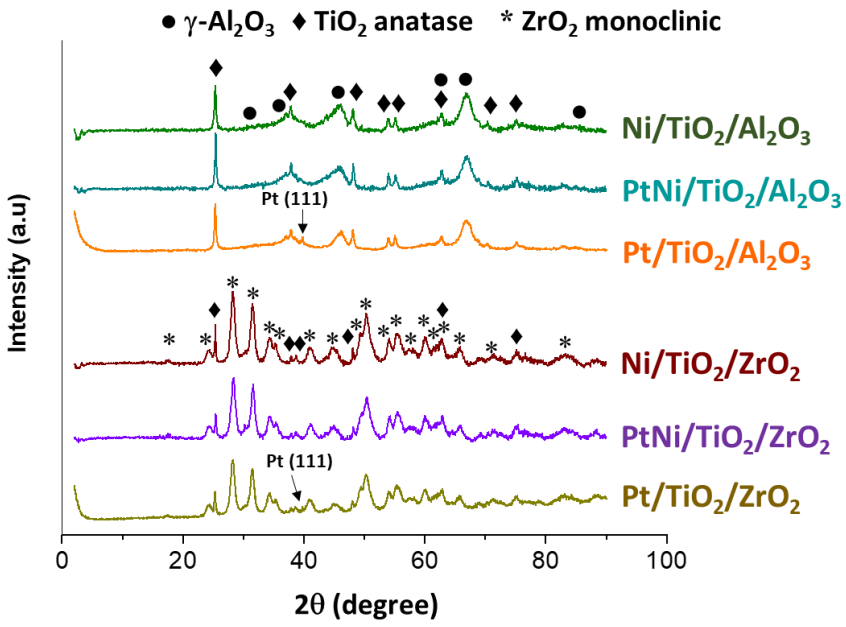

Figure 6.12. X-ray diffraction patterns of Ni, PtNi and Pt supported on TiO_2/Al_2O_3 and TiO_2/ZrO_2 catalysts.

6.3.10.2. Temperature-programmed reduction (TPR)

Additionally, the hydrogen consumption and the reducibility of metal species on the surface of the Ni-based catalysts were investigated by performing temperature-programmed reduction (TPR) experiments. Thus, H_2-TPR profiles of the Ni, Pt and PtNi supported on TiO_2/Al_2O_3 and TiO_2/ZrO_2 catalysts are shown in Figures 6.13 and 6.14, respectively, while data calculated from the H_2 uptake in each case are listed in Table 6.6.

As can be seen, Ni/Al_2O_3 showed the maximum peak at 495 ºC, while lower reduction temperatures were encountered for both Ni/TiO_2

and Ni/ZrO_2 materials. In addition, maximum temperature peaks ranging from 314 ºC to 423 ºC were found for Ni supported on mixed metal oxides synthesized by co-precipitation method. Interestingly, a maximum peak at 475 ºC was observed for $Ni/TiO_2/Al_2O_3$ catalyst. In addition, two peaks at 300 ºC and 427 ºC were detected in the case of $Ni/TiO_2/ZrO_2$. According to previously reported study [22], the reduction of bulk Ni^{2+}, which interacts weakly with the support, occurred at lower temperature, whereas the higher temperature peak is attributed to the reduction of highly dispersed Ni^{2+} species with strong interaction with the support. From the attained data, the reduction of these highly dispersed Ni^{2+} species occurred at 475 ºC and 427 ºC for our $Ni/TiO_2/Al_2O_3$ and $Ni/TiO_2/ZrO_2$ catalysts, respectively. More importantly, the temperature of these highly dispersed Ni species present in both PtNi-based materials ($PtNi/TiO_2/Al_2O_3$ and $PtNi/TiO_2/ZrO_2$ with maximum at 420 ºC and 354 ºC, respectively) shifted towards lower values compared with their analogous Ni-based samples. Therefore, as reported in previous studies investigating the effect of addition of another metal on the reduction of Ni species present in bimetallic systems such as NiCu [23] and PdNi [24], the addition of Pt seemed to facilitate the reduction of Ni species in our system. In addition, the low-temperature hydrogen consumption peaks (at 160 ºC and 120 ºC for $PtNi/TiO_2/Al_2O_3$ and $PtNi/TiO_2/ZrO_2$, respectively) shifted towards a higher temperature in comparison with Pt catalysts, probably due to the change of Pt crystallite size, as less Pt loading was encountered in the bimetallic samples [25].

As conclusion, H_2-TPR results clearly suggest that there is a synergic effect between Ni and Pt nanoparticles on enhanced redox properties of the catalysts. Thus, the presence of Pt increases Ni reducibility, which together with the strong metal-support interaction exhibited by Ni supported on mixed metal oxides lead to enhanced hydrogenation capacities for these types of materials.

Table 6.6. Hydrogen consumption of monometallic Ni- and bimetallic PtNi-based catalysts.

Catalyst	Amount of adsorbed H_2 (μmol/g)	Max Temperature (ºC)
Ni/Al_2O_3	2232	495
Ni/TiO_2	2484	389
Ni/ZrO_2	2484	300
Ni/ZrO_2-Al_2O_3	2032	314
Ni/TiO_2-ZrO_2	2601	389
Ni/TiO_2-Al_2O_3	2270	423
$Ni/TiO_2/Al_2O_3$	2153	475
$PtNi/TiO_2/Al_2O_3$	2451	420
$Pt/TiO_2/Al_2O_3$	497	150 and 500
$Ni/TiO_2/ZrO_2$	2357	300 and 427
$PtNi/TiO_2/ZrO_2$	2163	354
$Pt/TiO_2/ZrO_2$	425	85 and 490

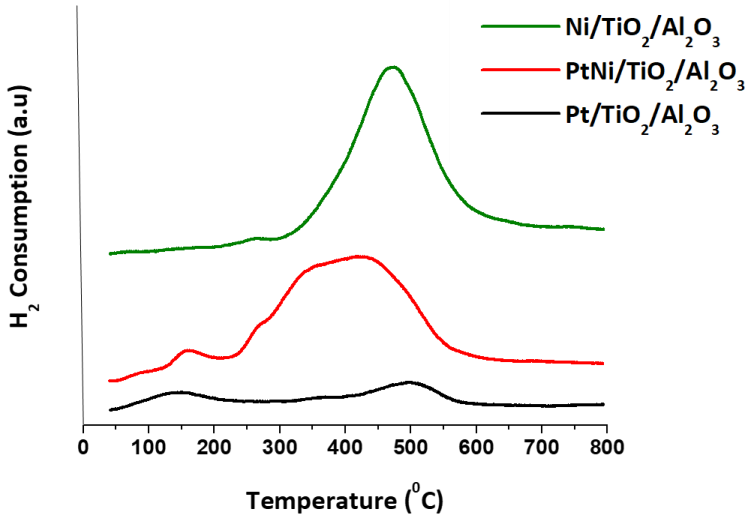

Figure 6.13. H_2-TPR profiles of Ni-, Pt- and PtNi supported on TiO_2/Al_2O_3 catalysts.

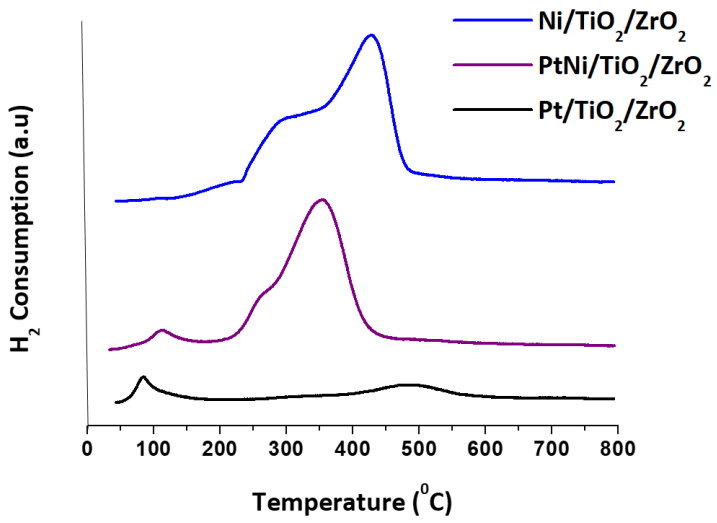

Figure 6.14. H_2-TPR profiles of Ni-, Pt- and PtNi supported on TiO_2/ZrO_2 catalysts.

6.3.10.3. Ammonia temperature-programmed adsorption-desorption (NH_3-TPD)

In addition, the total amount of acid sites was determined by temperature-programmed adsorption-desorption of ammonia (NH_3-TPD) measurements, and the corresponding data are listed in Table 6.7. Moreover, NH_3-TPD profiles of Ni- and PtNi-based catalysts are shown in Figure A6.11.

Table 6.7. Ammonia adsorption on monometallic Ni- and bimetallic PtNi-based catalysts.

Catalyst	Total amount of acid sites (μmol/g)
Ni/Al_2O_3	381
Ni/ZrO_2	273
Ni/TiO_2	188
Ni/TiO_2-Al_2O_3	359
Ni/TiO_2-ZrO_2	272
Ni/ZrO_2-Al_2O_3	304
$Ni/TiO_2/Al_2O_3$	330
$Ni/TiO_2/ZrO_2$	180
$PtNi/TiO_2/Al_2O_3$	324
$PtNi/TiO_2/ZrO_2$	161

As expected, the presence of Al_2O_3 support provides more acidity to the corresponding final catalytic materials. Thus, comparison of similar series of materials can be done, and the following order of acidity can be established:

$Ni/Al_2O_3 > Ni/TiO_2 > Ni/ZrO_2$;

$Ni/TiO_2\text{-}Al_2O_3 > Ni/ZrO_2\text{-}Al_2O_3 > Ni/TiO_2\text{-}ZrO_2$;

$Ni/TiO_2/Al_2O_3 > Ni/TiO_2/ZrO_2$;

$PtNi/TiO_2/Al_2O_3 > PtNi/TiO_2/ZrO_2$

In addition, the incorporation of TiO_2 layers via incipient wetness impregnation onto Al_2O_3 and ZrO_2 supports did not increase the total acidity of the samples in comparison with the analogous mixed metal oxides prepared by co-precipitation method. Remarkably, the Pt doping in the bimetallic PtNi-based catalysts did not highly affect the total acidity of the material, and only small decrease in the NH_3 adsorption capacity was observed in comparison with the analogous monometallic Ni-based samples.

6.3.10.4. Microscopy and H_2 chemisorption measurements

High-resolution transmission electron microscopy (HR-TEM) measurements of the most representative Ni- and PtNi-based catalysts were also performed. For instance, HR-TEM images of $Ni/TiO_2/Al_2O_3$ and $Ni/TiO_2/ZrO_2$ catalysts are shown in Figure 6.15, and the presence of Ni species can be clearly recognized. In addition, average Ni nanoparticle size values for Ni/Al_2O_3, Ni/TiO_2, $Ni/TiO_2/Al_2O_3$ and $Ni/TiO_2\text{-}Al_2O_3$ samples are listed in Table 6.8. When comparing the particle size distributions obtained from TEM measurements of the catalysts (Figure 6.16), Ni/Al_2O_3 presented small Ni nanoparticle sizes centered between 1.5-2.0 nm, while nanoparticle size distributions moved towards higher values centered between 4.0-6.0 nm and 6.0-8.0

nm for Ni/TiO_2-Al_2O_3 and Ni/TiO_2, respectively. In the case of $Ni/TiO_2/Al_2O_3$ material, a dual metal particle distribution with small and a few big Ni nanoparticles was observed.

Data from H_2 chemisorption (Table 6.8) showed that Ni nanoparticle size was 41.3 and 47.6 nm for $Ni/TiO_2/Al_2O_3$ and $Ni/TiO_2/ZrO_2$, respectively. Additionally, the amount of chemisorbed H_2 was higher for the bimetallic PtNi systems compared with their analogous monometallic Ni systems; this could suggest both higher metal dispersion and active metal surface area, along with smaller particle size in the bimetallic catalysts in comparison with their analogous monometallic samples.

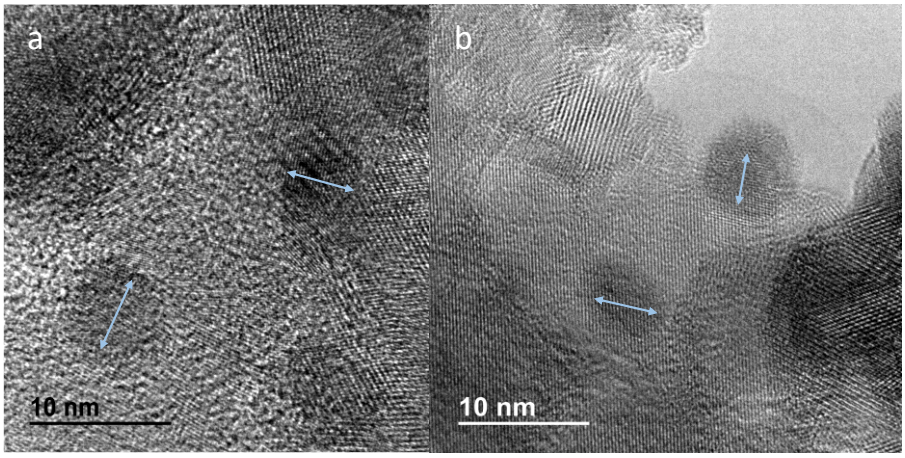

Figure 6.15. HR-TEM images of a) $Ni/TiO_2/Al_2O_3$ and b) $Ni/TiO_2/ZrO_2$ catalysts (blue: Ni (111), d≈0.20 nm).

Table 6.8. Average particle size and amount of chemisorbed H_2 of different Ni- and PtNi-based catalysts.

Catalyst	Particle size (nm)[a]	Particle size (nm)[b]	Ni dispersion (%)[b]	Amount of chemisorbed H_2 (μmol/g)[b]
Ni/Al_2O_3	2.0	-	-	-
Ni/ZrO_2	-	-	-	-
Ni/TiO_2	7.5	-	-	-
Ni/TiO_2-Al_2O_3	6.2	-	-	-
$Ni/TiO_2/Al_2O_3$	4.1	41.3	2.5	29
$Ni/TiO_2/ZrO_2$	-	47.6	2.1	25
$PtNi/TiO_2/Al_2O_3$	-	-	-	148
$PtNi/TiO_2/ZrO_2$	-	-	-	53

[a] Average diameter of Ni nanoparticles calculated from TEM measurements of, at least, 100 particles. [b] Values calculated by H_2 chemisorption assuming a stoichiometry of Ni/H = 1.

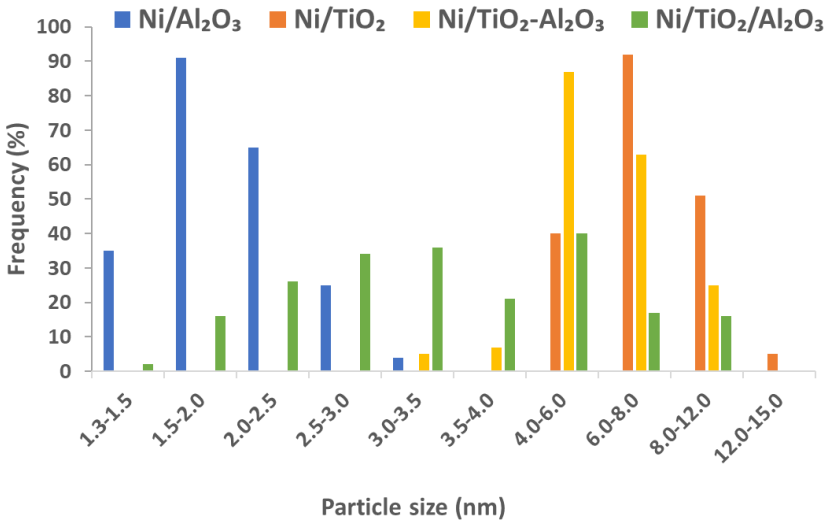

Figure 6.16. Ni particle size distribution of different monometallic Ni catalysts.

HR-STEM images of bimetallic $PtNi/TiO_2/Al_2O_3$ catalyst, along with the corresponding elemental composition are shown in Figures 6.17 and A6.12. As can be seen, the latter catalyst consists of Pt nanoparticles possessing small particle size, Ni nanoparticles with bigger particle size and bimetallic PtNi nanoparticles with intermediate particle size.

In addition, HRTEM-EDX mapping images of monometallic $Ni/TiO_2/Al_2O_3$ and $Ni/TiO_2/ZrO_2$, and bimetallic $PtNi/TiO_2/Al_2O_3$ and $PtNi/TiO_2/ZrO_2$ catalysts are shown in Figures 6.18, 6.19, 6.20 and 6.21, respectively. SEM-EDX mapping images of these selected catalysts are also shown in Figures A6.13, A6.14, A6.15 and A6.16. It is worth noting that the Ti element (and consequently the TiO_2) was found to be homogeneously dispersed onto both Al_2O_3 and ZrO_2 supports in all the cases. In addition, Ni nanoparticles were well dispersed and homogeneously distributed in the monometallic Ni systems. The same finding could be stressed in the case of bimetallic PtNi-based materials, Ni and Pt nanoparticles being homogeneously dispersed as well. As it was above-mentioned, the presence of small Pt nanoparticles and relatively bigger Ni nanoparticles together with PtNi combined nanoparticles could be ascertained.

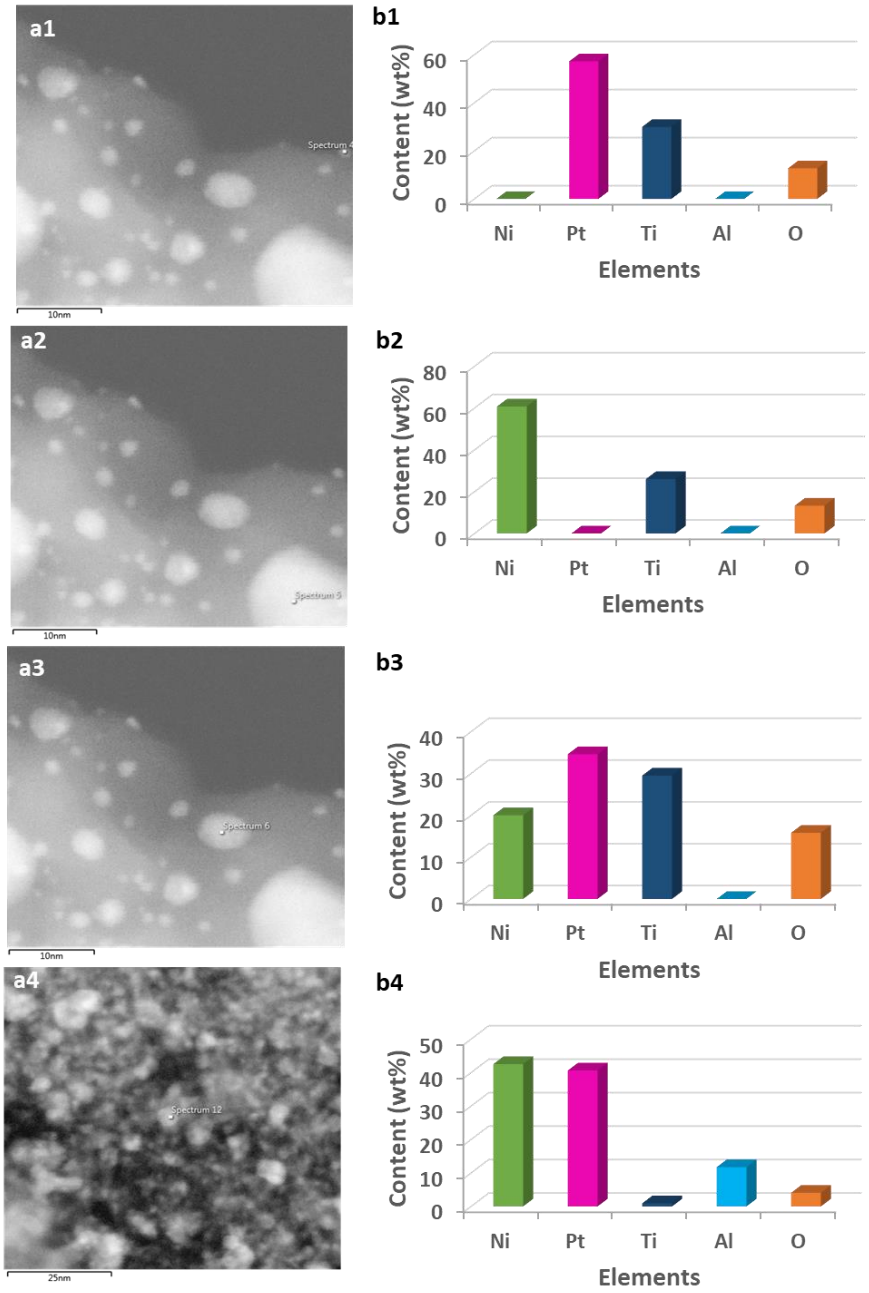

Figure 6.17. a) HR-STEM images and b) elemental composition of $PtNi/TiO_2/Al_2O_3$ catalyst.

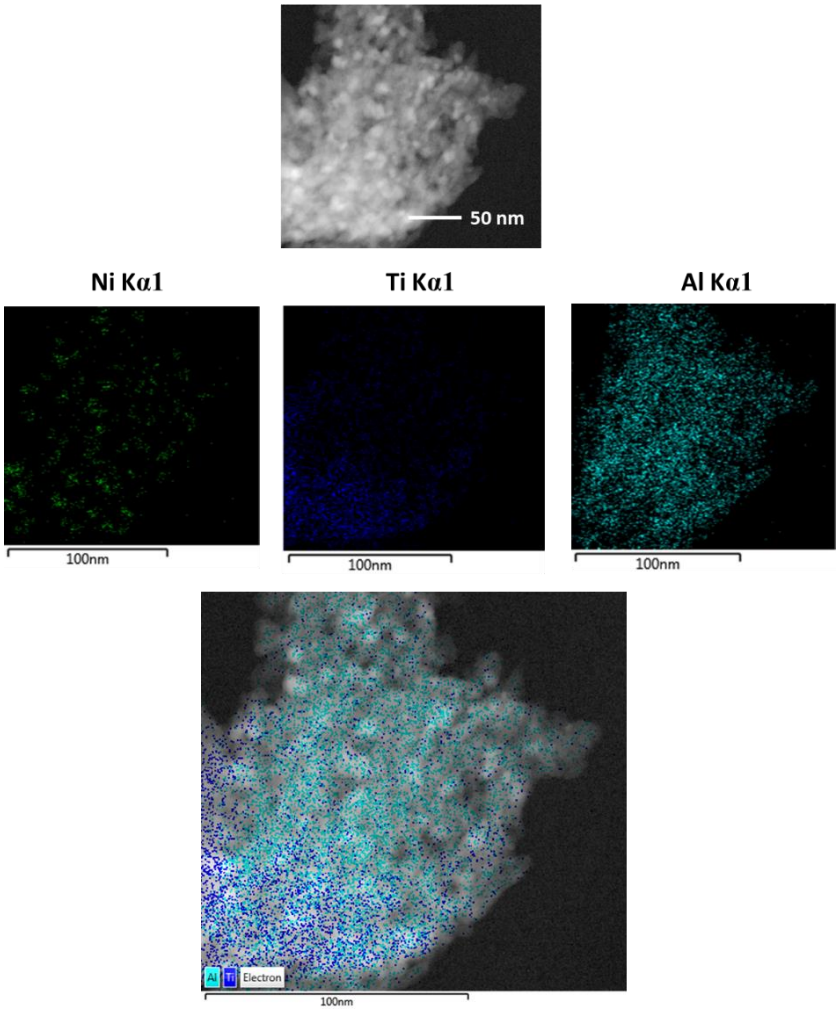

Figure 6.18. HRTEM-EDX mapping of $Ni/TiO_2/Al_2O_3$ catalyst.

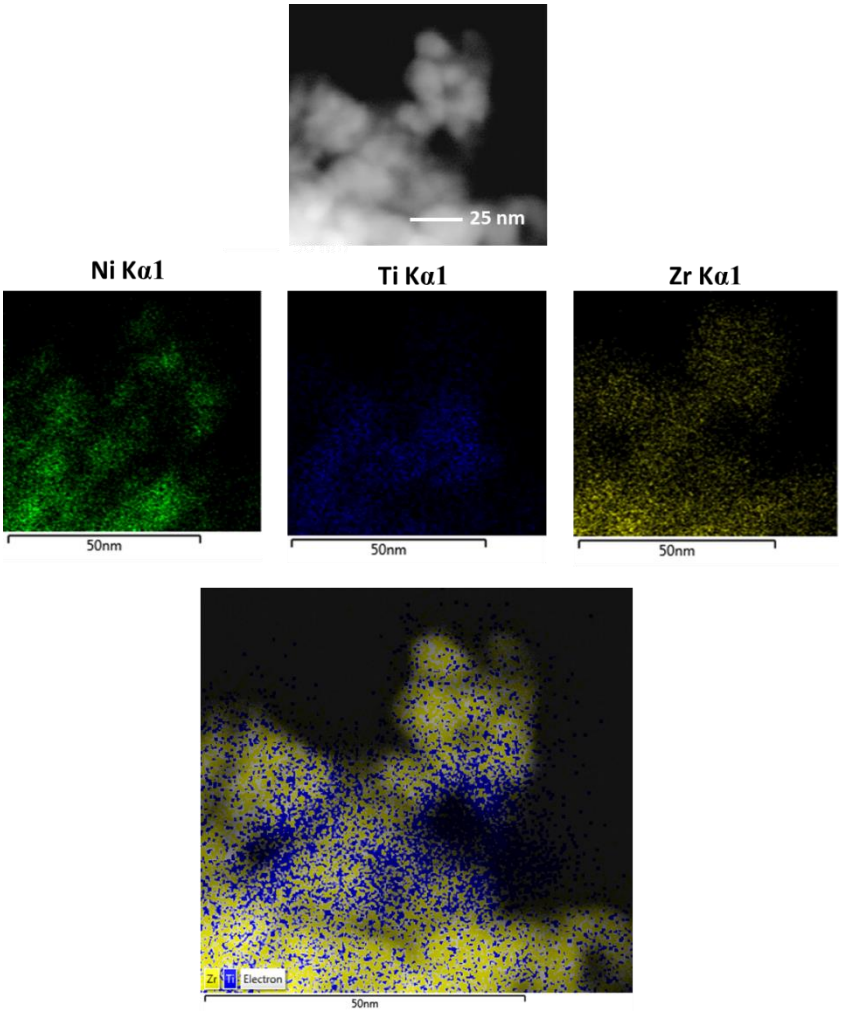

Figure 6.19. HRTEM-EDX mapping of Ni/TiO_2/ZrO_2 catalyst.

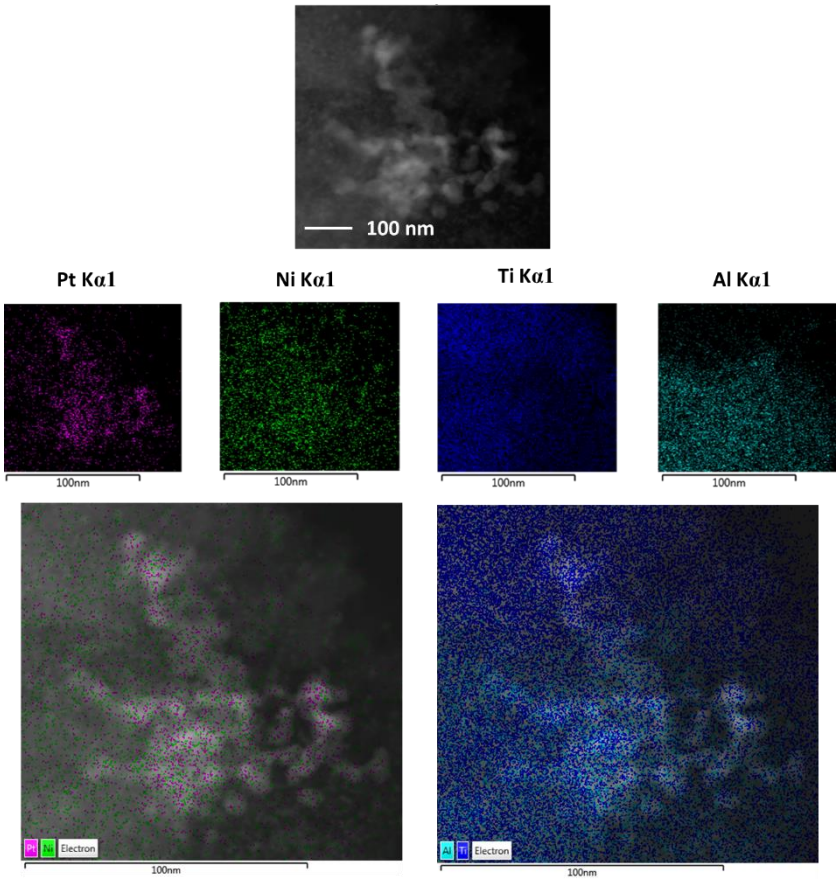

Figure 6.20. HRTEM-EDX mapping of PtNi/TiO_2/Al_2O_3 catalyst.

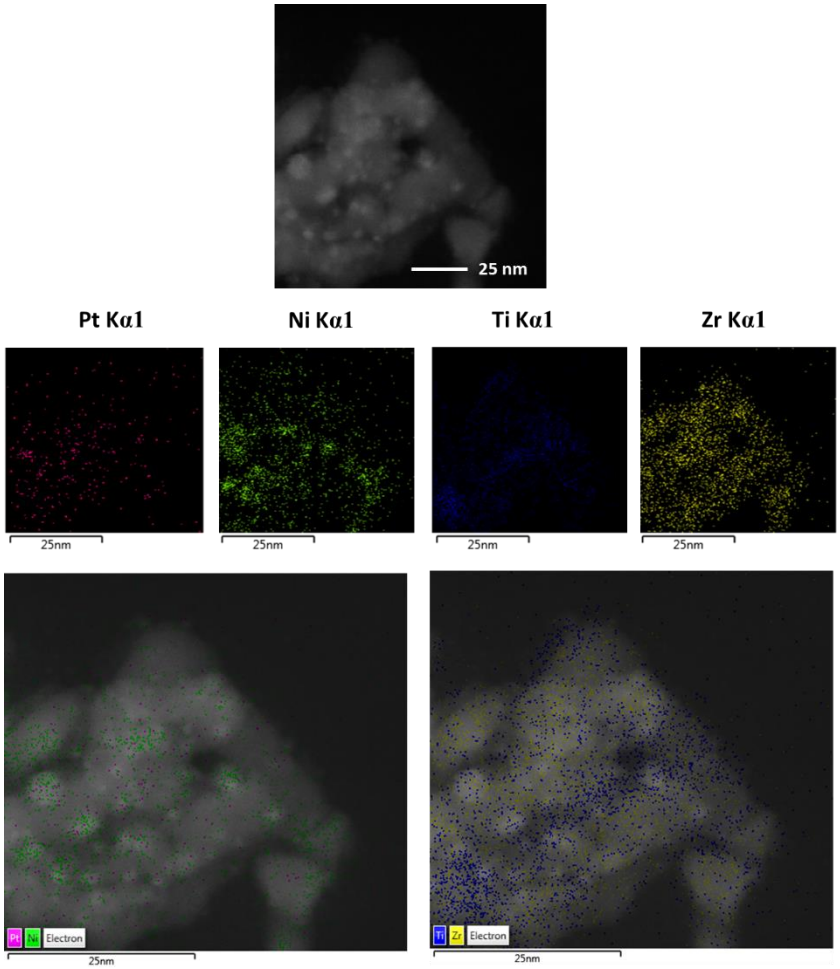

Figure 6.21. HRTEM-EDX mapping of PtNi/TiO_2/ZrO_2 catalyst.

6.3.10.5. XPS measurements

Aiming at gaining an insight into a likely interaction between both Ni and Pt metals, XPS analyses were carried out for the monometallic Ni- and Pt-based catalysts and the bimetallic PtNi-based one. In this sense, Pt*4f*, Ni*2p* and Al*2s* high-resolution XPS were acquired. However, the interpretation of the XPS spectra was challenging due to several regions overlapping with each other. Concretely, the Pt*4f* region overlaps with Al*2p* and Ni*3p*, so that seeing any shift in the Pt$4f_{5/2}$ binding energy (BE) is highly adventurous (see Figure A6.17).

On the contrary, the Ni*2p* XPS signal does appear relatively clean, and Figure 6.22 presents an approximated fitting for the Ni$2p_{3/2}$ region. It must be mentioned that any Ni*2p* curve fitting procedure not based on pure references is highly risky due to a multiplet splitting structure. Nonetheless, assuming the presence of Ni(0) (the precursor on the catalyst has been "*in-situ*" reduced), and another set of signals corresponding to oxidized Ni (with a vast majority of Ni(II) species since we started from a Ni(II) precursor), it is possible to reach an acceptable fitting. Notably, the fitting (see Table A6.3 for a more detailed procedure) is considering a multiplet splitting for this Ni(II) with a situation somewhere between isolated Ni^{2+}, NiO and $Ni(OH)_2$ [26-28]. Although this fitting does not allow us to discriminate between the nature of these oxidized species, it is helpful to isolate the metallic part of the spectra.

In view of this functional isolation, both $Ni/TiO_2/Al_2O_3$ and $PtNi/TiO_2/Al_2O_3$ samples show nearly the same Ni^0/Ni-oxidized ratio (44.56 and 46.54, respectively). However, when Pt is present in the sample, the nanoparticle size distribution tends to be much more homogeneous. This can be seen in the two peaks for Ni^0 present in the $Ni/TiO_2/Al_2O_3$, pointing towards the existence of different phases with different conductivities. The peak at lower BE (849.5 eV) would correspond to bigger Ni^0 nanoparticles with a higher conductivity, and mistakenly corrected by the charge reference applied to the survey spectra, whereas the peak observed at higher BE (851.4 eV) can be ascribed to smaller Ni^0 nanoparticles with lower conductivities [29]. On the contrary, just the peak corresponding to the smaller Ni^0 nanoparticles (851.4 eV) is present in the bimetallic system $PtNi/TiO_2/Al_2O_3$. This fact is in good agreement with what literature has reported about adding a small amount of a noble metal to a system mainly comprising a first-row transition metal, the former controlling the size of the latter [30]. This constitutes a good prove that Pt is somehow influencing Ni, which is likely to reveal a strong interaction between both metals. Thus, data obtained by means of XPS measurements are in a good agreement with results from H_2-TPR, microscopy and H_2 chemisorption measurements of the samples.

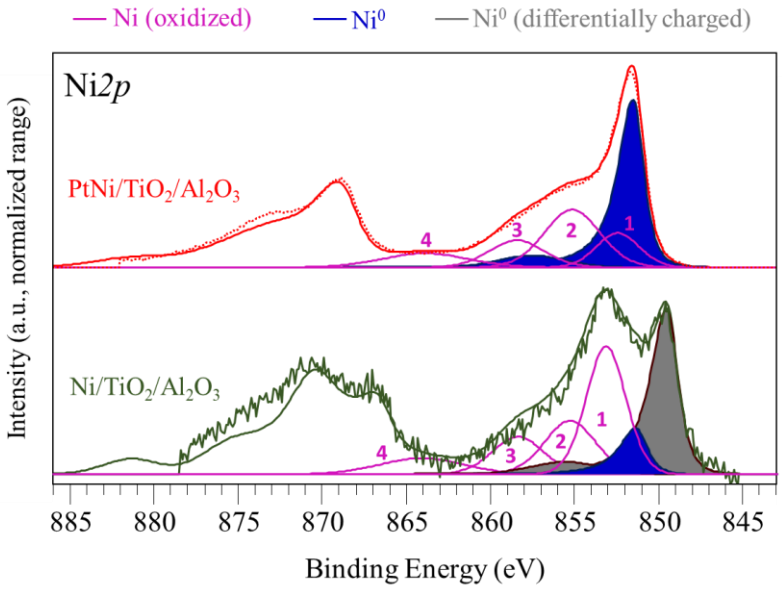

Figure 6.22. XPS patterns of Ni2p scan for $Ni/TiO_2/Al_2O_3$ and $PtNi/TiO_2/Al_2O_3$ catalysts.

Considering all the above-mentioned, the results obtained from the catalysts characterization by means of XPS, H_2-TPR, microscopy and H_2 chemisorption measurements correlate with the superior hydrogenation catalytic activity observed for the bimetallic PtNi catalytic materials compared with the monometallic Ni-based systems. This superior activity is mainly due to a synergic and strong interaction between Ni and Pt, resulting in smaller and well dispersed metal nanoparticles with highly reducible Ni species in the bimetallic catalyst. In addition, the homogeneously deposited TiO_2 layers onto the alumina and/or zirconia support appear to favour Ni nanoparticles dispersion, also enhancing their reducibility and, consequently, their hydrogenation capacity under reaction conditions.

6.4. Conclusions

- In the mild hydrotreatment of tars-type compounds, Ni supported on TiO_2/Al_2O_3 demonstrated to be the most efficient catalyst among the monometallic Ni-based catalysts tested, achieving higher selectivity to the desired hydrogenated products.
- Additionally, monometallic Ni-based catalysts were tested in the catalytic selective hydrogenation of fatty acids to produce hydrocarbons, and in this specific case monometallic Ni supported on TiO_2/Al_2O_3 and TiO_2/ZrO_2 were encountered as the most efficient catalysts for n-heptadecane (C17) formation.
- The effect of Pt addition to these Ni-based systems was evaluated at 275 ºC and 30 bar of H_2 by varying the catalyst loading. In this sense, bimetallic PtNi-based catalysts demonstrated higher activity than their analogous monometallic Ni-based systems, achieving maximum production of n-heptadecane (C17) with low amount of catalyst (only 10 mg).
- Additionally, the effect of reaction parameters, such as temperature and H_2 concentration, was investigated and the most relevant catalytic results were attained when performing the catalytic test at 275 ºC and 30 bar of pressure (H_2 concentration ≥60%). For instance, maximum C17 selectivity (≈85%, 96% in liquids) was reached with $PtNi/TiO_2/Al_2O_3$ catalyst, being slightly lower in the case of $PtNi/TiO_2/ZrO_2$ because of the competitive n-octadecane (C18) formation.

- The production of stearyl alcohol (C18OH) was also maximized in our catalytic system, its selectivity being slightly increased when increasing the H_2 pressure from 30 bar to 45 bar by working at 225 ºC. For instance, 51% and 55% selectivities to the stearyl alcohol were achieved working with 25 mg of bimetallic $PtNi/TiO_2/Al_2O_3$ and $PtNi/TiO_2/ZrO_2$ catalysts, respectively.
- Based on the attained catalytic results, a reaction mechanism was proposed, especially for explaining the activity of bimetallic PtNi-based catalysts. Thus, after a rapid hydrogenation of the oleic acid to the corresponding saturated stearic acid, the reaction proceeds with the formation of the stearyl alcohol intermediate. The latter could react with the stearic acid to produce stearyl stearate as by-product or, more interestingly, suffer decarbonylation and/or hydrodeoxygenation to produce n-heptadecane (C17) and/or n-octadecane (C18). The former pathway is clearly favoured over our catalytic system.
- Characterization of the catalytic materials by means of XPS, H_2-TPR, microscopy, H_2 chemisorption measurements, among others confirms the superior activity of the bimetallic PtNi systems compared with the monometallic Ni ones. This superior activity is mainly due to a synergic and strong interaction between Ni and Pt, resulting in smaller and well dispersed metal nanoparticles with the presence of highly reducible Ni species in the bimetallic catalyst.

6.5. References

[1] S. Hu, M. Xue, H. Chen, Y. Sun, J. Shen, Chinese Journal of Catalysis 32 (2011) 917-925.

[2] D. Zhang, J. Zhao, Y. Zhang, X. Lu, International Journal of Hydrogen Energy 41 (2016) 11675-11681.

[3] P. Vozka, D. Orazgaliyeva, P. Šimáček, J. Blažek, G. Kilaz, Fuel Processing Technology 167 (2017) 684-694.

[4] G.W. Huber, S. Iborra, A. Corma, Chemical Reviews 106 (2006) 4044-4098.

[5] M. Ventura, A. Marinas, M.E. Domine, Topics in Catalysis 63 (2020) 846-865.

[6] B.M.E Russbueldt, W.F. Hoelderich, Journal of Catalysis 271 (2010) 290-304.

[7] P. Benjumea, J. Agudelo, A. Agudelo, Fuel 87 (2008) 2069-2075.

[8] G. Knothe, Fuel Processing Technology 86 (2005) 1059-1070.

[9] R.W. Gosselink, S.A.W. Hollak, S.W. Chang, J. van Haveren, K.P. de Jong, J.H. Bitter, D.S. van Es, ChemSusChem 6 (2013) 1576-1594.

[10] A. Kiméné, R. Wojcieszak, S. Paul, F. Dumeignil, Journal of Chemical Technology & Biotechnology 94 (2019) 658-669.

[11] E. Santillan-Jimenez, M. Crocker, Journal of Chemical Technology & Biotechnology 87 (2012) 1041-1050.

[12] E. Santillan-Jimenez, T. Morgan, J. Lacny, S. Mohapatra, M. Crocker, Fuel 103 (2013) 1010-1017.

[13] C. Zhao, T. Bruck, J.A. Lercher, Green Chemistry 15 (2013) 1720-1739.

[14] J.G. Immer, M.J. Kelly, H.H. Lamb, Applied Catalysis A: General 375 (2010) 134-139.

[15] G. Li, F. Zhang, L. Chen, C. Zhang, H. Huang, X. Li, ChemCatChem 7 (2015) 2646-2653.

[16] L. Chen, F. Zhang, G. Li, X. Li, Applied Catalysis A: General 529 (2017) 175-184.

[17] K. Jeništová, I. Hachemi, P. Mäki-Arvela, N. Kumar, M. Peurla, L. Čapek, J. Wärnå, D.Y. Murzin, Chemical Engineering Journal 316 (2017) 401-409.

[18] W.F. Maier, W. Roth, I. Thies, P.V. Ragué Schleyer, Chemische Berichte 115 (1982) 808-812.

[19] J. Li, J. Zhang, S. Wang, G. Xu, H. Wang, D.G. Vlachos, ACS Catalysis 9 (2019) 1564-1577.

[20] P. Kumar, S.R. Yenumala, S.K. Maity, D. Shee, Applied Catalysis A: General 471 (2014) 28-38.

[21] M.W. Schreiber, D. Rodriguez-Niño, O.Y. Gutiérrez, J.A. Lercher, Catalysis Science & Technology 6 (2016) 7976-7984.

[22] J. Liu, C. Li, F. Wang, S. He, H. Chen, Y. Zhao, M. Wei, D.G. Evans, X. Duan, Catalysis Science & Technology 3 (2013) 2627-2633.

[23] C.P. Ferraz, A. Kiméné, K.S. Vargas, S. Heyte, C. Durlin, O. Simon, F. Dumeignil, S. Paul, R. Wojcieszak, Catalysis Science & Technology 11 (2021) 3025-3038.

[24] V.M. Shinde, G. Madras, Applied Catalysis B: Environmental 132-133 (2013) 28-38.

[25] E. Soszka, M. Jedrzejczyk, I. Kocemba, N. Keller, A.M. Ruppert, Catalysts 10 (2020) 1026.

[26] A.P. Grosvenor, M.C. Biesinger, R.S.C. Smart, N. Stewart McIntyre, Surface Science 600 (2006) 1771-1779.

[27] M.C. Biesinger, B.P. Payne, A.P. Grosvenor, L.W.M. Lau, A.R. Gerson, R.S.C. Smart, Applied Surface Science 257 (2011) 2717-2730.

[28] M.C. Biesinger, B.P. Payne, L.W.M. Lau, A. Gerson, R.S.C. Smart, Surface and Interface Analysis 41 (2009) 324-332.

[29] S.P. Yuan, P.X. Jiang, International Journal of Thermophysics 27 (2006) 581-595.

[30] J.-w. Zhang, K.-k. Sun, D.-d. Li, T. Deng, G.-p. Lu, C. Cai, Applied Catalysis A: General 569 (2019) 190-195.

CHAPTER 7.

GENERAL CONCLUSIONS

This work has shown the necessity of designing and developing new solid metal (Pd, Ni) nanoparticles supported on metallic oxides catalysts, with high activity and stability for the transformation of tars derived from petroleum refining and biomass gasification via mild hydrotreatment to produce partially hydrogenated products in the range of C9-C15. In addition, the application scope of the solid catalysts developed in this work was extended to other demanding hydrogenation reactions. Thus, Pd-based catalysts were employed for performing the reductive amination of bio-derived acetol with ethylenediamine to produce 2-methylpiperazine in an efficient way, while Ni-based catalysts demonstrated excellent activity to transform fatty acids (non-conventional feedstocks) into hydrocarbons via selective hydrogenation.

From the results attained during this thesis with the different solid catalysts designed and tested in different hydrotreatment and/or hydrogenation processes, the following general conclusions can be established:

Chapter 4: Titanium oxide-supported Pd as an efficient and stable catalyst for the mild hydrotreatment of tars-type compounds

The mild hydrotreatment of a model mixture of tars-type compounds (i.e., naphthalene, 1-methylnaphthalene, acenaphthylene and phenanthrene) simulating those produced from petroleum distillation or from biomass gasification, into hydrogenated and partially hydrogenated products in the range of C9-C15 was efficiently performed over Pd supported on TiO_2 catalysts.

The hydrotreatment activity and selectivity towards the desired hydrogenated products (i.e., tetralin and others) were strongly improved by increasing the amount of acid sites and surface area of the catalyst. TiO_2 Nano, possessing majorly titania Anatase crystalline phase, was found as the more adequate support to accommodate small Pd nanoparticles.

More interestingly, after consecutive reuses, 1.3wt%Pd/TiO_2 Nano catalyst remained active and stable, with very low carbon deposition, any Pd leaching detected, and practically no changes in the Pd nanoparticle size, even after regeneration (with H_2) of the used catalyst. Thus, although Pd^0 active species were transformed into Pd^{2+} species during the process, they were recovered via an *"in situ"* reduction under operational conditions.

Finally, the activity of Pd/TiO_2 Nano catalyst in tars mild hydrotreatment was compared with other previously reported commercial catalysts, demonstrating higher activity and selectivity than metal supported on alumina and CoMo-based catalysts, with conversion values comparable to those of NiMoS/Al_2O_3 but having much higher TON and less carbon deposition. Additionally, other types of products (higher amounts of gases, light hydrocarbons and monoaromatics) were generated with Pd/USY as catalyst, along with high carbon deposition on the catalyst surface. In addition, doping of the Pd-based catalyst with other metal did not improve the catalytic activity in tars mild hydrotreatment.

Chapter 5. Titania-alumina-supported Pd catalysts for the mild hydrotreatment of tars-type compounds

Better catalytic results in the tars mild hydrotreatment were obtained with Pd/TiO_2-Al_2O_3 material compared with Pd supported on other mixed metal oxides.

The synthesis of TiO_2-Al_2O_3 support was optimized, achieving better results when Pd is supported on TiO_2-Al_2O_3 having Ti/Al molar ratio ≈ 1.3, synthesized at pH = 9, with ammonia solution addition rate of 1000 mL/h, and being precipitated during 12 h (aging time) at 60 ºC. Additionally, Pd/TiO_2-Al_2O_3 catalyst is efficient and stable for the tars mild hydrotreatment after consecutive reuses. Thus, quite low carbon deposition, any Pd leaching and changes in the Pd particle size (and distribution) were observed after consecutive reuses and regeneration with H_2. The catalytic activity of Pd/TiO_2-Al_2O_3 catalyst is similar to that of Pd/TiO_2 Nano catalyst and better than Pd/γ-Al_2O_3 material in the tars mild hydrotreatment, the former catalysts being more resistant to carbon deposition than the latter one.

$Pd/TiO_2/\gamma$-Al_2O_3 catalyst, the support being synthesized via incipient wetness impregnation method, possesses similar activity compared to Pd/TiO_2 Nano. In addition, this material is cheaper and easier to prepare in comparison with Pd supported on co-precipitated Ti-Al mixed oxide.

Additionally, Pd/TiO_2-Al_2O_3 catalyst is efficient in another demanding hydrogenation reaction, such as the reductive amination of

bio-derived acetol with ethylenediamine to produce 2-methylpiperazine (2-MP), being more active than Pd supported on Al_2O_3 and TiO_2 Nano.

Chapter 6: Ni-based catalysts for hydrogenation reactions

In the mild hydrotreatment of tars-type molecules, $Ni/TiO_2/Al_2O_3$ was encountered as the most efficient catalyst among the Ni-based catalysts tested, being more selective to the desired hydrogenated products.

Additionally, monometallic Ni-based catalysts were tested in the selective hydrogenation of oleic acid to produce hydrocarbons, $Ni/TiO_2/Al_2O_3$ and $Ni/TiO_2/ZrO_2$ being the most efficient catalysts for n-heptadecane (C17) formation. Afterwards, bimetallic PtNi-based catalysts demonstrated higher activity than their analogous monometallic Ni-based systems, achieving maximum production of n-heptadecane (C17) with only 10 mg of catalyst, working at 275 ºC and 30 bar of H_2 pressure.

The effect of reaction parameters, such as catalyst loading, temperature and H_2 concentration was investigated, and the most relevant catalytic results were attained when performing the catalytic test at 275 ºC and 30 bar of pressure (H_2 concentration ≥60%). For instance, the maximum C17 selectivity (≈85%, 96% in liquids) was obtained with $PtNi/TiO_2/Al_2O_3$ catalyst, being slightly lower in the case of $PtNi/TiO_2/ZrO_2$ due to the competitive n-octadecane (C18) formation. In addition, the production of stearyl alcohol (C18OH) was

maximized for both bimetallic $PtNi/TiO_2/Al_2O_3$ and $PtNi/TiO_2/ZrO_2$ catalysts by working at 225 ºC and 45 bar of H_2.

Based on the achieved catalytic results, a reaction mechanism was proposed, particularly to explain the activity of bimetallic PtNi-based catalysts. The superior activity of bimetallic systems is mainly attributable to a synergic and strong interaction between Ni and Pt, resulting in smaller and well dispersed metal nanoparticles with the presence of highly reducible Ni species in the bimetallic material (confirmed by characterization studies performed by different techniques).

CHAPTER 8.
LIST OF FIGURES AND TABLES

8.1. List of figures

Chapter 1. Introduction

Chapter 3. Experimental procedure

Chapter 4. Titanium oxide-supported Pd as an efficient and stable catalyst for the mild hydrotreatment of tars-type compounds

Chapter 5. Titania-alumina-supported Pd catalysts for the mild hydrotreatment of tars-type compounds

Chapter 6. Ni-based catalysts for hydrogenation reactions

8.2. List of tables

Chapter 1. Introduction

Chapter 3. Experimental procedure

Chapter 4. Titanium oxide-supported Pd as an efficient and stable catalyst for the mild hydrotreatment of tars-type compounds

Chapter 5. Titania-alumina-supported Pd catalysts for the mild hydrotreatment of tars-type compounds

Chapter 6. Ni-based catalysts for hydrogenation reactions

CHAPTER 9.
ANNEX

9.1. For Chapter 4: Titanium oxide-supported Pd as an efficient and stable catalyst for the mild hydrotreatment of tars-type compounds

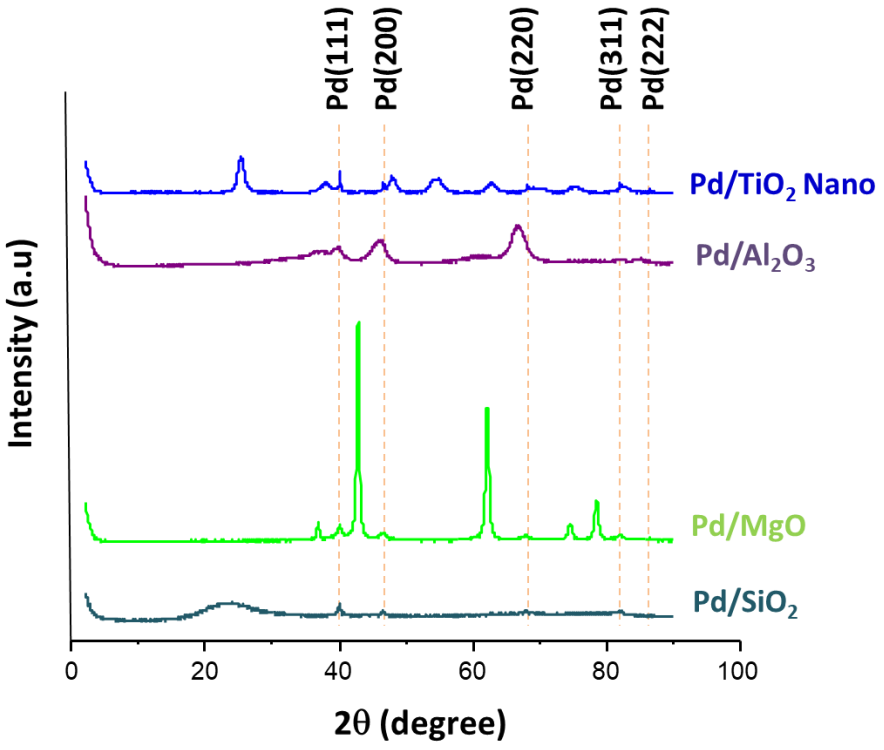

Figure A4.1. XRD patterns of different metal oxides-supported Pd catalysts.

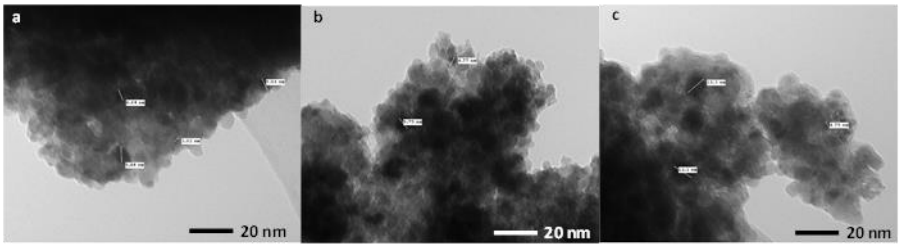

Figure A4.2. TEM images of a) 0.8wt%Pd/TiO_2 Nano (4-7 nm), b) 1.3wt%Pd/TiO_2 Nano (5-9 nm), and c) 2.2wt% Pd/TiO_2 Nano (6-12 nm).

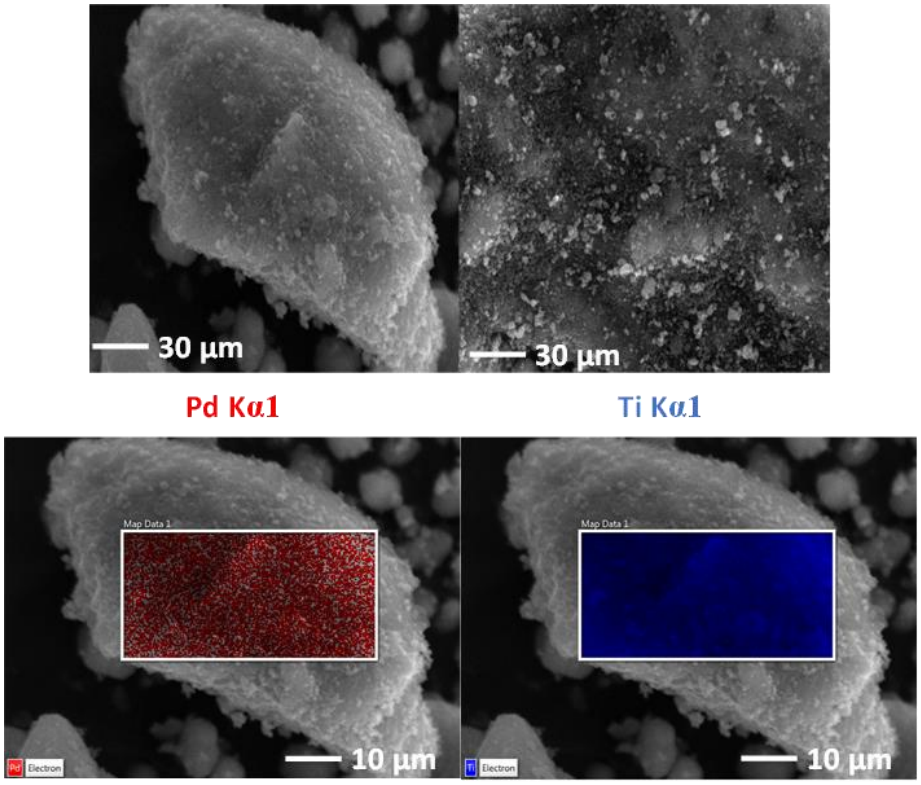

Figure A4.3. SEM-EDX images of fresh Pd/TiO_2 Nano catalyst.

Table A4.1. Catalytic activity comparison between Pd/TiO_2 Nano and other commercial catalysts in the tars mild hydrotreatment.[a]

Catalyst	Conv (mol%)	TON	Mass balance (%)	C after reaction (%)	Product selectivity (mol%)								
					Alkylcyclo-hexane	MonoAr	Tetralin	Decalin	Ace	HAce-1	HPhe-1	HPhe-2	HAce-2/HPhe-3
Pd/TiO_2 Nano	88	103	98	0.8	0.0	1.2	55.2	0.5	0.0	25.3	6.0	9.0	0.3
Pd/Al_2O_3	69	97	91	0.9	0.0	1.4	37.4	0.0	0.0	31.9	11.9	3.1	0.0
Pt/Al_2O_3	57	143	91	0.7	0.0	2.2	27.1	0.0	19.9	18.3	14.9	0.0	0.0
$NiMoS/Al_2O_3$	93	7	94	2.0	0.0	1.3	54.3	2.1	0.0	21.0	5.2	9.1	0.3
CoMoS/SiAl	73	7	90	1.7	0.0	1.8	42.2	0.4	0.0	27.5	10.4	3.0	0.0
Pd/USY	98	85	54	10.0	1.6	5.5	33.6	6.5	0.0	1.1	1.3	3.4	2.4
Pt/USY	98	144	54	15.7	1.2	5.0	36.7	4.5	0.0	1.6	1.1	4.2	2.0

[a] Reaction conditions: 0.5 g of tars-type compounds, 4.0 g of n-hexadecane, 275 °C, 30 bar of H_2 during 7 h. For Pd- and Pt-based catalysts, metal content ≈ 1.0wt%, except for Pd/TiO_2 Nano (1.3wt%). In $NiMoS/Al_2O_3$ Ni content = 3.3wt% and Mo content = 12.0wt%; and in $CoMoS/SiO_2$-Al_2O_3, Co content = 2.8wt%; and Mo content = 8.0wt%. TON = mols of products / mols of metal in catalyst.

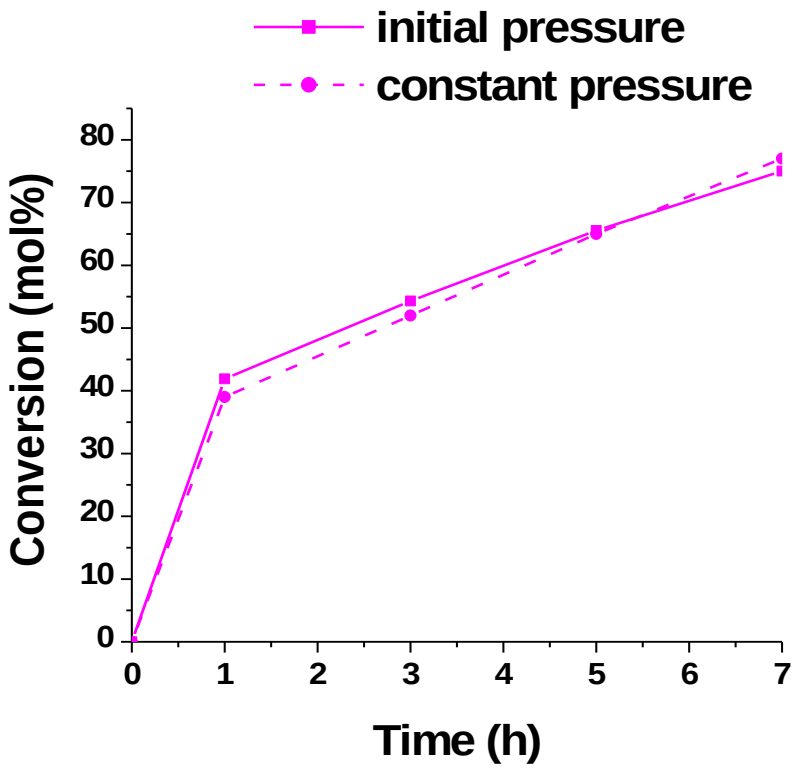

Figure A4.4. Conversion vs time in tars mild hydrotreatment over 1.3wt%Pd/TiO_2 Nano. Reaction conditions: 0.5 g of tars-type compounds, 4.0 g of n-hexadecane, 0.2 g of catalyst, 250 ºC, 30 bar of H_2 (initial and constant pressure) during 7 h.

9.2. For Chapter 5. Titania-alumina-supported Pd catalysts for the mild hydrotreatment of tars-type compounds

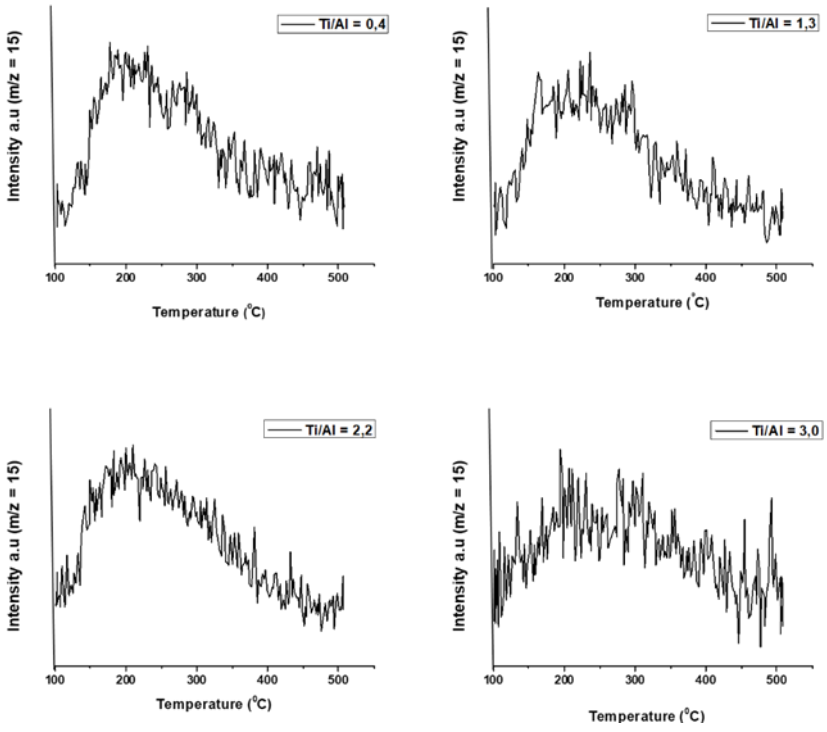

Figure A5.1. NH_3-TPD desorption profiles of TiO_2-Al_2O_3 samples having different Ti/Al molar ratios.

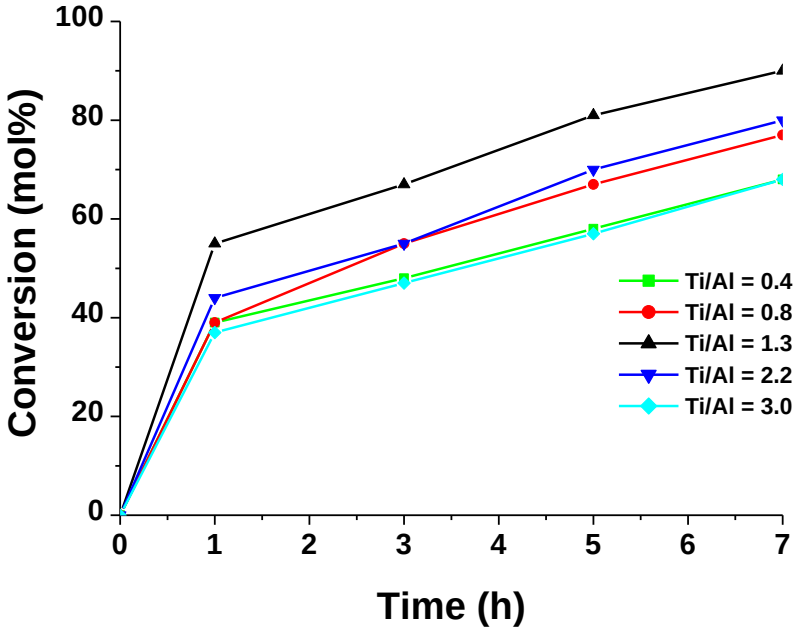

Figure A5.2. Conversion of tars-type compounds over Pd/TiO_2-Al_2O_3 catalysts with different Ti/Al molar ratio. Reaction conditions: 0.5 g of tars-type compounds, 4.0 g of n-hexadecane, 0.2 g of catalyst, 30 bar of H_2, 250 °C, during 7 h.

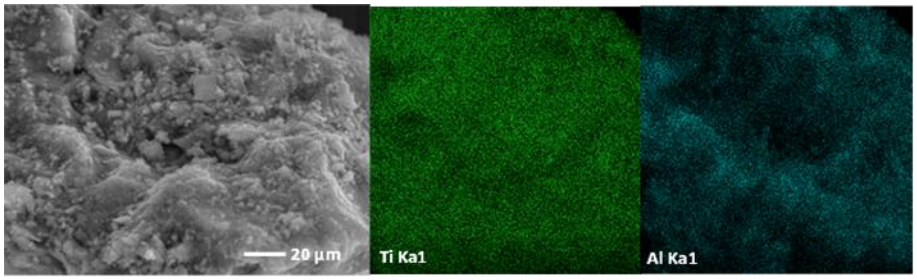

Figure A5.3. SEM-EDX mapping of TiO_2-Al_2O_3 mixed metal oxide.

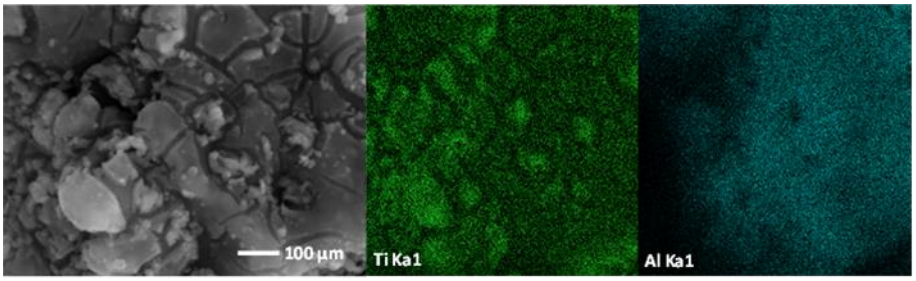

Figure A5.4. SEM-EDX mapping of TiO_2/Al_2O_3 mixed metal oxide.

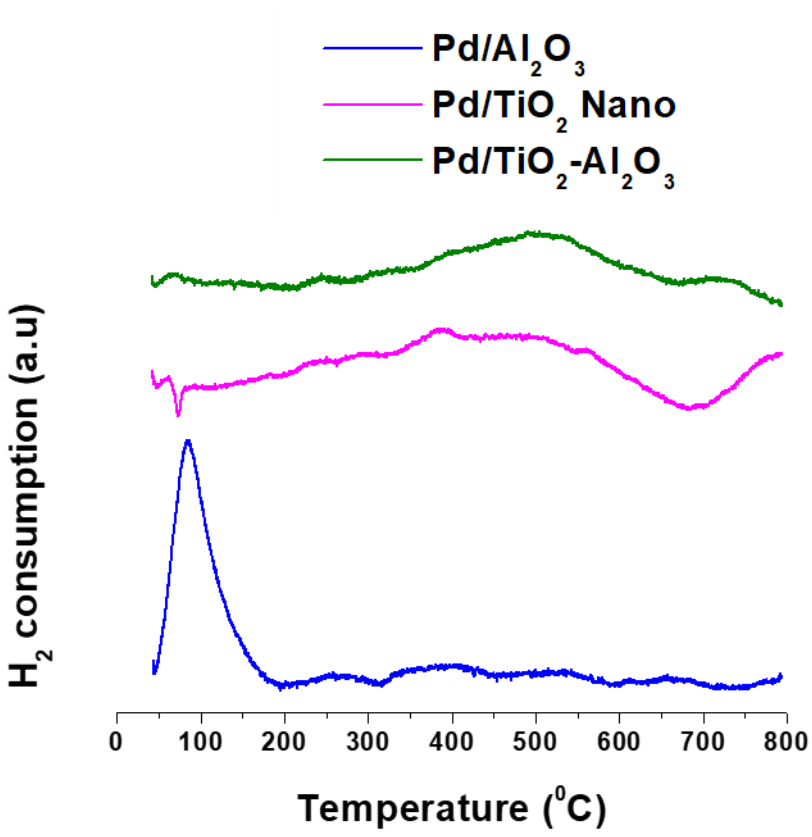

Figure A5.5. H_2-TPR profiles for Pd-based catalysts.

TPR experiments were carried out starting from ≈ 40 ºC.

9.3. For Chapter 6: Ni-based catalysts for hydrogenation reactions

Table A6.1. Liquid lost values in the blank test.

Reactor	Liquid lost (mg)	Liquid lost (%)
R1	-126.4	-8.8
R2	-104.7	-7.2
R3	-132.2	-9.1
R4	-102.4	-7.0
R5	-105.8	-7.3
R6	-111.0	-7.7
R7	-102.1	-7.0
R8	-93.2	-6.4
R9	-94.9	-6.5
R10	-89.2	-6.1
R11	-92.3	-6.4
R12	-103.5	-7.1
R13	-94.4	-6.5
R14	-91.3	-6.3
R15	-96.9	-6.7
R16	-94.0	-6.5
R17	-97.0	-6.9
R18	-104.3	-7.3
R19	-104.9	-7.3
R20	-98.9	-6.8
R21	-95.8	-6.6
R22	-104.9	-7.3
R23	-101.8	-7.1
R24	-105.0	-7.3

Reactions conditions: 1.56 mL of 15wt% oleic acid in decalin solution, 275 ºC, 30 bar of H_2, during 3 h.

Table A6.2. Selectivity to n-heptadecane (C17) with and without catalysts pre-activation.

Catalyst	Without pre-activation	With pre-activation
Ni/Al_2O_3	29	31
Ni/ZrO_2	27	22
Ni/TiO_2	25	10
Ni/TiO_2-Al_2O_3	3	2
Ni/ZrO_2-Al_2O_3	6	5
Ni/TiO_2-ZrO_2	7	5
$Ni/TiO_2/Al_2O_3$	83	87
$Ni/TiO_2/ZrO_2$	81	71
$Pt/TiO_2/Al_2O_3$	5	6
$Pt/TiO_2/ZrO_2$	5	4
$PtNi/TiO_2/Al_2O_3$	80	85
$PtNi/TiO_2/ZrO_2$	78	81

Reactions conditions: 1.56 mL of 15wt% oleic acid in decalin solution, 275 ^oC, 30 bar of H_2, 25 mg of catalyst during 3 h.

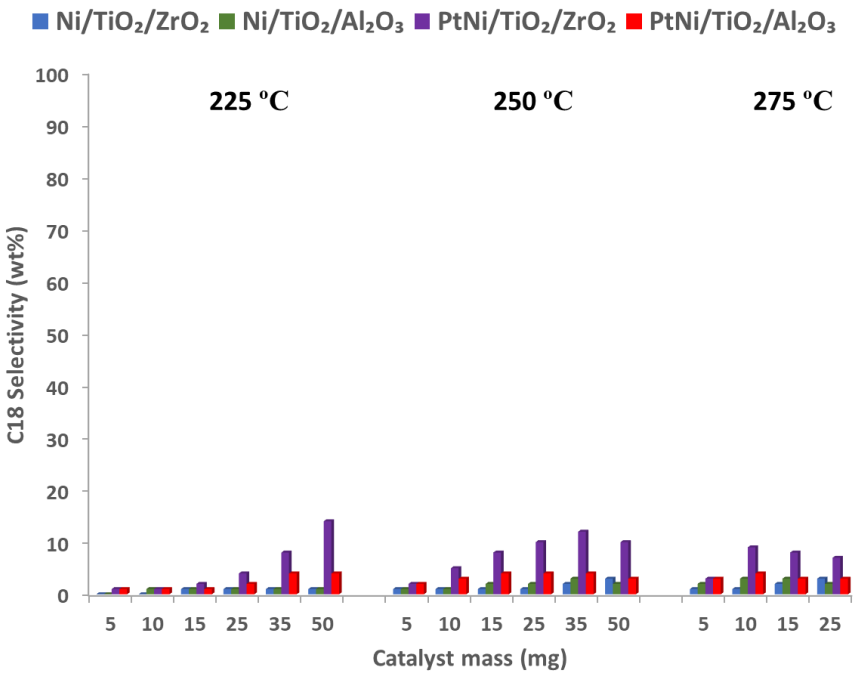

Figure A6.1. Influence of the temperature on the selectivity to n-octadecane (C18) over monometallic Ni and bimetallic PtNi supported on TiO_2/Al_2O_3 and TiO_2/ZrO_2 (Conversion = 100%). Reactions conditions: 1.56 mL of 15wt% oleic acid in decalin solution, 30 bar of H_2, during 3 h.

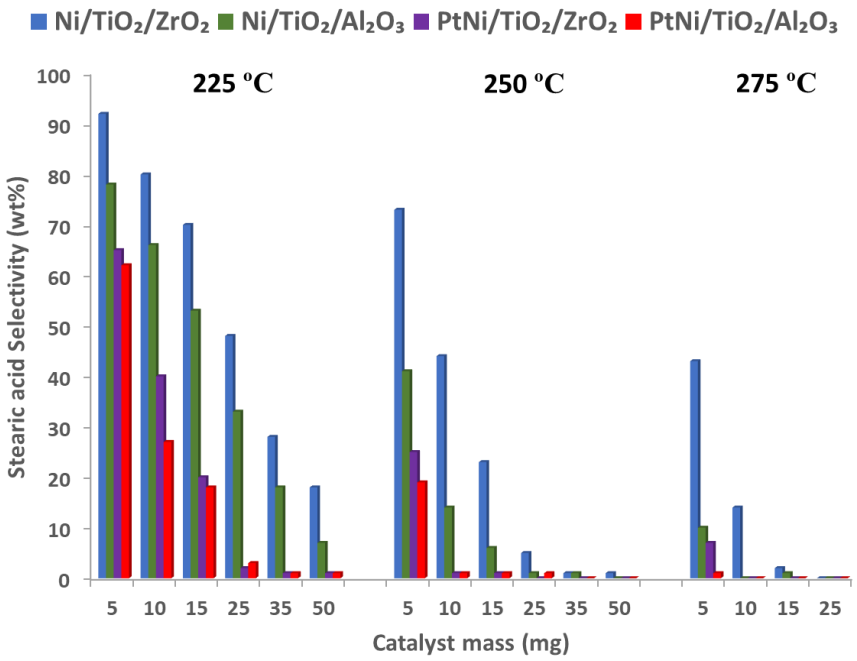

Figure A6.2. Influence of the temperature on the selectivity to stearic acid over monometallic Ni and bimetallic PtNi supported on TiO_2/Al_2O_3 and TiO_2/ZrO_2 (Conversion = 100%). Reactions conditions: 1.56 mL of 15wt% oleic acid in decalin solution, 30 bar of H_2, during 3 h.

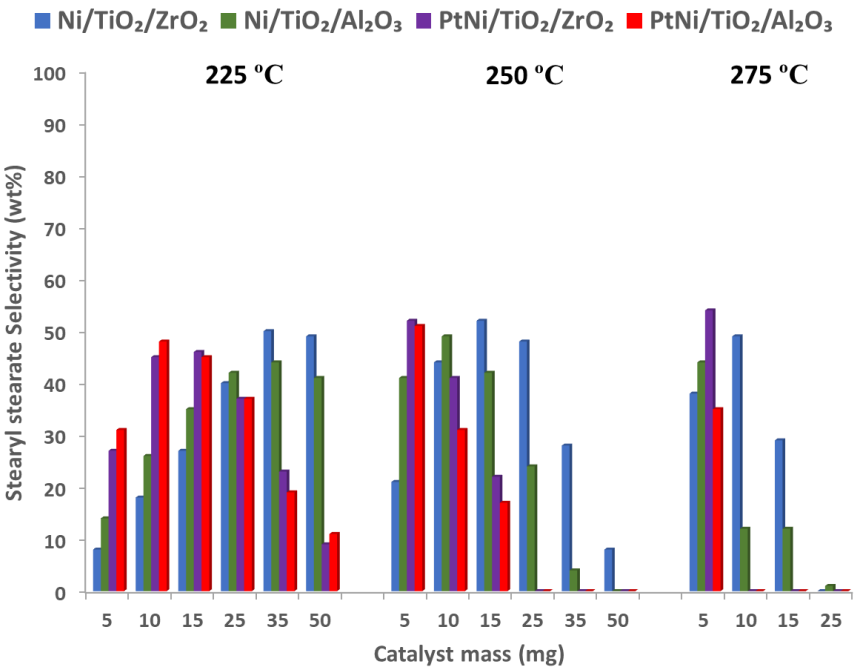

Figure A6.3. Influence of the temperature on the selectivity to stearyl stearate over monometallic Ni and bimetallic PtNi supported on TiO_2/Al_2O_3 and TiO_2/ZrO_2 (Conversion = 100%). Reactions conditions: 1.56 mL of 15wt% oleic acid in decalin solution, 30 bar of H_2, during 3 h.

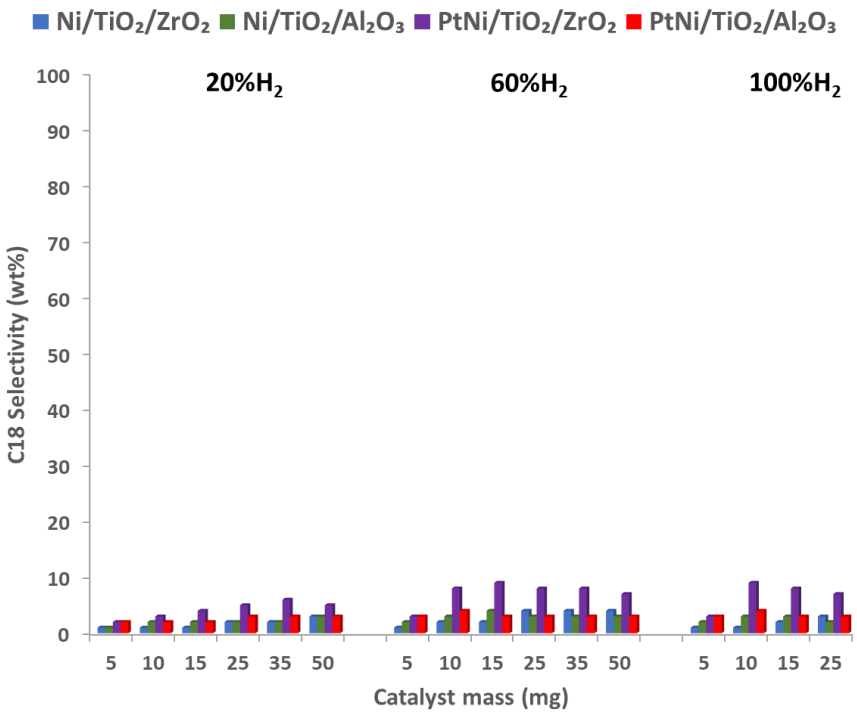

Figure A6.4. Influence of the H_2 concentration on the selectivity to n-octadecane (C18) over monometallic Ni and bimetallic PtNi supported on TiO_2/Al_2O_3 and TiO_2/ZrO_2 (Conversion = 100%). Reactions conditions: 1.56 mL of 15wt% oleic acid in decalin solution, 275 ºC, 30 bar, during 3 h.

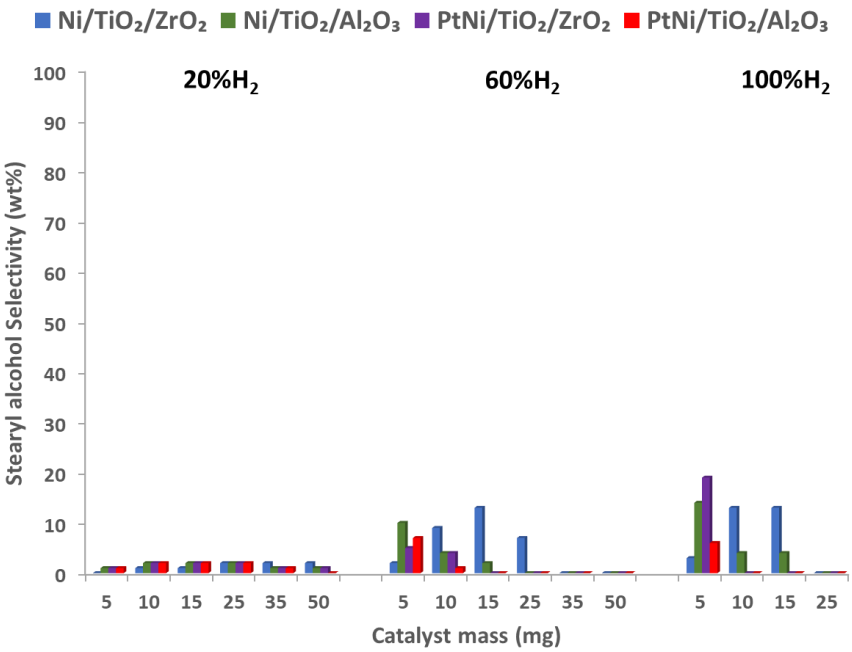

Figure A6.5. Influence of the H_2 concentration on the selectivity to stearyl alcohol (C18OH) over monometallic Ni and bimetallic PtNi supported on TiO_2/Al_2O_3 and TiO_2/ZrO_2 (Conversion = 100%). Reactions conditions: 1.56 mL of 15wt% oleic acid in decalin solution, 275 ºC, 30 bar, during 3 h.

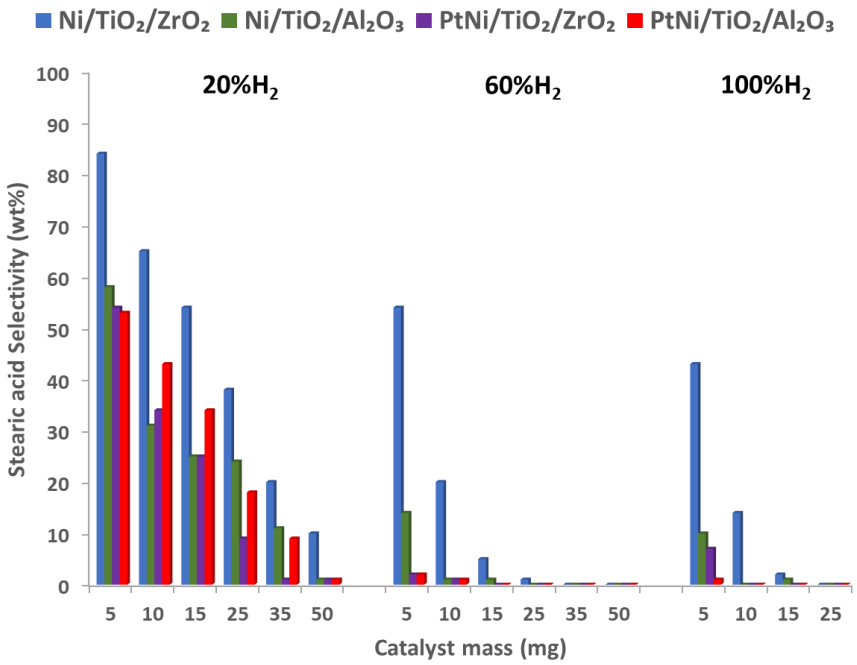

Figure A6.6. Influence of the H_2 concentration on the selectivity to stearic acid over monometallic Ni and bimetallic PtNi supported on TiO_2/Al_2O_3 and TiO_2/ZrO_2 (Conversion = 100%). Reactions conditions: 1.56 mL of 15wt% oleic acid in decalin solution, 275 ºC, 30 bar, during 3 h.

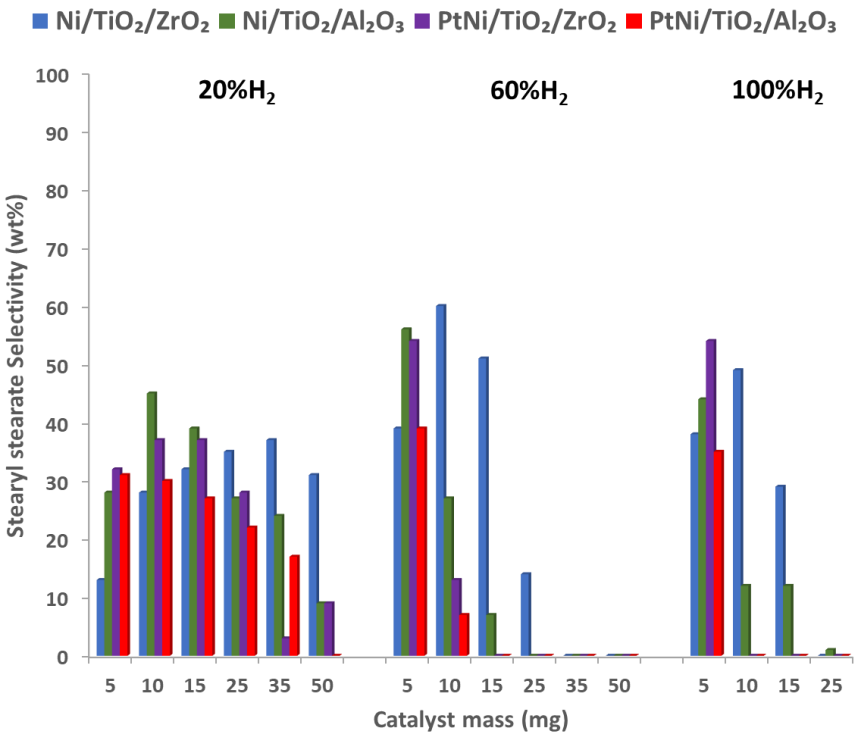

Figure A6.7. Influence of the H_2 concentration on the selectivity to stearyl stearate over monometallic Ni and bimetallic PtNi supported on TiO_2/Al_2O_3 and TiO_2/ZrO_2 (Conversion = 100%). Reactions conditions: 1.56 mL of 15wt% oleic acid in decalin solution, 275 ºC, 30 bar, during 3 h.

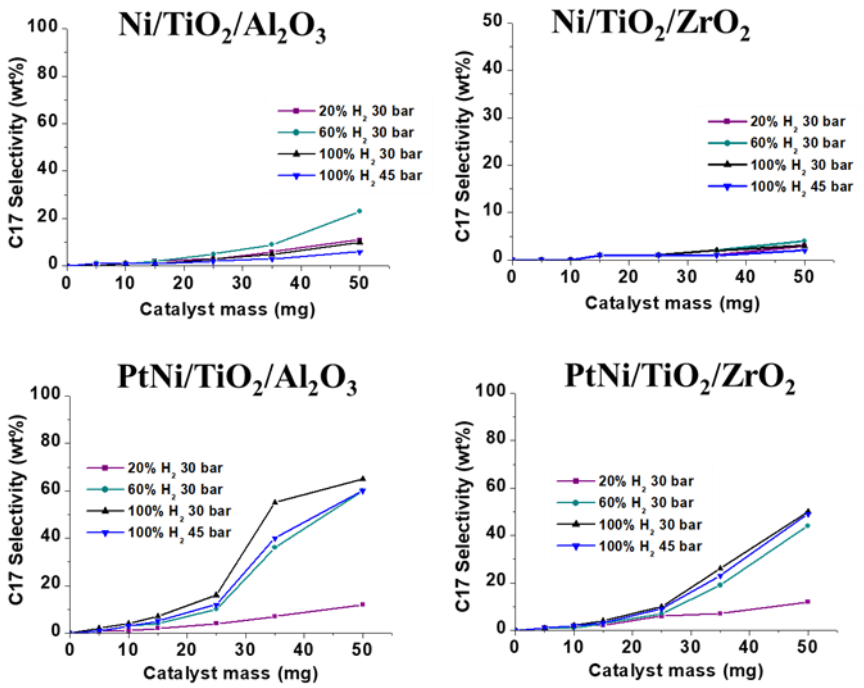

Figure A6.8. Influence of the H_2 concentration (and pressure) on the selectivity to n-heptadecane (C17) over monometallic Ni and bimetallic PtNi supported on TiO_2/Al_2O_3 and TiO_2/ZrO_2 (Conversion = 100%). <u>Reactions conditions</u>: 1.56 mL of 15wt% oleic acid in decalin solution, 225 ºC, during 3 h.

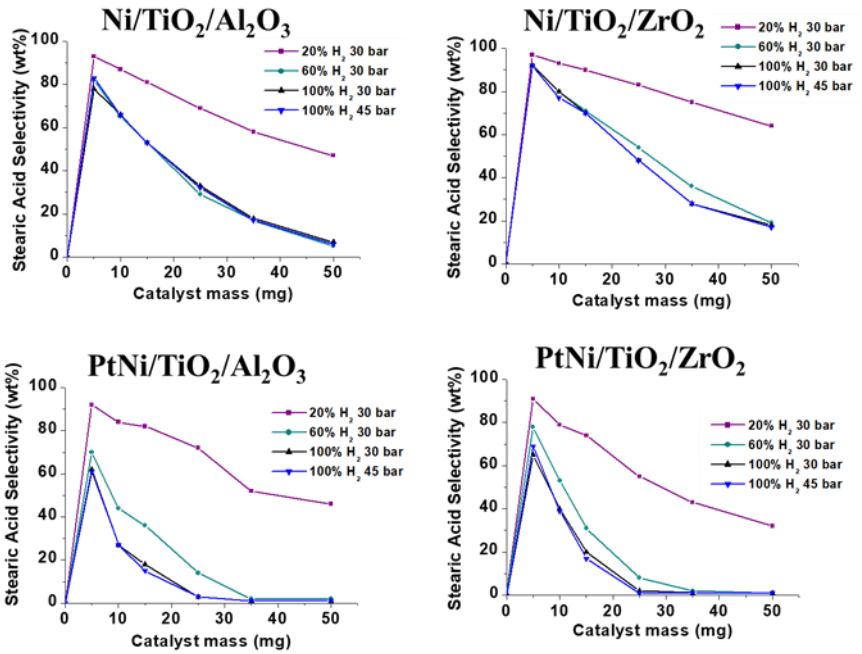

Figure A6.9. Influence of the H_2 concentration (and pressure) on the selectivity to stearic acid over monometallic Ni and bimetallic PtNi supported on TiO_2/Al_2O_3 and TiO_2/ZrO_2 (Conversion = 100%). Reactions conditions: 1.56 mL of 15wt% oleic acid in decalin solution, 225 ºC, during 3 h.

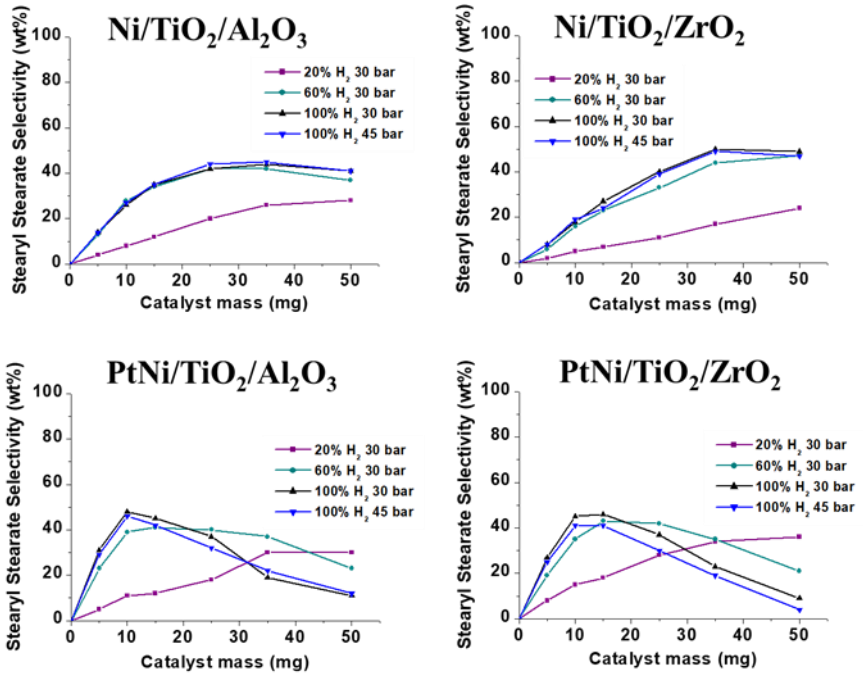

Figure A6.10. Influence of the H_2 concentration (and pressure) on the selectivity to stearyl stearate over monometallic Ni and bimetallic PtNi supported on TiO_2/Al_2O_3 and TiO_2/ZrO_2 (Conversion = 100%). Reactions conditions: 1.56 mL of 15wt% oleic acid in decalin solution, 225 ºC, during 3 h.

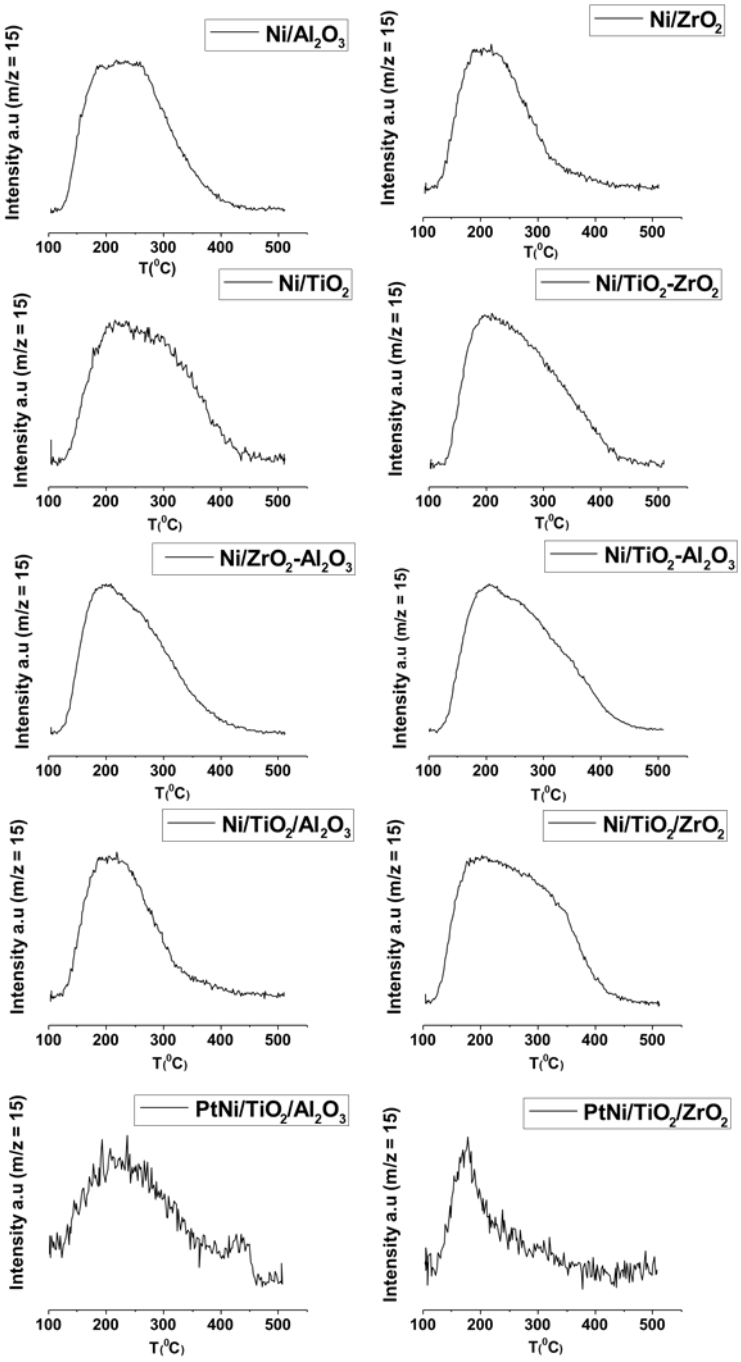

Figure A6.11. NH_3-TPD profiles of Ni- and PtNi-based catalysts.

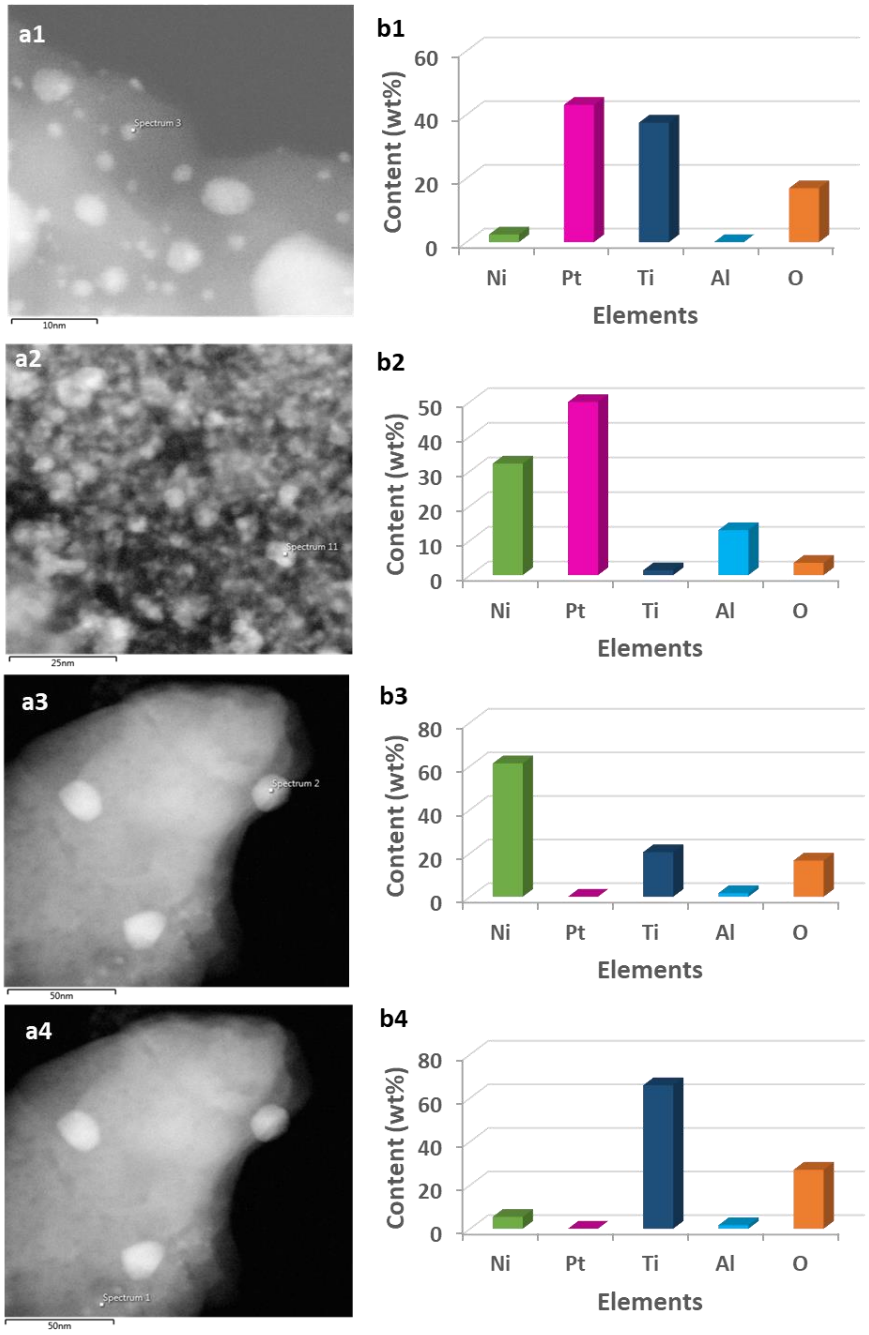

Figure A6.12. a) HR-STEM images and b) elemental composition of $PtNi/TiO_2/Al_2O_3$ *catalyst.*

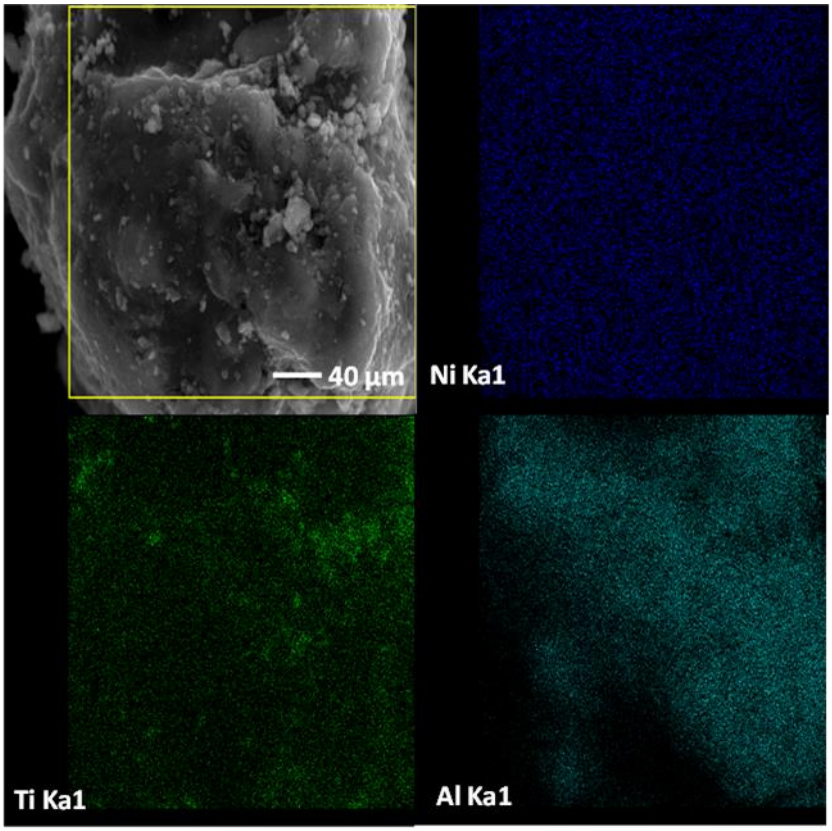

Figure A6.13. SEM-EDX mapping of $Ni/TiO_2/Al_2O_3$ catalyst.

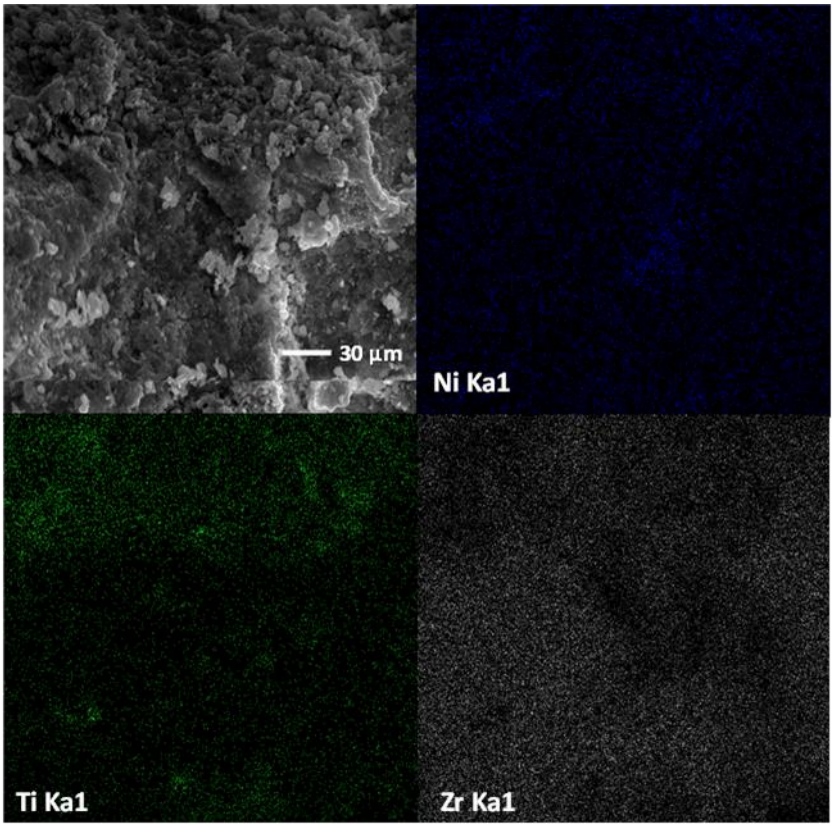

Figure A6.14. SEM-EDX mapping of $Ni/TiO_2/ZrO_2$ catalyst.

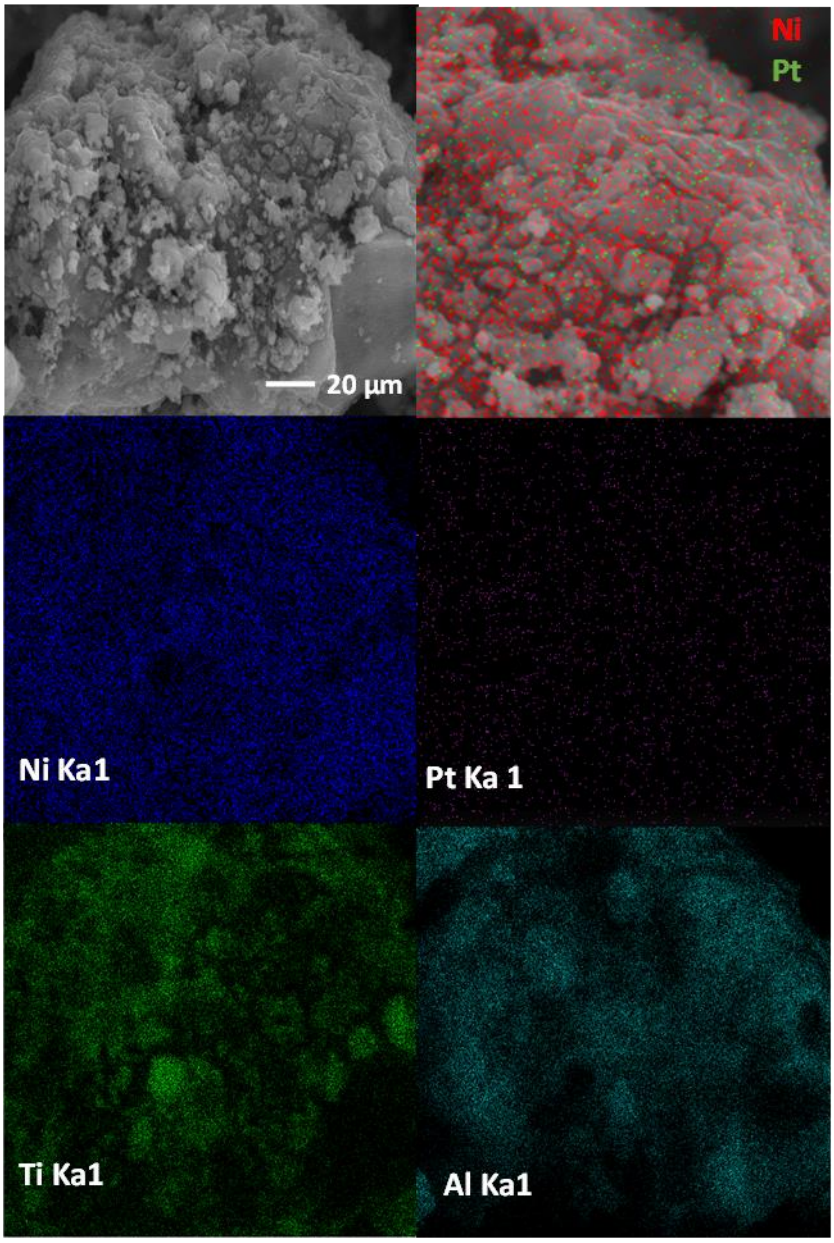

Figure A6.15. SEM-EDX mapping of PtNi/TiO_2/Al_2O_3 catalyst.

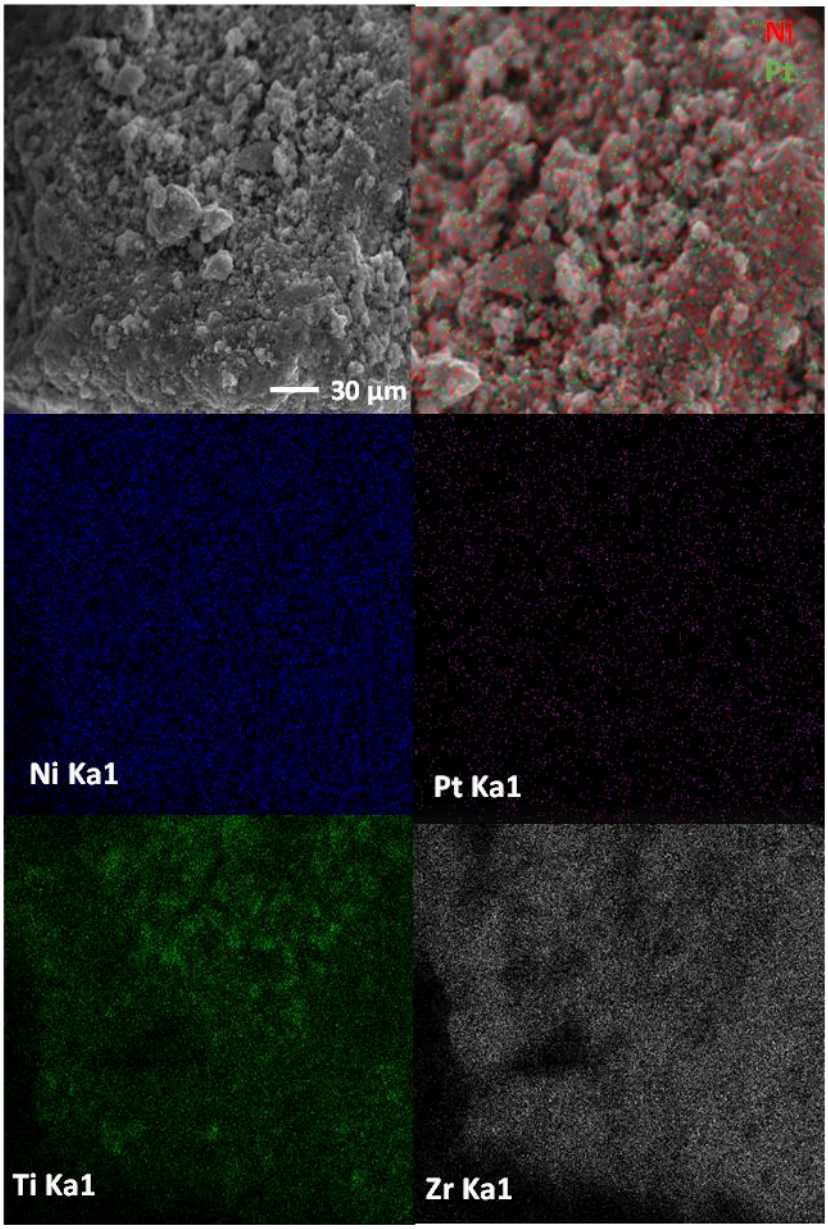

Figure A6.16. SEM-EDX mapping of PtNi/TiO_2/ZrO_2 catalyst.

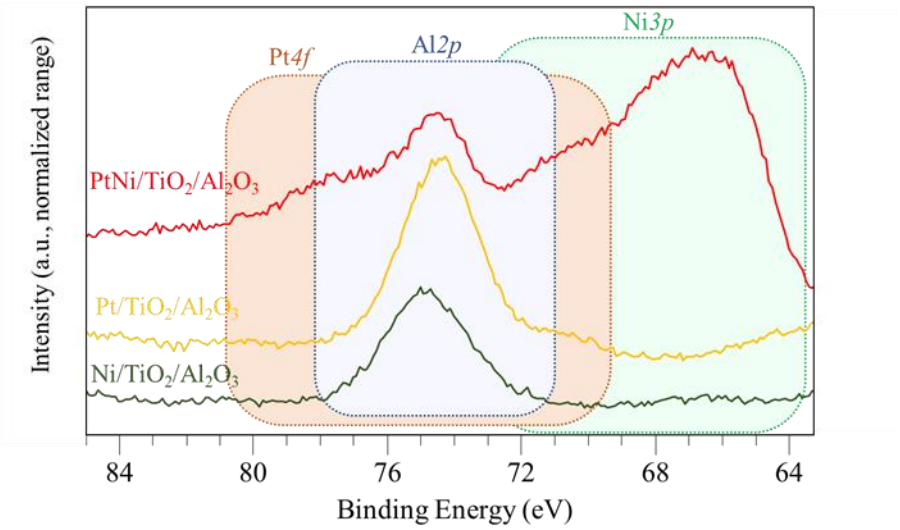

Figure A6.17. XPS patterns of Pt4f, Al2p and Ni3p scan for Ni, Pt and PtNi supported on TiO_2/Al_2O_3 catalysts.

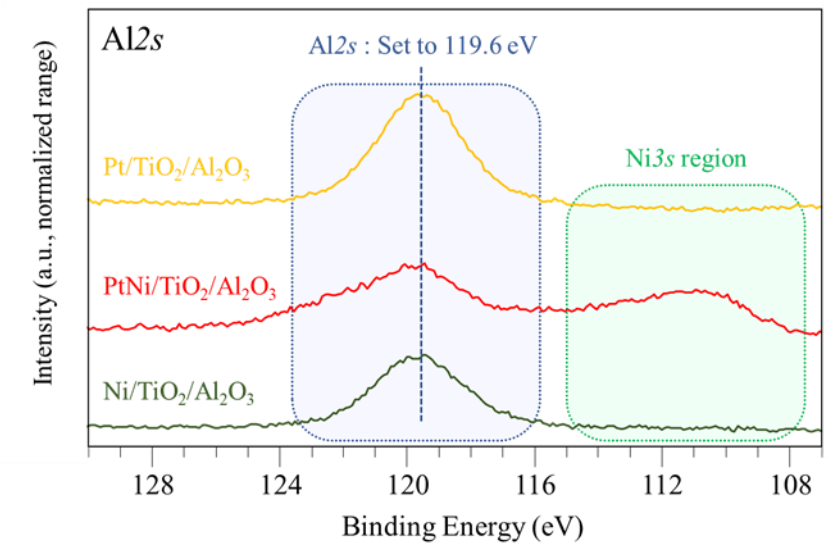

Figure A6.18. XPS patterns of Al2s scan for Ni, Pt and PtNi supported on TiO_2/Al_2O_3 catalysts (charge correction made with respect to 119.6 eV).

Table A6.3. Restrictions or special parameters applied in the $Ni2p_{3/2}$ XPS peak fitting.

Component	Parameter	Restriction
Ni(0)*	Line shape	Line shape for metallic nickel taken from refs. [1,2].
Ni(0)-satellite*	Position	Ni(0) + 6.03 eV [2]
Ni(0)-satellite*	Area	Restricted to Ni(0) x 0.15 [2]
Ni(0)*	Fwhm (eV)	Restricted to a maximum of 1.5 eV (PtNi) and 1.6 eV (Ni) [3]
Oxidized Ni (1)	Position	Firstly, set at 853.7 eV, then allowed to vary
Oxidized Ni (2,3,4)	Position	Restricted to be between those values found for NiO and $Ni(OH)_2$ and Ni^{2+} [1,2,4]
Oxidized Ni (2,3)	Fwhm (eV)	Not allowed to go beyond the value for oxidized Ni (1) x 1.3 [2,5]

* This restriction applied to Ni(0) and Ni(0) differentially charged.

[1] M.C. Biesinger, B. Payne, L.W.M. Lau, A. Gerson, R.S.C. Smart, Surface and Interface Analysis 41 (2009) 324–332.

[2] M.C. Biesinger, B.P. Payne, A.P. Grosvenor, L.W.M. Lau, A.R. Gerson, R.S.C. Smart, Applied Surface Science 257 (2011) 2717–2730.

[3] G. Bodelón, S. Mourdikoudis, L. Yate, I. Pastoriza-Santos, J. Pérez-Juste, L.M. Liz-Marzán, ACS Nano 8 (2014) 6221–621.

[4] A.P. Grosvenor, M.C. Biesinger, R.S.C. Smart, N.S. McIntyre, Surface Science 600 (2006) 1771–1779.

[5] R. Arrigo, S. Gallarati, M.E. Schuster, J.M. Seymour, D. Gianolio, I. da Silva, J. Callison, H. Feng, J.E. Proctor, P. Ferrer, F. Venturini, D. Grinter, G. Held, ChemCatChem. 12 (2020) 1491–1503.